

การพัฒนาการสังเคราะห์พอลิเอทิลีนเอไทนิลินและการประยุกต์เป็นฟลูออเรสเซนซ์เซนเซอร์



นางสาวนพรัตน์ ถาวรสิน

จุฬาลงกรณ์มหาวิทยาลัย

บทคัดย่อและแฟ้มข้อมูลฉบับเต็มของวิทยานิพนธ์ตั้งแต่ปีการศึกษา 2554 ที่ให้บริการในคลังปัญญาจุฬาฯ (CUIR)
เป็นแฟ้มข้อมูลของนิสิตเจ้าของวิทยานิพนธ์ ที่ส่งผ่านทางบัณฑิตวิทยาลัย

The abstract and full text of theses from the academic year 2011 in Chulalongkorn University Intellectual Repository (CUIR)
are the thesis authors' files submitted through the University Graduate School.

วิทยานิพนธ์นี้เป็นส่วนหนึ่งของการศึกษาตามหลักสูตรปริญญาวิทยาศาสตรดุษฎีบัณฑิต

สาขาวิชาปิโตรเคมี

คณะวิทยาศาสตร์ จุฬาลงกรณ์มหาวิทยาลัย

ปีการศึกษา 2560

ลิขสิทธิ์ของจุฬาลงกรณ์มหาวิทยาลัย

DEVELOPMENT OF POLY(ARYLENEETHYNYLENE)S SYNTHESIS AND
APPLICATION AS FLUORESCENT SENSOR

Miss Nopparat Thavornsini



A Dissertation Submitted in Partial Fulfillment of the Requirements
for the Degree of Doctor of Philosophy Program in Petrochemistry

Faculty of Science

Chulalongkorn University

Academic Year 2017

Copyright of Chulalongkorn University

นพรัตน์ ถาวรสิน : การพัฒนาการสังเคราะห์พอลิเอทรีนเอไทนิลีนและการประยุกต์เป็นฟลูออเรสเซนต์เซนเซอร์ (DEVELOPMENT OF POLY(ARYLENEETHYNYLENE)S SYNTHESIS AND APPLICATION AS FLUORESCENT SENSOR) อ.ที่ปรึกษาวิทยานิพนธ์หลัก: รศ. ดร.สัมฤทธิ์ วัชรสินธุ์, อ.ที่ปรึกษาวิทยานิพนธ์ร่วม: ศ. ดร.มงคล สุขวัฒนาสินธุ์, 141 หน้า.

ในงานวิจัยนี้มุ่งเน้นการเตรียมและการนำพอลิเอทรีนเอไทนิลีนมาประยุกต์ใช้เป็นเซนเซอร์ งานวิจัยนี้แบ่งออกเป็น 2 ส่วน ในส่วนแรกคือ การนำซาลิไซลัลดีไฮด์ฟังกชันนัลไรซ์พอลิ(เมทา-ฟีนิลีนเอไทนิลีน)มาใช้เป็นซีโมเซนเซอร์แบบเปิดสำหรับไอออนเหล็ก (Fe^{3+}) และในส่วนที่สองคือ การพัฒนาการเตรียมพอลิเอทรีนเอไทนิลีนที่มีความบริสุทธิ์สูงโดยใช้แพลเลเดียมบนแคลเซียมคาร์บอเนต ($Pd/CaCO_3$) เป็นตัวเร่งปฏิกิริยาแบบบิวทิรพันธุ์

ในส่วนแรก เราได้พัฒนาตัวตรวจวัดฟลูออเรสเซนต์แบบเปิดชนิดใหม่สำหรับไอออนเหล็กที่มีโครงสร้างพื้นฐานเป็นพอลิ(เมทา-ฟีนิลีนเอไทนิลีนซาลิไซลัลดีไฮด์) (PPE-IM) การเตรียม PPE-IM ทำได้โดยการโพลีเมอไรเซชันฟังกชันนัลไรเซชันของเอมีนพอลิเมอร์, (PPE-AM) ผ่านการควบแน่นกับซาลิไซลัลดีไฮด์ โดยมีองศาการเกิดพอลิเมอร์ของทั้ง PPE-AM และ PPE-IM เท่ากับ 17 พร้อมด้วยดัชนีการกระจายตัวของพอลิเมอร์เท่ากับ 1.5 ในสารละลายที่เป็นน้ำพอลิเมอร์ PPE-IM มีความเสถียรต่อการไฮโดรไลซิสสูงแตกต่างจากอนุพันธ์เดียวกันของโมเลกุลขนาดเล็กซึ่งจะเกิดการไฮโดรไลซิสอย่างช้าๆ ฟลูออเรสเซนต์เริ่มต้นที่ต่ำของ PPE-IM ที่ความยาวคลื่น 470 นาโนเมตร ถูกทำให้เพิ่มขึ้นมากถึง 300 เท่าเมื่อเติมไอออนเหล็กลงไป จาก ^1H-NMR แสดงให้เห็นว่า การเพิ่มขึ้นของฟลูออเรสเซนต์มีสาเหตุมาจากไอออนเหล็กเหนี่ยวนำให้เกิดปฏิกิริยาไฮโดรไลซิสของหมู่เอมีน ระบบการตรวจวัดไอออนเหล็กนี้ให้ค่าต่ำสุดที่สามารถตรวจวัดได้เท่ากับ 0.14 ไมโครโมลาร์

ในส่วนที่สอง ตัวเร่งปฏิกิริยาแพลเลเดียมรองรับบนแคลเซียมคาร์บอเนต ($Pd/CaCO_3$) ซึ่งเป็นตัวเร่งปฏิกิริยาแบบบิวทิรพันธุ์ที่หาซื้อได้ง่าย ถูกนำมาใช้เป็นครั้งแรกเพื่อสังเคราะห์พอลิเอทรีนเอไทนิลีน (PAEs) ผ่านปฏิกิริยาโซโนคาซิกซ์คัปปลิงพอลิเมอไรเซชัน จากการศึกษาเพื่อหาสภาวะที่เหมาะสมในการเกิดปฏิกิริยาพบว่า การใช้ 10 โมลเปอร์เซ็นต์ของ $Pd/CaCO_3$ ร่วมกับสารตั้งต้นที่หาซื้อได้ง่ายและมีราคาถูกสามารถเร่งปฏิกิริยา C-C คัปปลิงพอลิเมอไรเซชันระหว่างแอริลไดเอทรีนและแอริลไดไฮไดรด์/ไดโบรไมด์ที่หลากหลายที่อุณหภูมิ 80 องศาเซลเซียส โดยให้ร้อยละผลได้ PAEs สูง (79-100%) กลุ่มของ PAEs ที่ถูกสังเคราะห์ขึ้นมีองศาการเกิดพอลิเมอร์ (DP) สูงอยู่ในช่วงตั้งแต่ 15 ถึง 143 พร้อมทั้งมีค่าดัชนีการกระจายตัวของพอลิเมอร์ (PDI) เปลี่ยนแปลงในช่วง 1.5 ถึง 3.8 เมื่อประเมินความสามารถในการเร่งปฏิกิริยาเคมีของตัวเร่งปฏิกิริยา $Pd/CaCO_3$ เปรียบเทียบกับตัวเร่งปฏิกิริยาดั้งเดิมแบบบิวทิรพันธุ์, Pd/C และตัวเร่งปฏิกิริยาดั้งเดิมแบบเอกพันธุ์ $Pd(PPh_3)_4$ พบว่าการใช้ $Pd/CaCO_3$ สามารถเทียบเคียงกันได้ในด้าน DP และ PDI ที่สำคัญคือ พอลิเมอร์ที่สังเคราะห์ได้จาก $Pd/CaCO_3$ มีการปนเปื้อนของโลหะแพลเลเดียมและโลหะทองแดงอยู่ในปริมาณน้อยกว่าพอลิเมอร์ที่เตรียมได้จาก Pd/C และตัวเร่งปฏิกิริยาแบบเอกพันธุ์ $Pd(PPh_3)_4$

งานวิจัยโดยรวมของวิทยานิพนธ์นี้ประสบความสำเร็จในการเตรียมฟลูออเรสเซนต์เซนเซอร์แบบเปิดที่มีพื้นฐานโครงสร้างเป็นพอลิเอทรีนเอไทนิลีนสำหรับการตรวจวัดไอออนเหล็กอย่างมีความไวและความจำเพาะเจาะจงได้ (ภาค ก) และสามารถสังเคราะห์พอลิเอทรีนเอไทนิลีนที่มีความบริสุทธิ์สูงโดยใช้ตัวเร่งปฏิกิริยาแบบบิวทิรพันธุ์ $Pd/CaCO_3$ (ภาค ข)

สาขาวิชา ปีโตรเคมี

ปีการศึกษา 2560

ลายมือชื่อนิสิต

ลายมือชื่อ อ.ที่ปรึกษาหลัก

ลายมือชื่อ อ.ที่ปรึกษาร่วม

5672881323 : MAJOR PETROCHEMISTRY

KEYWORDS: POLY(ARYLENEETHYNYLENE)S / HETEROGENEOUS CATALYST / FLUORESCENT SENSORS / SONOGASHIRA COUPLING / HYDROLYSIS

NOPPARAT THAVORNIN: DEVELOPMENT OF POLY(ARYLENEETHYNYLENE)S SYNTHESIS AND APPLICATION AS FLUORESCENT SENSOR. ADVISOR: ASSOC. PROF. SUMRIT WACHARASINDHU, Ph.D., CO-ADVISOR: PROF. MONGKOL SUKWATTANASINITT, Ph.D., 141 pp.

In this research, we focus on preparation and sensor application of poly(aryleneethynylene)s. Our work is divided into two parts. The first study relates to the utilization of salicylaldehyde-functionalized poly(*m*-phenyleneethynylene) as a turn-on chemosensor for ferric ion (Fe^{3+}). The second part is the preparation of highly pure poly(aryleneethynylene)s using Pd/CaCO₃ as a heterogeneous catalyst.

In the first part, a new turn-on fluorescent probe for ferric ion based on poly(*m*-phenyleneethynylene salicylaldehyde) (PPE-IM) is developed. The preparation of PPE-IM involves post-polymerization functionalization of corresponding polymeric amine, PPE-AM, via condensation with salicylaldehyde. Degree of polymerization of both PPE-AM and PPE-IM are 17 with polydispersity index of 1.5. In aqueous solution, polymeric PPE-IM is hydrolytically stable unlike its small molecule analogue which is gradually hydrolyzed. The weak fluorescence of initial PPE-IM at wavelength 470 nm is greatly enhanced by 300 folds upon the addition of Fe^{3+} . ¹H-NMR analysis reveals that the fluorescence enhancement is caused by Fe^{3+} induced hydrolysis of the imine group. The sensing system shows a detection limit of 0.14 micromolar of Fe^{3+} .

In the second part, a commercially available heterogeneous palladium catalyst supported on calcium carbonate (Pd/CaCO₃) is studied for preparation of poly(aryleneethynylene)s (PAEs) via Sonogashira coupling polymerization for the first time. The study shows that the use of 10 mol% of Pd/CaCO₃ together with commercially available and inexpensive reagents can catalyze C-C coupling polymerization between aryl diethyne and a variety of aryl diiodides/dibromides at 80 °C to provide corresponding PAEs in excellent yields (79-100%) and high degree of polymerization (DP) ranging from 15 to 143 along with polydispersity index (PDI) range of 1.5 to 3.8. The catalytic activity of this Pd/CaCO₃ is comparable to the classical heterogeneous, Pd/C catalyst and homogeneous Pd(PPh₃)₄ catalyst. While Pd/CaCO₃ catalysed reaction gives much lower Pd and Cu contaminations in the resulting polymers.

In summary, a highly sensitive and selective fluorescence turn-on sensor for Fe^{3+} is developed from poly(aryleneethynylene)s via post polymerization functionalization (part A). The heterogeneous polymerization using Pd/CaCO₃ catalyst is developed for preparation of highly pure poly(aryleneethynylene)s (part B).

Field of Study: Petrochemistry

Academic Year: 2017

Student's Signature

Advisor's Signature

Co-Advisor's Signature

ACKNOWLEDGEMENTS

First, of all, I would like to express my sincere gratitude to my advisor, Associate Professor Sumrit Wacharasindhu, Ph.D. and my co-advisor, Professor Mongkol Sukwattanasinitt, Ph.D. for giving me opportunities, valuable advice, guidance and kindness throughout this research. Sincere thanks are also extended to my group member, Associate Professor Paitoon Rashatasakhon, Ph.D., Assistant Professor Anawat Ajavakom, Ph.D. and Sakulsuk Unarunotai, Ph.D. for their generous advice, invaluable guidance and encouragement. This thesis research would not be completed without their advice and guidance.

My appreciation is also given to Associate Professor Warinthorn Chavasiri, Ph.D., Chatr Panithipongwut Kowalski, Ph.D., Associate Professor Paitoon Rashatasakhon, Ph.D. thesis defense committee, for their kind attention, valuable suggestion and recommendations. I would like to thank Assistant Professor Rakchart Tripol, Ph.D., the external thesis defense committee from Mahidol University for suggestions.

Furthermore, I gratefully thank to my friends for their genuine, Kanokthorn Boonkitpatarakul, Ph.D., Kannigar Vongnam, Ph.D., Eakkaphon Rattanangkool, Ph.D. and everyone in MAPS-group for spirit, smile, good wish and their helps in everything.

I would like to thank the Thailand Research Fund (TRF-RSA6080018) and Nanotechnology Center (NANOTEC), NSTDA, Ministry of Science and Technology, Thailand, through its International Research Integration: Chula Research Scholar, program of Center of Excellence Network, Ratchadapiseksomphot Endowment Fund of Chulalongkorn University, Center of Excellence on Petrochemicals and Materials Technology (PETROMAT).

Finally, I would like to express thankfulness to Miss Suporn Panyataranont, Miss Patamavadee Phanpanya and my exceptional family for their love, care, encouragement and support throughout my life and study. I would not be able to reach this success without them.

CONTENTS

	Page
THAI ABSTRACT	iv
ENGLISH ABSTRACT	v
ACKNOWLEDGEMENTS	vi
CONTENTS	vii
LIST OF SCHEMES	xi
LIST OF FIGURES	xiii
LIST OF TABLES	xx
LIST OF ABBREVIATIONS	xxi
CHAPTER I INTRODUCTION	1
1.1 Overview of acetylenic polymer sensors (Part A).....	1
1.1.1 Structures of conjugated polymer fluorophores	1
1.1.2 Fluorescent spectral	4
1.1.3 Sensing mechanism	5
1.1.4 Optical sensor application of poly(aryleneethynylene)s (PAE)s.....	6
1.1.5 Importance of Ferric ion (Fe^{3+}).....	15
1.2.6 Objectives of this work.....	21
1.2 Introduction (Part B).....	22
1.2.1 Introduction of Sonogashira coupling reaction	23
1.2.2 Introduction of Pd-catalyzed polymerization.....	24
1.2.3 Introduction of Heterogeneous Pd catalyst.....	25
1.2.4 Literature reviews	26
1.2.5 Objectives of this research.....	33

CHAPTER II EXPERIMENTAL	34
2.1 Chemicals and materials	34
2.2 Analytical instruments	34
2.3 Experimental strategy for the synthesis of salicylaldimine-functionalized poly(phenyleneethynylene) used as turn-on sensor for ferric ion (part A)	35
2.3.1 Synthesis of small molecules.....	35
2.3.1.1 Preparation of 2,4-diiodoaniline (AM) [107] and (E)-2-((2,4- diiodo phenylimino)methyl)phenol (IM)	35
2.3.1.2 Preparation of 2,4-bis(phenylethynyl)amino derivatives	36
2.3.2 Synthesis of acetylenic polymers.....	37
2.4 Photophysical property study.....	38
2.4.1 UV-Visible spectroscopy	38
2.4.1.1. Molar Absorption Coefficients (ϵ).....	38
2.4.2 Fluorescence spectroscopy	39
2.4.3 Fluorophore quantum yields (Φ).....	39
2.4.4 Fluorescent sensor study (for part A)	40
2.4.4.1 Stability study	40
2.4.4.2 Selectivity study.....	40
2.4.4.3 Fluorescence titration.....	40
2.4.4.4 Competition with other metal ions.....	40
2.4.4.5 Limit of detection	41
2.5 Experimental strategy for the synthesis of highly pure poly(aryleneethynylene)s using Pd/CaCO ₃ as eco-friendly heterogeneous catalyst (part B).....	41

	Page
2.5.1 Sonogashira coupling polymerization using Pd/CaCO ₃ as catalyst.....	41
2.5.1.1 Preparation of model monomers	41
2.5.1.2 Optimization conditions	43
2.5.1.3 Polymer (4aa) preparation	45
2.5.2 Comparative study between obtained PAE 4aa using Pd/CaCO ₃ with other conventional catalyst.	45
2.5.2.1 Characterization of PAE 4aa obtained using Pd/CaCO ₃ and other conventional catalysts and determination of molecular weight by GPC.	45
2.5.2.2 Determination of Palladium and copper contents in PAEs by ICP-OES analysis.....	47
2.5.3 Reusability test of Pd/CaCO ₃ catalyst.....	47
2.5.4 Substrate scope of aryl dihalides coupled with aryl diethyne (3b) for examining generality of Pd/CaCO ₃ -catalyzed Sonogashira polymerization.....	48
2.5.4.1 Preparation of aryldihalide monomers.....	48
2.5.4.2 Preparation of aryldiethynyl monomer.....	52
2.5.5 Preparation PAEs (4cb-4jb) from dihalide monomers (2c-2j) and 1,4- dibutoxy-2,5-diethynylbenzene monomer (3b).....	53
CHAPTER III RESULTS AND DISCUSSION	57
3.1 Fluorescence turn-on sensor based on imine Schiff base-functionalized poly(phenyleneethynylene) (PPE-IM) for ferric ion (Fe ³⁺) detection (Part A).....	57
3.1.1 Synthesis and characterization of PE-AM, PE-IM, PPE-AM and PPE-IM.....	57
3.1.2 Photophysical properties of PE-AM, PE-IM, PPE-AM and PPE-IM.....	61
3.1.3 Molecular stability of imine sensors (PE-IM, PPE-IM).....	63

	Page
3.1.4 Fluorescence studies of PPE-IM toward Fe ³⁺ ion and other metal ions. . .	65
3.1.5 Machanistic investigation	68
3.2 Synthesis of highly pure poly(aryleneethynylene)s using palladium supported on calcium carbonate as eco-friendly heterogeneous catalyst (Part A).....	71
3.2.1 Optimization of the reaction conditions	71
3.2.1.1 Effect of Catalyst loading and ligand	72
3.2.1.2 Effect of base	74
3.2.1.3 Effect of solvent.....	76
3.2.1.4 Effect of reaction temperature	77
3.2.2 Aryl diiodide (2a), aryl diethyne (3a) and PAE 4aa characterization.....	78
3.2.3 Comparative study between PAE 4aa obtained using Pd/CaCO ₃ versus compound obtained from conventional catalysts.	81
3.2.4 Reusability test of Pd/CaCO ₃ catalyst	84
3.2.5 Substrate scope of aryl dihalides coupled with aryl diethyne (3b) for examining generality of Pd/CaCO ₃ -catalyzed Sonogashira polymerization.....	86
CHAPTER IV CONCLUSION.....	95
4.1 Salicylaldimine-functionalized poly(<i>m</i> -phenyleneethynylene) as turn-on chemosensor for ferric ion (part A)	95
4.2 Synthesis of highly pure poly(aryleneethynylene)s using palladium supported on calcium carbonate as eco-friendly heterogeneous catalyst (part B).....	95
REFERENCES	97
APPENDIX A.....	114

VITA..... 141



จุฬาลงกรณ์มหาวิทยาลัย
CHULALONGKORN UNIVERSITY

LIST OF SCHEMES

Scheme 1.1 Bio-compatible post-polymerization functionalization of a water soluble poly(<i>p</i> -phenyleneethynylene).....	3
Scheme 1.2 General synthetic method for PAEs	23
Scheme 1.3 Sonogashira coupling reaction	23
Scheme 1.4 Synthesis of PAEs from aromatic dihalide and aromatic alkyne	25
Scheme 1.5 Sonogashira coupling reaction catalyzed by heterogeneous catalyst.....	26
Scheme 1.6 Pd/C-catalyzed Sonogashira coupling of aryl bromide with acetylenes.....	26
Scheme 1.7 LDH-Pd(0)-catalyzed Sonogashira reaction of chloroarenes with phenylacetylene.....	27
Scheme 1.8 Pd-supported on zeolite catalyzed Cu-free Sonogashira reactions	27
Scheme 1.9 Pd supported on silica catalyzed Cu-free Sonogashira coupling.....	27
Scheme 1.10 Metal oxide supported Pd-catalyzed Sonogashira reactions.....	28
Scheme 1.11 Pd/CaCO ₃ catalyzed Heck coupling reaction between aryl halide and methyl acrylate.....	29
Scheme 1.12 Pd/CaCO ₃ catalyzed Stille cross coupling reaction between iodo-benzene and tributylphenyltin	29
Scheme 1.13 Pd/CaCO ₃ catalyzed Sonogashira cross-coupling reaction between aryl iodides and terminal alkynes.....	30
Scheme 1.14 Pd/Gr-catalyzed Heck reaction for preparing of polycinnamamide.....	30
Scheme 1.15 Pd/C-catalyzed copolymerization of polyketone	30
Scheme 1.16 Synthetic method and properties of polymers via cross coupling polymerizations catalyzed by Pd/C	31
Scheme 1.17 Pd-Fe ₃ O ₄ catalyzed Suzuki coupling polymerization	31

Scheme 1.18 Pd-catalyzed direct arylation polycondensation of 2-bromo-3-hexylthiophene	32
Scheme 1.19 Pd/C catalyzed direct arylation polycondensation of EDOT with various dibromoarenes.....	32
Scheme 1.20 Pd/CaCO ₃ -catalyzed Sonogashira coupling polymerization	33
Scheme 3.1 Synthetic procedures of PE-IM and PPE-IM	58
Scheme 3.2 Synthesis of PAE 4aa	71
Scheme 3.3 Synthesis of compound 2a	72
Scheme 3.4 Synthesis of compound 3a	72
Scheme 3.5 Pd/CaCO ₃ -catalyzed Sonogashira coupling polymerization	86
Scheme 3.6 Synthesis of compounds 2c and 2d	87
Scheme 3.7 Synthesis of compound 2e	87
Scheme 3.8 Synthesis of compound 2f	87
Scheme 3.9 Synthesis of compound 2g	88
Scheme 3.10 Synthesis of compound 2j	88
Scheme 3.11 Synthesis of compound 3b	88

LIST OF FIGURES

Figure 1.1 Molecular structures of some common conjugated polymers (CPs).....	2
Figure 1.2 Examples of PAEs with different structural modifications	3
Figure 1.3 Simple Jablonski diagram illustrating fluorescent processes	4
Figure 1.4 Schematic representations of various types of fluorescent sensors.....	5
Figure 1.5 Molecular structures of unbridged and bridged C=N compounds (left). The cleavage of C=N bond by hydrolysis (right).	6
Figure 1.6 Schematic representation of principal photophysics of ESIPT	6
Figure 1.7 Molecular structures of carboxylated model compound 9 and carboxylated PPE 10 , respectively.	7
Figure 1.8 (I) Fluorescent images of carboxylated PPE 10 in the presence of A) 10 - papain complex ([10] = 5 μ M, [papain] = 5 μ M). B) All 10 metal ions added to 10 -papain complex ([metal ion] = 0.4 mM). C) All ions except Hg ²⁺ add to 10 . (II) Schematic representation of the agglutinating mechanism induced FL quenching. A) 10 alone. B) Electrostatic complex from 10 -papain. C) After addition of Hg ²⁺ to 10 -papain complex leads to its precipitation by cross-linking of the papain molecules through Hg ²⁺	8
Figure 1.9 Structures of (<i>p</i> -phenyleneethynylene)s (11 - 14).....	8
Figure 1.10 A) fluorescence spectra and B) absorption spectra of 13 in THF with increasing amounts of Hg ²⁺ . Inset showing the fluorescence and visual color changes of 13 before (left) and after (right) the addition of 20 equiv. of Hg ²⁺	9
Figure 1.11 Schematic illustration of process for detecting cuprous ions (Cu ⁺), hydrogen peroxide and glucose assays.....	9
Figure 1.12 Structures of the four conjugated polyelectrolytes (16-19).....	10
Figure 1.13 A) Response patterns constructed based on fluorescence quenching of 16-19 the by eight metal ions at 5 μ M each. B) 3-D canonical score plot of the	

fluorescence response patterns obtained by 16-19 PPE sensors array against 5 μM of eight metal ions.....	10
Figure 1.14 (Left) structure of PPE 20 and (right) fluorescence enhancement of 20 in THF upon the addition of Hg^{2+}	11
Figure 1.15 Fluorescence enhancements in different sensory system upon various cations: (A) PPE 20 (5 μM) with and (B) without Cu^{2+} (5 μM) mixture system in THF solution.....	12
Figure 1.16 (A) Structures and (B) fluorescence spectra of PPE 21 , 22 , 23 and 24 . (C) Fluorescence spectral changes of PPE 24 upon titration of $\text{Cd}(\text{ClO}_4)_2$ in water.	13
Figure 1.17 Structure of PPE 25 and schematic representation of the Al^{3+} assay.....	13
Figure 1.18 (A) Molecular structures of PPE 26-32 (B) Response patterns for different cations constructed based on fluorescence responses of seven polymers upon 2 μM of cations.....	14
Figure 1.19 Molecular structure of PPE 33 (left) and Relative fluorescence change of PPE 33 (10 μM) in the presence of various metal ions (each 33.3 μM) in $\text{DMSO}/\text{H}_2\text{O}$ (right). Benesi-Hildebrand plot for Fe^{3+} -bound PPE 33 , obtained from Uv-vis spectra (inset).....	16
Figure 1.20 Design concept of fluorescence “on” Fe^{3+} chemodosimeter. The inset shows the visual fluorescence emission of 35 only (left) and 35 + Fe^{3+} ions (right) using UV lamp.....	17
Figure 1.21 Schematic representation of the Fe^{3+} -induced Schiff base hydrolysis and the spirolactam ring opening of rhodamine in 36 and Confocal microscopic analysis of Hep G2 cells with 36 for 40 min.....	18
Figure 1.22 The possible mechanism of 37 toward Fe^{3+} and the photographs of 37 after the addition of metal ions (5.0 equiv.) using a UV lamp at room temperature.....	19
Figure 1.23 Objectives of this work.....	21

Figure 1.24 Sonogashira catalytic cycle.....	24
Figure 2.1 The calibration curve for turn-on sensing.	41
Figure 2.2 Example of calibration curve of Palladium standard	47
Figure 3.1 ¹ H NMR spectra of compounds A) PE-AM B) PE-IM in acetone- <i>d</i> ₆ C) PPE-AM and D) PPE-IM in CDCl ₃	59
Figure 3.2 Structure of PPE-IM in head- tail (left) and head- head (right) forms.....	59
Figure 3.3 FT-IR spectra of compounds A) PPE-AM and B) PPE-IM	60
Figure 3.4 GPC data of compounds A) PPE-AM and B) PPE-IM	61
Figure 3.5 Normalized spectra of absorption and emission of PE-AM , PE-IM , PPE-AM and PPE-IM	62
Figure 3.6 A) FL changes of PE-IM (25 μM) and PPE-IM (25 μM) in 10%milliQ water/THF with increasing time (0-120 min). Appearance images of B) PE-IM and C) PPE-IM at 0 min and 120 min, respectively. D) Schematic presentation of hydrolysis process of PE-IM	64
Figure 3.7 FL intensity of PPE-IM ($\lambda_{em} = 475$ nm) (25 μM) in 10%MilliQ pH 4-8/THF in 120 min. ($\lambda_{ex} = 410$ nm).	64
Figure 3.8 A) Fluorescent spectra of PPE-IM (25 μM) upon the addition of various metal ions (5 equiv.) in 10%milliQ water/THF. B) Change ratio (I/I_0) of FL intensity of PPE-IM (25 μM) in 10%milliQ water/THF containing various metal ions (5.0 equiv.). C) Fluorescent images of PPE-IM in the presence of different cations. The spectra were obtained after 30 min with $\lambda_{ex} = 410$ nm.	65
Figure 3.9 A) Fluorescent spectra of PPE-IM (25 μM) upon addition of Fe ³⁺ (125 μM) in 10%milliQ water/THF with increasing time (0 – 90 min), B) Plots of intensity versus time after added Fe ³⁺	66
Figure 3.10 A) and B) Fluorescence titration ($\lambda_{ex} = 410$ nm) of PPE-IM (25 μM) upon addition of difference concentration of Fe ³⁺ in 10%milliQ water/THF. The	

inset shows the calibration curves of ratio of PPE-IM to Fe^{3+} concentration. Each spectrum was obtained after 60 min of mixing.	66
Figure 3.11 Time dependence of fluorescence intensity of PPE-IM ($\lambda_{\text{em}} = 475$ nm) (25 μM) in the presence and absence of Fe^{3+} (5 equiv.) at pH 3.5. ($\lambda_{\text{ex}} = 410$ nm).....	67
Figure 3.12 Relative fluorescence of PPE-IM (25 μM) in 10% milliQ water/THF in the presence of Fe^{3+} (125 μM) plus another metal ion (625 μM) tested for interference.....	68
Figure 3.13 ^1H NMR of PPE-IM in CDCl_3 A) before and B) after addition of $\text{Fe}(\text{NO}_3)_3$ at 30 min.	69
Figure 3.14 Normalized spectra of absorption of PPE-IM (25 μM) upon the addition of Fe^{3+} (0-5 equiv.) in 10% H_2O /THF. Each spectrum was measured after 60 min at room temperature.....	69
Figure 3.15 Particle size changes of PPE-IM (50 μM) in 10%milliQ water/THF before (blue line) and after (red line) addition of Fe^{3+} (100 μM) with increasing time.....	70
Figure 3.16 Schematic representation of the plausible behavior of the PPE-IM before and after treatment with Fe^{3+}	70
Figure 3.17 Structure of seven ligands	72
Figure 3.18 FT-IR spectra of PAE 4aa	79
Figure 3.19 ^1H NMR spectra of monomer 2a , 3a and PAE 4aa in CDCl_3	79
Figure 3.20 ^{13}C NMR spectra of PAE 4aa in CDCl_3	80
Figure 3.21 GPC data of PAE 4aa	80
Figure 3.22 ^1H NMR spectra of PAE 4aa from Pd/CaCO_3 , Pd/C , $\text{PdCl}_2(\text{PPh}_3)_2$ and $\text{Pd}(\text{PPh}_3)_4$	83
Figure 3.23 Aryl dihalide monomers used in this section.....	86

Figure 3.24 PAEs (4aa-4jb) obtained from our optimized condition.....	92
Figure 3.25 Normalized absorption (top) and emission (bottom) spectra of PAEs in THF solution	92
Figure A.1 ^1H NMR of IM in acetone- d_6	114
Figure A.2 ^{13}C NMR of IM in acetone- d_6	114
Figure A.3 ^1H NMR of PE-AM in acetone- d_6	115
Figure A.4 FT-IR of PE-AM	115
Figure A.5 MALDI-TOF MS of PE-AM	116
Figure A.6 ^1H NMR of PE-IM in acetone- d_6	116
Figure A.7 ^{13}C NMR of PE-IM in acetone- d_6	117
Figure A.8 FT-IR of PE-IM	117
Figure A.9 MALDI-TOF MS of PE-IM	118
Figure A.10 ^1H NMR of PPE-AM in CDCl_3	118
Figure A.11 ^{13}C NMR of PPE-AM in CDCl_3	119
Figure A.12 FT-IR of PPE-AM	119
Figure A.13 ^1H NMR of PPE-IM in CDCl_3	120
Figure A.14 ^{13}C NMR of PPE-IM in CDCl_3	120
Figure A.15 FT-IR of PPE-IM	121
Figure A.16 ^1H NMR of 2a in CDCl_3	121
Figure A.17 ^1H NMR of 3a in CDCl_3	122
Figure A.18 ^1H NMR of 4aa obtained from Pd/CaCO_3 catalyst in CDCl_3	122
Figure A.19 ^{13}C NMR of 4aa obtained from Pd/CaCO_3 catalyst in CDCl_3	123
Figure A.20 FT-IR of 4aa obtained from Pd/CaCO_3 catalyst.....	123
Figure A.21 ^1H NMR of 4aa obtained from $\text{PdCl}_2(\text{PPh}_3)_2$ catalyst in CDCl_3	124

Figure A.22	^1H NMR of 4aa obtained from Pd (PPh ₃) ₄ catalyst in CDCl ₃	124
Figure A.23	^1H NMR of 4aa obtained from Pd/C catalyst in CDCl ₃	125
Figure A.24	GPC data of 4aa obtained from PdCl ₂ (PPh ₃) ₂ catalyst	125
Figure A.25	GPC data of 4aa obtained from Pd(PPh ₃) ₄ catalyst	126
Figure A.26	GPC data of 4aa obtained from Pd/C catalyst	126
Figure A.27	^1H NMR of 4db in CDCl ₃	127
Figure A.28	^{13}C NMR of 4db in CDCl ₃	127
Figure A.29	GPC data of 4db	128
Figure A.30	^1H NMR of 4eb in CDCl ₃	128
Figure A.31	^{13}C NMR of 4eb in CDCl ₃	129
Figure A.32	FT-IR of 4eb	129
Figure A.33	^1H NMR of 4fb in CDCl ₃	130
Figure A.34	^{13}C NMR of 4fb in CDCl ₃	130
Figure A.35	GPC data of 4fb	131
Figure A.36	^1H NMR of 4gb in CDCl ₃	131
Figure A.37	^{13}C NMR of 4gb in CDCl ₃	132
Figure A.38	FT-IR of 4gb	132
Figure A.39	GPC data of 4gb	133
Figure A.40	^1H NMR of 4hb in CDCl ₃	133
Figure A.41	^{13}C NMR of 4hb in CDCl ₃	134
Figure A.42	FT-IR of 4hb	134
Figure A.43	GPC data of 4hb	135
Figure A.44	^1H NMR of 4ib in CDCl ₃	135
Figure A.45	^{13}C NMR of 4ib in CDCl ₃	136

Figure A.46 FT-IR of 4ib	136
Figure A.47 GPC data of 4ib	137
Figure A.48 ^1H NMR of 4jb in CDCl_3	137
Figure A.49 ^{13}C NMR of 4jb in CDCl_3	138
Figure A.50 FT-IR of 4jb	138
Figure A.51 GPC data of 4jb	139



LIST OF TABLES

Table 1.1 Summary of some imine Schiff base fluorescence chemosensor for Fe^{3+}	20
Table 3.1 Photophysical properties of PE-AM, PE-IM, PPE-AM and PPE-IM.....	63
Table 3.2 Effect of catalyst loading and ligand.....	73
Table 3.3 Effect of Base	75
Table 3.4 Effect of solvent.....	76
Table 3.5 Effect of reaction temperature.....	78
Table 3.6 Comparison study between PAE 4aa was synthesized by using Pd/CaCO ₃ with other catalysts.....	82
Table 3.7 Palladium and copper contents in PAEs 4aa	84
Table 3.8 Reusability test of Pd/CaCO ₃ catalyst on polymerization	85
Table 3.9 PAE substrate scope.....	89
Table 3.10 Photophysical properties and color appearance of PAEs 4aa-4jb	93

LIST OF ABBREVIATIONS

Ar	aromatic
calcd	calculated
^{13}C NMR	carbon-13 nuclear magnetic resonance
CDCl_3	deuterated chloroform
CPs	conjugated polymers
DIPEA	N,N-Diisopropylethylamine
$\text{DMSO-}d_6$	deuterated dimethyl sulfoxide
DP	degree of polymerization
DLS	dynamic light scattering
d	doublet (NMR)
dd	doublet of doublet (NMR)
equiv	equivalent (s)
FETs	field-effect transistors
FT-IR	fourier transform infrared spectroscopy
^1H NMR	proton-1 nuclear magnetic resonance
h	hour (s)
J	coupling constant
K_a	Association constant
m	multiplet (NMR)
Mw	molecular weight
M	molar
PAEs	poly(aryleneethynylene)s

PDI	polydispersity index
rt	room temperature
s	singlet (NMR)
THF	tetrahydrofuran
TLC	thin layer chromatography
UV	ultraviolet
°C	degree Celsius
ϵ	molar absorption coefficient
Φ_f	quantum yield
% yield	percentage yield
δ	chemical shift

CHAPTER I

INTRODUCTION

1.1 Overview of acetylenic polymer sensors (Part A)

Of all acetylenic compounds mentioned in the first part, poly(aryleneethynylene)s (PAE)s are an important subclass of conjugated polymer genre which are highly fluorescent, chemically stable, and can be easily synthesized by either the Heck-Cassar-Sonogashira coupling or by alkyne metathesis. The photophysical properties of PAEs are dependent upon chain ordering, conformation and substitution of functional groups on aromatic building blocks. During the past decade, PAEs have been utilized in light emitting diodes, transistor applications and advanced biological or chemical sensor. Particularly, a number of precious extensions of these polymeric sensory systems have been developed into more sensitive and selective sensors for wider applications. This part of our report will focus on the synthesis, photophysical investigations and sensing applications for metal cations.

1.1.1 Structures of conjugated polymer fluorophores

Fluorescent chemosensors are used widely in chemical, biological, and environmental contaminant detection. Examples include detection of metal ion, anion, neutral molecules and biomolecules. Fluorescent technique is considered a powerful method owing to significant advantages such as high selectivity, high sensitivity, short response time, cost-effectiveness in instrumentation, operational simplicity, and also no destruction of samples. Typically, fluorescent chemosensors are composed of two main components: (1) a receptor unit for selective binding with the analytes (2) a transducer to provide the means of signaling this bonding, whether by fluorescence quenching, enhancement or wavelength shift. Many conjugated polymers have become a popular transducer material due to their extraordinary signal amplification capabilities as well as versatile optical and electrical properties. Many research groups have worked on the utilization of well-known conjugated polymers as shown in Figure 1.1, including polythiophene (1) [1], polypyrrole (2) [2],

polyfluorene (3) [3], poly(*p*-phenylenevinylene) (4) [4], and poly(*p*-phenyleneethynylene) (5) [5].

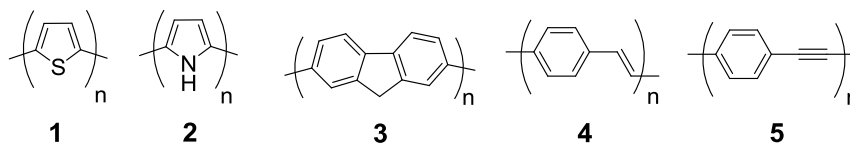


Figure 1.1 Molecular structures of some common conjugated polymers (CPs)

Poly(aryleneethynylene)s (PAEs) are polymers in which arene groups are separated by alkyne linkers. The simplest PAEs structures are the poly(*p*-phenyleneethynylene)s (PPEs), and a structurally related conjugated polymers, the poly(*p*-phenylenevinylene)s (PPVs) [6]. The molecular structure of PPEs and PPVs are closely related but their properties are different. When compared to the PPVs, PPEs generally display high emissive fluorescent quantum yields both in solution and in the solid state. They are stable up to 300 °C in air, and usually present enhanced photostability. Moreover, their optical properties are sensitively dependent upon the specific environment with distinct chromogenic behavior including the solvatochromicity, thermochromicity, ionochromicity, surfactochromicity, and biochromicity [7-9] not found in the PPVs. As a consequence, PPEs are used for sensing and also serve as potential transducers. They are alternatively of great interest as sensory materials to detect explosive compounds [10, 11], proteins [12], anions [13] and metal ions [14]. Structurally, different aromatic building blocks can also be introduced into the conjugated backbone by adjusted isomers of *ortho*-, *meta*- and *para*- of arene to create the desired electronic properties. The variable side chains can also be modified to adjust the polymer structures and their interactions with specific target. Figure 1.2 shows the examples of PAEs with different structural modifications.

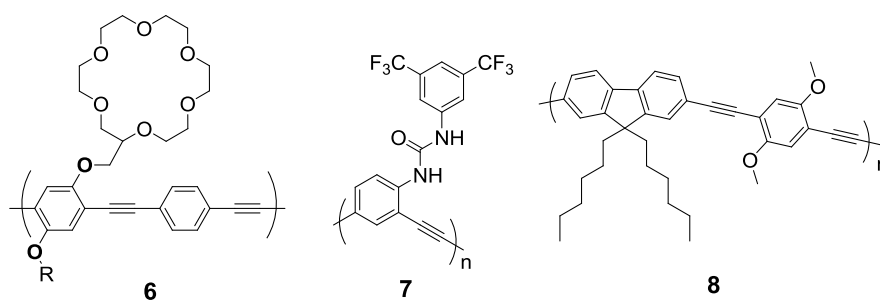
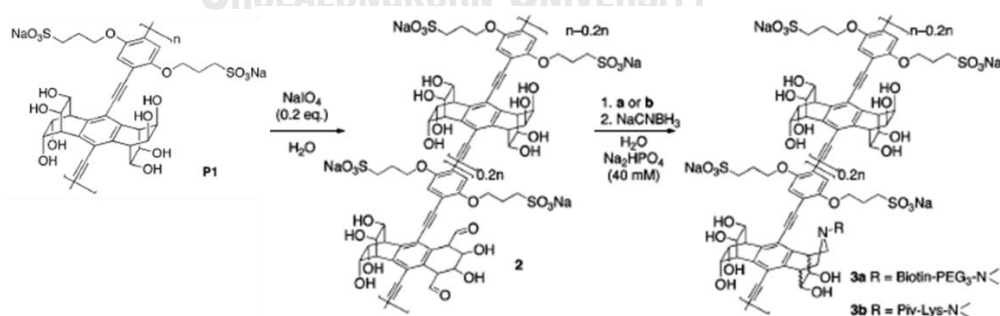


Figure 1.2 Examples of PAEs with different structural modifications

Side-chain post functionalization

The occurrence of macroscopic properties of polymers is caused by different molecular assemblies that are highly dependent upon side chain and main chain nature. Generally, the construction of pendent groups on PPE backbone has been commonly prepared through pre-polymerization functionalization approach by polymerizing well-defined monomer. In some case, the incorporation of functional groups may be incompatible with polymerization leading to failure in the preparation of target polymer. In recent years, alternative synthetic method, namely the post-polymerization functionalization (PPF) has been introduced. PPF strategy allows for tuning of a polymer's properties without synthetically retreating to the monomer stage (Scheme 1.1). Such advantages, a few reports applied PPF to attach some groups including protecting group [15], biotin [16], glucose [17] and alkyne compounds [18] to main chain for well-defined conjugated polymer.



Scheme 1.1 Bio-compatible post-polymerization functionalization of a water soluble poly(*p*-phenyleneethynylene).

1.1.2 Fluorescent spectral

Fluorescence is the emission of light typically occurring with aromatic compounds or highly conjugated molecules. The fluorescence processes that occur between the absorption and emission of light can be usually described by the Jablonski diagram as shown in Figure 1.3. After an electron absorbs a high energy photon, the molecule is excited electronically and vibrationally to excited states (S_1 or S_2) and forms an excited molecule. The molecule then rapidly relaxes vibrationally to the lowest excited level of S_1 which is called internal conversion process. Eventually, the molecule returns to ground state (S_0) via emission fluorescence of a longer wavelength. The time required to complete this process takes nano-second [19].

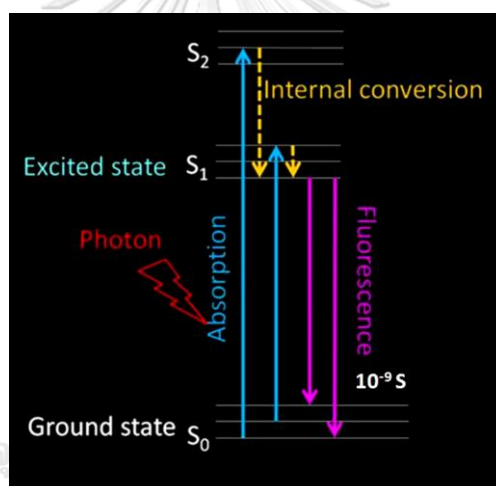


Figure 1.3 Simple Jablonski diagram illustrating fluorescent processes

Various molecular and supramolecular fluorescent sensors have been developed in recent years. They can be categorized into four different groups according to their fluorescence signaling process: (a) turn-OFF, (b) turn-ON, (c) ratiometric and (d) chemodosimeters. The first three processes are quenched, enhanced and wavelength shifted respectively, upon recognition of the target analyte and the processes are generally reversible (Figure 1.4). On the other hand fluorescent chemodosimeter is a molecular system that uses abiotic receptors to achieve analyte recognition with irreversible transduction of a fluorescent signal [20].

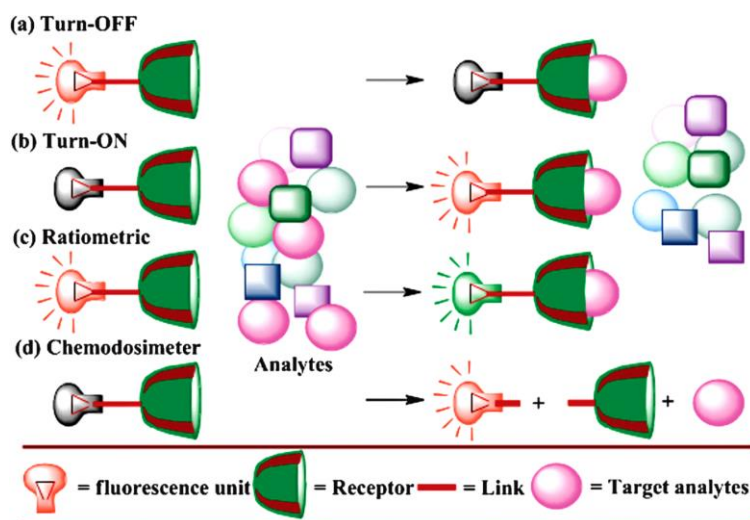


Figure 1.4 Schematic representations of various types of fluorescent sensors

The photophysical signaling mechanisms which controls the response of a fluorophore to analytes binding include photoinduced electron transfer (PET) [21-23], intramolecular charge transfer (ICT) [24, 25], Förster resonance energy transfer (FRET) [26], excited-state intramolecular proton transfer (ESIPT) [27], C=N isomerization [28], aggregation-induced enhancement fluorescence (AIE) [29], aggregation-caused quenching (ACQ) [30] and so on.

1.1.3 Sensing mechanism

The sensing mechanism of receptor in our fluorescence probe in this thesis have been designed based on C=N isomerization and ESIPT.

C=N bond isomerization

C=N bond isomerization is a fluorescence quenching mechanism that occurs through rotation of the double bond. The process occurs after the ground state geometry of the fluorophore is excited to a higher energy level [28]. For the fluorophores with an unbridged double bond structure, the predominant decay processes of the excited fluorophore are often non-fluorescent. On the other hand, their analogs containing covalently bridged double bond structure usually exhibit dramatic increases in fluorescence intensities due to either the suppression of double bond isomerization in the excited states or cleavage of this bond by hydrolysis reaction as depicted in Figure 1.5

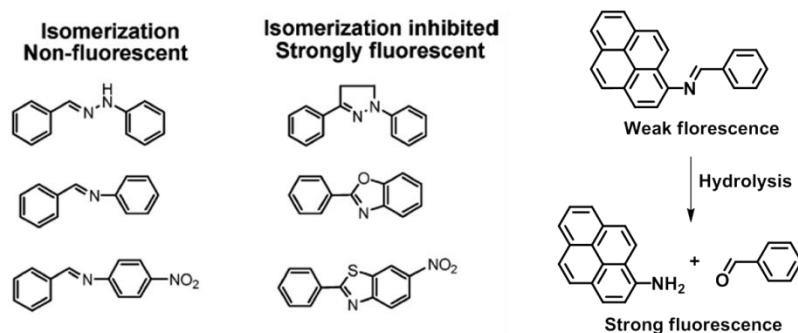


Figure 1.5 Molecular structures of unbridged and bridged C=N compounds (left). The cleavage of C=N bond by hydrolysis (right).

Excited state intramolecular proton transfer (ESIPT)

The ESIPT process is associated with the transfer of a proton of a hydroxyl (or amino) group to a carbonyl oxygen (or imine nitrogen) through a pre-existing six- or five-membered ring hydrogen bonding configuration. [31] The classic example of the ESIPT photophysical process was observed for 2-(20-hydroxyphenyl)-benzoxazole (HBO) as illustrated in Figure. 1.6. After irradiation, the HBO in enol form (E^*) is converted to the excited-state keto form (K^*) in the sub picosecond time scale resulting in significantly red shift emission compared with the absorption and unusually large Stoke shift. A large Stoke shift is beneficial in fluorescence sensing to avoid self-absorption or inner filter effect.

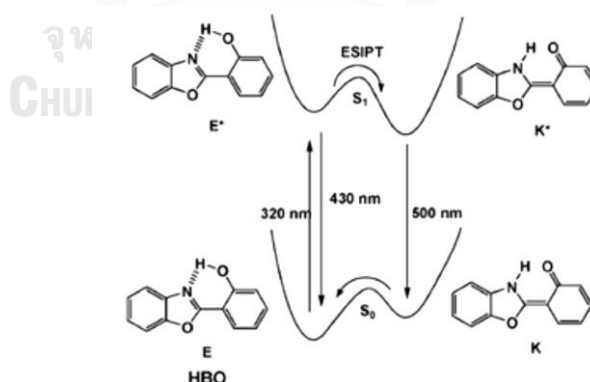


Figure 1.6 Schematic representation of principal photophysics of ESIPT

1.1.4 Optical sensor application of poly(aryleneethynylene)s (PAE)s

PAEs based fluorescence sensor often show exquisite sensitive changes either in colorimetric or in fluorometric systems when exposed to analytes. Fluorometric assay provides inherently high sensitivity as well as versatility in the detection of

various analyte. The change in fluorescent signal can be either enhanced intensity to give a turn-on signal, quenched intensity to give a turn-off signal or shifted wavelength to give a new emission, upon direct or indirect interaction with targets. PAEs-based sensors usually utilize more than one sensing mechanism in order to enhance the response of signal transduction. As a representative class of PAEs, PPEs have been well studied and applied detect various analytes, including DNA, TNT, anion sensors and metal ion. In the next section, the past reports on the detection of heavy metal poisoning which as environmental pollutants using PAEs-based on chemosensor will be discussed.

Metal sensor form PAEs (Turn off mode)

In 2005, Bunz et al. [32] reported the use of aqueous soluble carboxylated PPE **10** as a sensitive and selective sensor for lead (II) ion (Pb^{2+}). Such compound induced fluorescence quenching ($K_{sv} = 8.8 \times 10^5$) which is significantly higher than small molecule **9** ($K_{sv} = 600$) as depicted in Figure 1.7. Multivalent binding between **10** and Pb^{2+} as well as the exciton migration along the polymer chain played essential factors for the superior sensitivity of this sensor. Afterwards, the researcher expanded the sensing scope of their carboxylated polymer **10** that would form an electrostatic complex with the positively charged papain. This assay was applied as a selective fluorescence quenching probe for mercury (II) ion (Hg^{2+}) [33]. The agglutination mechanism of anionic polymer and cationic papain forming a supramolecular structure explains more selectivity than either **10** or papain alone as shown in the Figure 1.8.

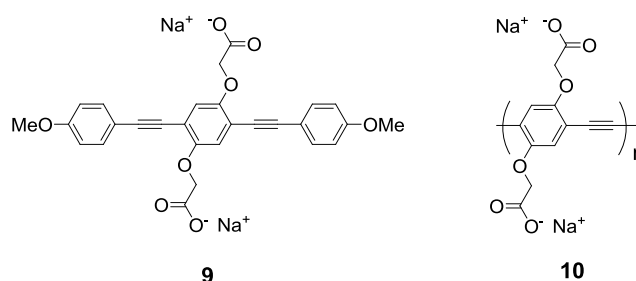


Figure 1.7 Molecular structures of carboxylated model compound **9** and carboxylated PPE **10**, respectively.

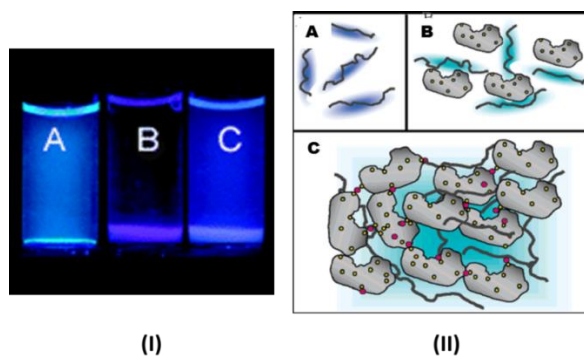


Figure 1.8 (I) Fluorescent images of carboxylated PPE **10** in the presence of A) **10**-papain complex ($[\mathbf{10}] = 5 \mu\text{M}$, $[\text{papain}] = 5 \mu\text{M}$). B) All 10 metal ions added to **10**-papain complex ($[\text{metal ion}] = 0.4 \text{ mM}$). C) All ions except Hg^{2+} add to **10**. (II) Schematic representation of the agglutinating mechanism induced FL quenching. A) **10** alone. B) Electrostatic complex from **10**-papain. C) After addition of Hg^{2+} to **10**-papain complex leads to its precipitation by cross-linking of the papain molecules through Hg^{2+} .

In 2009, Zhu et al. [34] successfully synthesized a panels of (*p*-phenyleneethynylene)s (**11** - **14**) and screened them with various transition metal (Figure 1.9). The results indicated that only **11** displayed a significant decrease in fluorescence intensity towards Ni^{2+} as well as an instant color change from light red to colorless. This could be attributed to the electron-transfer interactions between metal ions with an open shell electronic structure such as Ni^{2+} (d8) that may enable the occurrence of strong metal-ligand orbital interactions with conjugated polymer backbone. The Stern–Volmer fluorescence quenching constant (K_{sv}) was determined to be $2.57 \times 10^9 \text{ M}^{-1}$ with limit of detection (LOD) as low as $6.5 \times 10^{-12} \text{ M}$.

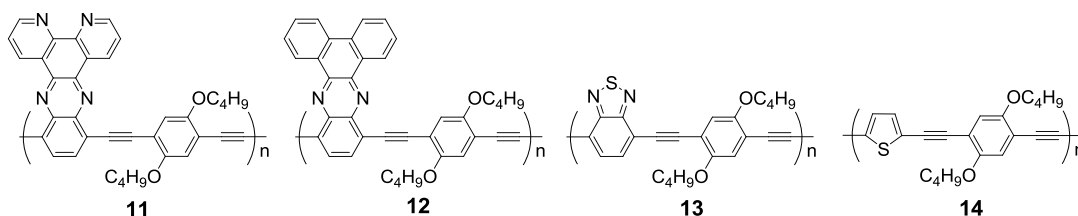


Figure 1.9 Structures of (*p*-phenyleneethynylene)s (**11** - **14**)

More recently, Zhu et al. [35] demonstrated that **13** containing benzo [2,1,3]thiadiazole (BDT), can bind Hg^{2+} with N or S atom on polymer backbone. [36]

Therefore, **13** could be applied as a calorimetric and fluorometric sensor for Hg^+ . After treatment with Hg^+ , the polymer exhibited prominent fluorescence turn-off response along with the color change from bright yellow to colorless. This behavior could be affected by intramolecular photoinduced charge transfer (PCT) between CP backbone and BDT- Hg^+ complex (Figure 1.10).

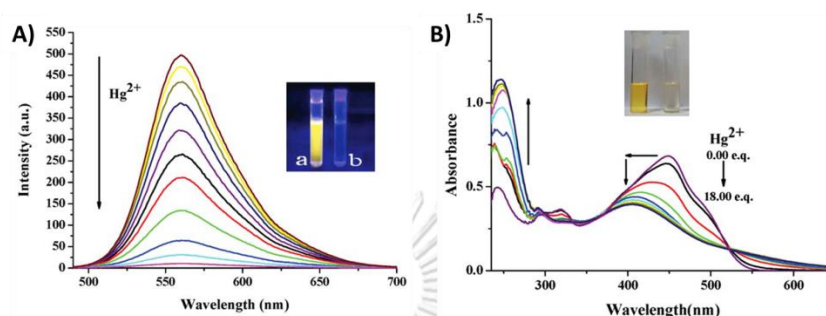


Figure 1.10 A) fluorescence spectra and B) absorption spectra of **13** in THF with increasing amounts of Hg^{2+} . Inset showing the fluorescence and visual color changes of **13** before (left) and after (right) the addition of 20 equiv. of Hg^{2+} .

In 2014, Liu et al. [37] developed a novel poly(phenyleneethynylene) bearing 2-thiohydantoin moieties (**15**) for cuprous ions (Cu^+) detecting via quenching process with $K_{sv} = 6.1 \times 10^4 \text{ M}^{-1}$ whereas cupric ions (Cu^{2+}) displayed no change (Figure 1.11). This could be explained by the chelating complex between the sulfur atom, considered as a “soft base” with Cu^+ as softer acid atom in comparison with Cu^{2+} . Besides, the “turn off” fluorescence from (**15**)/ Cu^+ mixture, the signal could also be recovered by the addition of H_2O_2 released from glucose oxidation of glucose oxidase (GOD), which caused Cu^+ is oxidized into Cu^{2+} . This system could be applied for glucose detection.

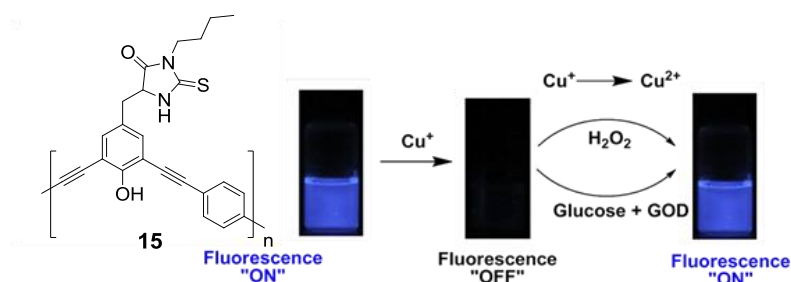


Figure 1.11 Schematic illustration of process for detecting cuprous ions (Cu^+), hydrogen peroxide and glucose assays.

In 2015, Tan et al. [38] prepared four anionic conjugated polyelectrolytes (CPEs) based on poly(*p*-pheynyleneethynylene) (PPE) backbone containing various pendant ionic side chains as shown in Figure 1.12. A set of PPEs (**16-19**) were utilized as array-based sensor for the detection of various metal ions including Pb^{2+} , Hg^{2+} , Fe^{3+} , Cr^{3+} , Cu^{2+} , Mn^{2+} , Ni^{2+} , and Co^{2+} . They showed clear differentiation in fluorescence response between metal ions using 2-D and 3-D linear discrimination analysis (LDA) (Figure 1.13). In particular, the array could readily differentiate as low as 100 nM of each metal. These distinct responses presumably arose from either the conformational change of the polymers upon interaction with metal ions or a heavy-atom quenching effect (spin-orbit coupling). [39]

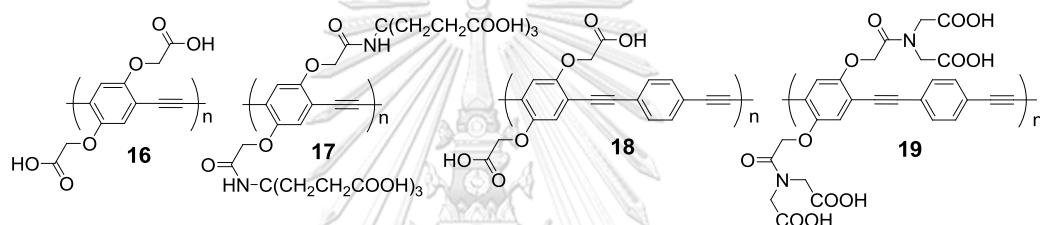


Figure 1.12 Structures of the four conjugated polyelectrolytes (**16-19**)

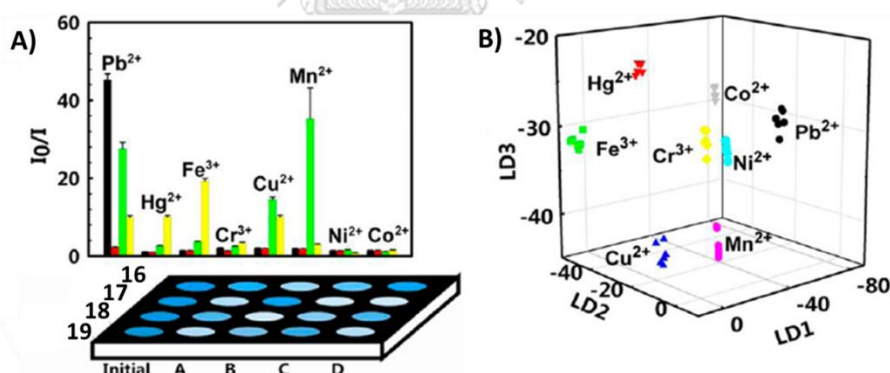


Figure 1.13 A) Response patterns constructed based on fluorescence quenching of **16-19** the by eight metal ions at 5 μM each. B) 3-D canonical score plot of the fluorescence response patterns obtained by **16-19** PPE sensors array against 5 μM of eight metal ions.

Metal sensor form PAEs (Turn-on mode)

In principle, fluorescence “turn-on” sensor has numerous advantages over “turn-off” sensors, for example: (1) higher sensitivity as a result of contrasting

fluorescence signal with a dark background (2) higher selectivity as the signal is generated by specific binding, whereas fluorescence quenching can occur in multiple ways. In recent years, several PPEs display direct or indirect turn-on fluorescence towards metal ion. The new mechanism was involved either analyte-induced deaggregation or through coordination of a metal cations to a covalently attached appropriate functional group acting as an internal quencher.

In 2005, Jones et al. [40] discovered a novel turn-on fluorescence chemosensors based-on amino functionalized conjugated polymer for the first time (**20**) (Figure 1.14). At the initial state, **20** displayed a weak emission at λ_{max} 480 nm along with poor quantum yields of 0.09 in THF solution. Upon the addition of metal ions, only Hg^{2+} caused fluorescence enhancement by a factor of 2.7. This approach was consistent with a prior PET mechanism for PPE fluorescence quenching, which was interrupted upon binding of the analyte. Although this mechanism was effective, it has only attained weak fluorescence enhancement due to the restriction of relatively high background fluorescence as shown in Figure 1.14 (right).

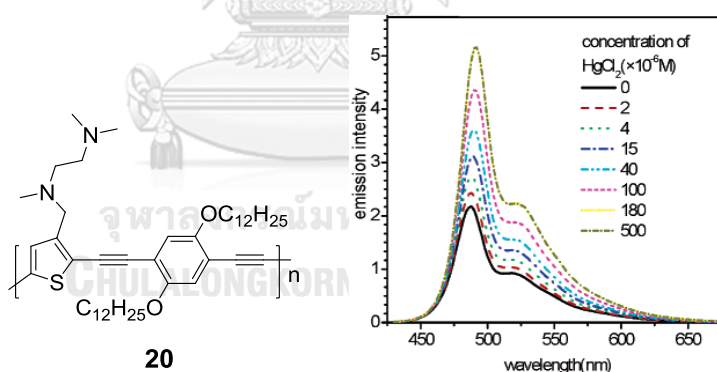


Figure 1.14 (Left) structure of PPE **20** and (right) fluorescence enhancement of **20** in THF upon the addition of Hg^{2+} .

To increase the sensitivity of this sensing, Jones et al. [41] discovered proficient strategy to enhance sensitivity of the sensing **20** by preloading 5 μM of Cu^{2+} onto the polymer with a repeat unit concentration of 5 μM . This amount is sufficient to quench fluorescence signal of **20**, completely. Subsequently, the fluorescence intensity of PPE **20**/ Cu^{2+} hybrid system was enhanced more than 150-

fold enhancement towards titration of 10 μM of aqueous FeCl_2 . According to the wavelength intensity of PPE **20**/ Cu^{2+} after titration of Fe^{2+} ions was negligible change both in emission ($\lambda_{\text{max}} = 494 \text{ nm}$) and in absorption ($\lambda_{\text{max}} = 440 \text{ nm}$), this suggests no significant change in the overall electronic structure of the polymer (Figure 1.15). They hence assumed that the Fe^{2+} has displaced the Cu^{2+} already in coordination with the receptor. This unique hybrid inorganic/organic polymer method should be useful in the detection of iron cations or modified for other analytes.

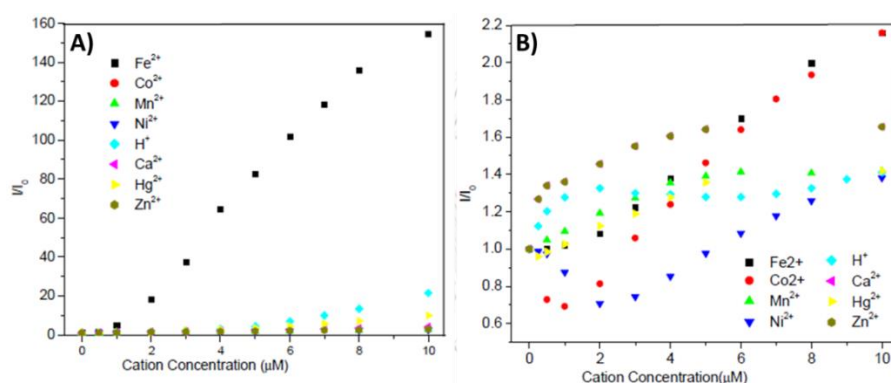


Figure 1.15 Fluorescence enhancements in different sensory system upon various cations: (A) PPE **20** (5 μM) with and (B) without Cu^{2+} (5 μM) mixture system in THF solution.

In 2011, Zhao et al. [42] attempted to design low-emissive PPE by incorporating N-containing groups into the side chains of polymer as depicted in Figure 1.16. Of the four polymers, only PPE **21** carrying both aminophenyl and triazole groups showed low emission with quantum yield of 0.038. Such extinguished fluorescence was proposed by a relay of energy transfer (ENT) sensitizes the donor (amino) group which triggering an Intramolecular Charge Transfer (ICT) process from the donor (amino) to the acceptor (triazole) group. The non-emissive PPE **21** acts as a highly selective and sensitive for Zn^{2+} and Cd^{2+} ions in THF (LOD $\approx 1 \mu\text{M}$). In addition, water soluble PPE **24** was also synthesized to overcome the aggregation effect in aqueous solution of PPE **21**. They found that PPE **24** showed prominent fluorescence turn-on responses to Cd^{2+} ions (LOD = 3 mM) and H^+ (LOD = 0.3 mM) in

water. The binding mode with 1:4 binding ratio ($24 \cdot [\text{Cd}^{2+}]_4$) occurred due to effective interaction of both amino and triazole receptors with analyte.

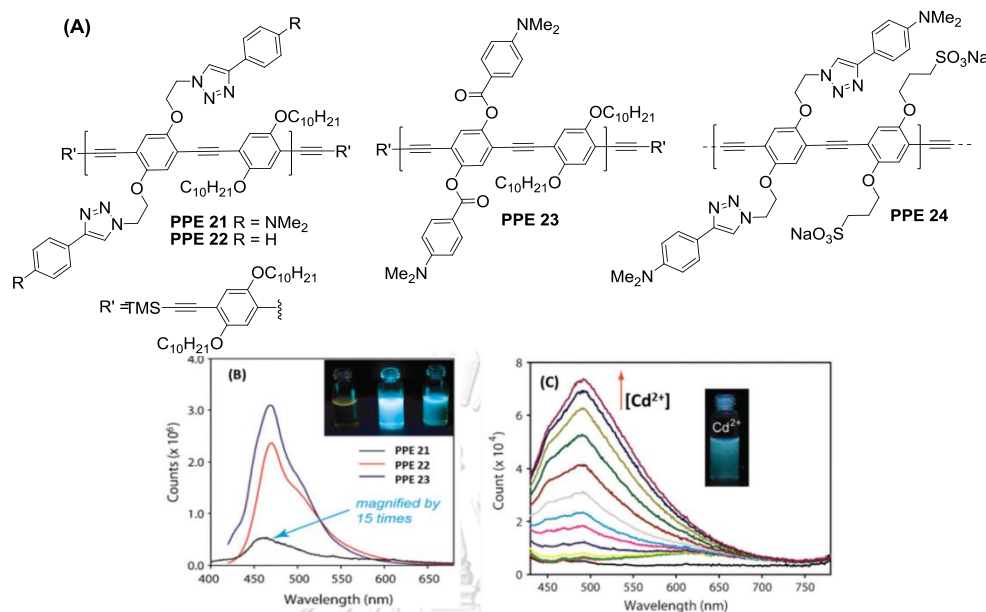


Figure 1.16 (A) Structures and (B) fluorescence spectra of PPE 21, 22, 23 and 24. (C) Fluorescence spectral changes of PPE 24 upon titration of Cd(ClO₄)₂ in water.

In 2013, Li et al. [43] synthesized planar cationic conjugated polyelectrolyte, poly(fluoreneethynylene) (**25**) and investigated its aggregation-induced photophysical properties (Figure 1.17). They found that the addition of sodium citrate which has opposite charge could induce efficient π -stacking aggregation of **25** in aqueous solution through relatively strong electrostatic interactions resulting in the self-quenching of fluorescence. The quenching efficiency of the citrate demonstrated a K_{SV} value of $2.66 \times 10^5 \text{ M}^{-1}$. The signal can be recovery upon the treatment with Al³⁺ showing the limit of detection of 0.37 μM . The retrieval fluorescence caused by a strong chelation ability of citrate with Al³⁺.

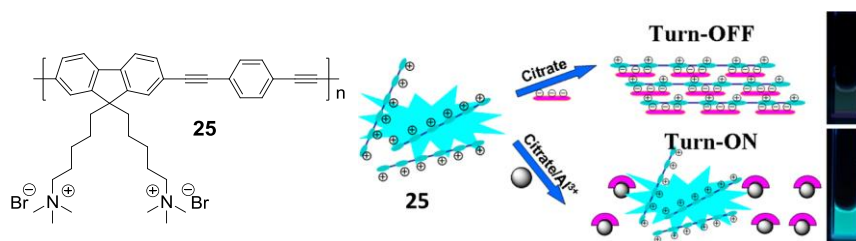


Figure 1.17 Structure of PPE 25 and schematic representation of the Al³⁺ assay.

In 2014, Fan et al. [44] combined seven different conjugated polymers into a sensor array for metal sensing including Na^+ , K^+ , Mg^{2+} , Ca^{2+} , Mn^{2+} , Zn^{2+} , Cd^{2+} detection (Figure 1.18). The response patterns for each cation were constructed by collecting the individual fluorescence responses from seven polymers in the array. Each ion owns a characteristic pattern. Some of them have similar fluorescence response patterns with subtle differences, while some patterns are distinctively different. This can be attributed to the differential interactions between cations and polymers. Limit of detection of this array was determined to be lower than $0.125 \mu\text{M}$.

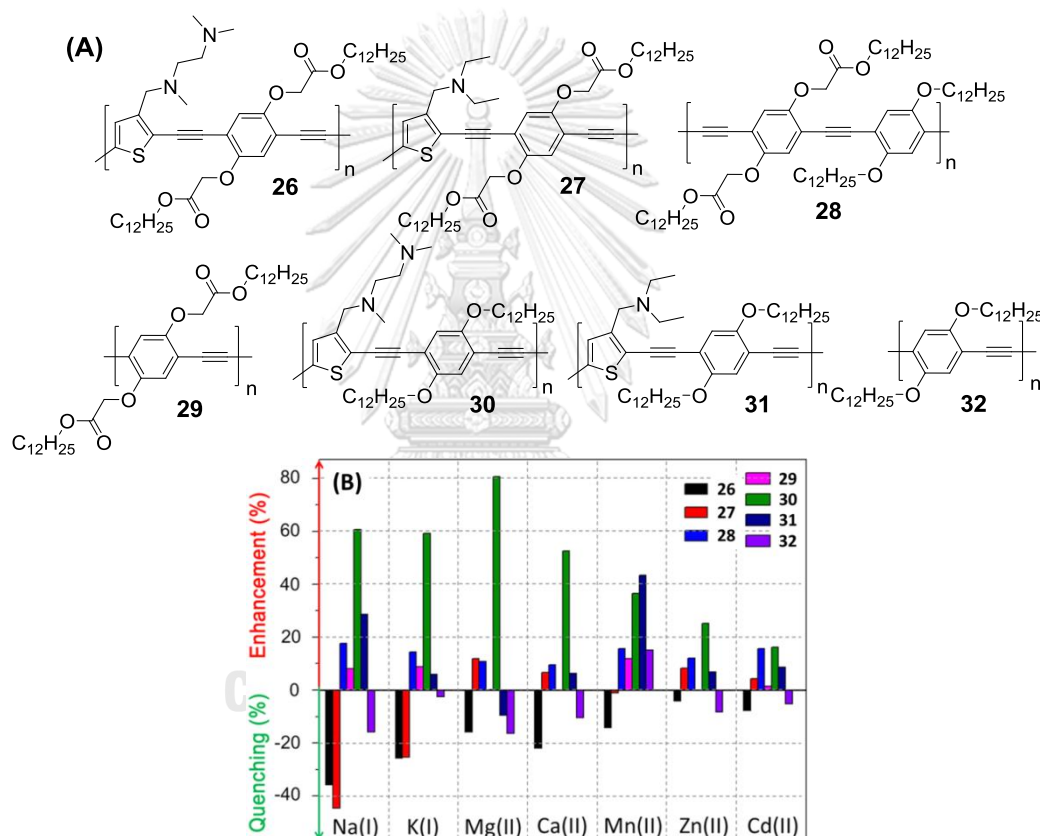


Figure 1.18 (A) Molecular structures of PPE **26-32** (B) Response patterns for different cations constructed based on fluorescence responses of seven polymers upon $2 \mu\text{M}$ of cations.

Till now, turn-on PPEs sensors were mostly observed for mono- or divalent cations (Na^+ , K^+ , Ca^{2+} , Mg^{2+} , Mn^{2+} , Zn^{2+} , Cd^{2+} , Hg^{2+} , Fe^{2+}) detection. While, there are few reports for recognition of trivalent cations such as Fe^{3+} , Al^{3+} . Particularly, Fe^{3+} as well known has a paramagnetic nature that usually induced the fluorescent

quenching mechanism. Therefore, there are remained challenges to develop selective as well as sensitive, fluorescence turn-on Fe^{3+} probes.

1.1.5 Importance of Ferric ion (Fe^{3+})

Iron is the most abundant trace mineral in creatures which is considered to be a crucial element in biological systems and play the essential role in human body. Normally, about 70% of the iron in mammals is found in hemoglobin, and about 5% to 10% is found in myoglobin. When bound to normal hemoglobin and myoglobin, iron is in the ferrous (Fe^{2+}) form [45, 46]. Up to 25% of iron in the body is in the ferric (Fe^{3+}) form and is stored in hemosiderin, ferritin, and transferrin in the liver, spleen, and bone marrow [47]. Nonetheless, Fe^{3+} species in excessive amounts can be toxic because of its ability to promote oxidation of lipids, proteins, and other cellular components [48]. Consequently, high levels of Fe^{3+} ion within the body have been associated with increased incidence of certain cancer and dysfunction of organs such as heart, pancreas and liver. [49, 50] Moreover, ingested iron can have an extremely corrosive effect on the gastrointestinal (GI) mucosa, which can manifest as nausea, vomiting, abdominal pain, hematemesis, and diarrhea; patients may become hypovolemic because of significant fluid and blood loss. Individuals demonstrate symptoms of toxicity after ingestion of more than 20 mg/kg of body weight. Moderate intoxication occurs when ingestion of elemental iron exceeds 40 mg/kg. Ingestions exceeding 60 mg/kg can cause severe toxicity may be lethal. Treatment is necessary provided when a serum iron level $> 500 \mu\text{g/dL}$ ($> 5 \text{ mM}$) [51]. Accordingly, development of a sensing system for the reliable quantification of ferric ions (Fe^{3+}) is still importance for medical diagnosis and nutritional analysis.

Fluorescent turn-on sensor for ferric ions (Fe^{3+}) based on PPE

As mention above, the detection of trace amounts of Fe^{3+} ions is critical. Indeed, there are many reports on Fe^{3+} probes. In term of PPE sensors, most of them undergo a fluorescence quenching response [52] but until now there has only one literature reports using direct turn-on PPE sensor for Fe^{3+} detection.

In 2015, Lei et al. [53] reported benzoselenadiazole-based PPE (**33**) as highly sensitive and selective turn-on chemosensor for Fe^{3+} in DMSO/ H_2O , resulted from Fe^{3+} ions inhibited the photoinduced electron transfer (PET) from triethylamino group receptor to conjugated polymer backbone. The enhanced intensity was significant for Fe^{3+} concentrations ranging from 0.1 to 33.3 μM , and resulted in a 5.5-fold total fluorescence enhancement with detection limit as low as 7.7×10^{-8} M (Figure 1.19). Additionally, increasing fluorescence of PPE metal complex could be recovered by adding EDTA. For binding analysis, measurement using the Benesi-Hildebrand expression based on UV-vis absorption spectra confirmed that the stoichiometry of $\mathbf{33}\text{-Fe}^{3+}$ was 1:1 and found an association constant (K_a) of 1.57×10^3 mol^{-1} .

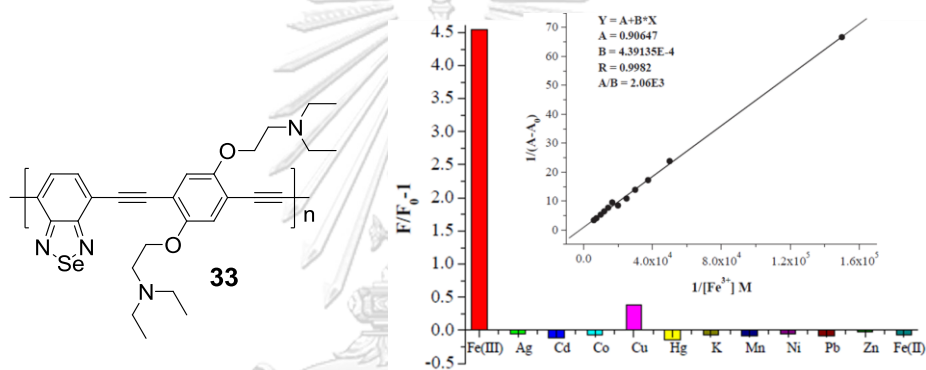


Figure 1.19 Molecular structure of PPE **33** (left) and Relative fluorescence change of PPE **33** (10 μM) in the presence of various metal ions (each 33.3 μM) in DMSO/ H_2O (right). Benesi-Hildebrand plot for Fe^{3+} -bound PPE **33**, obtained from Uv-vis spectra (inset).

There are limited numbers of reports on metal sensing by PPEs due to highly emissive nature of PPEs at the initial state. Alternatively, Fe^{3+} also has a paramagnetic nature that induced the fluorescent quenching behavior. Nevertheless, a small number of fluorescence-enhanced Fe^{3+} sensors have been reported recently. Most of the works employed chemodosimetric approach involving the use of reactions induced by a specific analyte such as an anion or cation or other molecule. This reaction resulted in a significant chemical transformation involving bond breaking or forming in the probes [54]. They are generally irreversible and reflect a cumulative response related directly to the concentration of the analyte.

Mostly, derivatives of imine Schiff base were incorporated as receptor for Fe^{3+} fluorescence turn-on probe. The isomerization effect of $\text{C}=\text{N}$ lead to a completely weak fluorescent signal of probe at the initial state. Because of the instability of the Schiff bases in either unsuitable acid or basic environment, they are easily hydrolyzed by coordinated with acidic water molecules. Thus, Fe^{3+} is a strong Lewis acid may also hydrolyze Schiff bases in an analogous way. Nonetheless, all of these sensors are merely based on small molecules.

Fluorescent turn-on sensors for ferric ions (Fe^{3+}) based on Schiff base molecules

In 2008, Lin et al. [55] designed and synthesized a fluorescence turn-on chemodosimeter for Fe^{3+} based on metal-promoted hydrolysis of bis-(coumarinyl) Schiff base (Figure 1.20). The addition of Fe^{3+} ($60 \mu\text{M}$) to **34** ($5 \mu\text{M}$) in MeOH- H_2O (98/2, v/v) induced fluorescence enhancement by 140-fold within 50 min. Furthermore, others metals ions exhibited negligible detection interference. This could be explained by the fact that the pK_a of Fe^{3+} is much lower than those of other metal ions surveyed. In the same year [56], they also developed this type of coumarin sensor for Fe^{3+} (**35**) to a large ratiometric fluorescence response by spectral shift based on regulation of intramolecular charge transfer (ICT).

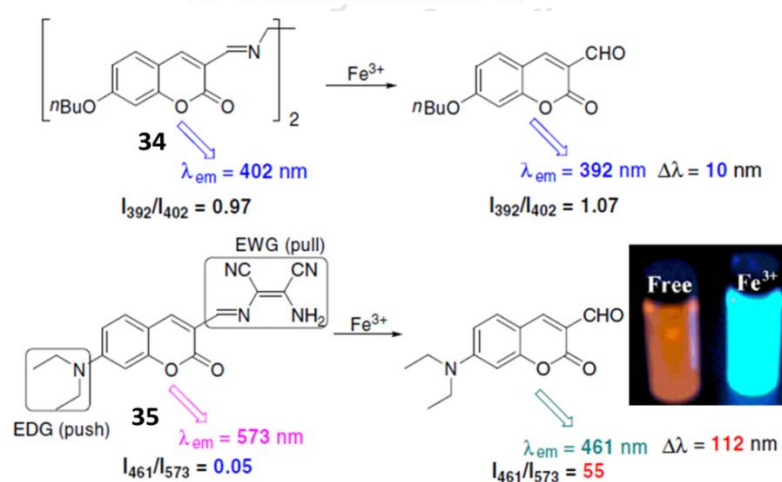


Figure 1.20 Design concept of fluorescence “on” Fe^{3+} chemodosimeter. The inset shows the visual fluorescence emission of **35** only (left) and **35** + Fe^{3+} ions (right) using UV lamp.

In 2010, Lee et al. [57] reported the synthesis of rhodamine-based probe (**36**) and studied its fluorescence properties and application to an iron-overloaded cell (Figure 1.21). There notably displayed fluorogenic changes by the Fe^{3+} -catalyzed hydrolysis reaction that caused spirolactam ring opening in H_2O -MeCN (95/5, v/v). The detection limit was as low as $0.1 \mu\text{M}$. Moreover, chemodosimeter **36** was very selective towards the Fe^{3+} ion even in the presence of other metal cations *in vitro* as well as in hepatocytes.

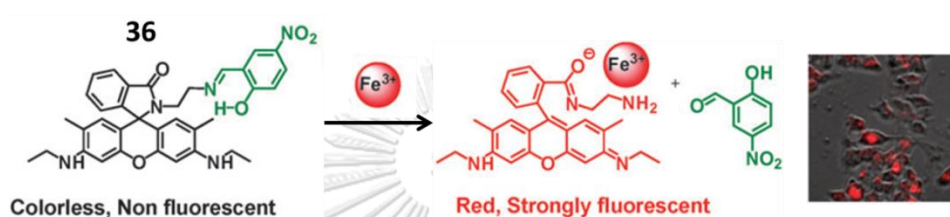


Figure 1.21 Schematic representation of the Fe^{3+} -induced Schiff base hydrolysis and the spirolactam ring opening of rhodamine in **36** and Confocal microscopic analysis of Hep G2 cells with **36** for 40 min.

In 2016, Chen et al. [58] successfully prepared multichannel sensor, triphenylamine-BODIPY based Schiff base fluorescent probe (**37**) with an emission in the near-infrared (NIR) region (Figure 1.22). It can detect Fe^{3+} and Hg^{2+} ions with remarkable fluorescence enhancement in THF/ H_2O (v/v, 1:1, buffered with 10 mM HEPES pH = 7.4) based on the hydrolysis reaction of the $-\text{C}=\text{N}$ bond, and naked eye detection was also realized with an obvious change from red to green. Another feature for Fe^{3+} detection was the 4-hydroxystyryl groups that bound with Fe^{3+} and contribute the enhancement of fluorescence, while Hg^{2+} did not bind. The stoichiometry between the probe and ions was calculated to be 1:3 for Fe^{3+} and 1:2 for Hg^{2+} , respectively. The low detection limits of Fe^{3+} and Hg^{2+} were calculated from the titration results with the values of $5.15 \times 10^{-7} \text{ M}$ and $6.81 \times 10^{-7} \text{ M}$, respectively.

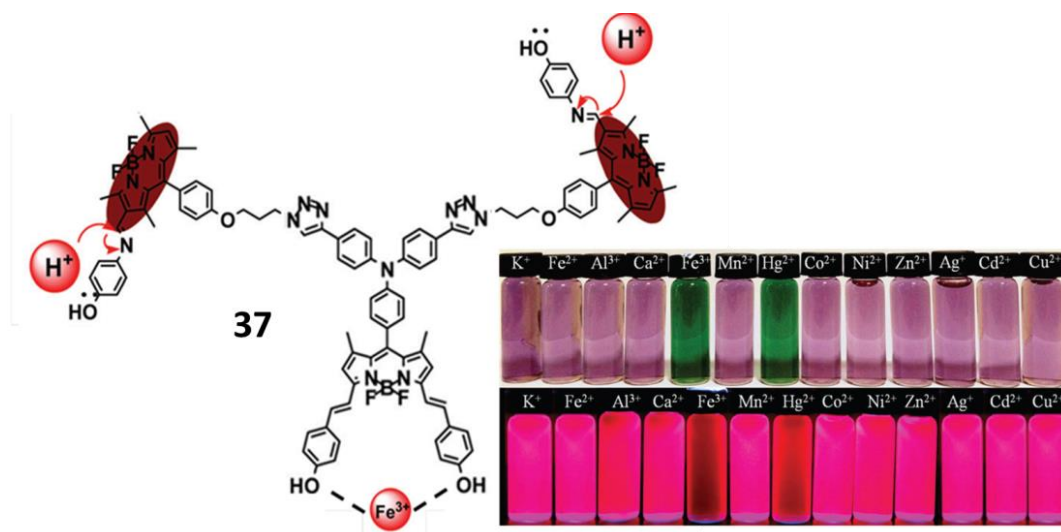
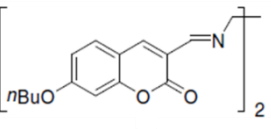
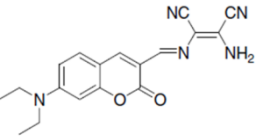
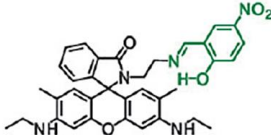
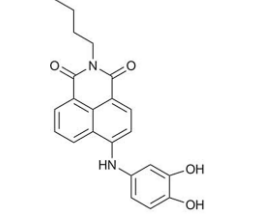
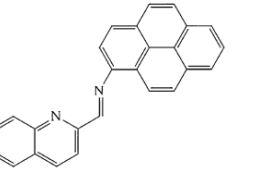
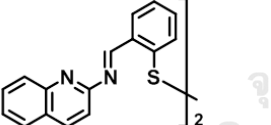
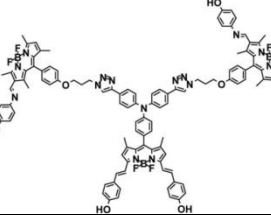


Figure 1.22 The possible mechanism of **37** toward Fe^{3+} and the photographs of **37** after the addition of metal ions (5.0 equiv.) using a UV lamp at room temperature.

Some of the imine Schiff base fluorescent sensors for selective detection of Fe^{3+} have been reported in Table 1.1.

Table 1.1 Summary of some imine Schiff base fluorescence chemosensor for Fe³⁺

Ligand	$\lambda_{em,I0}$	$\lambda_{em,I}$	Testing Media	Time (min)	LOD	Ref.
	402	392	MeOH/H ₂ O (98/2)	50	-	[55]
	573	461	MeOH/H ₂ O (99/1)	35	-	[56]
	551	551	H ₂ O/MeCN (95/5)	20	0.1 μ M	[57]
	520	520	MeCN/H ₂ O (99/1)	> 48	-	[59]
	440	440	DMSO/H ₂ O (70/30)	-	1.37 μ M	[60]
	406	413	100% H ₂ O	-	2.0 μ M	[61]
	668	510	THF/HEPES pH 7.4 (1/1)	-	0.5 μ M	[58]

According to the literature reviews above, the imine Schiff base compounds are promising sensors for Fe³⁺ detection giving remarkably fluorescence turn-on based on hydrolysis process. Nevertheless, those Schiff base molecules are unstable in an aqueous environment. Therefore, PPE-based fluorescent chemosensors which

have advantages of high structure stability and high aggregation will be introduced as matrices of Schiff base ligands to prevent the hydrolysis process.

1.2.6 Objectives of this work

This research aim to construct low emissive poly(phenyleneethynylene) composed of salicylaldehyde Schiff base as a receptor unit (**PPE-IM**) and to study the potential for applications in turn-on sensor for ferric ion detection. Additionally, the comparison of sensing abilities of our polymer and corresponding small molecule counterpart (**PE-IM**) will be explored (Figure 1.23).

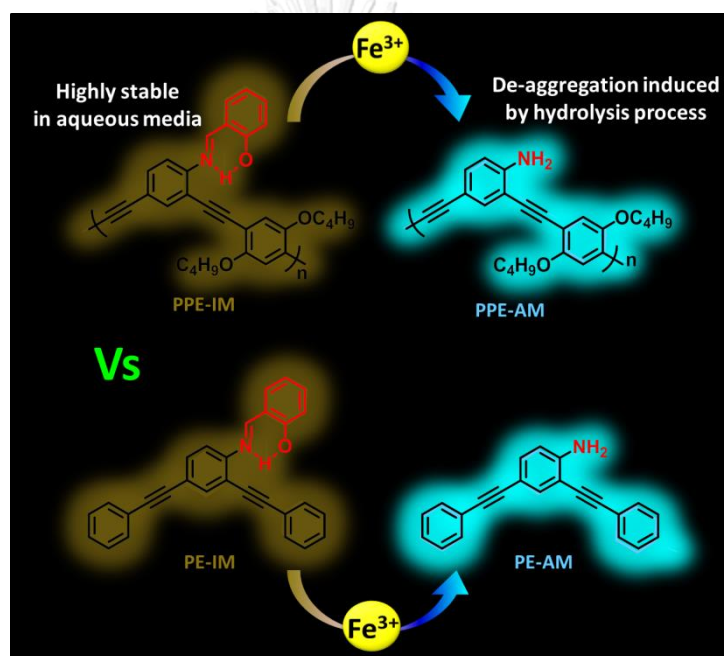
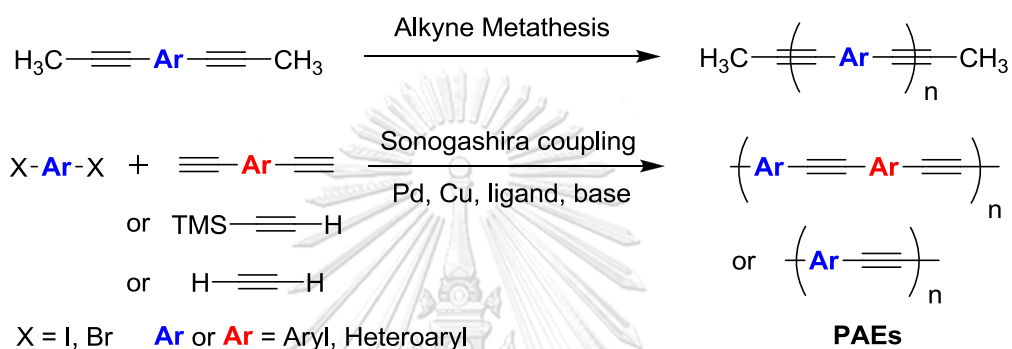


Figure 1.23 Objectives of this work

1.2 Introduction (Part B)

Phenylacetylenic compounds are unsaturated hydrocarbon containing at least one carbon-carbon triple bond with 180° bond angle between the phenyl carbon and sp^1 carbon [62]. Such structures are important building blocks of natural products, pharmaceuticals and molecular materials small molecules as well as polymers. Conjugated acetylenic polymers, so called poly(aryleneethynylene)s (PAEs) [63-65], possess more predictable geometry and attractive photophysical properties. They are an attractive component for semiconductor devices [66], molecular wire [67-69], photovoltaic devices [70], molecular electronics and sensory materials [5]. In general, there are two available methods to make PAEs as presented in Scheme 1.2. The first one is the alkyne metathesis polymerization of alkyne. [71, 72] Although this method allows to construct a high molecular weight polymer, but it requires high reaction temperature, high pressure and expensive catalyst such as molybdenum hexacarbonyl ($Mo(CO)_6$) and metalcarbene catalyst. The second method is a step-growth polycondensation method such as Heck-Cassar-Sonogashira reaction. It is a Pd-catalyzed coupling reaction between aryl dihalide and terminal alkyne [63-65, 73]. This method is the most widely used method because of its high activity, specificity, efficiency, versatility and inexpensive catalyst required. Homogeneous Pd is commonly employed as catalytic polymerization in PAE preparation. However, it has several drawbacks. The catalyst is unrecoverable, air-sensitive, post-treatment is required and residual toxic metal can affect electronic performance of semiconducting polymer [74-76]. In order to address these problems, the solid support-stabilized Pd as heterogeneous catalyst has been developed in organic synthetic methodology over recent years [77]. Numerous heterogeneous Pd have been used in Sonogashira coupling reaction, such as Pd fixed on zeolite [78-80], Pd on metal oxide ($\gamma-Fe_2O_3$) [81], Pd on modified silica [82], Pd on clay [83] and Pd on charcoal [84-86]. Although these Pd catalysts showed high potential of reactivity, stability and reusability but most of all requires multistep synthesis. On the other hands, Pd on charcoal, one of the most inexpensive supports, is flammable from its pyrophoric behavior. Alternatively, $CaCO_3$ which is non-toxic and natural abundant

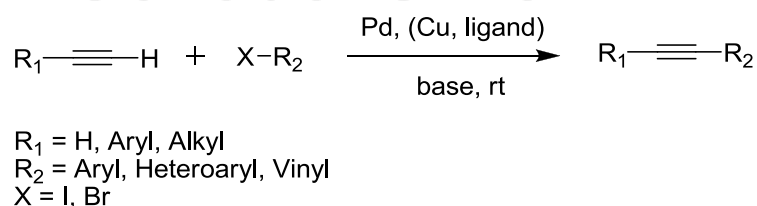
has been recently established for Pd supported catalyst in many reactions such as Heck [87, 88] and Stille [89] coupling reaction in small molecules. Importantly, not only catalyst supported on CaCO_3 can be reused in many cycles but the palladium leaching from those reports are quite low. To the best of our knowledge, Pd supported on CaCO_3 has not been reported for polymer preparation. Therefore, the aim of our research is to use Pd/ CaCO_3 as catalyst for PAE preparation and to compare a quality of resulting polymer with one from conventional Pd catalyst.



Scheme 1.2 General synthetic method for PAEs

1.2.1 Introduction of Sonogashira coupling reaction

In 1975, Sonogashira coupling reaction was firstly reported by Sonogashira and his co-worker. [90] In this reaction, the palladium catalyzed sp^2 - sp coupling reaction between aryl or vinyl halide and terminal alkyne with or without Cu as co-catalyst providing acetylenic compounds (Scheme 1.3).



Scheme 1.3 Sonogashira coupling reaction

The mechanism of reaction is unclear. Previous report hypothesized involvement of Pd and Cu catalytic cycles shown in Figure 1.24. The reaction begins with Pd(0) species (A) oxidizes with the aryl halide in the oxidative addition step to form the Pd(II) species (B), then transformed into a Pd(II) complex (C) after

transmetalation with a copper acetylide formed in the Cu-cycle. Next, the complex undergoes trans/cis isomerization and reductive elimination to produce the desired product with regeneration of the active Pd(0) species catalyst which are ready for a recycle loop. In case of Cu-cycle, start with copper halide reacts with terminal alkyne for deprotonation of base to form copper acetylide (F). [91]

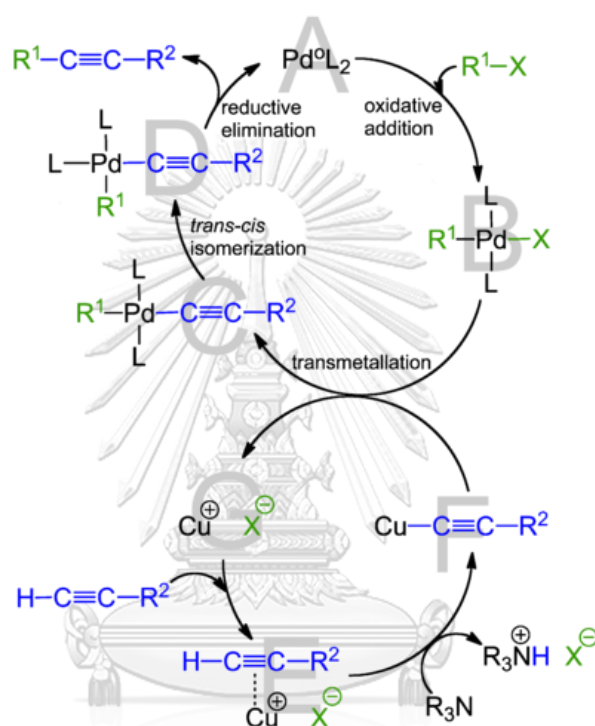
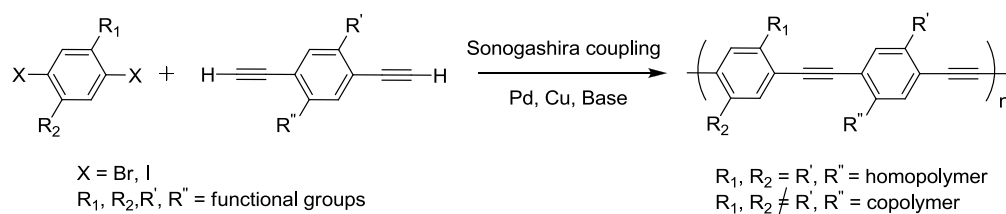


Figure 1.24 Sonogashira catalytic cycle

1.2.2 Introduction of Pd-catalyzed polymerization

Giesa and Schulz [92] first reported the use of Pd-catalyzed Sonogashira coupling for the synthesis of poly(aryleneethynylene)s (PAEs) (Scheme 1.4). Generally, it involves a palladium-mediated coupling between aromatic dihalide and aromatic diyne in an amine solvent to create arene groups separated by alkyne linkers. This method is general and compatible with most functional groups to afford highly soluble copolymer in good yield with low molecular weight ($\text{DP} = 9\text{-}15$).

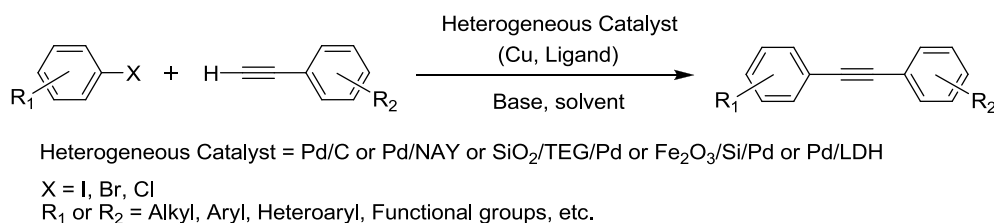


Scheme 1.4 Synthesis of PAEs from aromatic dihalide and aromatic alkyne

Most of C–C coupling polymerizations for preparation of conjugated polymers (CPs) are usually catalyzed by soluble ligand stabilized homogeneous palladium which has several of obstacles. Such catalysts frequently cause a high level of residual palladium obstinately embedded in the chains of resulting polymers. Even with the slightest amount may lead to dramatically destructive effect on the electronic performance of semiconducting polymers. [75]. As such, the post treatment of polymers with palladium scavenger is required which is unfavorable and impractical for large scale production. The exchange between aryl groups on the phosphine ligands and those on the Pd center [93] causes incorporation of phosphorus contaminant and potentially lowering the molecular weight of synthesized polymers. [94, 95] Many catalysts are composed of large molecular weight ligands that are expensive, unrecoverable, and air-sensitive, presenting problems for process economic and sustainability. Therefore, the application of homogeneous Pd catalyst for the synthesis of conjugated polymers remains a challenge to be solved.

1.2.3 Introduction of Heterogeneous Pd catalyst

Pd-supported on solid matrix called “heterogeneous Pd catalysis” is a promising option to conquer the problems outlined above. For Sonogashira reaction, several solid substrates were used to support active Pd catalysts such as Pd immobilized on zeolite [78-80], metal oxide [81], modified silica [82], clay [83] and carbon [84-86] as shown in Scheme 1.5.



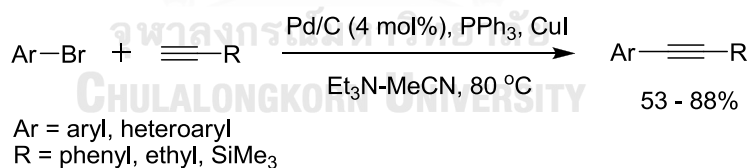
Scheme 1.5 Sonogashira coupling reaction catalyzed by heterogeneous catalyst

Those catalysts have several advantages such as reusability, stability, simplicity, low level of residual Pd, no contaminant of ligand. Consequently, numerous of solid support-stabilized Pd catalysts have been well established for C-C couplings reaction commonly applied to small molecules syntheses [77, 96].

1.2.4 Literature reviews

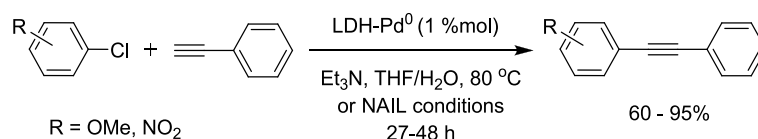
Sonogashira coupling reaction using heterogeneous Pd catalyst

In 1990, Pd/C-catalyzed Sonogashira coupling was pioneered by Guzman and co-workers. [97] This method was used with the anhydrous mixture of acetonitrile and triethylamine in the presence of PPh₃ and CuI to catalyze coupling reaction between aryl or heteroaryl bromides and trimethylsilylacetylene, phenyl acetylene, and butyne (Scheme 1.6). Notably, the coupled products were yielded higher than those reported under homogeneous Pd(0) catalysis.



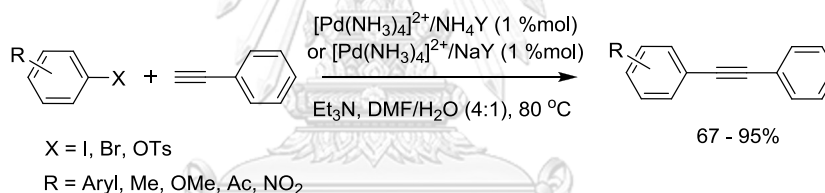
Scheme 1.6 Pd/C-catalyzed Sonogashira coupling of aryl bromide with acetylenes

In 2002, Choudary and co-workers [83] demonstrated that even Sonogashira coupling of electron-rich chloroarenes could be carried out using active palladium nanoparticles sustained on layered double hydroxide (LDH-Pd(0)) as catalyst. The catalyst (1 %mol) was used under Cu-free conditions in five cycles and showed consistent activity in the coupling of phenylacetylene and chlorobenzene. Non-aqueous ionic liquids (NAIL) could also be used for this catalytic system as shown in Scheme 1.7.



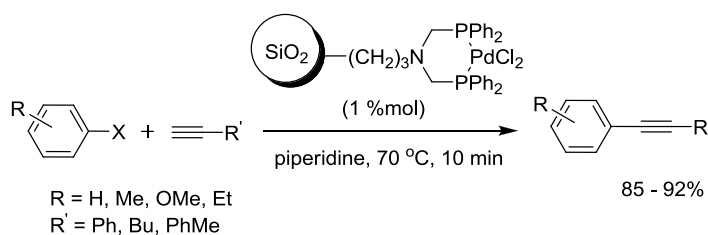
Scheme 1.7 LDH-Pd(0)-catalyzed Sonogashira reaction of chloroarenes with phenylacetylene

In 2004 and later, the heterogeneous Sonogashira reactions using Pd-supported on zeolites $[\text{Pd}-(\text{NH}_3)_4]^{2+}/\text{NH}_4\text{Y}$ [78, 79] and $[\text{Pd}-(\text{NH}_3)_4]^{2+}/\text{NaY}$ [80] under copper-free and ligand-free conditions was reported by Djakovitch and co-workers. The optimal condition used only 1% mol of catalyst with triethylamine as base and mixture of DMF and water at 80 °C in 3 hours for transforming aryl halides and terminal alkynes to desired products in good yield (Scheme 1.8). Even though the catalysts showed excellent stability toward leaching, they exhibited remarkable loss of activity in the first reuse.



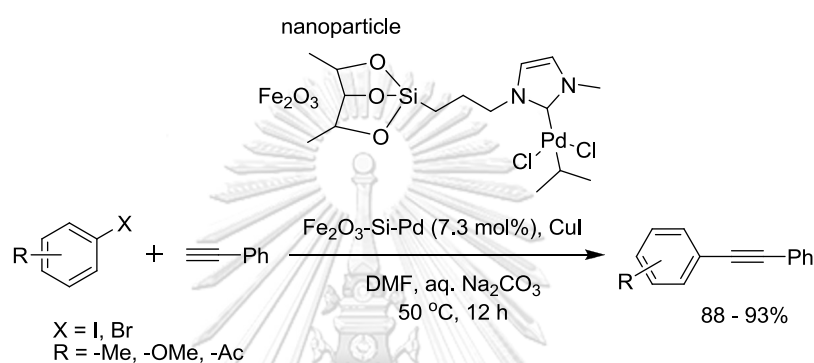
Scheme 1.8 Pd-supported on zeolite catalyzed Cu-free Sonogashira reactions

In 2005, the stable Pd catalyst on silica was first developed by immobilization of Pd into 3-aminopropyl-modified silica gel (Scheme 1.8) by Tyrrell and co-workers. [98] The catalyst was successfully applied in a series of fast, copper-free Sonogashira coupling reactions between a variety of terminal alkynes and aryl iodides with piperidine as base and solvent (Scheme 1.9). The cross coupling products were obtained in 85-92 % yield.



Scheme 1.9 Pd supported on silica catalyzed Cu-free Sonogashira coupling

In the same year, Gao and co-workers [81] discovered Pd-nitrogen-heterocyclic carbene-immobilized on magnetic maghemite (γ - Fe_2O_3)-silica nanoparticle and successfully applied in Sonogashira reaction. The reaction proceeded smoothly under mild condition at 50°C to provide high yields (88 – 93%) of alkyne products by coupling aryl iodides or bromides with phenylacetylene as shown in Scheme 1.10. The catalyst could be separated and reused for five rounds with negligible change of yield.

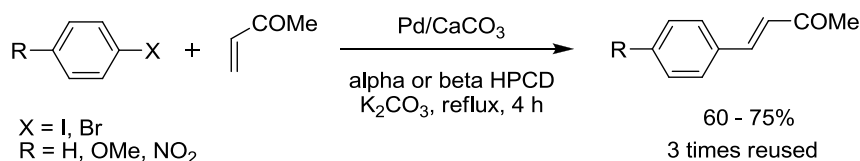


Scheme 1.10 Metal oxide supported Pd-catalyzed Sonogashira reactions

Palladium supported on calcium carbonate (Pd/CaCO_3) as catalyst for cross coupling reaction

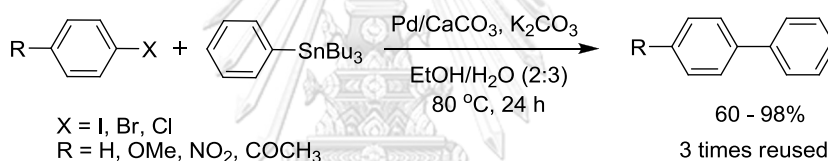
Among solid support for Pd catalyst, calcium carbonate, which is a common substance found in nature, has received much attention as an environmentally friendly solid support due to its low price, high stability and non-pyrophoric behavior. It also has a high affinity for palladium metals due to the presence of carbonyl functional groups. [99] Hence, palladium supported on calcium carbonate catalyst was used effectively in the cross coupling reaction including Heck and Stille reactions.

In 2007, Senra and co-workers [88] reported the use of Pd/CaCO_3 for phosphine-free Heck reactions in aqueous media to couple aryl halide and methyl acrylate. Hydroxyl propylated cyclodextrins were consumed as supramolecular hosts contributing the activity of catalyst (Scheme 1.11). The system can be reused up to three times with no significant loss of activity.



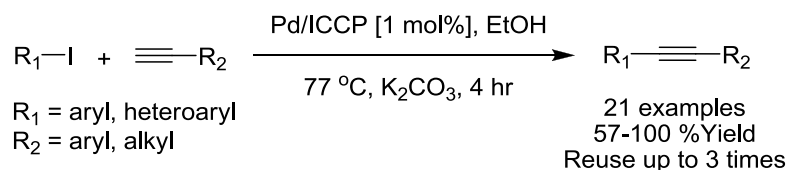
Scheme 1.11 Pd/CaCO₃ catalyzed Heck coupling reaction between aryl halide and methyl acrylate

In the same year, Coelho and co-workers [89] reported the coupling between substituted arylhalides and tributylphenyltin which were carried out in ethanol–water solution using Pd/CaCO₃ as catalyst in a ligand-free system via Stille reactions. The catalyst could be recycled three times without any loss of activity. The ethanol–water solution, after removal of the catalyst and extraction of the product, was found to have catalytic activity, thus showing the presence of soluble Pd(0)/Pd(II) species that can be regarded as the true catalysts (Scheme 1.12).



Scheme 1.12 Pd/CaCO₃ catalyzed Stille cross coupling reaction between iodo-benzene and tributylphenyltin

Most recently, our research group [100] successfully prepared heterogeneous palladium nanoparticles (3-6 nm) which are deposited on individual calcium carbonate plates (ICCPs) derived from mussel shell. Pd/ICCP efficiently catalyzed Sonogashira cross-coupling reactions between aryl iodides and terminal alkynes to generate alkyne compounds in high yields (57-100%) without the use of any copper metal or external ligand. Such catalyst could also be reused up to three times with no significant loss of activity. In addition, this catalyst was carried out with negligible Pd-metal leaching in reaction (Scheme 1.13).

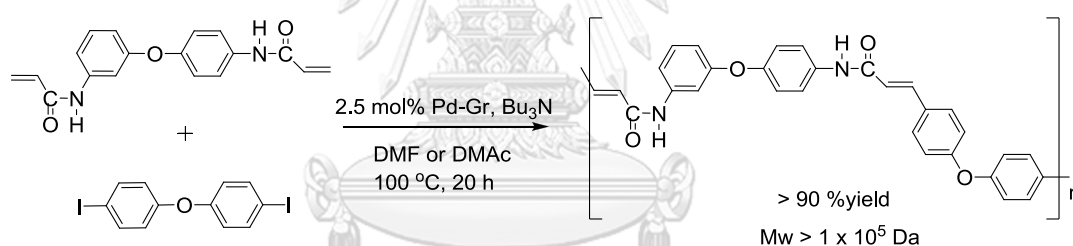


Scheme 1.13 Pd/CaCO₃ catalyzed Sonogashira cross-coupling reaction between aryl iodides and terminal alkynes

In addition to above literature reviews, there are a few reports about the use of heterogeneous Pd catalysts to promote the C–C coupling polymerization for preparation of conjugate polymer.

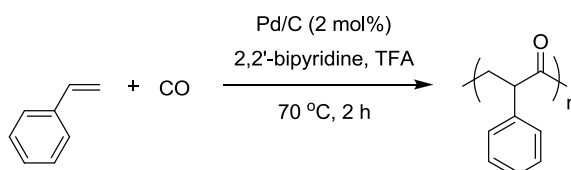
C-C coupling polymerization using heterogeneous Pd catalyst

In 1995, the first investigation was described by Kakimoto and co-workers [101] about polycondensation using the Palladium supported on graphite (Pd/Gr) catalyzed Heck reaction for preparing of polycinnamamide by polymerization of N,N'-(3,4'-oxydiphenylene)bis-(acrylamide) and bis(4-iodophenyl) ether (Scheme 1.14). Such reaction proceeded efficiently with 2.5 mol% Pd/Gr without any ligand compounds in the presence of tributylamine in DMF at 100 °C for 20 h to obtain high molecular weight polymer in excellent yield.



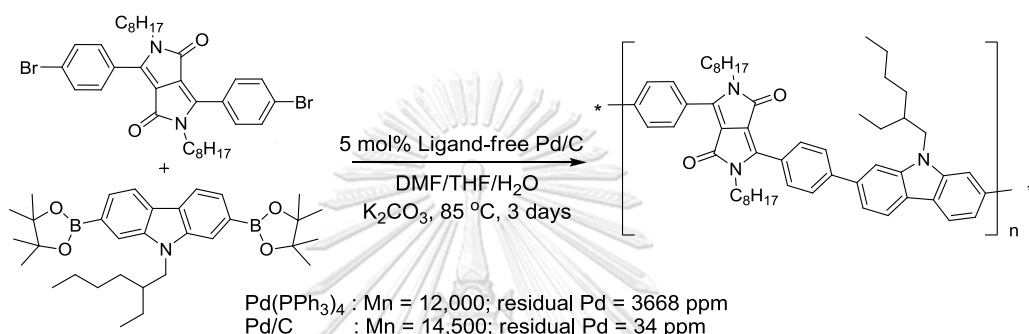
Scheme 1.14 Pd/Gr-catalyzed Heck reaction for preparing of polycinnamamide

In 2009, Guo and co-workers [102] revealed that polyketone (STCO) was successfully synthesized by applied of carbon monoxide (CO) and styrene (ST) in the presence of Pd/C (5.4 wt%) with bipyridine and *p*-toluenesulfonic acid as shown in Scheme 1.15. In the copolymerization system, Pd/C catalyst can be reused for 6 times with higher catalytic activity of 1255.17 STCO/(g Pd h) than that of homogeneous catalyst (palladium acetate).



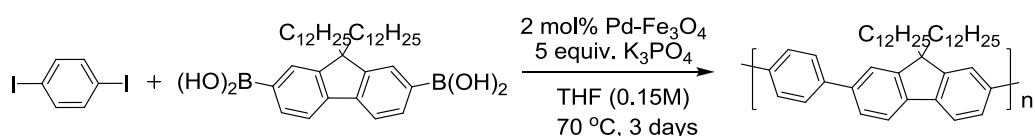
Scheme 1.15 Pd/C-catalyzed copolymerization of polyketone

Ligand-free heterogeneous Pd/C catalyzed Suzuki, Heck, and Stille coupling polymerizations toward conjugated polymers were first developed in 2012 by Chen and co-workers [103]. The reaction proceeded under mild condition using 5 mol% Pd/C in mixture solvent of DMF/H₂O/THF at 85 °C for 3 days (Scheme 1.16). The preparing polymers displayed higher molecular weight ($M_n = 14,500$) with less Pd residue ($Pd_{res} = 34$ ppm) which is lower than classical homogeneous catalyst ($Pd(PPh_3)_4$) leading to enhanced electronic performance (FETs).



Scheme 1.16 Synthetic method and properties of polymers via cross coupling polymerizations catalyzed by Pd/C

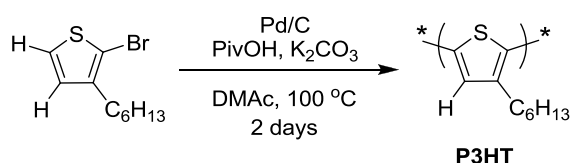
In 2014, the application of Pd-Fe₃O₄ heterodimer nanocrystal catalysis towards Suzuki coupling polymerization was initially illustrated by Choi and co-workers [104]. The optimized reaction conditions: 0.15 M substrate in the presence of 2 mol% Pd-Fe₃O₄ and K₃PO₄ in THF at 70 °C for 3 days showed good reactivity to afford various moderate to high molecular weight conjugated polymers (Scheme 1.17). Moreover, the catalyst was easily separated using an external magnet followed by reused in the polymerization for up to the 11th run with maintained the catalytic activity.



Scheme 1.17 Pd-Fe₃O₄ catalyzed Suzuki coupling polymerization

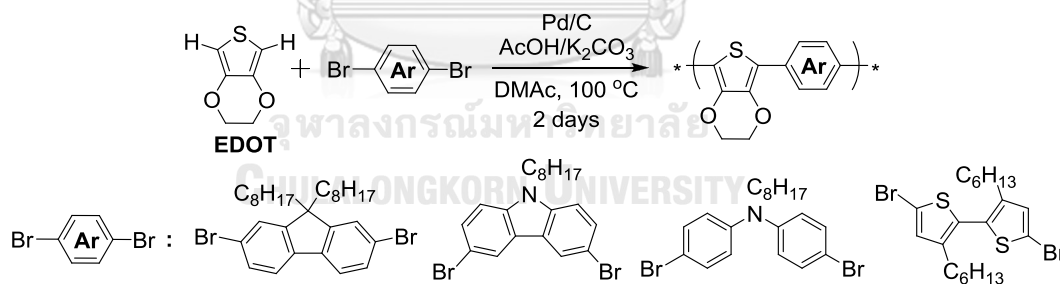
In 2015, Hayashi and co-workers [105] succeeded in the synthesis of linear π -conjugated polymer *via* Pd/C catalyzed direct arylation (dehydrohalogenative)

polycondensation. The optimal condition was carried out in the presence of 2.5 mol% Pd/C with phosphine-free in dimethylacetamide (DMAc) at 100 °C for 2 days, giving linear and highly regioregular head-to-tail poly(3-hexylthiophene-2,5-diyl) (P3HT) in high yield with high molecular weight (Scheme 1.18).



Scheme 1.18 Pd-catalyzed direct arylation polycondensation of 2-bromo-3-hexylthiophene

In 2017, direct arylation polycondensation of 3,4-ethylenedioxy-thiophene (EDOT) with 2,7-dibromo-9,9-dioctylfluorene using a Pd/C catalyst was demonstrated by Koizumi and co-workers [106]. Under the optimized conditions, 2.5 mol% Pd/C with acetic acid/potassium carbonate in N,N-dimethylacetamide at 100 °C for 2 days also resulted in a high molecular weight p-conjugated alternating copolymer of various dibromoarene derivatives, giving EDOT-carbazole, EDOT-dialylamine and EDOT-bithiophene polymers in high yield (Scheme 1.19).



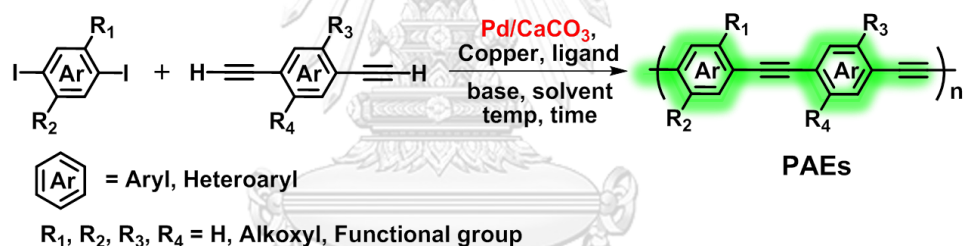
Scheme 1.19 Pd/C catalyzed direct arylation polycondensation of EDOT with various dibromoarenes.

According to background literature above, several examples of heterogeneous Pd-catalyzed Suzuki–Miyaura, Stille and Mizoroki–Heck cross-coupling polycondensations for π -conjugated polymers have been reported so far. However, there has been no report on palladium supported on calcium carbonate (Pd/CaCO₃). It is therefore our goal to use this abundant naturally occurring, cheap, stable and

environmentally friendly substance as palladium catalyst support for Sonogashira cross coupling polymerization.

1.2.5 Objectives of this research

In this research, we purpose to use heterogeneous palladium supported on calcium carbonate as an alternative catalyst for Sonogashira coupling polymerization between diiodo aromatics and terminal alkynes to synthesize the corresponding PAEs (Scheme 1.20). The catalyst loading, reaction concentration, reaction time, temperature, type of ligand, base and solvent will be screened. The molecular weight, photophysical properties, palladium contamination and electronic performances of prepared PAEs from optimal condition will be determined and compare to PAEs from homogeneous catalyst and Pd/C. Finally, to extend the scope of the reaction, varieties diiodo coupling partner will be subjected to our optimal reaction condition to prepare a variety of PAEs.



Scheme 1.20 Pd/CaCO₃-catalyzed Sonogashira coupling polymerization

CHAPTER II

EXPERIMENTAL

2.1 Chemicals and materials

Aniline, trimethylsilylacetylene, and bis(triphenylphosphine)palladium(II) dichloride ($\text{PdCl}_2(\text{PPh}_3)_2$) were purchased from Fluka (Switzerland). 1-bromobutane, 2-ethylhexylbromide, iodine-monochloride, copper (I) iodide, 1, 8-diazabicyclo [5.4.0] undec-7-ene (DBU), diisopropylamine, salicylaldehyde and quinine sulfate were purchased from Aldrich. Ammonium chloride, potassium hydroxide, potassium carbonate, potassium iodide, sodium sulfate, sodium thiosulphate and sodium chloride were purchased from Carlo Erba Reagent. All other reagents were non-selectively purchased from Sigma-Aldrich, Fluka, Merck (Germany) or Tokyo Chemical Industry (TCI). For most reactions, solvents such as dichloromethane, tetrahydrofuran, methanol, ethanol, dimethylformamide, dimethylsulphoxide, toluene and acetonitrile were reagent grade stored over molecular sieves before used. All column chromatography were operated using Merck silica gel 60 (70-230 mesh). Thin layer chromatography (TLC) was performed on silica gel plates (Merck F245). Solvents used for extraction, precipitation and chromatography such as dichloromethane, hexane, ethyl acetate, methanol and diethyl ether were commercial grade which were used without distillation. Milli-Q water was used in all experiments unless specified otherwise. The most reactions were carried out under positive pressure of N_2 filled in rubber balloons.

2.2 Analytical instruments

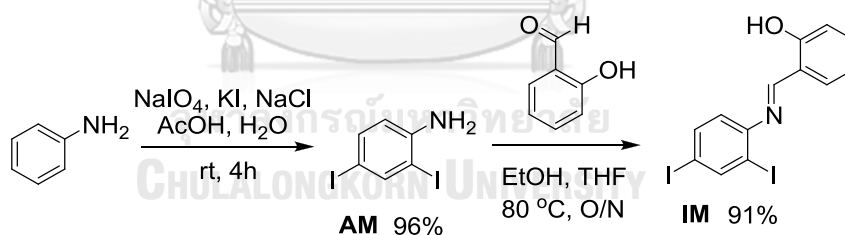
Elemental (C, H, N) analyses were performed on a PE 2400 series II analyzer (Perkin-Elmer, USA). Mass spectra were recorded on a Microflex MALDI-TOF mass spectrometer (Bruker Daltonics) using doubly recrystallized α -cyano-4-hydroxy cinnamic acid (CCA) as a matrix. Fourier transform infrared spectra were acquired on Nicolet 6700 FT-IR spectrometer equipped with a mercury-cadmium telluride (MCT) detector (Nicolet, USA). $^1\text{H-NMR}$ and $^{13}\text{C-NMR}$ spectra were acquired from sample

solution in CDCl_3 , $(\text{CD}_3)_2\text{CO}-d_6$, CD_3OD and $\text{DMSO}-d_6$ on Varian Mercury NMR spectrometer (Varian, USA) at 400 MHz and 100 MHz, respectively. The UV-visible absorption spectra were obtained from a Varian Cary 50 UV-Vis spectrophotometer (Varian, USA) and the fluorescence emission spectra were recorded on a Varian Cary Eclipse spectrofluorometer (Varian, USA). All polymer solutions were filtered through $0.45 \mu\text{m}$ syringe filters prior to use. Polymer molecular weights were determined at 25°C on a HP series 1100 GPC system in THF at 1.0 mL/min (4 mg/mL sample concentrations) equipped with a diode array detector (254 nm and 450 nm). Polymer molecular weights are reported relative to polystyrene standards. Prepared polymer at concentration of $100 \mu\text{M}$ in 10%water/THF was measured particle sizes at various temperatures ($25 - 60^\circ\text{C}$) by dynamic light scattering zetasizer nano ZS.

2.3 Experimental strategy for the synthesis of salicylaldehyde-functionalized poly(phenyleneethynylene) used as turn-on sensor for ferric ion (part A).

2.3.1 Synthesis of small molecules

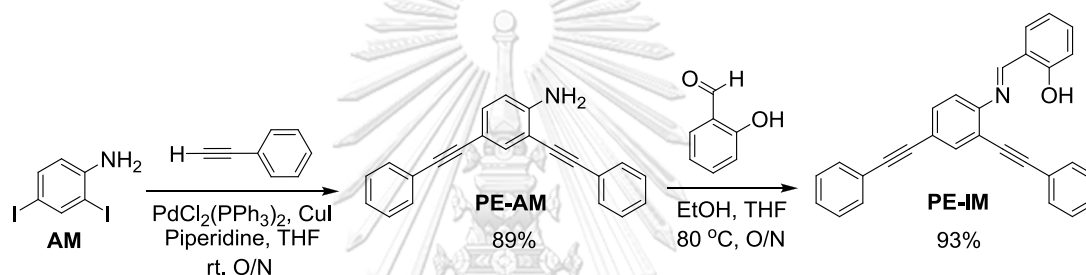
2.3.1.1 Preparation of 2,4-diiodoaniline (AM) [107] and (E)-2-((2,4-diiodo phenylimino)methyl)phenol (IM)



AM: A typical procedure was followed according to the previous literature by using aniline (1.00 g, 10.75 mmol), sodium periodate (2.29 g, 10.75 mmol), potassium iodide (5.35 g, 32.25 mmol) and sodium chloride (2.51 g, 43.00 mmol) dissolved in the mixture of acetic acid (32 mL) and water (4 mL). After the reaction proceeded under ambient for 4 hours, the mixture was extracted with CH_2Cl_2 ($3 \times 50 \text{ mL}$) and washed with $\text{Na}_2\text{S}_2\text{O}_3$, NaHCO_3 and brine. The residue was purified by column chromatography using 5% EtOAc /hexane to yield AM as brown powder 3.56 g (10.31 mmol, 96%) ^1H NMR (400 MHz, CDCl_3) δ ppm 7.89 (s, 1H), 7.37 (d, $J = 8.4 \text{ Hz}$, 1H), 6.52 (d, $J = 8.4 \text{ Hz}$, 1H), 4.13 (s, 2H).

IM: A mixture of **AM** (100 mg, 0.29 mmol), salicylaldehyde (33.87 μL , 0.32 mmol) in EtOH (3 mL) was stirred at 80 $^{\circ}\text{C}$ for 3 h. The precipitated bright yellow solid was washed with cold EtOH (3 \times 25 mL) to obtain desired product (yield: 118.2 mg, 91%) ^1H NMR (400 MHz, *acetone*) δ ppm 12.69 (s, 1H), 8.86 (s, 1H), 8.33 (s, 1H), 7.87 (d, J = 7.4 Hz, 1H), 7.63 (m, 1H), 7.48 (m, 1H), 7.31 (d, J = 7.0 Hz, 1H), 7.00 (d, J = 7.7 Hz, 2H). ^{13}C NMR (101 MHz, *acetone*) δ ppm 166.08, 162.15, 147.57, 139.91, 134.99, 134.37, 121.65, 120.37, 120.17, 120.13, 118.05, 117.95, 98.40, 92.25. MALDI-TOF MS calcd. $\text{C}_{13}\text{H}_9\text{I}_2\text{NO}$ 448.877, found 450.042.

2.3.1.2 Preparation of 2,4-bis(phenylethynyl)amino derivatives

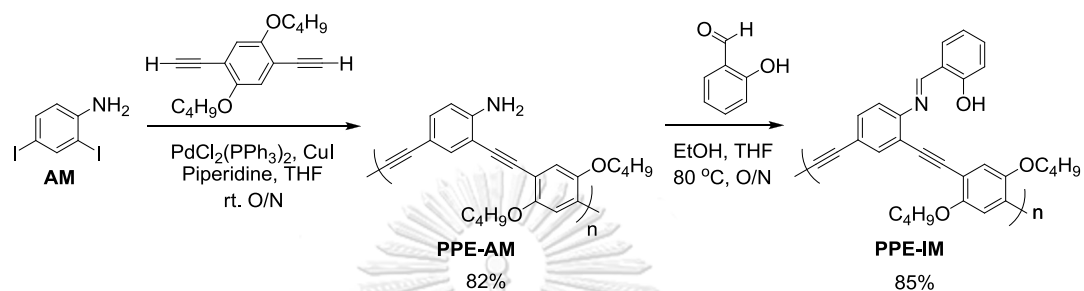


2,4-bis(phenylethynyl)aniline (PE-AM): A typical procedure was followed according to the literature. [108] A yellow powder of **PE-AM** was obtained. ^1H NMR (400 MHz, *acetone*) δ ppm 7.62-7.57 (m, 2H), 7.49 (d, J = 8.2 Hz, 3H), 7.43-7.33 (m, 6H), 7.28 (d, J = 8.5 Hz, 1H), 6.83 (d, J = 8.5 Hz, 1H), 5.57 (s, 2H). FTIR (neat, cm^{-1}) 3465, 3373, 3029, 2362, 2202, 1612, 1500. MALDI-TOF MS calcd. $\text{C}_{22}\text{H}_{15}\text{N}$ 293.1204, found 292.2350.

(E)-2-((2,4-bis(phenylethynyl)phenylimino)methyl)phenol (PE-IM): Compound **PE-AM** (94 mg, 0.32 mmol) was dissolved in 2.5 ml of EtOH and then the solution was stirred at 50 $^{\circ}\text{C}$ for 15 min after the addition of salicylaldehyde (40.8 μL , 0.38 mmol). The reaction mixture was stirred at reflux for 2 h. After filtration, the filter was collected and washed with cold EtOH (5 \times 10 mL). After drying under a vacuum, an orange powder (**PE-IM**) was obtained (yield: 118 mg, 93%) ^1H NMR (400 MHz, *acetone*) δ ppm 13.51 (s, 1H), 9.12 (s, 2H), 7.83 (s, 2H), 7.68 (dd, J = 8.0, 2.1 Hz, 10H), 7.62-7.58 (m, 4H), 7.50-7.43 (m, 14H), 7.00 (dd, J = 14.2, 7.6 Hz, 4H). ^{13}C NMR (101 MHz, *acetone*) δ 165.10, 165.06, 162.56, 162.16, 149.83, 136.33, 134.68, 134.08,

133.45, 132.65, 132.42, 129.71, 129.65, 129.52, 129.44, 123.81, 123.77, 122.84, 120.78, 120.33, 120.10, 120.03, 119.27, 118.00, 117.90, 96.03, 91.45, 88.90, 86.67. FTIR (neat, cm^{-1}) 3055, 2359, 2201, 1606. MALDI-TOF MS calcd. $\text{C}_{29}\text{H}_{19}\text{NO}$ 397.1467, found 397.4780.

2.3.2 Synthesis of acetylenic polymers.



Poly(*m*-anilineethynylene-*p*-phenyleneethynylene) copolymer (PPE-AM):

In a typical experiment, a mixture of compound **AM** (100 mg, 0.29 mmol), 2,4-diethynyldibutoxybenzene (78.4 mg, 0.29 mmol), PdCl₂(PPh₃)₂ (20.4 mg, 0.03 mmol), CuI (11.0 mg, 0.06 mmol), PPh₃ (15.2 mg, 0.06 mmol), were stirred in the mixture solvent of THF (2 mL) and DBU (1 mL). The reaction was carried out under pressure of N₂ filled in rubber balloons and stirred at room temperature for 24 hours. Then the solution was added with dichloromethane (10 mL) to dissolve part of gelly polymer for 15 min. The rotary evaporator was used to concentrate total solvent to a small volume (\approx 1 mL) and the polymer was precipitated by dropping the solution into 150 mL of cold methanol. The precipitate that formed was collected by centrifuge, washed repeatedly with methanol (5 \times 30 mL) and evaporated under vacuum to afford greenish yellow powder of **PPE-AM** (yield: 85 mg, 82%) $M_w = 6.3 \times 10^3$ Da., DP = 17, PDI = 1.5, ¹H NMR (400 MHz, CDCl₃) δ ppm 7.86, 7.57, 7.29, 7.00, 6.71, 4.76, 4.05, 1.85, 1.58, 1.03. ¹³C NMR (101 MHz, CDCl₃) δ ppm 155.08, 153.29, 148.29, 142.02, 134.52, 133.12, 132.65, 117.90, 116.94, 116.72, 116.41, 115.78, 115.16, 113.86, 107.93, 92.19, 84.92, 84.15, 82.84, 69.47, 68.92, 31.44, 19.22, 13.90. FTIR (neat, cm^{-1}) 3470, 3362, 2958, 2866, 2357, 2190, 1612, 1506, 1211.

Salicylaldimine-functionalized poly(*m*-anilineethynylene-*p*-phenyleneethynylene) copolymer (PPE-IM): Polymer **PPE-AM** (67 mg, 0.18 mmol based on

repeating unit) was dissolved in 2 mL of EtOH at 70 °C for 15 min. Then salicylaldehyde (540 mg, 0.47 mL) was added and the reaction was stirred for 24 hours. The reaction mixture was cooled to room temperature and concentrated to small volume by rotary evaporator before precipitation in cold methanol. After precipitated polymer was formed, there was collected by centrifuge and washed repeatedly with cold methanol (5 × 30 mL) to afford orange powder of **PPE-IM** (yield: 75 mg, 85%). ^1H NMR (400 MHz, CDCl_3) δ ppm 13.44, 12.83, 8.79, 8.57, 8.12, 7.77, 7.54, 7.43, 7.29, 6.98, 4.05, 1.83, 1.55, 1.02. ^{13}C NMR (101 MHz, CDCl_3) δ ppm 162.63, 161.49, 153.67, 153.32, 149.13, 148.59, 142.04, 136.79, 135.55, 133.41, 132.58, 132.43, 132.33, 119.15, 118.94, 117.38, 117.14, 96.05, 92.04, 91.22, 69.35, 68.88, 31.15, 19.11, 13.75, FTIR (neat, cm^{-1}) 2955, 2929, 2866, 2193, 1609, 1497, 1205.

2.4 Photophysical property study

For two parts mentioned above, all conjugated compounds were fully examined photophysical properties by following methods of spectroscopic measurements that described in the next section.

2.4.1 UV-Visible spectroscopy

The stock solutions of all polymers in THF and small molecules (**PE-AM**, **PE-IM**) in acetone were prepared at concentration of 1 mM. The absorption spectra of all fluorophores were determined from 250 nm to 600 nm at ambient temperature.

2.4.1.1. Molar Absorption Coefficients (ϵ)

Molar Absorption Coefficients (ϵ) of such fluorophores were estimated from UV absorption spectra of analytical samples at various concentrations. For small molecule (**PE-AM**, **PE-IM**) and all polymers were measured in acetone and in THF, respectively. The intensities at absorption maximum wavelength (λ_{max}) of each compound were plotted against the concentrations. Each plot should be a straight line goes through origin. Molar Absorption Coefficients (ϵ) can be obtained from plotting of maximum absorption (A) vs. concentration (C) represented into the following equation:

$$A = \epsilon b C \quad (1)$$

*b is the cell path length.

2.4.2 Fluorescence spectroscopy

For prepared polymer in part A, the polymer solution was diluted to 10 μM in THF. The solutions of small molecules (**PE-AM**, **PE-IM**) and all polymers (**PPE-AM**, **PPE-IM**) were diluted to 10 μM in 10% H_2O /acetone and 10% H_2O /THF, respectively. The emission spectra of fluorophores were recorded from 350 nm to 700 nm at ambient temperature using an excitation wavelength at 300 to 410 nm.

2.4.3 Fluorophore quantum yields (Φ)

The fluorescence quantum yields of **PE-AM** and **PE-IM** were performed in acetone, while those of **PPE-AM**, **PPE-IM** and treated **PPE-IM** with Fe^{3+} were performed in 10% H_2O /THF. Each sample used quinine sulphate ($\Phi_{\text{ST}} = 0.54$, $\lambda_{\text{ex}} 336$ nm) in 0.5 M H_2SO_4 as a reference [109]. The UV-Vis absorption spectra of all analytical samples and reference samples at varied concentrations were recorded. The maximum absorbance of all samples should never exceed 0.1 (a.u.). The fluorescence emission spectra of the same solution using appropriate excitation wavelengths selected were recorded based on the absorption maximum wavelength (λ_{max}) of each compound. Graphs of integrated fluorescence intensities were plotted against the absorbance at the respective excitation wavelengths. Each plot should be a straight line with 0 interception and gradient m [110].

In addition, the fluorescence quantum yield (Φ_x) was obtained from plotting of integrated fluorescence intensity vs absorbance represented into the following

$$\Phi_x = \Phi_{\text{ST}} \left(\frac{\text{Grad}_x}{\text{Grad}_{\text{ST}}} \right) \left(\frac{\eta_x^2}{\eta_{\text{ST}}^2} \right) \quad (2)$$

The subscripts Φ_{ST} denote the fluorescence quantum yield of a standard reference which used quinine sulphate in 0.1 M H_2SO_4 ($\Phi = 0.54$) and Φ_x is the fluorescence quantum yield of sample and η is the refractive index of the solvent.

2.4.4 Fluorescent sensor study (for part A)

2.4.4.1 Stability study

The stock solutions 1 mM of the imine fluorophores (**PE-IM** and **PPE-IM**) were prepared in THF. To afford the fluorophores concentration of 10 μM , there were diluted in 10% $\text{H}_2\text{O}/\text{THF}$ and adjusted to 1 mL. The spectra were recorded after mixing from 1 to 120 min.

2.4.4.2 Selectivity study

The stock solution 1 mM of the **PPE-IM** was prepared in THF. All metal ion solutions were prepared in Milli-Q water and adjusted to 2 mM. The stock solutions of the fluorophore and analyte were mixed and diluted to the designated concentrations in 10% $\text{H}_2\text{O}/\text{THF}$. The final volumes of the mixtures were adjusted to 1 mL to afford concentration of 25 μM for the **PPE-IM** and 250 μM for metal ions at the ratio 1:10 in 10% $\text{H}_2\text{O}/\text{THF}$. The spectra were recorded after mixing for 60 minutes.

2.4.4.3 Fluorescence titration

The stock solution of **PPE-IM** in THF (1 mM, 25 μL) was diluted with H_2O 100 μL and THF (875 μL) in a 1 mL quartz cuvette. Designated volumes of the Fe^{3+} stock solution (0-100 μL) for 2 mM to afford 1-8 equiv. of Fe^{3+} and 0-12.5 μL for 20 mM to afford 8-10 equiv. of Fe^{3+} in milliQ water was added into the sensor solution. The final volumes were adjusted to 1 mL by adding milliQ water. The final concentration of each fluorophore is 25 μM in 10% $\text{H}_2\text{O}/\text{THF}$. The spectra were recorded after mixing for 60 minutes.

2.4.4.4 Competition with other metal ions

The mixture of each **PPE-IM**/ Fe^{3+} /other metal ions in concentration of 25/125/625 μM with ratio of 1/5/25 were used to investigate the interference of other metal ions to Fe^{3+} treating with sensors.

2.4.4.5 Limit of detection

In fluorescent sensing, limit of detection (LOD) is the lowest concentration of analyte in a sample that is required to produce a signal greater than three times the standard deviation of the a blank sample. But the value is not necessarily quantitated as an exact value. The limit of detection can be calculated according to the equation (3)

$$\text{LOD} = [(I_0 + 3\text{SD})/I_0 - \text{Intercept}]/K \quad (3)$$

The variables were similar to those in turn-on sensing. Except K is the slope of the straight line of the plot of I/I_0 against the concentration of an analyte [A]. Example of the calibration curve is shown in Figure 2.1.

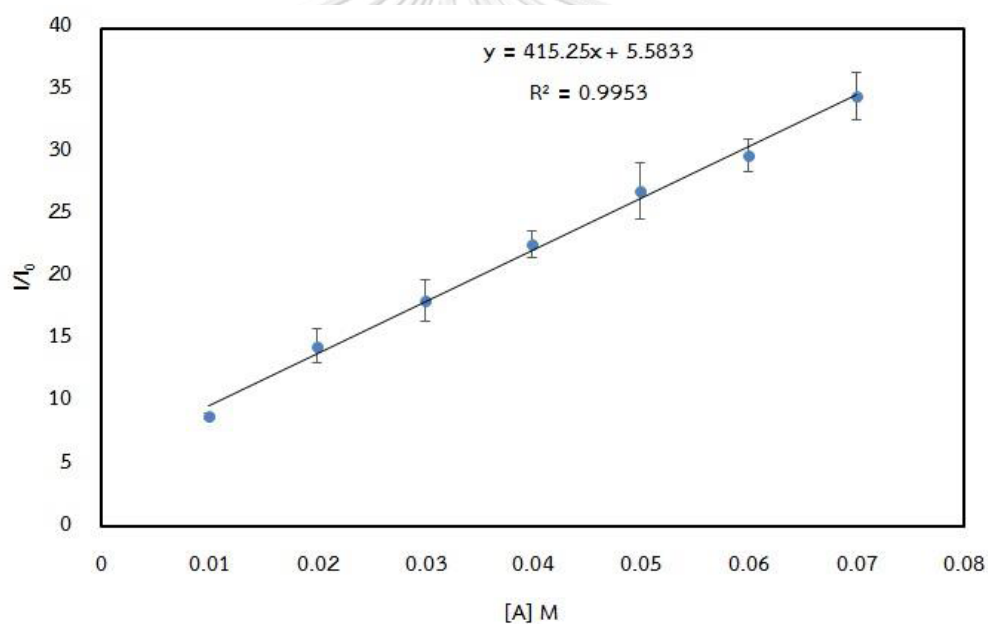


Figure 2.1 The calibration curve for turn-on sensing.

2.5 Experimental strategy for the synthesis of highly pure poly(aryleneethynylene)s using Pd/CaCO₃ as eco-friendly heterogeneous catalyst (part B).

2.5.1 Sonogashira coupling polymerization using Pd/CaCO₃ as catalyst.

2.5.1.1 Preparation of model monomers

1,4-di-2-ethylxyloxy-2,5-diiodobenzene (2a) [111]

1a: KOH (4.59 g, 81.72 mmol) and dried DMSO (15 mL) were stirred for 15 min in 100 mL round bottom flask. Hydroquinone (2.00 g, 18.16 mmol) was charged before 2-ethylhexyl bromide (14.03 g, 72.64 mmol) was gradually dropped in solution. The mixture was carried out at room temperature for overnight. The mixture was extracted three times with CH_2Cl_2 (3 \times 100 mL). The combined organic phase was modulated to neutral pH and then was washed with water, brine, dried over anhydrous Na_2SO_4 and evaporated under vacuum. Column chromatography was used to purify the desired product which provided 5.59 g (18.16 mmol, 92%) of **1a** as a colorless oil. ^1H NMR (400 MHz, CDCl_3) δ ppm 6.83 (s, 4H), 3.79 (d, J = 4.5 Hz, 4H), 1.69 (dd, J = 11.2, 5.4 Hz, 2H), 1.56 – 1.21 (m, 16H), 1.06 – 0.85 (m, 12H). ^{13}C NMR (101 MHz, CDCl_3) δ ppm 153.7, 115.6, 71.5, 39.8, 30.8, 29.4, 24.1, 23.3, 14.3, 11.3.

2a: Dialkoxybenzene **1a** (0.50 g, 1.49 mmol) in MeOH (35 mL) was stirred at temperature below 15 $^\circ\text{C}$ before iodine (I) chloride (1.07 g, 5.96 mmol) was added dropwise and the reaction mixture was then allowed to reflux for 1 day under pressure of N_2 . The mixture was extracted three times with CH_2Cl_2 (3 \times 50 mL). The combined organic phase was washed with aqueous $\text{Na}_2\text{S}_2\text{O}_3$, water, brine and dried over anhydrous Na_2SO_4 . The solution was evaporated and the residue was eluted through a silica gel column by hexane to afford 0.69 g (1.49 mmol, 78%) of **2a** as a colorless oil. ^1H NMR (400 MHz, CDCl_3) δ ppm 7.16 (s, 2H), 3.81 (d, J = 5.1 Hz, 4H), 1.74-1.72 (m, 2H), 1.54 – 1.43 (m, 8H), 1.33 (d, J = 2.5 Hz, 8H), 0.97-0.88 (m, 12H). ^{13}C NMR (101 MHz, CDCl_3) δ ppm 152.4, 121.9, 85.6, 71.9, 39.0, 30.0, 28.6, 23.5, 22.5, 13.6, 10.8.

1,4-diethynylbenzene (**3a**) [112]

3a-TMS: A 100 mL of round bottom flask equipped with a magnetic stirring bar was charged with 1,4-diiodobenzene (0.50 g, 1.52 mmol), Tetrakis(triphenyl phosphine)palladium(0) ($\text{Pd}(\text{PPh}_3)_4$) (0.09 g, 0.08 mmol), copper (I) iodide (CuI) (0.03 g, 0.15 mmol) were dissolved in anhydrous THF (30 mL) at room temperature for 10 min and then added trimethylsilylacetylene (TMSA) (0.59 g, 6.06 mmol), along with triethylamine (TEA) (0.91 g, 9.09 mmol). The substrate concentration was adjusted to

0.1 M with trace of THF. After the solution color became deep brown, the reaction was allowed to proceed at 80 °C under positive pressure of N₂ for overnight. After cooling the reaction, such solution was extracted with EtOAc (3 × 50 mL) and washed with NH₄Cl, brine and dried over Na₂SO₄. The reaction was evaporated to small volume and further purified through silica gel with hexane as eluent to afford **3a-TMS** (0.41 g, 1.52 mmol, 100%) as a pale-yellow solid. ¹H NMR (400 MHz, CDCl₃) δ ppm 7.52 (d, 2H), 0.08 (s, 9H).

3a: 1,4-bis((trimethylsilyl)ethynyl)benzene (**3a-TMS**) (0.40 g, 1.49 mmol), was dissolved in mixture of MeOH (3 mL) and CH₂Cl₂ (3 mL) and then added with potassium carbonate (K₂CO₃) (0.31 g, 2.23 mmol). After the reaction was mixed at room temperature for 3 hours, there was extracted with EtOAc (3 × 50 mL) and washed with water, brine and dried over Na₂SO₄. The reaction was evaporated to small volume and the residue was purified by silica chromatography, eluting with hexane to give **3a** (0.18 g, 1.49 mmol, 100%) as a brown solid. ¹H NMR (400 MHz, CDCl₃) δ ppm 7.44 (s, 2H), 3.17 (s, 1H). ¹³C NMR (101 MHz, CDCl₃) δ ppm 132.3, 122.7, 82.9, 80.6.

2.5.1.2 Optimization conditions

General procedure for screening the optimized polymerization condition by using Pd/CaCO₃ as catalyst (procedure A): Sealed tube equipped with a magnetic stirring bar was charged with 1,4-di-2-ethylxyloxy-2,5-diiodobenzene (**2a**), 1,4-diethynylbenzene (**3a**), Pd/CaCO₃, Cul, PPh₃ and solvent. The mixture was deoxygenated with nitrogen gas for 30 seconds, after that base was added. The concentration of the mixture was fixed at 0.05 M. All reaction proceeded under N₂ atmosphere at 80 °C for 24 hours. After the reaction completely proceeded and cooled to room temperature, the reaction mixture was then filtered through a cotton wool and washed with CH₂Cl₂ several times until the emissive light of polymer solution disappeared. The filtrate was evaporated under vacuum and then dissolved again with 1-2 mL of CH₂Cl₂, followed by dropping into 150 mL of cold MeOH. The precipitate was collected by centrifuge, washed repeatedly with MeOH and evaporated under vacuum to obtain poly (1,4-di-2-ethylhexyloxy-*p*-

phenyleneethynylene) (**4aa**) in corresponding yields. After that, the desired polymers were characterized by ^1H , ^{13}C NMR spectroscopy, FT-IR and further determined the molecular weight (M_w and M_n) and polydispersity index (PDI) by gel permeation chromatography (GPC).

Table 3.2 Effect of Catalyst loading and ligand: Synthesized according to procedure A, sealed tube equipped with a magnetic stirring bar that was charged with 1,4-di-2-ethylxyloxy-2,5-diiodobenzene (**2a**) (1 equiv.), 1,4-dibutoxy-2,5-diethynylbenzene (**3a**) (1.01 equiv.), Pd/CaCO₃ (0.01-0.10 equiv.), CuI (2 equiv. of Pd catalyst), ligands (2 equiv. of Pd catalyst) and the mixture of DIPEA/THF (1/2, v/v). The desired product of PAE **4aa** was obtained in corresponding yield.

Although the bidentate ligands were efficient to drive the reaction at 5%mol of palladium catalyst but most of bidentate ligands were costly more than the original one, triphenylphosphine (PPh₃), resulting that some economic problems in industrial scale. Therefore, we adjusted other factors by using 10%mol of palladium catalyst to evaluate optimal condition.

Table 3.3 Effect of base: Synthesized according to procedure A, sealed tube equipped with a magnetic stirring bar was charged with 1,4-di-2-ethylhexyloxy-2,5-diiodobenzene (**2a**) (1 equiv.), 1,4-dibutoxy-2,5-diethynyl benzene (**3a**) (1.01 equiv.), Pd/CaCO₃ (0.10 equiv.), CuI (0.20 equiv.), PPh₃ (0.20 equiv.), THF (2.27 mL), organic base (1.13 mL) or inorganic base (5 equiv.), giving desired product of PPE **4aa** in consistent yield.

Table 3.4 Effect of solvent: Synthesized according to procedure A, sealed tube equipped with a magnetic stirring bar was charged with 1,4-di-2-ethylxyloxy-2,5-diiodobenzene (**2a**) (1 equiv.), 1,4-dibutoxy-2,5-diethynylbenzene (**3a**) (1.01 equiv.), Pd/CaCO₃ (0.10 equiv.), CuI (0.20 equiv.), PPh₃ (0.20 equiv.), solvent (2.27 mL) and diisopropylethylamine (DIPEA) (1.13 mL), resulting desired product of PPE **4aa** in consistent yield.

In order to find the optimal temperature, we operated the polymerization from 40 °C to 120 °C. The desired product from the reaction that performed at lower

and higher temperature than 80 °C resulted in the lower yield along with low molecular weight even though the reaction was carried over 2 days, indicating that at 80 °C as optimal temperature of the reaction as depicted in Table 3.5.

Table 3.5 Effect of reaction temperature: Synthesized according to procedure A, 1,4-di-2-ethylxyloxy-2,5-diiodobenzene (**2a**) (1 equiv.), 1,4-dibutoxy-2,5-diethynylbenzene (**3a**) (1.01 equiv.), Pd/CaCO₃ (0.10 equiv.), CuI (0.20 equiv.), PPh₃ (0.20 equiv.) and the mixture of DIPEA/THF (1/2, v/v) were charged into the sealed tube that equipped with a magnetic stirring bar and stirred at corresponding temperature under nitrogen for 24 hours. The desired product of PAE **4aa** was provided in corresponding yield.

2.5.1.3 Polymer (**4aa**) preparation

PAE 4aa: Synthesized according to procedure A, monomer **2a** (100 mg, 0.17 mmol), monomer **3a** (21.52 mg, 0.17 mmol), Pd/CaCO₃ (36.18 mg, 0.017 mmol), copper iodide (CuI) (6.48 mg, 0.034 mmol), triphenylphosphine (PPh₃) (8.47 mg, 0.034 mmol), DIPEA (1.13 mL) and THF (2.27 mL) were introduced in oven-dried sealed tube equipped with a magnetic stirring bar. The bright-yellow powder of **4aa** was obtained 72.94 mg (0.16 mmol, 94%). GPC (vs. polystyrene standards in tetrahydrofuran): M_w = 65,287 Da., M_w/M_n = 3.1, DP = 143. ¹H NMR (400 MHz, CDCl₃) δ ppm 7.48 (br, 2H), 7.01 (br, 1H), 3.92 (br, 2H), 1.78 (br, 1H), 1.51 (br, 2H), 1.32 (br, 4H), 0.89 (br, 6H). ¹³C NMR (101 MHz, CDCl₃) δ ppm 153.78, 131.26, 131.22, 123.52, 123.17, 116.46, 113.82, 94.57, 87.94, 71.97, 39.53, 30.56, 29.04, 23.89, 22.92, 13.91, 11.12. FTIR (neat, cm⁻¹) 2961, 2924, 2858, 2205, 1460, 1208.

2.5.2 Comparative study between obtained PAE **4aa** using Pd/CaCO₃ with other conventional catalyst.

2.5.2.1 Characterization of PAE **4aa** obtained using Pd/CaCO₃ and other conventional catalysts and determination of molecular weight by GPC.

With the optimized condition in hand, we next focused on the comparison of degree of polymerization and amount of palladium and copper residues that

contaminated in resulting polymer obtained by using Pd/C and homogeneous palladium as catalyst as shown in Table 3.6 and 3.7, respectively.

PAE 4aa from PdCl₂(PPh₃)₂: Synthesized according to procedure A, monomer **2a** (100 mg, 0.17 mmol), monomer **3a** (21.52 mg, 0.17 mmol), PdCl₂(PPh₃)₂ (11.90 mg, 0.017 mmol), copper iodide (CuI) (6.48 mg, 0.034 mmol), triphenylphosphine (PPh₃) (8.47 mg, 0.034 mmol), DIPEA (1.13 mL) and THF (2.27 mL) were introduced in oven-dried sealed tube equipped with a magnetic stirring bar. The bright-yellow powder of **4aa** was obtained 75.0 mg (0.16 mmol, 97%). GPC (vs. polystyrene standards in tetrahydrofuran): $M_w = 33,149$, $M_w/M_n = 2.9$, DP = 73. ¹H NMR (400 MHz, CDCl₃) δ ppm 7.49 (s, 2H), 7.01 (s, 1H), 3.90 (d, $J = 22.5$ Hz, 4H), 1.80 (s, 1H), 1.54 (s, 4H), 1.34 (s, 4H), 0.94 (d, $J = 33.3$ Hz, 6H).

PAE 4aa from Pd(PPh₃)₄: Synthesized according to procedure A, monomer **2a** (100 mg, 0.17 mmol), monomer **3a** (21.52 mg, 0.17 mmol), Pd(PPh₃)₄ (19.64 mg, 0.017 mmol), copper iodide (CuI) (6.48 mg, 0.034 mmol), triphenylphosphine (PPh₃) (8.47 mg, 0.034 mmol), DIPEA (1.13 mL) and THF (2.27 mL) were introduced in oven-dried sealed tube equipped with a magnetic stirring bar. The bright-yellow powder of **4aa** was obtained 76.2 mg (0.17 mmol, 99%). GPC (vs. polystyrene standards in tetrahydrofuran): $M_w = 60,063$, $M_w/M_n = 3.8$, DP = 132. ¹H NMR (400 MHz, CDCl₃) δ ppm 7.49 (s, 2H), 7.01 (s, 1H), 3.90 (d, $J = 22.9$ Hz, 4H), 1.80 (s, 1H), 1.56 (s, 4H), 1.34 (s, 4H), 0.94 (d, $J = 32.6$ Hz, 6H).

PAE 4aa from Pd/C: Synthesized according to procedure A, monomer **2a** (100 mg, 0.17 mmol), monomer **3a** (21.52 mg, 0.17 mmol), Pd/C (18.17 mg, 0.017 mmol), copper iodide (CuI) (6.48 mg, 0.034 mmol), triphenylphosphine (PPh₃) (8.47 mg, 0.034 mmol), DIPEA (1.13 mL) and THF (2.27 mL) were introduced in oven-dried sealed tube equipped with a magnetic stirring bar. The bright-yellow powder of **4aa** was obtained 66.7 mg (0.15 mmol, 86%). GPC (vs. polystyrene standards in tetrahydrofuran): $M_w = 41,412$ Da., $M_w/M_n = 3.1$, DP = 91. ¹H NMR (400 MHz, CDCl₃) δ ppm 7.49 (d, $J = 3.0$ Hz, 4H), 7.02 (s, 2H), 3.90 (d, $J = 22.6$ Hz, 4H), 1.81 (m, 2H), 1.55 (m, 8H), 1.35 (m, 8H), 0.94 (m, 12H).

2.5.2.2 Determination of Palladium and copper contents in PAEs by ICP-OES analysis

1) Calibration curve method.

Palladium and copper standard for ICP (1000 mg/L) were used to prepare calibration curve between 0.1-30 ppm as shown in Figure 2.2.

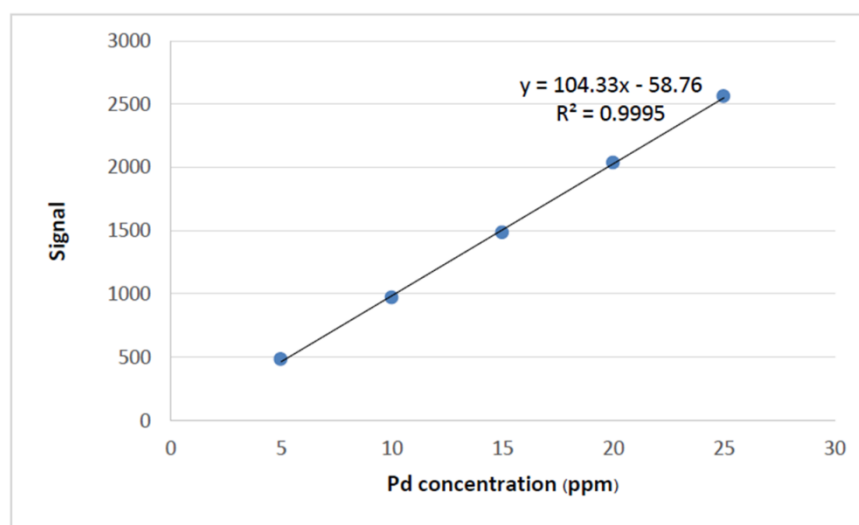


Figure 2.2 Example of calibration curve of Palladium standard

2) General procedure for preparation of sample.

After the reaction finished, the mixture was collected by centrifugation after washing for several times with THF to dissolve totally residual polymer from the catalysts. The gathering polymer solution was precipitated out following procedure A. The overall polymer solid (≈ 70 mg) was introduced into sealed tube and then charged with aquaregia (5 mL). Then, the mixture was stirred at $100\text{ }^{\circ}\text{C}$ for 1 day. After cooling to room temperature, the mixture was poured into 25 mL volumetric flask and adjusted by deionized water. Finally, such solutions were filtered through $0.45\text{ }\mu\text{m}$ syringe filters prior to measure. Amount of residual palladium and copper in prepared polymers are depicted in Table 3.7.

2.5.3 Reusability test of Pd/CaCO₃ catalyst

After the reaction for synthesis of PAE **4aa** according to procedure A, the Pd/CaCO₃ was separated from the reaction mixture by centrifugation and washed

several times until the emissive solution disappeared. The reused palladium catalyst was dispersed in THF (0.5 mL) by sonication before the next reaction. The results of this experiment are highlighted in Table 3.8.

In an attempt to extend the application of our system under optimal condition, we further investigated PAEs substrate scopes and studied their photo-physical properties.

2.5.4 Substrate scope of aryl dihalides coupled with aryl diethyne (**3b**) for examining generality of Pd/CaCO₃-catalyzed Sonogashira polymerization

2.5.4.1 Preparation of aryldihalide monomers

General procedure for synthesizing dialkoxybenzene derivatives (procedure B): Hydroquinone (1 equiv.), base (5 equiv.) and solvent was charged in round bottom flask equipped with a magnetic stirring bar and stirred at room temperature for 30 min before aliphatic halide derivatives (2.5 equiv.) was added. After the reaction proceeded overnight, the mixture was extracted with CH₂Cl₂ (3 × 100 mL). The combined organic phase was modulated to neutral pH and then was washed with water, brine, dried over anhydrous Na₂SO₄ and evaporated under vacuum. Column chromatography was used to purify the desired product giving compound.

General procedure for synthesizing aryldiodide compounds (procedure C): Dialkoxybenzene derivatives (1 equiv.) was dissolved in MeOH at temperature below 15 °C for 15 min and then gradually added iodine(I) chloride (ICl) (3 equiv.). After the mixture was stirred to reflux for 1 day under pressure of N₂, the mixture was extracted three times with CH₂Cl₂ (3 × 100 mL). The separated organic phase was washed with aqueous Na₂S₂O₃, water, brine and dried over anhydrous Na₂SO₄. The organic volume was concentrated *in vacuo* and purified by column chromatography to afford corresponding product.

1,4-dibutoxy-2,5-diiodobenzene (**2b**) [113]

1b: Synthesized according to procedure B, hydroquinone (2.00 g, 18.16 mmol), KOH (4.58 g, 81.72 mmol) and n-butyl bromide (9.95 g, 72.64 mmol) in DMF (15 mL) was charged and stirred at room temperature for overnight. Such reaction

was poured into 300 mL of cold water and the organic precipitate was collected by simple filtration and then washed with MeOH and water to afford compound **1b** in 8.82 g (18.16 mmol, 76%) as needle-like white crystal. ^1H NMR (400 MHz, CDCl_3) δ ppm 6.82 (s, 4H), 3.92-3.89 (t, 4H), 1.77-1.70 (m, 4H), 1.52-1.43 (m, 4H), 0.98-0.94 (t, 6H). ^{13}C NMR (101 MHz, CDCl_3) δ ppm 153.7, 115.9, 68.9, 32.0, 19.7, 14.3.

2b: Synthesized according to procedure C, **1b** (4.00 g, 17.99 mmol) and ICl (12.76 g, 78.61 mmol) was dissolved in MeOH (30 mL) to give 6.25 g (17.99 mmol, 74%) of **2b** as a white solid. ^1H NMR (400 MHz, CDCl_3) δ ppm 7.17 (s, 2H), 3.93 (t, $J = 6.4$ Hz, 4H), 1.82-1.75 (m, 4H), 1.58-1.49 (m, 4H), 0.98 (t, $J = 7.4$ Hz, 6H). ^{13}C NMR (101 MHz, CDCl_3) δ ppm 153.2, 123.2, 86.6, 70.4, 31.6, 19.6, 14.1. This spectral data agreed with the results reported in the literature.

3,3'-(2,5-diiodo-1,4-phenylene)bis(oxy)dipropyl-1-ol (**2c**) [114]

1c: Synthesized according to procedure B, hydroquinone (1 g, 9.08 mmol), K_2CO_3 (4.5 g, 32.56 mmol) and 3-chloropropan-1-ol (2.58 g, 27.25 mmol) in MeCN (10 mL) to provide 1.26 g (9.08 mmol, 76%) of **1c** as a white powder. ^1H NMR (400 MHz, CDCl_3) δ ppm 6.83 (s, 4H), 4.07 (t, $J = 5.9$ Hz, 4H), 3.86 (t, $J = 5.9$ Hz, 4H), 2.10 – 1.98 (m, 4H), 1.89 (s, 2H). ^{13}C NMR (101 MHz, CDCl_3) δ ppm 153.0, 115.4, 66.5, 60.5, 31.9.

2c: Synthesized according to procedure C, **1c** (1.50 g, 5.64 mmol) and ICl (4.57 g, 28.18 mmol) in MeOH (15 mL) to afford 2.64 g (5.52 mmol, 98%) of **2c** as a white solid. ^1H NMR (400 MHz, $\text{DMSO}-d_6$) δ ppm 7.33 (s, 2H), 4.52 (s, 2H), 4.01 (t, $J = 6.2$ Hz, 4H), 3.58 (t, $J = 5.9$ Hz, 4H), 1.83 (p, $J = 6.2$ Hz, 4H). ^{13}C NMR (101 MHz, $\text{DMSO}-d_6$) δ ppm 152.3, 122.4, 86.9, 66.8, 57.3, 32.1. This spectral data agreed with the results reported in the literature.

3,3'-(2,5-diiodo-1,4-phenylene)bis(oxy)bis(propyl-3,1-diyl)diacetate (**2d**) [115]

2d: A mixture of **2c** (0.10 g, 0.21 mmol) and 4-dimethylaminopyridine (DMAP) in pyridine (1.5 mL) was charged with acetic anhydride (0.08 g, 0.84 mmol). The reaction mixture was carried out at reflux temperature for 3 hours. The warm white powder was formed after the reaction was cooled to room temperature. The

resulting solid was filtered and washed several times with MeOH, water and brine. The collecting solid was dried with vacuum pump to prepare 0.11 g (0.20 mmol, 96%) of **2d**. ^1H NMR (400 MHz, CDCl_3) δ ppm 7.18 (s, 2H), 4.32 (t, $J = 6.2$ Hz, 4H), 4.02 (t, $J = 6.0$ Hz, 4H), 2.17 - 2.11 (m, 4H), 2.07 (s, 6H). ^{13}C NMR (101 MHz, CDCl_3) δ ppm 171.0, 152.8, 122.9, 86.3, 66.7, 61.2, 28.6, 21.0.

1,4-diiodo-2,5-bis(2-(2-methoxyethoxy)ethoxy)benzene (**2e**) [116]

e: Diethyleneglycol monomethylether (10.38 g, 86.31 mmol) and DMAP in CH_2Cl_2 (150 mL) were dissolved in triethylamine (25.00 mL, 178 mmol). The reaction mixture was stirred at 0 °C for 10 min and then dropwise with mesylchloride (10.92 g, 95.2 mmol) was added. After the reaction mixture was stirred at room temperature for 2 h, there was extracted with CH_2Cl_2 (3 \times 50 mL) and the combined organic layer was dried over Na_2SO_4 . The solution was concentrated and the residue was purified by column chromatography to provide 15.47 g (78.0 mmol, 90%) of **e** as a light yellow oil. ^1H NMR (400 MHz, CDCl_3) δ ppm 4.33 (t, $J = 4.60$ Hz, 2H), 3.72 (t, $J = 4.40$ Hz, 2H), 3.60 (t, $J = 4.40$ Hz, 2H), 3.49 (t, $J = 4.60$ Hz, 2H), 3.32 (s, 3H), 3.02 (s, 3H).

1e: A solution of hydroquinone (1.53 g, 13.89 mmol) and KOH (2.44 g, 43.5 mmol) in DMF (30 mL) was added with **e** (5.81 g, 29.3 mmol) and was then stirred at 60 °C for 20 h. After the resulting solution was extracted with CH_2Cl_2 and was adjusted a pH with saturated NH_4Cl , the combined organic phase was washed with water (10 \times 100 mL). Next, the solvent was evaporated. The residue was purified by column chromatography on silica gel to get 4.21 g (13.34 mmol, 96%) of **1e** as a light brown oil. ^1H NMR (400 MHz, CDCl_3) δ ppm 6.80 (s, 4H), 4.05 (t, $J = 5.00$ Hz, 4H), 3.79 (t, $J = 4.80$ Hz, 4H), 3.68 (t, $J = 4.60$ Hz, 4H), 3.54 (t, $J = 4.60$ Hz, 4H), 3.35 (s, 6H).

2e: A solution of **1e** (0.50 g, 1.59 mmol), H_5IO_6 (0.18 g, 0.79 mmol) and I_2 (0.80 g, 3.18 mmol) in acetic acid (4.5 mL), sulfuric acid (3 mL) and water (6 mL) was stirred at 70 °C for 12 h. After cooling to room temperature, the mixture was extracted with CH_2Cl_2 (3 \times 50 mL). The organic layer was washed with aqueous $\text{Na}_2\text{S}_2\text{O}_3$, water, brine and dried over anhydrous Na_2SO_4 . Then, gathered organic solvent was evaporated to small volume and was purified by column chromatography to furnish 0.59 g (1.04

mmol, 66%) of **2e** as a white powder. ^1H NMR (400 MHz, CDCl_3) δ ppm 7.23 (s, 2H), 4.11 (t, $J = 4.80$ Hz, 4H), 3.89 (t, $J = 4.80$ Hz, 4H), 3.78 (t, $J = 4.40$ Hz, 4H), 3.58 (t, $J = 4.40$ Hz, 4H), 3.40 (s, 6H). ^{13}C NMR (101 MHz, CDCl_3) δ ppm 153.4, 123.8, 86.6, 72.3, 71.3, 70.6, 69.8, 60.7, 59.3.

1,2,4,5-tetrafluoro-3,6-diiodobenzene (**2f**) [117]

2f: Iodine (12.7 g, 50 mmol) and fuming sulfuric acid (15 mL) were mixed and stirred at room temperature for 30 minutes. Then 3 g (20 mmol) of 1,2,4,5-tetrafluorobenzene was added gradually over a period of 10 minutes. Subsequently, the mixture was heated on a water bath at 60°C for 3 hours. The mixture was cooled and poured over crushed ice. Dark solid formed which was filtered, washed with aqueous NaHCO_3 and dried. This material was recrystallized from a methanol giving 6.99 g (17.39 mmol, 87%) of **2f** as a white crystal. ^{13}C NMR (101 MHz, CDCl_3) δ ppm 147.8, 72.9. This spectral data agreed with the results reported in the literature.

3,6-diiodo-9-octyl-9H-carbazole (**2g**) [118]

1g: A mixture of carbazole (5.0 g, 29.9 mmol), potassium iodate (6.6 g, 39.8 mmol) and potassium iodide (9.6 g, 44.9 mmol) were dissolved in acetic acid (50 mL) and then heated to reflux for 20 minute. The resulting solution was allowed to cool to room temperature and diluted with EtOAc (50 mL) and water (50 mL). The aqueous layer was separated and extracted with EtOAc (3 \times 100 mL). The combined organic layer was dried over Na_2SO_4 , and concentrated under reduced pressure to give a brown solid residue. The residue was purified by crystallization from hexane to yield **1g** as light brown crystals. (12.3 g, 98%). ^1H NMR (400 MHz, $\text{DMSO-}d_6$) δ ppm 11.56 (s, 1H), 8.58 (s, 2H), 7.66 (d, $J = 8.5$ Hz, 2H), 7.35 (d, $J = 8.5$ Hz, 2H). ^{13}C NMR (101 MHz, $\text{DMSO-}d_6$) δ ppm 138.7, 134.0, 129.1, 123.8, 113.5, 81.8.

2g: Synthesized according to procedure B, **1g** (0.20 g, 0.48 mmol), sodium hydride (0.15 g, 6.20 mmol) and octyl bromide (0.18 g, 0.96 mmol) in dried DMF (3 mL). The reaction mixture was carried out at room temperature for 1 h giving 0.20 g (0.39 mmol, 80%) of **2g** as yellowish brown crystal. ^1H NMR (400 MHz, CDCl_3) δ ppm 8.28 (d, $J = 1.4$ Hz, 2H), 7.68 (dd, $J = 8.6, 1.6$ Hz, 2H), 7.11 (d, $J = 8.6$ Hz, 2H), 4.01 (dd,

$J = 7.2, 2.4$ Hz, 2H), 1.95 (dt, $J = 11.3, 5.5$ Hz, 1H), 1.26 (d, $J = 7.2$ Hz, 8H), 0.88 (dd, $J = 14.3, 6.7$ Hz, 6H). ^{13}C NMR (101 MHz, CDCl_3) δ ppm 140.0, 134.5, 129.3, 124.0, 111.2, 81.8, 47.6, 39.4, 31.1, 28.9, 24.5, 23.1, 14.1, 11.0.

2,7-dibromo-9H-fluoren-9-one (**2j**) [119]

2j: The compound of 2,7-dibromo-9H-fluorene (**2i**) (3.19 g, 9.85 mmol) was dissolved in acetic acid (30 mL) before that $\text{K}_2\text{Cr}_2\text{O}_7$ (3.63g , 12.34 mmol) was introduced carefully. The mixture was refluxed for 6 hours. The precipitate formed was initially washed with water (50 mL) followed by 2% HCl solution (100 mL). The yellow solid thus obtained was dried under vacuum to afford 2.40 g (7.09 mmol, 72%) of **2j** as a yellow solid. ^1H NMR (400 MHz, CDCl_3) δ ppm 7.76 (s, 1H), 7.62 (d, $J = 6.3$ Hz, 1H), 7.38 (d, $J = 7.8$ Hz, 1H). The data agreed with previous reported in literature.

2.5.4.2 Preparation of aryldiethynyl monomer

Compound **3b** [120]

3b-TMS: A 100 mL of round bottom flask equipped with a magnetic stirring bar was charged with 1,4-dibutoxy-2,5-diiodobenzene (**2b**) (1.0 g, 2.11 mmol), $\text{PdCl}_2(\text{PPh}_3)_2$ (0.07 g, 0.10 mmol), CuI (0.04 g, 0.21 mmol), PPh_3 (0.06 g, 0.21 mmol) were dissolved in anhydrous THF (18 mL) at room temperature for 10 min and then added trimethylsilylacetylene (TMSA) (0.62 g, 6.32 mmol), along with triethylamine (TEA) (1.27 g, 12.6 mmol). The substrate concentration was adjusted to 0.1 M with trace of THF. After the solution color became deep brown, the reaction was allowed to proceed at 80°C under positive pressure of N_2 for overnight. After cooling the reaction, such solution was extracted with EtOAc (3 \times 50 mL) and washed with NH_4Cl , brine and dried over Na_2SO_4 . The reaction was evaporated to small volume and further purified through silica gel with hexane as eluent to afford **3b-TMS** 0.79 mg (1.90 mmol, 90%) as a bright yellow solid. ^1H NMR (400 MHz, CDCl_3) δ ppm 6.89 (s, 2H), 3.95 (t, $J = 6.3$ Hz, 4H), 1.80 – 1.73 (m, 4H), 1.56 – 1.49 (m, 4H), 0.97 (t, $J = 7.4$ Hz, 6H), 0.25 (s, 18H).

3b: 1,4-dibutoxy-2,5-bis(2-(trimethylsilyl)ethynyl)benzene (**3b-TMS**) (0.79 g, 1.90 mmol) was dissolved in MeOH/CH₂Cl₂ (1/1, v/v) and then added with K₂CO₃ (0.79 g, 5.71 mmol). After the reaction was mixed at room temperature for 3 hours, there was extracted with EtOAc (3 × 50 mL) and washed with water, brine and dried over Na₂SO₄. The reaction was evaporated to small volume and the residue was purified by silica chromatography, eluting with hexane to give **3b** 0.47 g (1.74 mmol, 92%) as a yellow solid. ¹H NMR (400 MHz, CDCl₃) δ ppm 6.95 (s, 2H), 3.98 (t, *J* = 6.5 Hz, 4H), 3.33 (s, 2H), 1.82 – 1.75 (m, 4H), 1.56 – 1.47 (m, 4H), 0.97 (t, *J* = 7.4 Hz, 6H).

2.5.5 Preparation PAEs (**4cb-4jb**) from dihalide monomers (**2c-2j**) and 1,4-dibutoxy-2,5-diethynylbenzene monomer (**3b**)

Table 3.9 PAE substrate scope

General procedure for polymerization of aryl diiodides coupling with aryl diethynes (procedure D): A sealed tube with a magnetic bar was introduced with aryl diiodides (1 equiv.), aryl diethynes (1.01 equiv.), Pd/CaCO₃ (0.10 equiv.), CuI (0.20 equiv.), PPh₃ (0.20 equiv.) and added with the mixture of DIPEA and THF at ratio of 1:2. The concentration of the mixture was fixed at 0.05 M. All reactions were carried out under N₂ atmosphere at 80 °C for 20 hours. After cooling the reaction to room temperature, the reaction mixture was then filtered through a cotton wool and washed with CH₂Cl₂ several times until disappearance of the emissive polymer solution which could be checked under black light. The filtrate was evaporated under vacuum and then dissolved again with 1-2 mL of CH₂Cl₂, followed by dropping into 150 mL of cold MeOH. The precipitated solid was collected by centrifuge, washed repeatedly with MeOH and evaporated under vacuum to obtain desired PAEs in corresponding yields. After that, the desired polymers were characterized by ¹H-, ¹³C-NMR spectroscopy, FT-IR and were further measured the molecular weight (M_w and M_n) and polydispersity index (PDI) by gel permeation chromatography (GPC).

PAE (4db): Synthesis as declared in procedure D, using **2d** (100 mg, 0.18 mmol), **3b** (48.67 mg, 0.18 mmol), Pd/CaCO₃ (38.48 mg, 0.018 mmol), CuI (6.86 mg, 0.036 mmol), PPh₃ (9.44 mg, 0.036 mmol), DIPEA (1.2 mL) and THF (2.4 mL) to afford

94 mg (0.16 mmol, 91%) of **4db** as an orange-yellow solid. GPC (vs. polystyrene standards in THF): $M_w = 20375$, $M_n = 9828$, PDI = 2.2, $DP_n = 36$, $^1\text{H NMR}$ (400 MHz, CDCl_3) δ ppm 7.03 (br, 2H), 4.34 (br, 2H), 4.14 (br, 2H), 4.07 (br, 2H), 2.18 (br, 2H), 2.05 (br, 3H), 1.83 (br, 2H), 1.56 (br, 2H), 1.00 (br, 3H). $^{13}\text{C NMR}$ (101 MHz, CDCl_3) δ ppm 170.74, 153.45, 153.16, 117.40, 117.11, 114.48, 114.42, 91.02, 69.24, 66.05, 61.11, 31.26, 28.65, 20.74, 19.11, 13.77.

PAE (4eb): Synthesis as declared in procedure D, using **2e** (100 mg, 0.18 mmol), **3b** (48.89 mg, 0.18 mmol), Pd/CaCO₃ (38.48 mg, 0.018 mmol), CuI (6.86 mg, 0.036 mmol), PPh₃ (9.44 mg, 0.036 mmol), DIPEA (1.2 mL) and THF (2.4 mL) to afford 100.31 mg (0.17 mmol, 96%) of **4eb** as a bright-yellow solid. GPC (vs. polystyrene standards in THF): $M_w = 32637$, $M_n = 15058$, PDI = 2.10, $DP_n = 56$, $^1\text{H NMR}$ (400 MHz, CDCl_3) δ ppm 7.06 (br, 1H), 7.01 (br, 1H), 4.24 (br, 2H), 4.05 (br, 2H), 3.92 (br, 2H), 3.79 (br, 2H), 3.53 (br, 2H), 3.36 (br, 3H), 1.84 (br, 2H), 1.57 (br, 2H), 1.00 (br, 3H). $^{13}\text{C NMR}$ (101 MHz, CDCl_3) δ ppm 153.48, 153.41, 132.01, 131.91, 128.39, 128.27, 117.95, 117.20, 91.60, 91.21, 71.91, 70.90, 69.58, 69.34, 63.48, 58.87, 31.28, 19.11, 13.77. FTIR (neat, cm^{-1}) 2929, 2869, 2196, 1423, 1205.

PAE (4fb): Synthesis according to procedure D, using **2f** (50 mg, 0.12 mmol), **3b** (33.64 mg, 0.12 mmol), Pd/CaCO₃ (26.51 mg, 0.012 mmol), CuI (4.74 mg, 0.024 mmol), PPh₃ (6.54 mg, 0.024 mmol), DIPEA (0.8 mL) and THF (1.6 mL) to afford 50.27 mg (0.11 mmol, 97%) of **4fb** as a yellowish-orange solid. GPC (vs. polystyrene standards in THF): $M_w = 6184$, $M_n = 4110$, PDI = 1.5, $DP_n = 15$, $^1\text{H NMR}$ (400 MHz, CDCl_3) δ ppm 7.01 (br, 1H), 4.01 (br, 2H), 1.82 (br, 2H), 1.55 (br, 2H), 1.00 (br, 3H). $^{13}\text{C NMR}$ (101 MHz, CDCl_3) δ ppm 154.91, 154.23, 147.56, 145.07, 117.62, 117.34, 113.42, 106.09, 99.78, 98.28, 79.77, 69.51, 31.22, 19.17, 13.82.

PAE (4gb): Synthesis according to procedure D, using **2g** (100 mg, 0.19 mmol), **3b** (50.89 mg, 0.19 mmol), Pd/CaCO₃ (40.62 mg, 0.019 mmol), CuI (7.24 mg, 0.038 mmol), PPh₃ (9.96 mg, 0.038 mmol), DIPEA (1.3 mL) and THF (2.6 mL) to afford 96.27 mg (0.18 mmol, 93%) of **4gb** as a yellow solid. GPC (vs. polystyrene standards in THF): $M_w = 43741$, $M_n = 15677$, PDI = 2.8, $DP_n = 80$, $^1\text{H NMR}$ (400 MHz, CDCl_3) δ ppm

8.28 (br, 1H), 7.67 (br, 1H), 7.38 (br, 1H), 7.11 (br, 1H), 4.30 (br, 2H), 4.12 (br, 2H), 1.90 (br, 2H), 1.61 (d, $J = 30.6$ Hz, 4H), 1.25 (br, 10H), 1.07 (br, 6H), 0.87 (br, 3H). ^{13}C NMR (101 MHz, CDCl_3) δ ppm 153.50, 140.31, 129.66, 123.85, 122.42, 117.78, 116.99, 114.09, 108.84, 95.87, 84.47, 69.37, 43.22, 31.59, 31.34, 29.15, 28.98, 28.81, 27.11, 22.42, 19.20, 13.87, 13.83. FTIR (neat, cm^{-1}) 2952, 2923, 2866, 2196, 1592, 1477, 1205.

PAE (4hb): Synthesis according to procedure D, using **2h** (50 mg, 0.15 mmol), **3b** (40.24 mg, 0.15 mmol), Pd/CaCO₃ (31.60 mg, 0.015 mmol), CuI (5.64 mg, 0.03 mmol), PPh₃ (7.74 mg, 0.03 mmol), DIPEA (1 mL) and THF (2 mL) to afford 51.27 mg (0.15 mmol, 99%) of **4hb** as a bright green solid. GPC (vs. polystyrene standards in THF): $M_w = 44211$, $M_n = 17303$, PDI = 2.6, $DP_n = 127$, ^1H NMR (400 MHz, CDCl_3) δ ppm 7.16 (br, 1H), 6.99 (br, 1H), 4.04 (br, 2H), 1.84 (br, 2H), 1.58 (br, 2H), 1.02 (br, 3H). ^{13}C NMR (101 MHz, CDCl_3) δ ppm 153.56, 131.71, 124.87, 116.43, 113.70, 90.91, 87.85, 69.31, 31.17, 19.13, 13.73. FTIR (neat, cm^{-1}) 2955, 2926, 2866, 2190, 1717, 1595, 1489, 1211.

PAE (4ib): Synthesis as declared in procedure D, using **2i** (50 mg, 0.15 mmol), **3b** (41.72 mg, 0.15 mmol), Pd/CaCO₃ (32.93 mg, 0.015 mmol), CuI (5.86 mg, 0.03 mmol), PPh₃ (8.07 mg, 0.03 mmol), DIPEA (1 mL) and THF (2 mL) to afford 65.58 mg (0.15 mmol, >99%) of **4ib** as a yellow solid. GPC (vs. polystyrene standards in THF): $M_w = 18882$, $M_n = 4959$, PDI = 3.8, $DP_n = 44$, ^1H NMR (400 MHz, CDCl_3) δ ppm 7.82 – 7.38 (br, 3H), 6.99 (br, 1H), 3.95 (br, 4H), 1.82 (br, 2H), 1.54 (br, 2H), 1.00 (br, 3H). ^{13}C NMR (101 MHz, CDCl_3) δ ppm 154.68, 153.37, 145.37, 142.68, 140.80, 139.95, 131.90, 130.57, 129.99, 127.98, 121.25, 120.90, 119.72, 117.58, 116.78, 96.06, 86.16, 69.33, 36.43, 31.00, 19.01, 13.67. FTIR (neat, cm^{-1}) 2955, 2926, 2869, 2204, 1715, 1595, 1495, 1211.

PAE (4jb): Synthesis according to procedure D, using **2j** (50 mg, 0.16 mmol), **3b** (42.99 mg, 0.16 mmol), Pd/CaCO₃ (34.12 mg, 0.016 mmol), CuI (6.24 mg, 0.032 mmol), PPh₃ (8.46 mg, 0.032 mmol), DIPEA (1 mL) and THF (2 mL) to afford 59.27 mg (0.14 mmol, 88%) of **4jb** as an orange solid. GPC (vs. polystyrene standards in THF): $M_w = 7719$, $M_n = 3212$, PDI = 2.4, $DP_n = 19$, ^1H NMR (400 MHz, CDCl_3) δ ppm 7.78 (br,

1H), 7.63 (br, 1H), 7.50 (br, 1H), 6.99 (br, 1H), 4.01 (br, 2H), 1.83 (br, 2H), 1.56 (br, 2H), 1.01 (br, 3H). ^{13}C NMR (101 MHz, CDCl_3) δ ppm 191.38, 154.85, 153.47, 142.71, 142.45, 137.67, 137.18, 127.57, 127.33, 121.81, 120.43, 120.27, 117.53, 116.78, 93.92, 87.96, 69.37, 31.08, 19.02, 13.70. FTIR (neat, cm^{-1}) 2957, 2929, 2869, 2201, 1715, 1594, 1214.

Table 3.10 Photophysical properties and color appearance of PAEs **4aa-4jb**



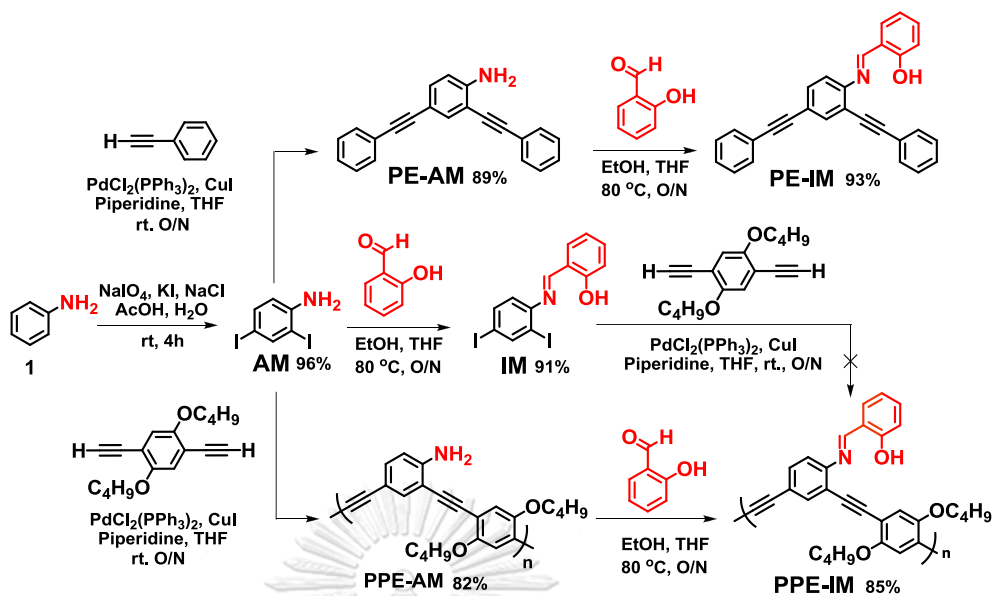
CHAPTER III

RESULTS AND DISCUSSION

3.1 Fluorescence turn-on sensor based on imine Schiff base-functionalized poly(phenyleneethynylene) (PPE-IM) for ferric ion (Fe^{3+}) detection (Part A)

3.1.1 Synthesis and characterization of PE-AM, PE-IM, PPE-AM and PPE-IM

As mentioned in the previous section, a dark background is a prerequisite for successful construction of a turn-on fluorescence sensor. Among known receptors, salicylaldimine is widely adopted for fluorescence signal quenching through either C=N isomerization or ESTPT behavior [121]. Herein, we introduced salicylaldimine, also called Schiff base, as a metal receptor that is attached to small acetylenic molecule (**PE-IM**) as well as on polymer backbone of PAEs (**PPE-IM**). The synthetic routes of **PE-IM** and **PPE-IM** are depicted in Scheme 3.1. The model compound **PE-IM** was prepared in high yield from diiodoaniline (**AM**) via two straightforward steps. The Sonogashira coupling reaction between **AM** with phenylacetylene gave **PE-AM** followed by the condensation with salicylaldehyde to yield the desired **PE-IM**. For the synthesis of **PPE-IM**, our initial attempt to condense **AM** with salicylaldehyde led to a hydrolytically unstable imine, **IM**. [122] Moreover, an attempt to polymerize **IM** into **PPE-IM** gave polymeric material with only low degree of polymerization. This is probably due to strong chelation of salicylaldimine to Pd species. [123, 124] Fortunately, **PPE-IM** could be obtained via post-polymerization functionalization (PPF) of **PPE-AM** via condensation with salicylaldehyde. All new compounds were characterized by ^1H , ^{13}C NMR spectroscopy, FTIR spectroscopy, MALDI-TOF mass spectrometry and gel permeation chromatography.



Scheme 3.1 Synthetic procedures of PE-IM and PPE-IM

The ^1H NMR spectra of small molecules (**PE-AM**, **PE-IM**) and polymer (**PPE-AM** and **PPE-IM**) are shown in Figure 3.1. Signals can be assigned to all protons in each corresponding structure. For amine derivatives, the broaden singlet signal of amine proton were appeared at around 5.57 (**PE-AM**) and 4.76 (**PPE-AM**) ppm. After reacting both amine compounds with salicylaldehyde, the conversion of amine ($-\text{NH}_2$) into imine ($-\text{HC}=\text{N}-$) resulted in complete disappearance of the amine protons around 5.0 ppm (peak g in **PE-IM** and peak j in **PPE-IM**). This result indicated an efficient imine formation in **PE-IM** and **PPE-IM**. Surprisingly, the characteristic phenolic proton ($-\text{OH}$) of **PE-IM** appeared as one singlet signal at 13.51 ppm, whereas **PPE-IM** showed two singlet peaks of those phenolic protons at 13.44 and 12.83 ppm. We reasoned that both peaks correspond to the intramolecular H-bonding interaction between N atom on $\text{C}=\text{N}$ of **PPE-IM** in head-head and head-tail forms (Figure 3.2). This could be supported by peak disappearance upon the addition of $\text{MeOH-}d_6$ into **PPE-IM** dissolved in CDCl_3 suggesting that both peaks are exchangeable proton.

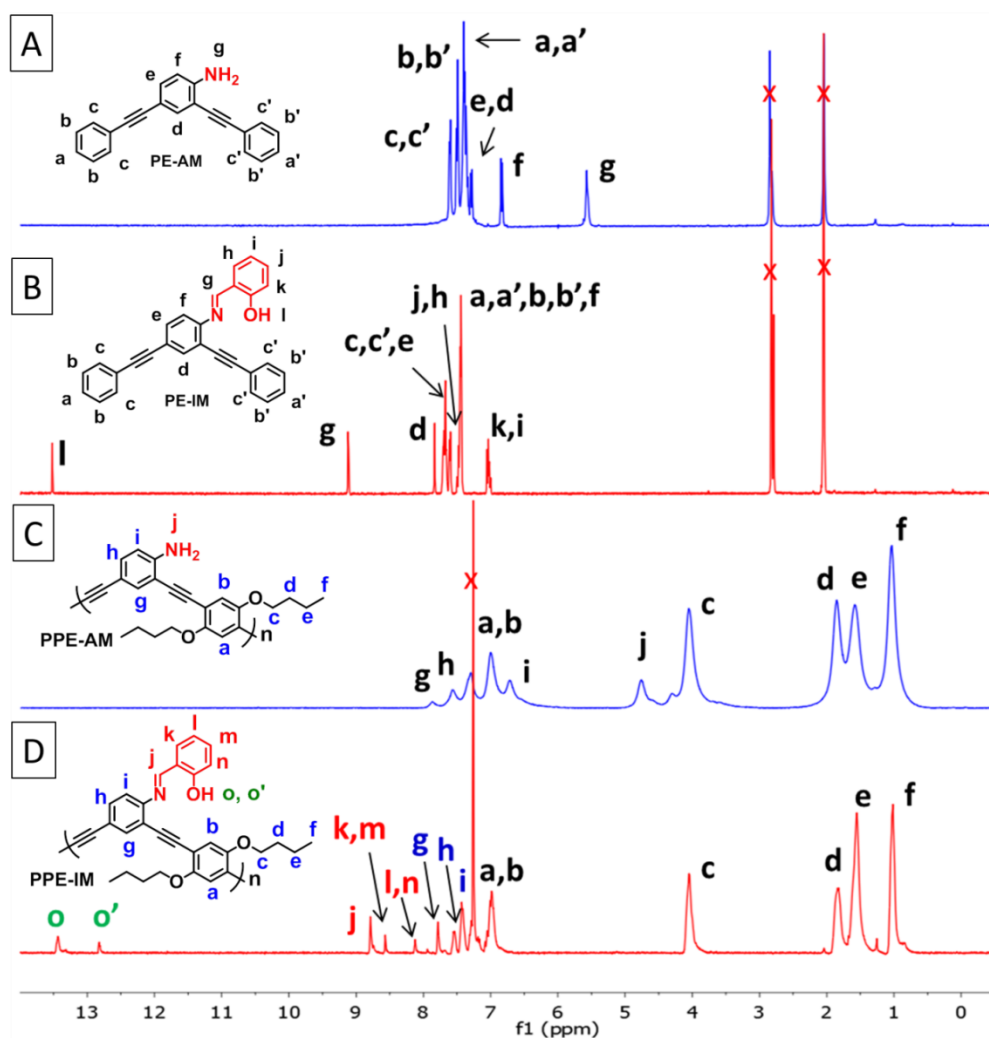


Figure 3.1 ^1H NMR spectra of compounds A) PE-AM B) PE-IM in acetone- d_6 C) PPE-AM and D) PPE-IM in CDCl_3 .

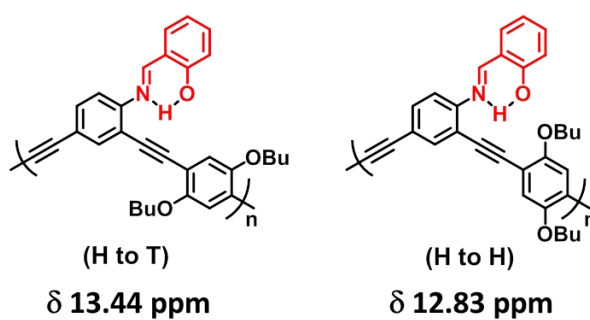


Figure 3.2 Structure of PPE-IM in head- tail (left) and head- head (right) forms.

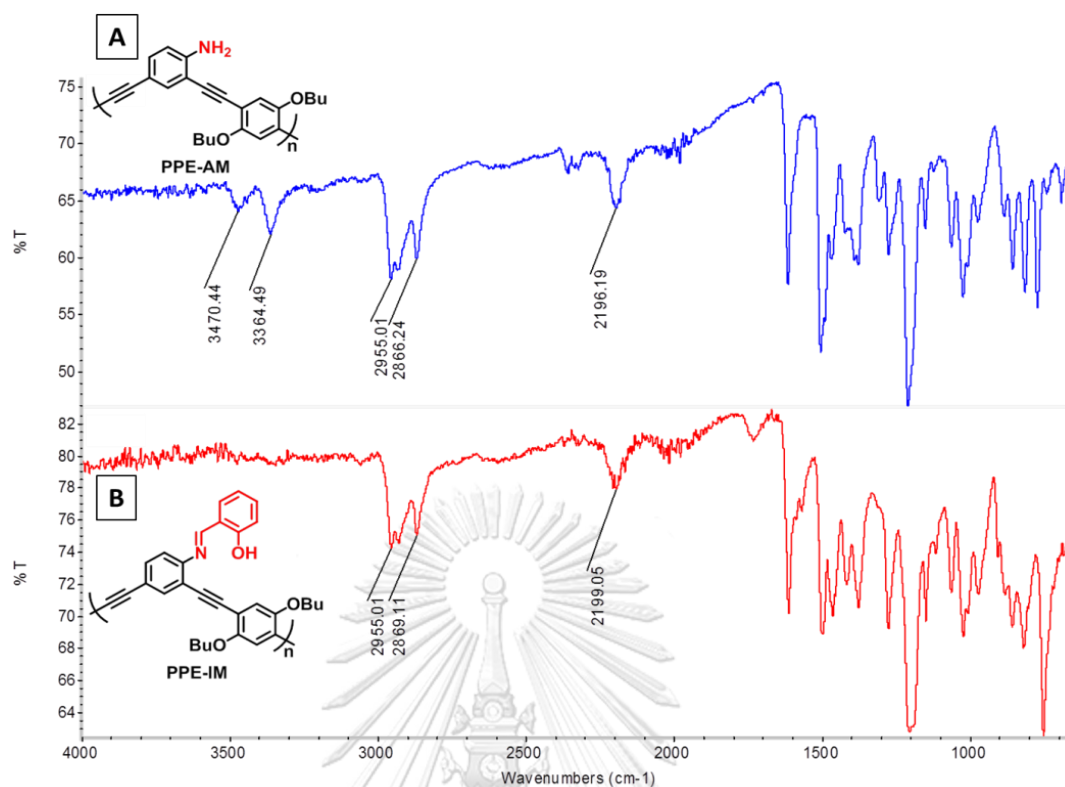


Figure 3.3 FT-IR spectra of compounds A) PPE-AM and B) PPE-IM.

In addition, IR data was in good agreement with expected structure from other reports [125, 126] (Figure 3.3). These findings indicated that carbon triple bond appeared as a broad peak at 2199 cm⁻¹, a signal corresponding to polymer formation. Conversion of PPE-AM into PPE-IM is clearly confirmed by IR spectrum. The N-H stretching of amine group in PPE-AM (Figure 3.3A) at 3,470 and 3,365 cm⁻¹ disappeared when compared to PPE-IM (Figure 3.3B). Further confirmation was provided by GPC data (Figure 3.4), upon observation of the molecular weight of PPE-IM ($M_w = 8455$ Da.) which is proportional to 100% imine post-functionalization of PPE-AM ($M_w = 6253$ Da.) From these evidences, it is possible that entire imine based-polymer was proficiently prepared.

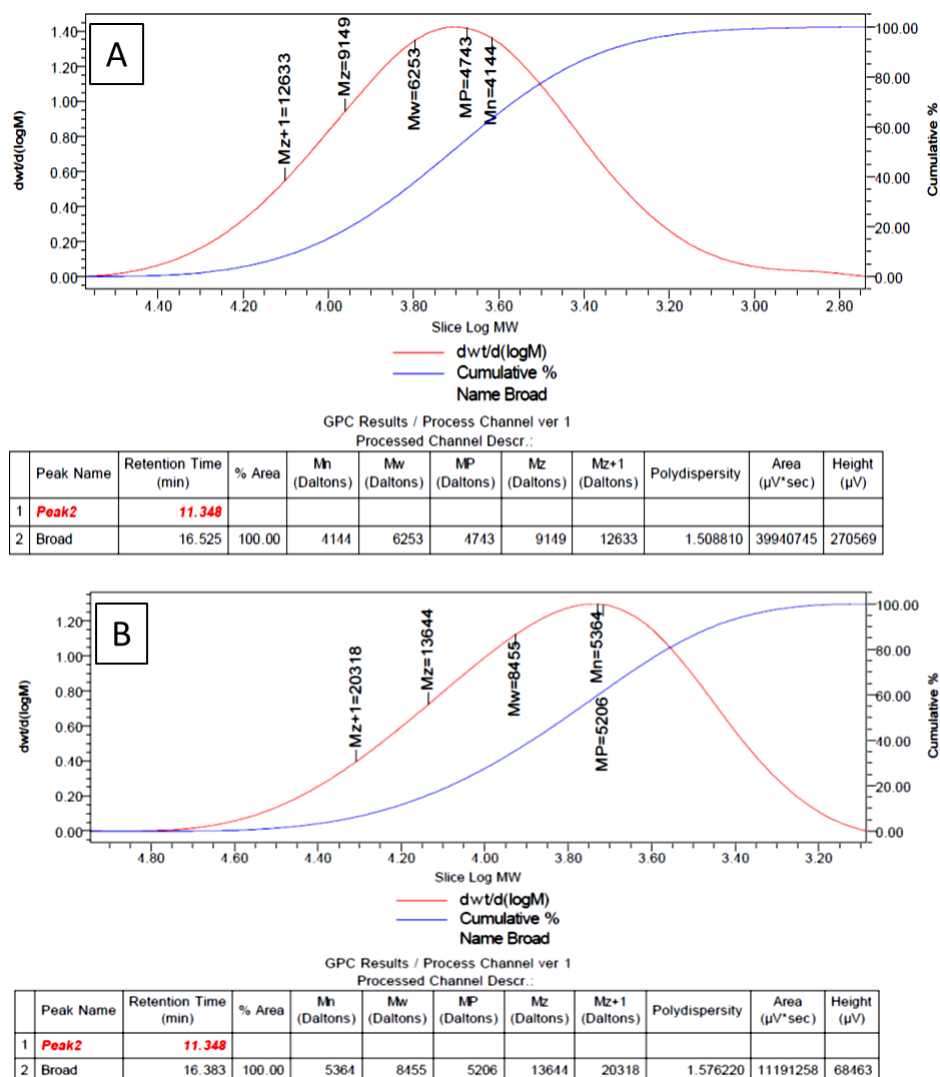


Figure 3.4 GPC data of compounds A) PPE-AM and B) PPE-IM

3.1.2 Photophysical properties of PE-AM, PE-IM, PPE-AM and PPE-IM

The absorption and emission of small molecules (PE-AM, PE-IM) fluorophores were studied in acetone, while the absorption and emission of polymers (PPE-AM, PPE-IM) were conducted in THF. The UV-vis absorption and fluorescence spectra are shown in Figure 3.5 and the photophysical properties are summarized in Table 3.1.

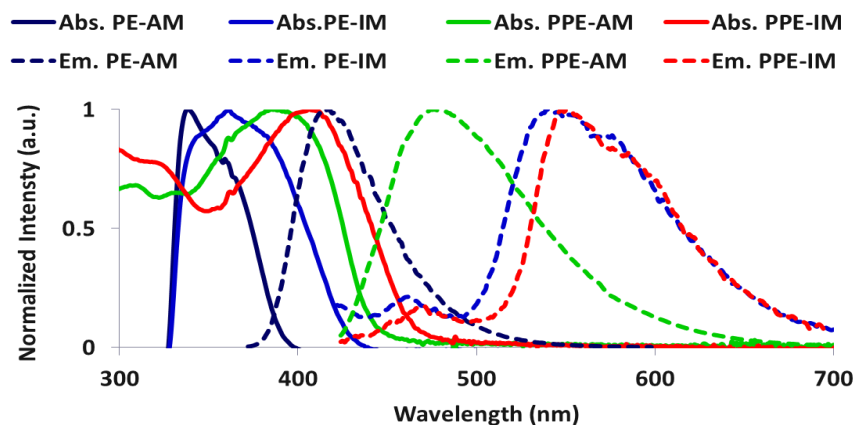


Figure 3.5 Normalized spectra of absorption and emission of PE-AM, PE-IM, PPE-AM and PPE-IM.

Comparing PE-AM and PPE-AM, the amine-containing polymer (PPE-AM) have longer absorption and emission maxima by ~ 60 nm (Table 3.1). This behavior can be attributed to an increase in π conjugation system from small molecule into conjugate polymer. As expected, both imine derivatives (PE-IM and PPE-IM) exhibited a red-shift of spectrum with weak fluorescent quantum yields ($\Phi_f = 0.001$ and 0.003). The low quantum yield of imine derivatives in comparison with amines is caused by the combination of ESIPT and C=N isomerization processes. In the emission spectra of imine derivatives (PE-IM and PPE-IM), two strong emission bands were observed. The former band around 469 nm in PE-IM and PPE-IM corresponds to normal tautomer (enol species) while the latter band around 545 nm is caused by ESIPT mechanism from the salicylaldimine Schiff bases. It involves the shifting of proton in excited state of normal tautomer into excited state of keto tautomer resulting in large Stokes shift values as large as 140-180 nm [127].

Table 3.1 Photophysical properties of PE-AM, PE-IM, PPE-AM and PPE-IM

Cmpd.	Absorption		Emission		Stokes' shift
	λ_{\max} (nm)	Log ϵ	λ_{\max} (nm)	Φ_f (%) ^c	
PE-AM	339 ^a , 341 ^b	4.22 ^a	417 ^a , 413 ^b	0.21 ^{a,b}	78 ^a , 72 ^b
PE-IM	360 ^a	4.26 ^a	469, 546 ^a	0.001 ^a	180
PPE-AM	385 ^b	4.10	474 ^b	0.32 ^b	89
PPE-IM	405 ^b	4.28	467, 545 ^b	0.003 ^b	140

^aDissolved in acetone, ^bDissolved in THF, ^cQuinine sulfate in 0.1 M H₂SO₄ ($\Phi_f = 0.54$) was used as the reference.

In general, the imine bonds are easily hydrolyzed under aqueous or acidic condition. Consequently, we next examined the stability of those low emissive imine fluorophores **PE-IM** compared to **PPE-IM**.

3.1.3 Molecular stability of imine sensors (**PE-IM**, **PPE-IM**)

In this section, we compared the stability between small molecule **PE-IM** and polymer **PPE-IM**. Both compounds were dissolved in 10% milliQ water/THF and the fluorescence intensity were monitored (Figure 3.6). We found that fluorescence intensity of **PE-IM** was gradually shifted and increased from 546 to 415 nm along with an increase in bright blue appearance. This indicates that the imine bond was cleaved and turned it back to original **PE-AM**. Whereas **PPE-IM** remained dark background without any fluorescence change at 475 nm under the identical condition (Figure 3.6A and C). It is interesting to note that even using 90% mixture of milliQ in THF, the fluorescent intensity of **PPE-IM** was still the same demonstrating that the polymeric imine is stable and can be used as a chemodosensor in an aqueous system whilst the use of **PE-IM** generate a false response in an aqueous media.

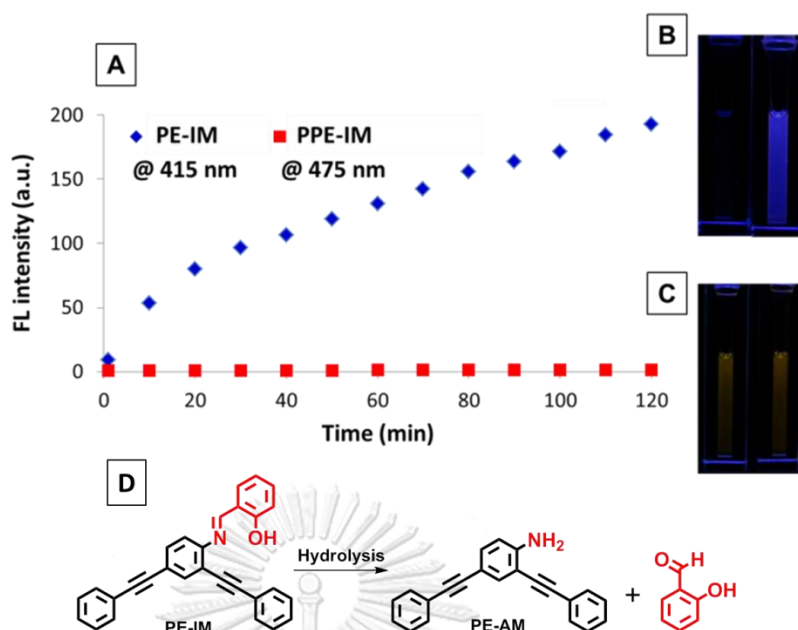


Figure 3.6 A) FL changes of PE-IM (25 μM) and PPE-IM (25 μM) in 10%milliQ water/THF with increasing time (0-120 min). Appearance images of B) PE-IM and C) PPE-IM at 0 min and 120 min, respectively. D) Schematic presentation of hydrolysis process of PE-IM.

Furthermore, the tolerance of imine-based polymer (PPE-IM) was also investigated by varying pH values of system from 4 to 8. It did not show any fluorescent change. We therefore found that such Schiff base polymer not only show the high stability in neutral pH but also in wide range of pH values (Figure 3.7).

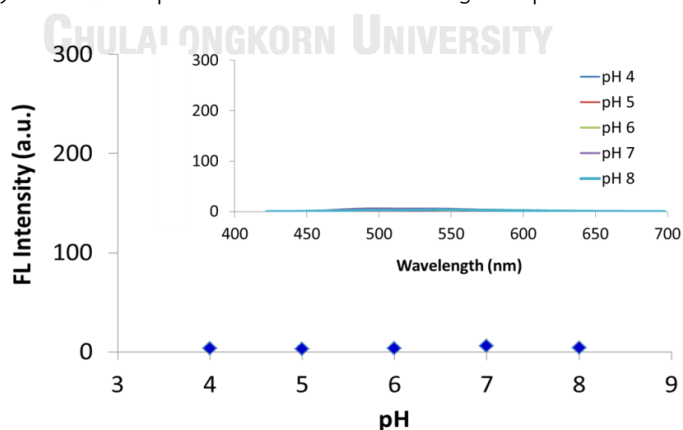


Figure 3.7 FL intensity of PPE-IM ($\lambda_{\text{em}} = 475 \text{ nm}$) (25 μM) in 10%MilliQ pH 4-8/THF in 120 min. ($\lambda_{\text{ex}} = 410 \text{ nm}$)

3.1.4 Fluorescence studies of PPE-IM toward Fe^{3+} ion and other metal ions.

The metal sensing ability of **PPE-IM** was investigated in 10%milliQ water/THF by addition of 5.0 equiv. of various metal ions (Li^+ , Na^+ , K^+ , Ag^+ , Mg^{2+} , Ca^{2+} , Co^{2+} , Ni^{2+} , Cu^{2+} , Zn^{2+} , Cd^{2+} , Ba^{2+} , Hg^{2+} , Pb^{2+} , Fe^{2+} , Fe^{3+} , Al^{3+} and Cr^{3+}). In fluorescence measurement, the addition of Fe^{3+} (125 μM) led to significant fluorescence enhancement with the change ratio around 300-fold in 30 min (Figure 3.8B). Also, the mixing solution (**PPE-IM** + Fe^{3+}) showed clearly bright blue luminescence light at $\lambda_{\text{em}} \approx 476$ nm which was blue-shifted by 69 nm from virgin **PPE-IM** (Figure 3.8C). For other metal ions treatment, the fluorescence intensity remains almost unchanged, except Al^{3+} , it slightly increased with the change ratio $I/I_0 = 17$. From time dependent study, fluorescence enhancement the signaling that treated with Fe^{3+} showed quite absolute increase within 55 min (Figure 3.9), resulting the quantum efficiency expanded from $\Phi_f = 0.003$ to $\Phi_f = 0.38$.

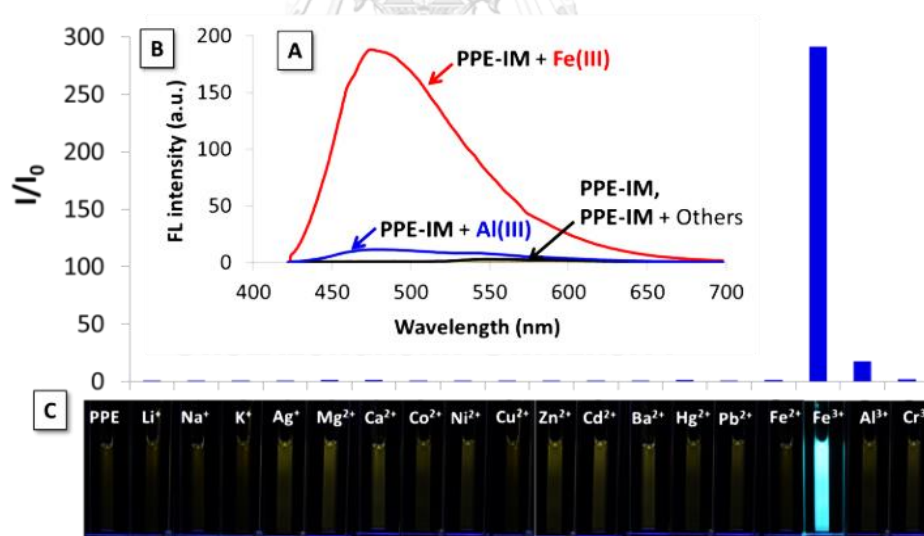


Figure 3.8 A) Fluorescent spectra of **PPE-IM** (25 μM) upon the addition of various metal ions (5 equiv.) in 10%milliQ water/THF. B) Change ratio (I/I_0) of FL intensity of **PPE-IM** (25 μM) in 10%milliQ water/THF containing various metal ions (5.0 equiv.). C) Fluorescent images of **PPE-IM** in the presence of different cations. The spectra were obtained after 30 min with $\lambda_{\text{ex}} = 410$ nm.

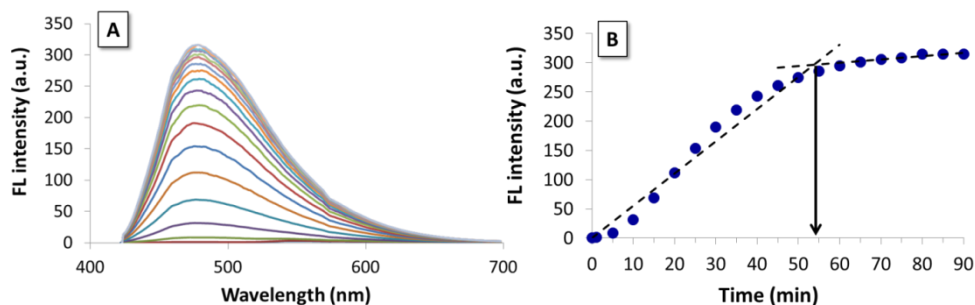


Figure 3.9 A) Fluorescent spectra of PPE-IM (25 μM) upon addition of Fe³⁺ (125 μM) in 10% milliQ water/THF with increasing time (0 – 90 min), B) Plots of intensity versus time after added Fe³⁺.

For quantitative analysis, the titration of Fe³⁺ at variable concentration was performed and the fluorescence emission was measured at 60 min to ensure the signal saturation. The fluorescent intensity increased almost linearly with the increasing Fe³⁺ concentration up to 5 equiv. (Figure 3.10A). To determine the detection limit of PPE-IM in 10% milliQ water/THF for Fe³⁺, a good linear response was obtained in micromolar range of Fe³⁺ around 2-12 μM (Figure 3.10B). The detection limit at three-fold standard deviation of the fluorescence obtained from a blank sample (PPE-IM) in the absence of Fe³⁺ ($3\sigma/K$) (σ : standard deviation, K: slope of the calibration plot) [128] was evaluated to be 0.14 μM. (Figure 3.10B inset).

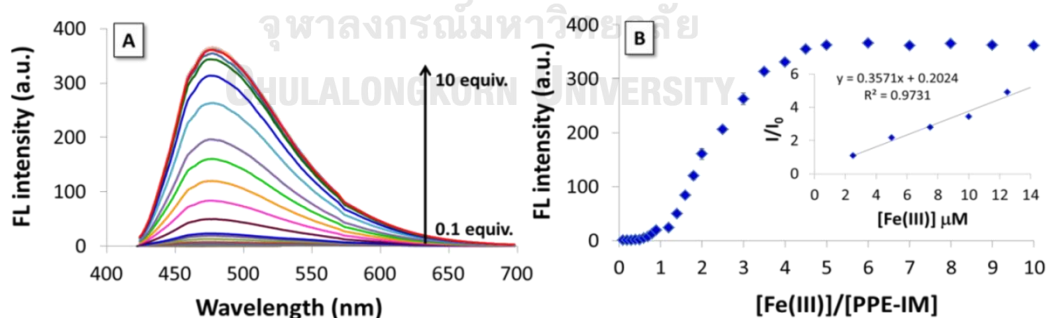


Figure 3.10 A) and B) Fluorescence titration ($\lambda_{\text{ex}} = 410 \text{ nm}$) of PPE-IM (25 μM) upon addition of difference concentration of Fe³⁺ in 10% milliQ water/THF. The inset shows the calibration curves of ratio of PPE-IM to Fe³⁺ concentration. Each spectrum was obtained after 60 min of mixing.

In addition, we would like to emphasize that the strong acidity of $\text{Fe}(\text{NO})_3$ in aqueous solution is not responsible for the hydrolysis of imine which is a possible cause of fluorescence enhancement. In our control experiment, the fluorescence increased insignificantly in the absence of $\text{Fe}(\text{NO})_3$ under the same pH (3.5) as in the presence of $\text{Fe}(\text{NO})_3$. This result strongly supports that the fluorescence enhancement of **PPE-IM** are solely from the Fe^{3+} (Figure 3.11) and our result also demonstrated the high stability of **PPE-IM** even at such high acidic condition.

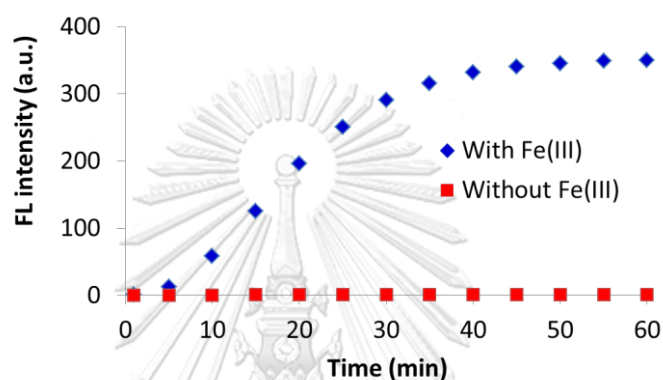


Figure 3.11 Time dependence of fluorescence intensity of **PPE-IM** ($\lambda_{\text{em}} = 475 \text{ nm}$) ($25 \mu\text{M}$) in the presence and absence of Fe^{3+} (5 equiv.) at pH 3.5. ($\lambda_{\text{ex}} = 410 \text{ nm}$)

To evaluate the interference from other metal ions, competition experiments were carried out by addition of Fe^{3+} and another metal cation (5 equiv. of Fe^{3+}) tested for interference to the **PPE-IM** solution (Figure 3.12). In the presence of other competing metal cations including Li^+ , Na^+ , K^+ , Ag^+ , Mg^{2+} , Ca^{2+} , Co^{2+} , Ni^{2+} , Cu^{2+} , Zn^{2+} , Cd^{2+} , Ba^{2+} , Pb^{2+} , Hg^{2+} , Fe^{2+} , Al^{3+} and Cr^{3+} , no significant interference was observed. The results indicate that **PPE-IM** is very selective for Fe^{3+} detection and quantification.

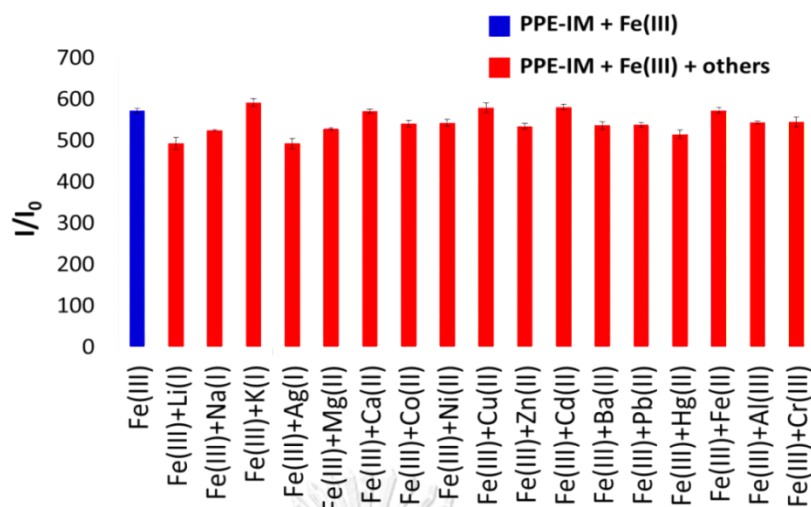


Figure 3.12 Relative fluorescence of **PPE-IM** (25 μM) in 10% milliQ water/THF in the presence of Fe^{3+} (125 μM) plus another metal ion (625 μM) tested for interference.

3.1.5 Mechanistic investigation

In order to prove the mechanism of this fluorescent turn-on phenomenon, we fully introduced the $^1\text{H-NMR}$ spectra of **PPE-IM** with and without $\text{Fe}(\text{NO}_3)_3$ which dissolved in MeOD as depicted in Figure 3.13. Upon the addition of $\text{Fe}(\text{NO}_3)_3$, imine proton signal at 8.79 ppm (j) disappeared along with the signal at 9.83 ppm (j') was developed which corresponding to proton of aldehyde functional group of salicylaldehyde molecules. Furthermore, the proton signal of aromatic region at 6.6 ppm (i) slightly emerged, indicating the possible existence of proton at *ortho*-position of aniline which substituted on **PPE-AM** structure. Unfortunately, in Figure 3.13B, both phenolic protons of **PPE-IM** and salicylaldehyde could not be revealed due to proton may be exchanged in MeOD.

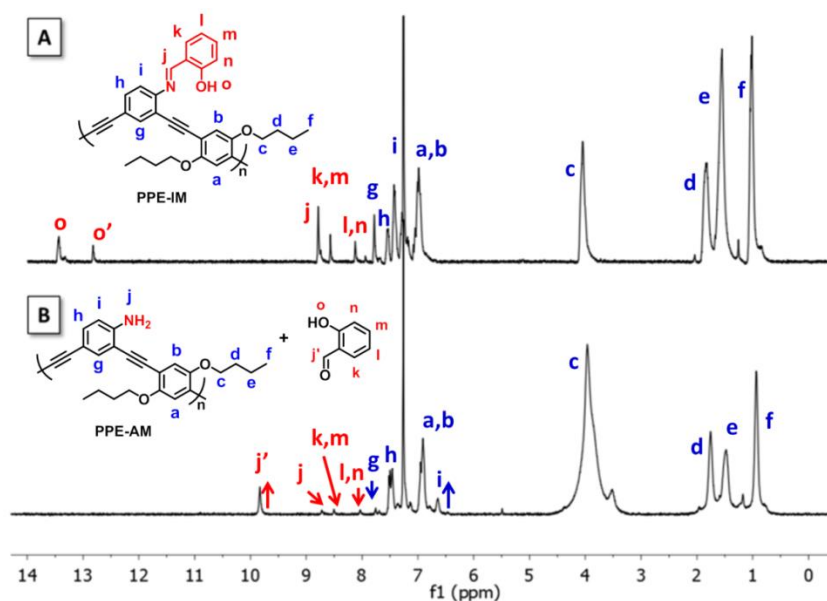


Figure 3.13 ^1H NMR of **PPE-IM** in CDCl_3 A) before and B) after addition of $\text{Fe}(\text{NO}_3)_3$ at 30 min.

In addition to the experiments above, we also monitored the reaction by UV spectroscopy. The result exhibited a new broad band at 380 nm with increasing amount of Fe^{3+} that could be assigned as the salicylaldehyde residue (Figure 3.14). These evidences indicated that irreversible binding of the Fe^{3+} ion with **PPE-IM** induced **PPE-AM** reforming. The changes could be attributed to the cleavage of imine linkage by Fe^{3+} -catalyzed though hydrolysis process.

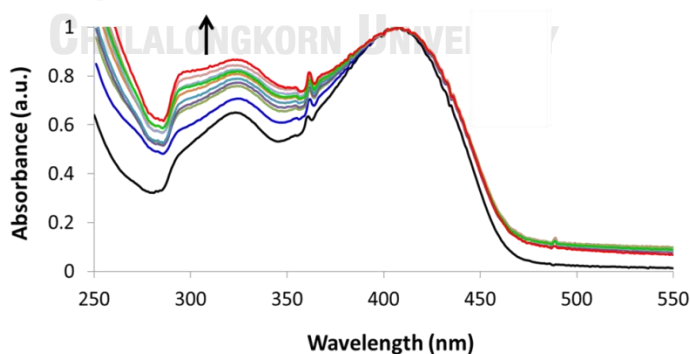


Figure 3.14 Normalized spectra of absorption of **PPE-IM** ($25 \mu\text{M}$) upon the addition of Fe^{3+} (0-5 equiv.) in $10\% \text{H}_2\text{O}/\text{THF}$. Each spectrum was measured after 60 min at room temperature.

To investigate the effect of intramolecular hydrogen bonding interaction on conformation change of our polymer, we further measured the particle size of **PPE-IM** before and after treatment with $\text{Fe}(\text{NO}_3)_3$ solution. The increase in particle size was observed upon addition of Fe^{3+} to the polymer solution (Figure 3.15). The result suggested that the hydrolysis diminished degree of self-coiling of the polymer chains as a result of hydrophobicity and intramolecular bonding reduction as illustrated in Figure 3.16.

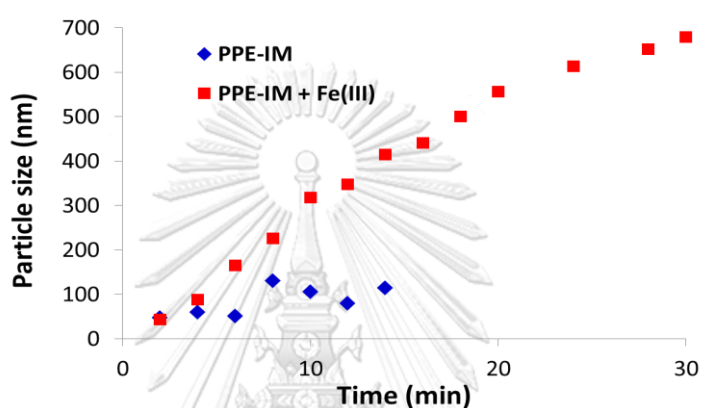


Figure 3.15 Particle size changes of **PPE-IM** ($50 \mu\text{M}$) in 10% milliQ water/THF before (blue line) and after (red line) addition of Fe^{3+} ($100 \mu\text{M}$) with increasing time

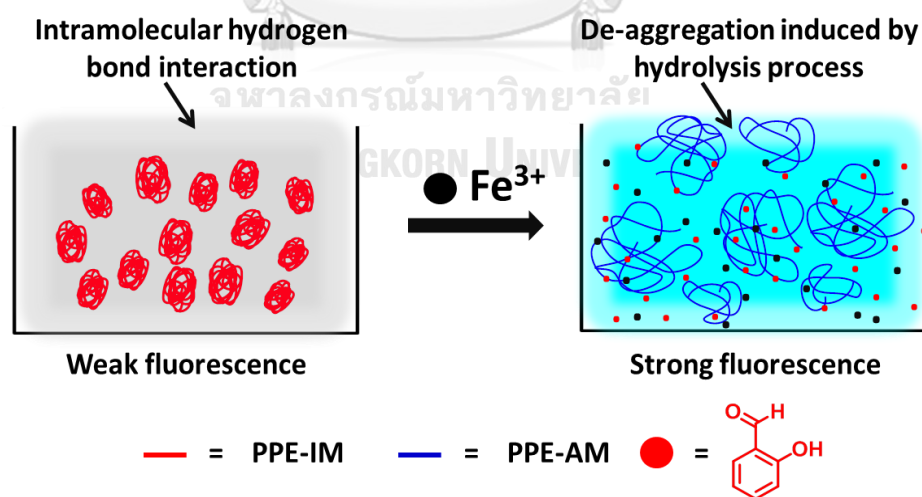


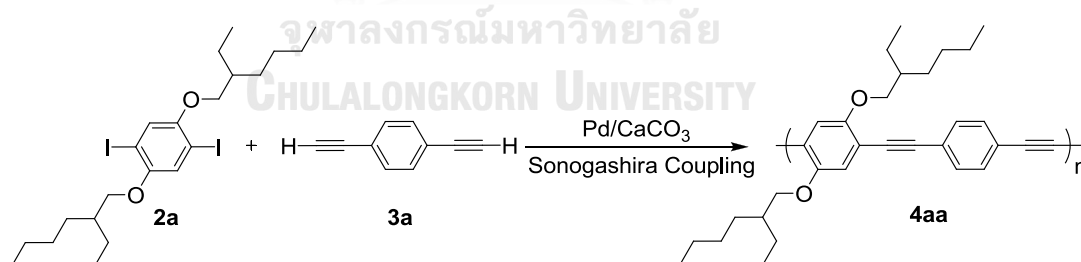
Figure 3.16 Schematic representation of the plausible behavior of the **PPE-IM** before and after treatment with Fe^{3+} .

3.2 Synthesis of highly pure poly(aryleneethynylene)s using palladium supported on calcium carbonate as eco-friendly heterogeneous catalyst (Part A)

3.2.1 Optimization of the reaction conditions

For the optimization study of Sonogashira coupling reaction using Pd/CaCO₃ as a catalyst, we decided to use aryl diiodides as a coupling partner because of its reactivity. The higher reactivity of aryl diiodides substrate compared to other aryl dihalides compounds is evident in the oxidative addition step, which is believed to be the rate determining steps in most Sonogashira coupling reactions [65]. Hence, aryl diiodides and aryl diethynes were first prepared to generate an alternating copolymer poly(aryleneethynylene)s under common Sonogashira coupling reaction. Heterogeneous Pd/CaCO₃ was used as a catalyst, in order to evaluate possibility of this process (Scheme 3.2).

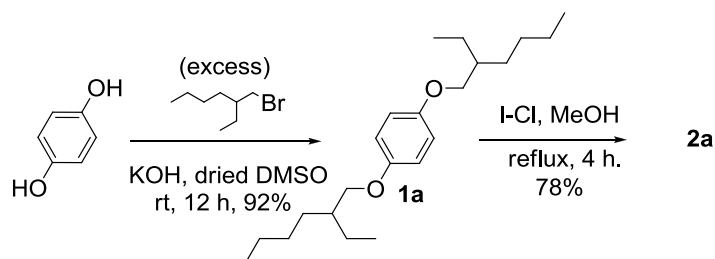
1,4-bis(2-ethylhexyloxy)-2,5-diiodobenzene (**2a**) and 1,4-diethynylbenzene (**3a**) were selected as starting monomers. The former has moderate electron donating power on the benzene ring and possesses flexible peripheral groups. Thus, corresponding polymers tend to dissolve well in various organic solvents. The latter has a rigid structure without any substituents that lead to the reduction of chain entanglement and ease of interpretation of resulting polymer.



Scheme 3.2 Synthesis of PAE **4aa**

1,4-bis(2-ethylhexyloxy)-2,5-diiodobenzene (**2a**)

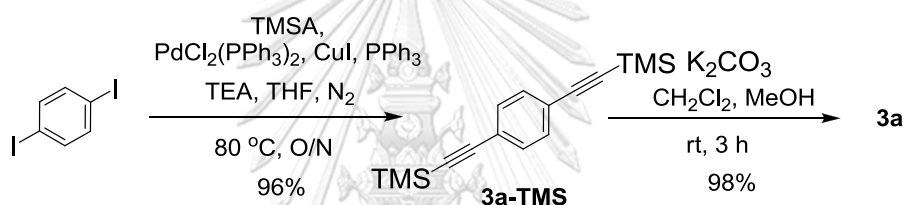
Compound **1a** was synthesized by alkylation of hydroquinone with 2-ethylhexyl bromide followed by iodination with iodine(I)chloride in methanol under reflux condition. Product **2a** was received in 78% yield as colorless oil (Scheme 3.3).



Scheme 3.3 Synthesis of compound **2a**

1,4-diethynylbenzene (**3a**)

For **3a**, we introduced 1,4-diethynylbenzene as a terminal source to diiodobenzene via Pd-catalyzed Sonogashira cross-coupling of trimethylsilylacetylene. After a base-catalyzed desilylation, the product **3a** was received in excellent yield (Scheme 3.4).



Scheme 3.4 Synthesis of compound **3a**

3.2.1.1 Effect of Catalyst loading and ligand

With the coupling partner **2a** and **3a** in hands, the amount of Pd/CaCO₃ catalyst and of ligands (Figure 3.17) were first screened under the conventional condition for Sonogashira coupling polymerization by reacting an 1:1 equivalent amount of 1,4-bis(2-ethylhexyloxy)-2,5-diiodobenzene (**2a**) and 1,4-diethynylbenzene (**3a**) in the presence of Pd/CaCO₃, CuI and ligands in mixture of DIPEA and THF. All reaction proceeded under N₂ atmosphere at 80°C for 20 h. The results were depicted in Table 3.2.

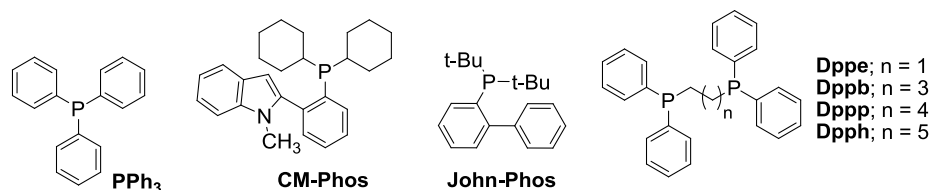
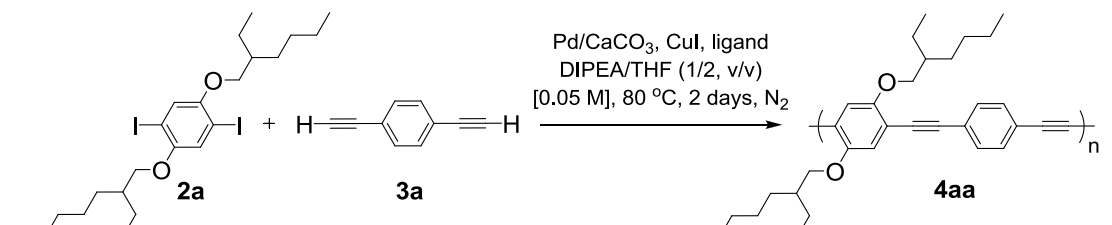


Figure 3.17 Structure of seven ligands

Table 3.2 Effect of catalyst loading and ligand


Entry	Pd (mol%)	Ligand ^a	Yield ^b (%)	M _w ^c (kDa)	DP _n ^c	PDI ^c
1 ^d	1	PPh ₃	N.A.	-	-	-
2 ^d	5	PPh ₃	N.A.	-	-	-
3	5	John-Phos	10	12.8	28	7.3
4	5	CM-Phos	N.A.	-	-	-
5	5	Dppe	N.A.	-	-	-
6	5	Dppb	84	22.0	48	3.0
7 ^d	5	Dppb	78	10.0	22	2.1
8	5	Dppp	76	21.6	47	3.5
9	5	Dpph	58	29.3	64	4.0
10 ^e	10	Dppb	90	32.1	71	3.4
11 ^e	10	PPh ₃	94	65.3	143	3.1
12 ^{d,e,f}	10	PPh ₃	N.A.	-	-	-

^a2 equiv. of Pd/CaCO₃ was used. ^bIsolated yield by single precipitation from MeOH/CH₂Cl₂, ^cDetermined by GPC, ^dPerformed at 0.2 M, ^eReaction time for 20 h, ^fNo Cul or ligands.

The results in Table 3.2 demonstrated that 1 and 5 mol% of Pd/CaCO₃ loading in the presence of PPh₃ as ligand failed to produce the polymer. Most of starting monomers **2a** remained and less emissive oligomers were observed (entries 1-2). Thus, both mono- and bidentate phosphine ligands were further examined in the hope for better activity. Among ligand testing (entries 3-9), Dppb ligand seemed to be the most active one, providing the highest polymer yield (84%), whereas

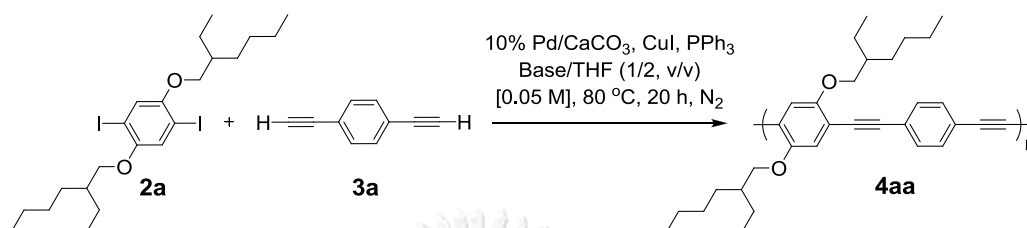
diphosphine bearing shortest linker (dppe; $n = 2$) produced clearly inferior results. This observation could be caused by the bite angle of palladium diphosphine complexes being too small. This caused a decrease in the rate of dissociation, leading to low catalytically active species (Pd^0) formation [129, 130]. Although most of these bidentate ligands possess significantly higher catalytic activities than said monodentate phosphine (entries 2-4), but they merely produced coupling polymer with modest degree of polymerization ($\text{DP}_n = 48\text{-}64$). The viscosity is too low for gravure printing [131] or electrospinning [132]. Even though substrate concentration was increased to 0.2 M, yield and molecular weight were reduced (78% yield, $\text{DP}_n = 22$). We hypothesized that dppb ligand has a high electron donating ability, therefore strong chelation is formed. As a result copper co-catalyst, whose presence is crucial for high activity catalyst used in Sonogashira coupling, is inhibited. To the best of our knowledge, the bulkiness of the phosphine ligands, which is determined by the cone angle, exerts a stronger influence on the rate determining step of oxidative additions than the electronic properties of the ligands [133, 134]. The previous report described that dppb have a lower cone angle ($\approx 130^\circ$) than traditional ligand (PPh_3) ($\approx 145^\circ$) [135]. In other words PPh_3 could be applied to enhance catalytic efficiency. In this work, we attempted to improve the polymerization efficiency and to prove that PPh_3 would be able to drive such coupling polymerization by increasing amount of Pd/CaCO_3 to 10 mol%. As shown in entry 11, it is noteworthy that the reaction was completed in 20 hours, resulting in the increase of DP_n of **4aa** up to 143. Thus, comparing the performance of several phosphines in the former Pd catalyzed reaction, PPh_3 turned out to be the most active ligand. Unfortunately, such system could not be performed without either copper or ligand (entry 12). As mentioned, we next adjusted other factors by using 10%mol of palladium catalyst and fixed concentration of 0.05 M to identify an optimal condition.

3.2.1.2 Effect of base

Rate of Pd-catalyzed coupling reactions are known to depend on the basicity of the base. A base is needed for the generation of copper acetylide by abstracting the acetylenic proton of the terminal alkyne before the transmetallation step. [65]

Hence, both organic and inorganic bases such as DIPEA, TEA, PIP, DBU, K_2CO_3 and KOH were investigated for the preparation of PAE (**4aa**). The results were summarized in Table 3.3

Table 3.3 Effect of Base



Entry	Base	Yield ^a (%)	M_w (kDa) ^b	DP ^b	PDI ^b
1	DIPEA	94	65.3	143	3.1
2 ^c	DIPEA	N.A.	-	-	-
3	TEA	92	16.6	36	2.1
4	PIP	67	7.6	17	2.1
5	DBU	100	27.8	61	2.4
6	K_2CO_3	94	21.9	48	2.3
7	KOH	N.A.	-	-	-

^aIsolated yield by single precipitation from MeOH/ CH_2Cl_2 , ^bDetermined by GPC, ^c5%v/v of DIPEA was used.

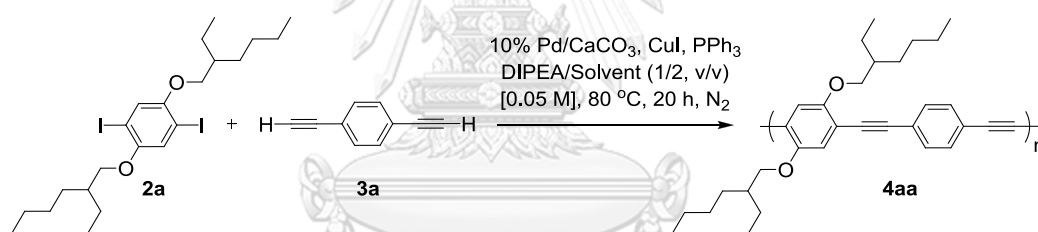
The results in Table 3.3 demonstrated that among six bases, DBU (entry 5) gave the highest yield ($\approx 100\%$) but DP_n remained low ($DP_n = 61$). It may be due to high molecular weight polymer obtained, leading to poor solubility in THF solvent which is needed for GPC analysis. Surprisingly, the result in entry 6 indicated that inorganic base (K_2CO_3) is efficient to cause complete conversion of starting material. However, low DP_n of corresponding polymer was obtained which exhibited poor dissolving of K_2CO_3 in THF. On the other hand, DIPEA proved to be the most useful in creating coupling polymer (**4aa**) in 94% yield along with the highest DP_n up to 143 (Table 3.3, entry 1). This result could be explained by the suitable basicity, leading to gradual polymerization. Notably, reducing the portion of DIPEA from 33% to 5% v/v of mixture solvent resulted in an incomplete conversion of the starting materials.

This led to an oligomer with low molecular weight formation (entry 2). Therefore, base is needed as a mixed solvent. Such system provides catalyst stabilizing effect of highly polar solvent as well as help to increase polymer dissolution. This led to higher yield of high molecular weight polymers [136].

3.2.1.3 Effect of solvent

Our next goal was to identify a suitable solvent which can accelerate the reaction at good rate. In the polymerization process, the appropriate solvent clearly plays an important role not only dissolve starting monomers and stabilize the catalyst but it must also maintain the growing polymer in solution for as long as possible in order to achieve high molecular weight. The further optimization investigation was carried out to determine types of solvents for polymerization were represented in Table 3.4.

Table 3.4 Effect of solvent



Entry	Solvent	Yield ^a (%)	M _w (kDa) ^b	DP ^b	PDI ^b
1	Toluene	88	16.1	35	2.0
2	CHCl ₃	NA	-	-	-
3	THF	94	65.3	143	3.1
4 ^c	-	78	18.0	40	2.4
5	DMF	70	22.4	49	2.3
6	MeCN	48	10.8	24	4.1
7	EtOH	19	11.3	25	1.3

^aIsolated yield by single precipitation from MeOH/ CH₂Cl₂, ^bDetermined by GPC,

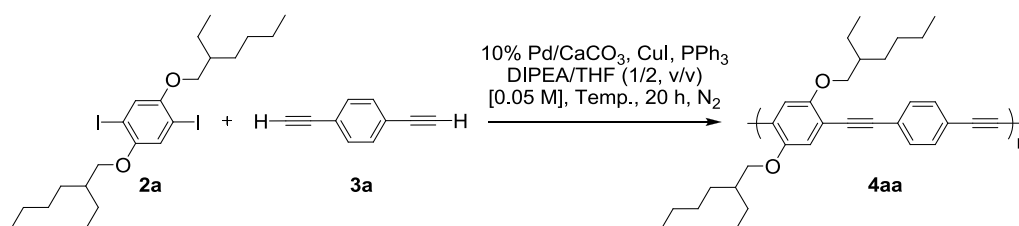
^cDIPEA was used as solvent.

Typically, the solvents employed in Sonogashira coupling polymerization vary as widely as those used in small molecule couplings, including toluene, chloroform,

THF, DMF, MeCN, and EtOH. Typically, polar solvents such as THF and DMF usually act as great solvents which led to a well dispersing Pd catalyst and likewise ensure enough solubility for the polymerizations. Even though, DMF was known to stabilize Pd catalysts [137], a modest yield with low molecular weight polymer was obtained (entry 5). Similarly, non-polar and highly polar solvents were introduced (entries 1, 6 and 7) which may be explained by the poor dispersion of the catalyst, resulting in an aggregation of the catalyst in the reaction system. In addition, the solubility of the polymer was also taken into consideration. We found some residues precipitated out from the reaction medium, which lower the molecular weight. The polymer prepared from THF gave the highest yield (94%) and degree of polymerization ($DP_n = 143$) (entry 3). The result could be attributed to the higher solubility of the polymer in THF than that in the others. In general, the reaction medium must be basic in order to neutralize the hydrogen halide produced as a by-product of this coupling reaction. [90] Hence, carrying the reaction in the absence of solvent was studied (entry 4). As expected, incomplete reaction and low molecular weight polymers were observed. As a result, therefore, THF was selected as the most appropriate solvent.

3.2.1.4 Effect of reaction temperature

With the optimum base (DIPEA) and solvent (THF) in hand, we examined the reaction temperature by carrying out the reaction under ambient temperature as well as at 80 and 120 °C as demonstrated in Table 3.5.

Table 3.5 Effect of reaction temperature

Entry	Temp (°C)	Yield ^a (%)	M _w (kDa) ^b	DP ^b	PDI ^b
1	RT	75	9.1	21	2.1
2	80	94	65.3	143	3.1
3	120	58	21.5	47	4.0

^aIsolated yield by single precipitation from MeOH/ CH₂Cl₂, ^bDetermined by GPC.

Based on the outstanding DP presented by using THF, we tried to reduce reaction temperature from 80 °C to ambient temperature. We found that lowering the temperature resulted in the lower yield and DP along with remaining starting monomers even though the reaction was conducted for 2 days (entry 1). On the other hand, when temperature was raised up to 120 °C, it gave a low yield of polymer with low DP. This may be caused by the more extensive P–C bond cleavage and phenyl–aryl occurred. Therefore, at 80 °C is necessary to ensure enough reactivity for polymerization.

As the above results, we concluded that the optimal condition for coupling polymerization is the use of Pd/CaCO₃ (10 %mol), CuI (20 %mol), PPh₃ (20 %mol), in the mixture of DIPEA/THF in a ratio 1:2 by fixed substrate concentration (0.05 M) at 80 °C under nitrogen atmosphere for 20 h. It must be noted that the structural confirmation and molecular weight determination of aryl diiodide (**2a**), aryl diethyne (**3a**) and PAE **4aa** using FT-IR, NMR and GPC spectroscopy will be further discussion in the next section.

3.2.2 Aryl diiodide (**2a**), aryl diethyne (**3a**) and PAE **4aa** characterization

The conversion of aryl diiodide (**2a**) and aryl diethyne monomer (**3a**) into PAE **4aa** was confirmed structures by FT-IR and ¹H, ¹³C NMR spectra of those monomers (**2a** and **3a**) with PAE **4aa** derived from optimized condition (Figure 3.18-3.20). Also,

the GPC results using THF as eluent and polystyrene as the internal calibration are depicted in Figure 3.21.

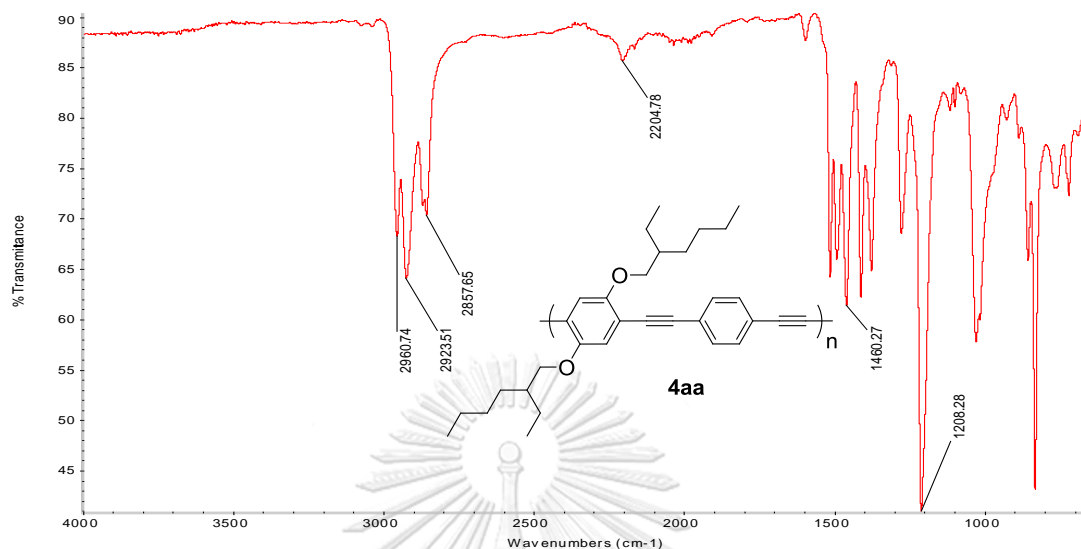


Figure 3.18 FT-IR spectra of PAE **4aa**

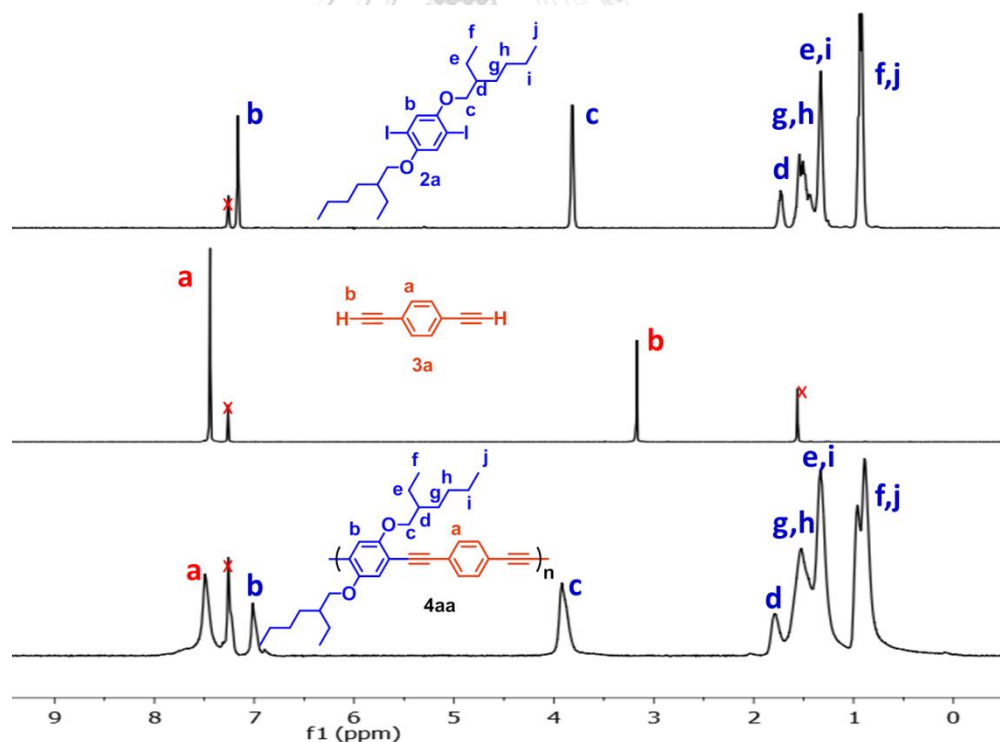


Figure 3.19 ^1H NMR spectra of monomer **2a**, **3a** and PAE **4aa** in CDCl_3

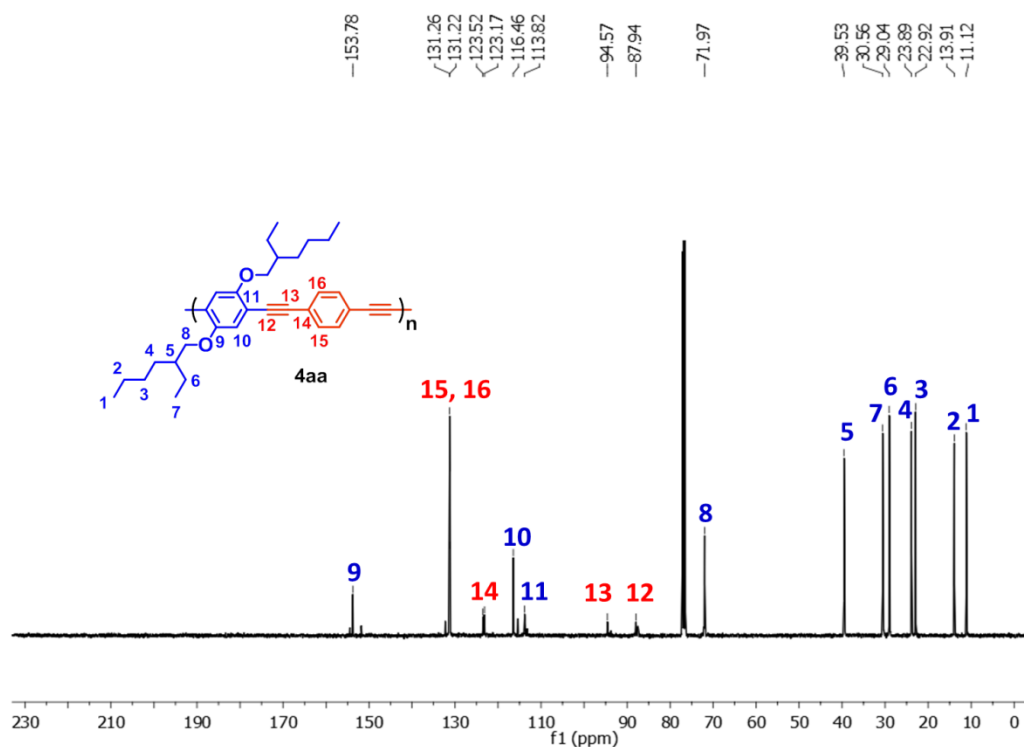


Figure 3.20 ^{13}C NMR spectra of PAE **4aa** in CDCl_3

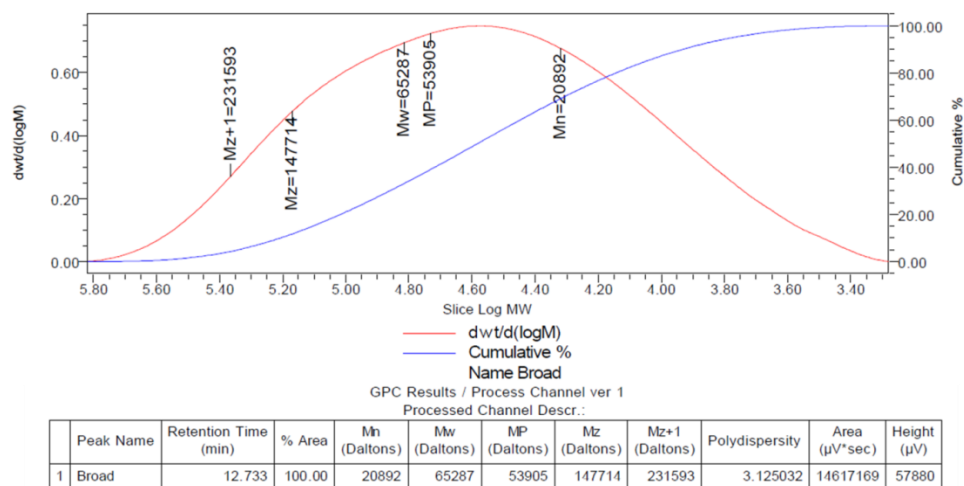


Figure 3.21 GPC data of PAE **4aa**

The FT-IR spectra of the PAE **4aa** is shown in Figure 3.18. The characteristic signals for the polymer formation appeared as a very weak broad signal at 2205 cm^{-1} . This can be assigned to a carbon triple bond ($-\text{C}\equiv\text{C}-$) stretching component. The medium signal around $1450 - 1600\text{ cm}^{-1}$ indicates vibrational modes of the conjugated backbone containing ring deformations and aryl ethynyl C—C stretching

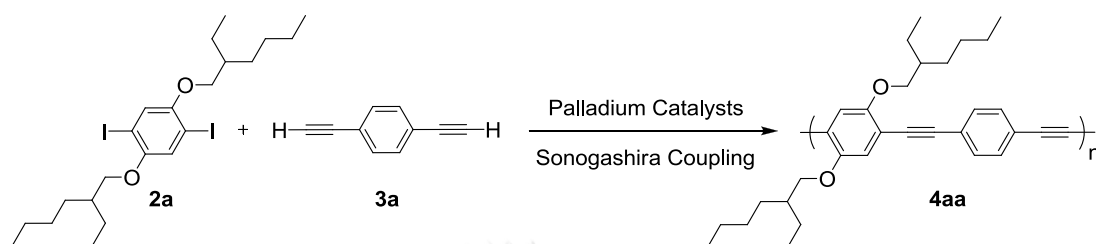
vibrations (Figure 3.18 above) [138]. In term of ^1H NMR spectra, the characteristic peaks of compound **2a**, **3a** and PAE **4aa** in CDCl_3 are shown in Figure 3.19. All signals can be assigned to all protons in each corresponding structure. The ^1H peaks of the polymer **4aa** were the integration of the monomers **2a** and **3a** but all resonances of such polymer are clearly broader than those of the two monomers, and no signal has been detected in the near 3.5 ppm region of the acetylenic proton. However, we noticed a very weak additional signal displayed in the aromatic region (at 6.90 ppm), which might be assigned to the phenyl end groups, carrying a nonreactive iodide atom. Moreover, resulting polymer was thoroughly analyzed by ^{13}C -NMR spectroscopy in order to confirm the triple bond formation and to detect potential diyne defects. Figure 3.20 represents the clearly visible spectra of acetylene carbon formation at $\delta \sim 88, 95$ ppm and no signals around $\delta \sim 73-71$ ppm which could be attributed to diyne defects[139]. Our result demonstrated efficiency of polymerization to produce high molecular weight polymer. The aromatic carbons of the main chains are detected at 154, 131, 124, 117 and 114 ppm. The small peak at 151 ppm may be assigned to the terminal carbons of the chain end. The carbons belonging to the alkoxy side chains appear as very strong signals at 72 and from 40 to 11 ppm. From ^1H and ^{13}C NMR data, the broaden peak along with no diyne defect was observed, indicating an unobstructed conjugated backbone structure leading to high molecular weight polymer obtained. This polymer can be verified by gel permeation chromatography (GPC) analysis in Figure 3.21, the spectrum represents molecular weight = 65,287 Da., degree of polymerization (DP_n) = 143 with satisfactory polydispersity index (PDI) = 3.10.

3.2.3 Comparative study between PAE **4aa** obtained using Pd/CaCO_3 versus compound obtained from conventional catalysts.

Although heterogeneous palladium Pd/CaCO_3 has been proven as a highly proficient catalyst for synthesizing PAE with high yield and molecular weight, but one may ask that can this method be employed instead of conventional catalysts. In the next section, we will compare the PAE from our Pd/CaCO_3 with PAE obtained from known homogeneous catalysts such as $\text{Pd}(\text{PPh}_3)_4$, and $\text{PdCl}_2(\text{PPh}_3)_2$ and

heterogeneous catalyst Pd/C under our optimized condition. The results were summarized in Table 3.6.

Table 3.6 Comparison study between PAE **4aa** was synthesized by using Pd/CaCO₃ with other catalysts.



Entry ^a	Pd catalyst	Yield ^b (%)	M _w ^c (kDa)	DP _n ^c	PDI ^c
1	PdCl ₂ (PPh ₃) ₂	88	33.2	73	2.9
2	Pd(PPh ₃) ₄	91	60.0	132	3.8
3 ^d	Pd/C	85	41.4	91	3.1
4	Pd/CaCO ₃	94	65.3	143	3.1

^aUnless noted, Pd cat. (10 mol%), PPh₃ (20 mol%), CuI (20 mol%), DIPEA/THF (1:2), [0.05 M], 80 °C, 20 h, N₂, ^bIsolated yield by single precipitation from MeOH/CH₂Cl₂, ^cDetermined by GPC, ^dPartially soluble.

1) Characterization of PAE **4aa** obtained using Pd/CaCO₃ and other conventional catalysts

With all the PAEs obtained from PdCl₂(PPh₃)₂, Pd(PPh₃)₄, Pd/C and Pd/CaCO₃ in hand, we then compared ¹H NMR spectra of all polymers by stacking NMR spectra of four catalysts (Figure 3.22). We found that all PAEs indicated similar peak patterns. The small peaks appeared in the aromatic regions around 6.9 and 7.3 ppm corresponds to the aromatic proton at *ortho* to the iodide and to the alkyne end group, respectively. Not surprise, the broaden peaks of PAE preparing from our method could be explained by higher molecular weight of pour PAE in the comparison with other catalysts.

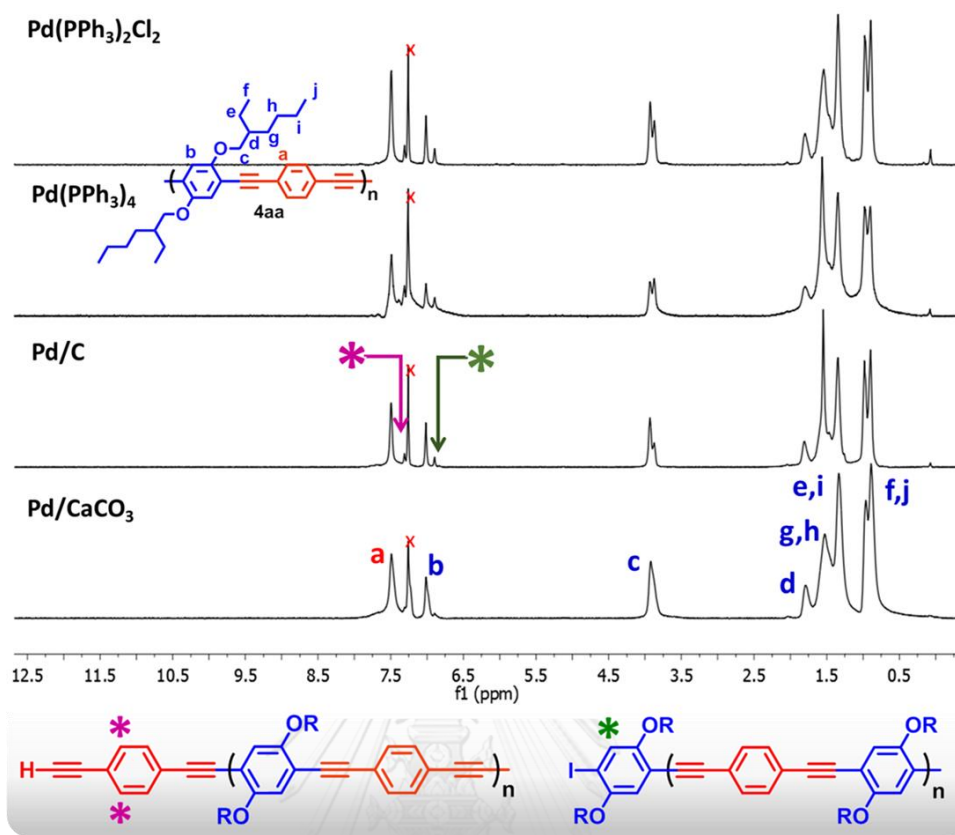


Figure 3.22 ^1H NMR spectra of PAE **4aa** from Pd/CaCO_3 , Pd/C , $\text{PdCl}_2(\text{PPh}_3)_2$ and $\text{Pd}(\text{PPh}_3)_4$

2) Determination of molecular weight by GPC

For the results demonstrated in Table 3.6, all of the resulting PAEs **4aa** gave excellent yields (85-94%) but possess different molecular weight. Polymer derived using $\text{PdCl}_2(\text{PPh}_3)_2$ gave the lowest M_w (33.2 kDa). It may be due to an inactive $\text{Pd}(\text{II})$ catalyst compared to other active species $\text{Pd}(0)$. While PAEs synthesized from active $\text{Pd}(0)$ both homogeneous and heterogeneous catalysts were able to produce PAE in high molecular weight around 40-65 kDa (entry 2-4). For comparison purposes, the smaller molecular weight and lower yield of the $\text{Pd}(\text{PPh}_3)_4$ -catalyzed polymer (entry 2) could be attributed to the side reactions through the phosphorus ligands which induces phenyl-aryl exchange from the PPh_3 to the catalytic palladium intermediate, resulting in polymer chains with phenyl end groups. [140] Notably, the slightly lower yield and M_w of PAE obtained using Pd/C (entry 3) is caused by cross linking of PAEs side chains with palladium nanoparticles [76], leading poorly soluble

in CH_2Cl_2 or THF solvents which is needed for precipitation and GPC analysis respectively.

3) *Determination of Palladium and copper contents in PAEs by ICP-OES analysis*

In addition to the use of Pd/CaCO_3 as highly effective catalyst to produce high M_w PAEs, the metal leaching was another purpose why we use supported heterogeneous catalyst. Hence, we further examined either palladium or copper leaching by determining those transition metal contents that contaminated into desired polymer. After the centrifugation and precipitation of PAE from $\text{PdCl}_2(\text{PPh}_3)_2$, $\text{Pd}(\text{PPh}_3)_4$, Pd/C and Pd/CaCO_3 , all polymer were investigated by ICP-OES analysis and Pd/Cu amount were shown in Table 3.7.

Table 3.7 Palladium and copper contents in PAEs **4aa**

Entry	Pd catalyst	Metal Contamination (ppm) ^a	
		Pd	Cu
1	$\text{PdCl}_2(\text{PPh}_3)_2$	18.6	21.4
2	$\text{Pd}(\text{PPh}_3)_4$	13.4	22.9
3	Pd/C	2.6	28.4
4	Pd/CaCO_3	1.9	3.4

^aDetected by ICP-OES and measured as ppm.

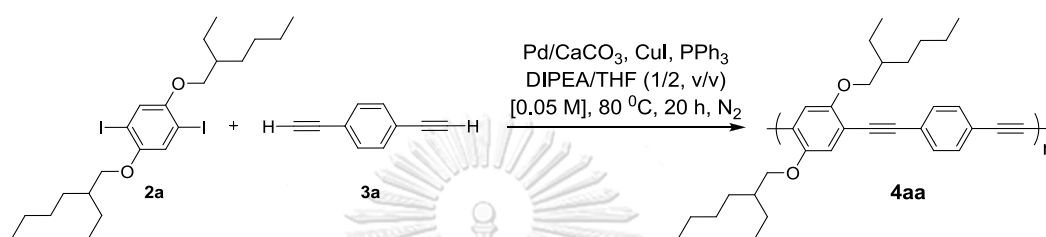
As expected, the contents of Pd residue in PAEs derived from heterogeneous catalysts, Pd/C and Pd/CaCO_3 (entries 3-4) are 5-6 times lower than PAEs derived from homogeneous catalysts. Particularly, Pd/CaCO_3 could minimize the Pd level to as low as 2 ppm. This could be caused by the chelating effect of the Pd with calcium carbonate particles [100]. It is interesting to note that the Cu level of synthesized PAEs via Pd/CaCO_3 (entry 4) was quite low compared with others which is probably caused by the physical adsorption of CuI on CaCO_3 [141].

3.2.4 Reusability test of Pd/CaCO_3 catalyst

To make our catalytic system greener and more economical, we next focused on the reusability of Pd/CaCO_3 for coupling polymerization and the result were

presented in Table 3.8. Unfortunately, the catalytic activity dropped precipitously, resulting the yield and molecular weight dramatic decrease after the first round. In attempt to recycle by the sonication of the catalyst before next reaction, the reusability of catalyst was not improved. It is presumably because of the strong aggregation of the catalyst during the recycling process [104].

Table 3.8 Reusability test of Pd/CaCO₃ catalyst on polymerization



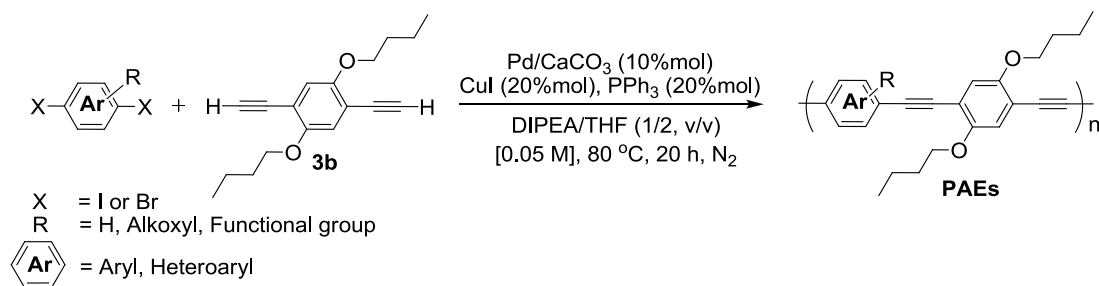
Entry ^a	Yield ^b (%)	M _w ^c (kDa)	DP _n ^c	PDI ^c
1	91	53.3	112	3.5
2	88	33.2	73	2.9
3 ^d	N.A.	-	-	-

^aUnless noted, Pd/CaCO₃ (10 mol%), CuI (20 mol%), PPh₃ (20 mol%),

^bIsolated yield by single precipitation from MeOH/ CH₂Cl₂, ^cDetermined by

GPC, ^dStarting monomers remained.

Encouraged by above results, Pd/CaCO₃ catalyst is proven to be an effective heterogeneous catalyst for PAE preparation. From a practical point of view, it is interesting to see whether the catalyst is compatible with a wide variety of substrates, which contain different structures and functional groups. With the optimal conditions in hand, the substrate scope of the Pd-catalyzed polymerization between different aromatic dihalides and 1,4-dibutoxy-2,5-diethynylbenzene (**3b**) were explored. In the next section, a panel of aryl dihalides carrying various side chains was then prepared and subjected to our optimal condition with Pd/CaCO₃ (Scheme 3.5).



Scheme 3.5 Pd/CaCO₃-catalyzed Sonogashira coupling polymerization

3.2.5 Substrate scope of aryl dihalides coupled with aryl diethyne (**3b**) for examining generality of Pd/CaCO₃-catalyzed Sonogashira polymerization

In this section, a wide range of aryl halides bearing electron-donating and electron-withdrawing groups (Figure 3.23) were thus prepared following reported literatures.

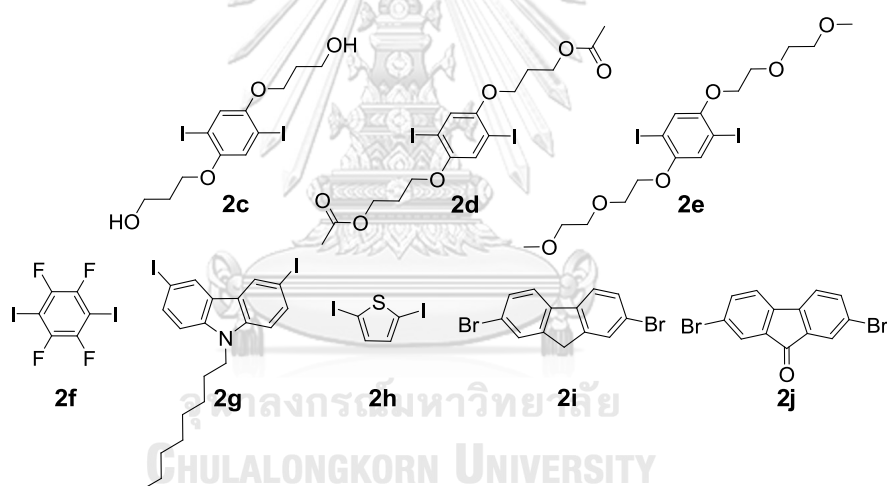
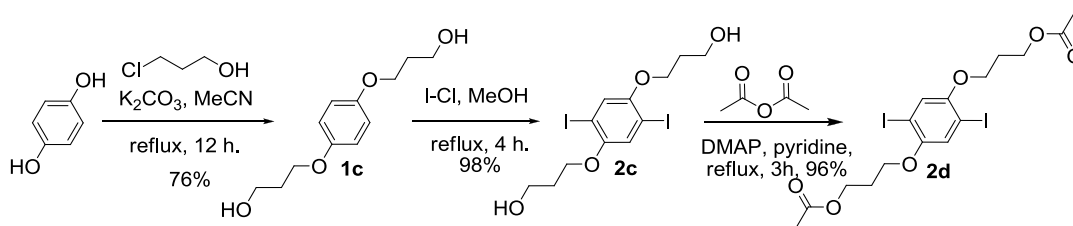


Figure 3.23 Aryl dihalide monomers used in this section

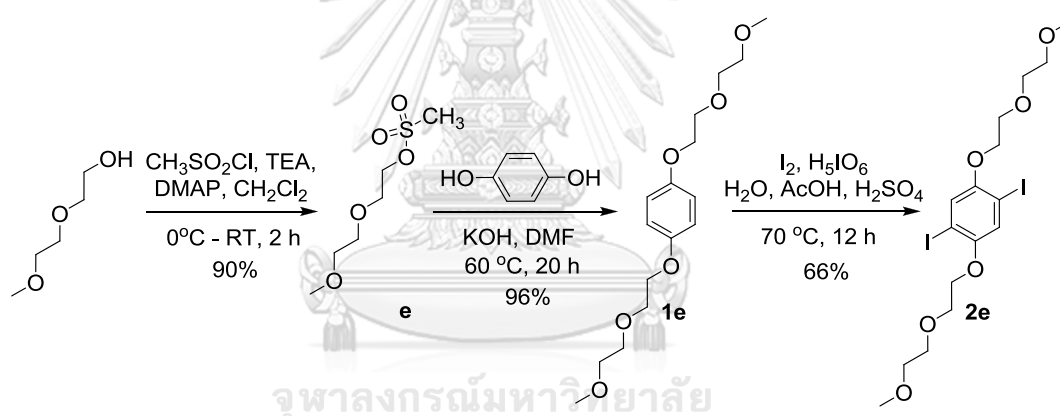
1) Preparation of aryl diiodides (**2c-2j**)

Compounds 2c and 2d: In order to verify that our method has high functional group tolerance, we demonstrate the reaction using various substrates carrying sensitive functional groups such as alcohol and ester. We first prepared the hydroxyl monomer (**2c**) followed by the alkylation and iodination, respectively, as shown in Scheme 3.6. With this starting alcohol substrate in hand, esterification of **2c** with acetic acid in pyridine under refluxing for 3 h also produced compounds **2d** in excellent yield.



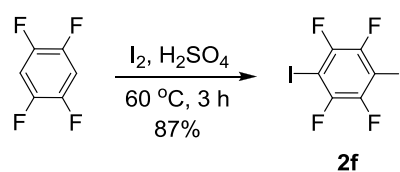
Scheme 3.6 Synthesis of compounds **2c** and **2d**

Compound 2e: Oxygen atom is well known to inhibit the catalyst efficiencies, probably by coordination to palladium. Therefore, we synthesized compound **2e** in order to prove that polyoxygeneous substrate would not affect under our reaction condition (Scheme 3.7). Activation of hydroxyl group on diethyleneglycol monomethylether with mesylchloride gives compound **e** in 90% yield. After that, compound **e** was reacted with hydroquinone followed by iodination to obtain **2e** in 66% yield for two steps.



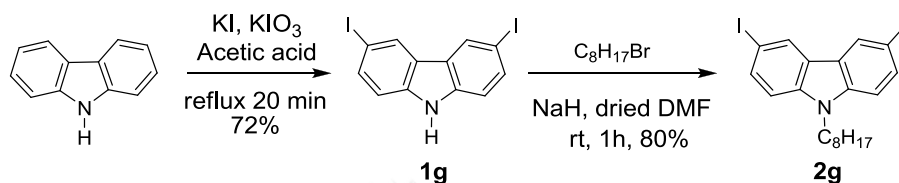
Scheme 3.7 Synthesis of compound **2e**

Compound 2f: In order to examine the feasibility of monomers bearing electron-withdrawing groups, we further prepared compound **2f** using known procedures. They were subjected to diiodination to afford **2f** in 87% yield (Scheme 3.8).



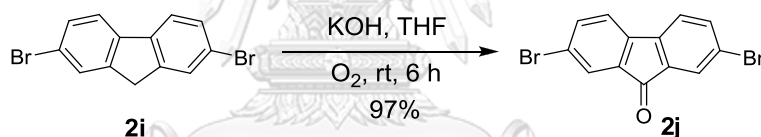
Scheme 3.8 Synthesis of compound **2f**

Compound 2g: Compound **2g** was prepared in order to see the potential of our method for the preparation of PAE containing heterocycle. We began with iodination of carbazole with potassium iodide to give **1g** in 72% yield. Then, alkylation using *n*-octylbromide was carried out in pyridine at room temperature providing compound **2g** in 80% yield (Scheme 3.9).



Scheme 3.9 Synthesis of compound **2g**

Compound 2j: In order to study the polymerization reaction in unreactive dibromide substrate, we designed to use **2i** and **2j** as coupling partner in our condition. With commercially available 2,7-dibromo-9H-fluorene (**2i**) in hand, **2j** was prepared by air-oxidation reaction to furnish desired product in 97% yield.

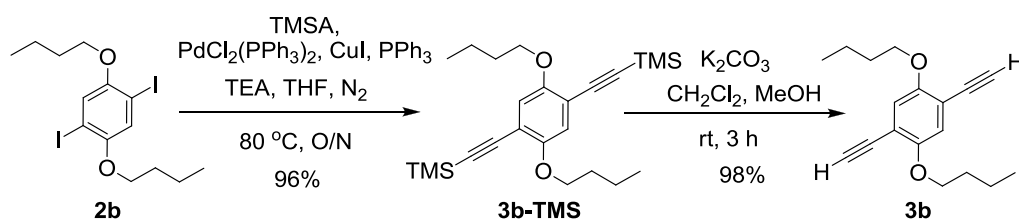


Scheme 3.10 Synthesis of compound **2j**

Noted; **2h** and **2i** were commercially available.

2) Preparation of 1,4-dibutoxy-2,5-diethynylbenzene (**3b**)

Compound 3b: As the following mentioned that flexible side chain can improve dissolution of polymer, compound **2b** was transformed into terminal alkyne **3b**. It was synthesized by the Pd-catalyzed Sonogashira cross-coupling between **2b** and trimethylsilylacetylene followed by a base-catalyzed desilylation (Scheme 3.11).

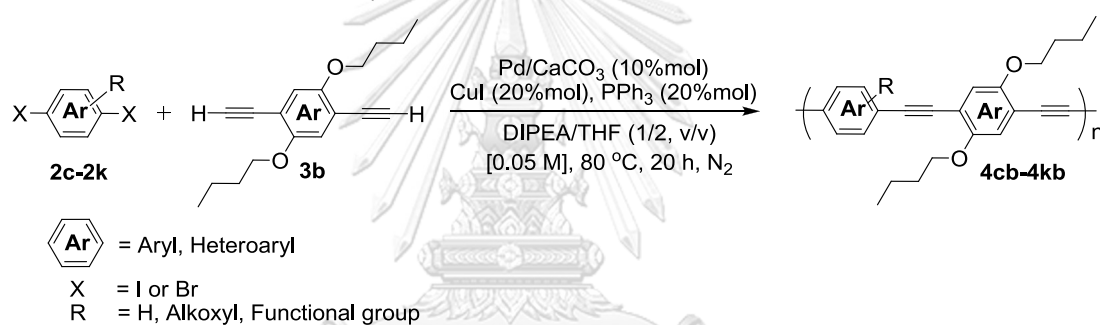


Scheme 3.11 Synthesis of compound **3b**

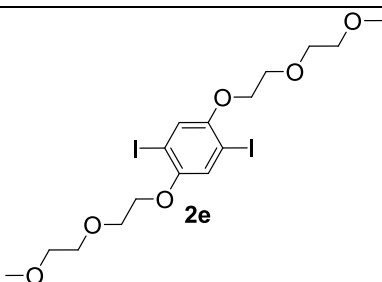
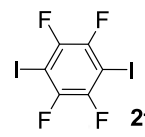
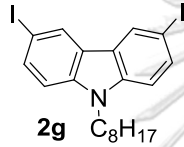
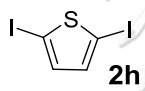
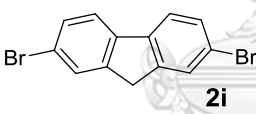
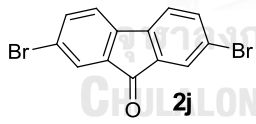
3) Preparation PAEs (**4cb-4jb**) from dihalide monomers (**2c-2j**) and 1,4-dibutoxy-2,5-diethynylbenzene monomer (**3b**)

To verify the scope and limitation of the present system, we tested several electronically diverse aryl dihalides (**2c-2j**) which were introduced to couple with terminal alkyne **3b** using Pd/CaCO₃ as a heterogeneous catalyst. The tests were conducted under the optimized reaction conditions: **2c-2j** (1 equiv), **3b** (1 equiv), Pd/CaCO₃ (10% mol), CuI (20% mol) and PPh₃ (20% mol) in the mixture of DIPEA/THF in a ratio 1:2 and reaction proceeded smoothly at 80 °C under a nitrogen atmosphere for 20 h to give the corresponding PAEs (**4cb-4jb**). The results obtained are presented in Table 3.9.

Table 3.9 PAE substrate scope



Entry	Dihalides	PAEs	Yield ^a (%)	M _w ^b (kDa)	DP _n ^b	PDI
1		4cb	N.A.	-	-	-
2		4db	90	20.4	36	2.2

Entry	Dihalides	PAEs	Yield ^a (%)	M _w ^b (kDa)	DP _n ^b	PDI
3		4eb	96	32.6	56	2.1
4		4fb	97	6.1	15	1.5
5		4gb	93	43.7	80	2.8
6		4hb	99	44.2	127	2.6
7		4ib	100	18.9	44	3.8
8		4jb	88	7.7	19	2.4

^aIsolated yield by precipitation in MeOH from CH₂Cl₂. ^bDetermined by GPC using universal calibration with standard polystyrene, N.A.= non-available.

The aryl diiodides containing oxygenous substituents (**2d** and **2e**) such as ester and glycol were well tolerated and proceed smoothly under our polymerization condition to yield the desired PAEs **4db** and **4eb** in excellent yields (entries 2 and 3). The polymer **4db** and **4eb** possess a high degree of polymerization (DP_n = 36 and 56, respectively) and narrow polydispersity index (PDI ≈ 2.1). Unfortunately, hydroxyl substituted monomer (**2c**) was not suitable for this system forming only oligomer with remaining starting materials even reaction was carried for

3 days. This may be owing to deprotonated hydroxyl side chains that performed as a binding site to coordinate with Cu ions [142], leading to inefficient transmetalation step. Again, the aryl diiodides bearing electron-withdrawing group (**2f**) (entries 4) was successfully polymerized with **3b** give **4fb** in high yields. However, the slightly low degree of polymerization of **4fb** ($DP_n = 15$) may result from its limited solubility in the reaction medium which leads the polymer precipitated from the reaction mixture during the course of polymerization. Next, the PAE containing heterocycle were successfully prepared from the diiodides **2g** and **2h** in high yields and high molecular weights (entries 5-6). Especially, thiophene based PAE (**4hb**) exhibited higher molecular weight than that from the original report. [64] It is important to note that all mentioned substituents are known to retard the oxidative addition step in catalytic cycle due to the hetero atoms complexation with palladium species resulting in the poor reaction rate. Moreover, the reaction proceeded well not only with aryl diiodides but also with aryl dibromides (entries 7-8). The coupling of either substituted electron deficient **2i** or electron rich aryl dibromide **2j** with alkyne (**3b**) underwent smoothly resulting in complete conversion and desired PAEs **4ib** and **4jb** were produced in excellent yields. Nonetheless, some of insoluble portion of **4jb** was formed after the reaction time which may be owing to rigidity of fluorene unit, resulting π - π stacking formation. This led to low degree of polymerization ($DP_n = 19$).

4) Photophysical properties and color appearance of PAEs (**4aa-4jb**)

In this section, photophysical properties of all the prepared PPEs were investigated. The photophysical properties can be correlated to the degree of conjugation along the backbone and can therefore be related to the molecular structure. Besides, the twisting around the backbone arising from the steric interactions between side chains on adjacent repeat units and the supermolecular packing may both have a strong influence on the electronic spectra [143]. To study their photophysical properties, the absorption and emission of the all polymers (Figure 3.24) were measured in THF solution. The normalized intensity of absorption and fluorescence spectra obtained for the polymers are shown in Figure 3.25. For the photophysical properties of the polymers including maximum absorption wavelength

(λ_{abs}), maximum emission wavelength (λ_{em}), molar absorptivity (ϵ) and fluorescence quantum efficiency (Φ_f) were determined as presented in Table 3.10.

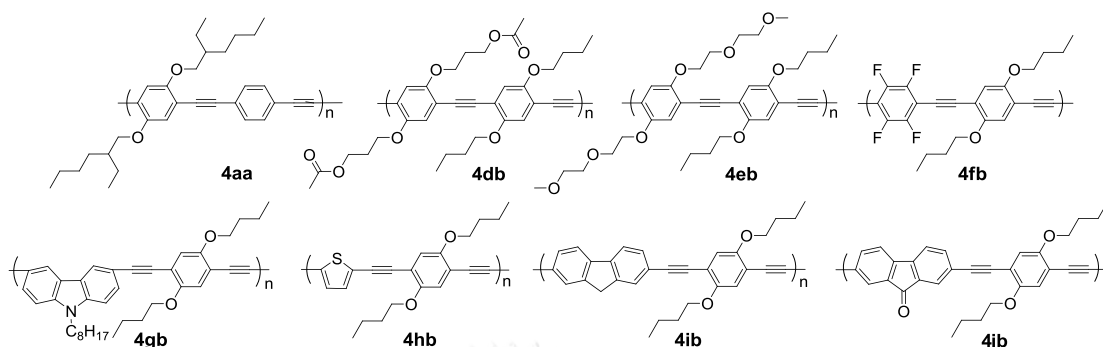


Figure 3.24 PAEs (4aa-4jb) obtained from our optimized condition

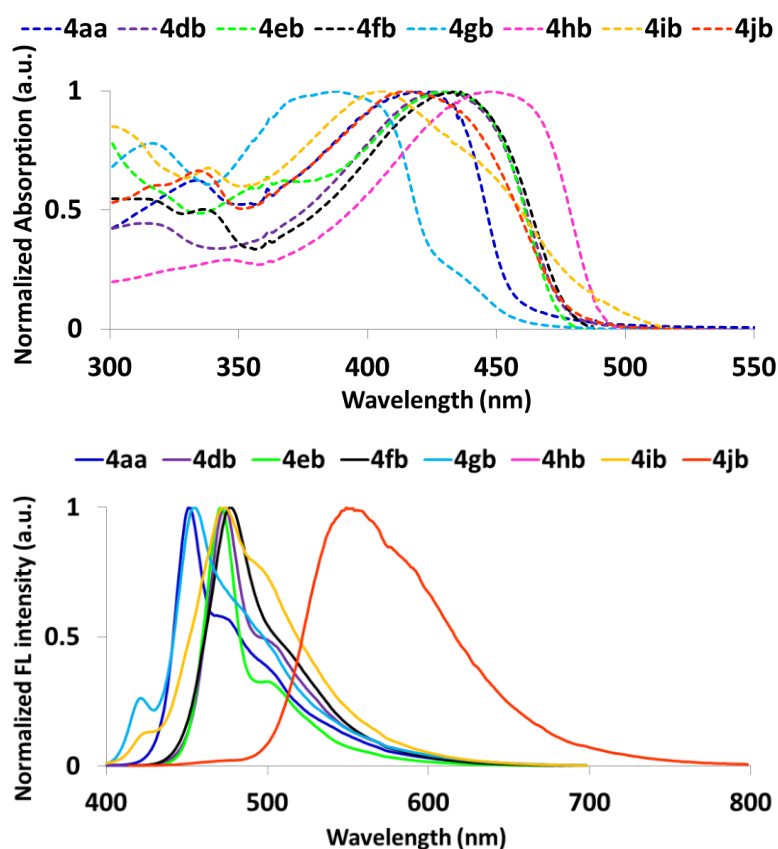









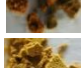




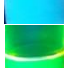






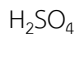
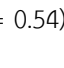
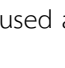


Figure 3.25 Normalized absorption (top) and emission (bottom) spectra of PAEs in THF solution

Table 3.10 Photophysical properties and color appearance of PAEs **4aa-4jb**

Entry ^a	PAEs	λ_{abs}^b	λ_{em}^b	ϵ	Φ_f^c	Solid	Visible ^d	BL ^d
1	4aa	423	449	4.51	0.47			
2	4db	312, 427	471	5.41	0.31			
3	4eb	360, 429	471	3.55	0.09			
4	4fb	300, 432	475	3.88	0.19			
5	4gb	315, 388	453	4.56	0.24			
6	4hb	344, 447	485	4.32	0.20			
7	4ib	333, 416	470	4.16	0.56			
8	4jb	300, 404	548	4.31	0.07			

^aDissolved in THF, ^bNormalized Spectra, ^cquinine sulphate in 0.1 M H₂SO₄ ($\Phi_f = 0.54$) was used as the standard, ^dDetermined at 1 mM

In accordance with the findings for photophysical properties of poly(2,5-dialkoxy-*p*-phenyleneethynylene)s, the PAEs of **4aa**, **4db** and **4eb** carrying bulky alkoxy derivatives exhibited similar absorption ($\lambda_{\text{abs}} \approx 430$ nm) and emission spectra ($\lambda_{\text{em}} \approx 470$ nm) to those reported earlier [113]. These results are in good agreement with other previous works that the photophysical properties of conjugated polymers are hardly influenced by the nature of the side chain substituents, but predominantly governed by the chemical structure of the polymer backbone. As seen in entries 4-8 (**4fb-4jb**) comprising various pendent groups in their backbone, the polymer solution displayed notable difference in maximum absorption and emission. As well known, absorption is presented as a function of electron density in the polymer chain. Hence electron-donating groups (ex. carbazole (**4gb**) and thiophene (**4hb**)) showed similar trend of having a longer maximum absorption wavelength than electron-withdrawing groups (ex. benzotrifluoride, carbonyl and nitro, particular). The latter group showed two absorption bands in the ultraviolet ($\lambda \approx 300$ -360 nm) and in the visible region ($\lambda \approx 400$ -460 nm) which corresponding to π - π^* transition of monomer and polymer, respectively.

For emission spectra investigation, these findings are well documented the fact that the emission maxima of the polymers appeared at almost the same wavelength. Our result suggested that these polymers have a similar π -conjugated system. Such spectra have almost identical features demonstrated a main peak with a maximum around 470-480 nm and a shoulder peak that extended into the low-energy, which might arise from energy migration to low-band gap defect sites as shown in Figure 3.25 (bottom). As expected, when more electron density is attached to the polymer main chain, there is a significant red shift of the emission spectrum. For instance, by comparing the emission spectra of **4aa** and **4hb**, it shows a 36 nm red shift for electron donating presented. While, polymer consisting carbonyl (**4jb**) group on backbone displayed the remarkably bathochromic shift around 540 nm. This may be associated with the present of alternated donor and acceptor substituents (ether-carbonyl copolymer) which shows intramolecular charge transfer behavior [138]. All polymers possess moderate molar absorptivity (ϵ) which were reported in $\log \epsilon$ around 3.90-4.60. Their fluorescence quantum efficiencies (Φ_f) were in range of 0.1-0.6.

The color appearance of each PAE in Table 3.10 illustrated that the prepared PAEs were greenish-yellow to deep orange powder. In solution state, all PAEs were dissolved in THF. Their color solutions were observed by naked eye which showed light brown to greenish yellow emission, unlike carbonyl (**4jb**) substituted backbone that displayed deep orange solution under visible light. In term of viewing under black-light, PAEs carrying electron donating units exhibited bright blue to green emission. While PAEs **4jb** was remarkable shifted to yellowish-orange color.

CHAPTER IV

CONCLUSION

4.1 Salicylaldimine-functionalized poly(*m*-phenyleneethynylene) as turn-on chemosensor for ferric ion (part A)

A new conjugated polymeric sensor (**PPE-IM**) based on salicylaldimine-functionalized poly(*m*-phenyleneethynylene)s was successfully prepared in excellent yield via Sonogashira coupling reaction and post-polymerization functionalization. Such polymer provides high hydrolytic stability in a wide pH range. This is caused by strong intramolecular hydrogen bonding and hydrophobic interaction among the side chains. The probe displays remarkably sensitive and selective turn-on fluorescence signal towards Fe^{3+} , through lewis acid-promoted hydrolysis process, with low detection limit of 0.14 μM and without significant interference from other metal ions. Thus **PPE-IM** developed herein could be a promising sensor for Fe^{3+} selective detection. It can be useful in several biological and environmental analysis as well as early rust detection.

4.2 Synthesis of highly pure poly(aryleneethynylene)s using palladium supported on calcium carbonate as eco-friendly heterogeneous catalyst (part B)

The heterogeneous palladium-catalyzed Sonogashira coupling polymerizations were developed for preparation of poly(aryleneethynylene)s (PAEs). Under the optimization condition, resulting polymers obtained from our developed method using Pd/CaCO_3 as catalyst provide a comparable yield with higher molecular weight comparing to that obtained from homogeneous catalyst ($\text{PdCl}_2(\text{PPh}_3)_2$ and $\text{Pd}(\text{PPh}_3)_4$). The PAEs containing various functional groups, either withdrawing or donating groups, were successfully synthesized in high yields (79-96%) with molecular weight ranging from 6-40 kDa. In addition, monomer containing heterocyclic thiophene or carbazole rings also compatible to give desired PAEs in excellent yields (88-100%). Most importantly, the PAEs prepared from this method contained significantly lower Pd and Cu level in comparison with those obtained

from Pd/C and classical homogeneous catalysts. The use of Pd/CaCO₃ as catalyst is cost-effective, user-friendly, and clean process which would be a valuable alternative for preparation of high purity PAEs.



REFERENCES

- [1] Perepichka, I.F., Perepichka, D.F., Meng, H., and Wudl, F. Light-Emitting Polythiophenes. Advanced Materials 17(19) (2005): 2281-2305.
- [2] Patil, A.O., Heeger, A.J., and Wudl, F. Optical properties of conducting polymers. Chemical Reviews 88(1) (1988): 183-200.
- [3] Scherf, U. and List, E.J.W. Semiconducting Polyfluorenes—Towards Reliable Structure–Property Relationships. Advanced Materials 14(7) (2002): 477-487.
- [4] Kraft, A., Grimsdale, A.C., and Holmes, A.B. Electroluminescent Conjugated Polymers—Seeing Polymers in a New Light. Angewandte Chemie International Edition 37(4) (1998): 402-428.
- [5] Bunz, U.H.F., Seehafer, K., Bender, M., and Porz, M. Poly(aryleneethynylene)s (PAE) as paradigmatic sensor cores. Chemical Society Reviews 44(13) (2015): 4322-4336.
- [6] Chen, L., McBranch, D.W., Wang, H.-L., Helgeson, R., Wudl, F., and Whitten, D.G. Highly sensitive biological and chemical sensors based on reversible fluorescence quenching in a conjugated polymer. Proceedings of the National Academy of Sciences, USA 96(22) (1999): 12287-12292.
- [7] Halkyard, C.E., Rampey, M.E., Kloppenburg, L., Studer-Martinez, S.L., and Bunz, U.H.F. Evidence of Aggregate Formation for 2,5-Dialkylpoly(*p*-phenyleneethynylenes) in Solution and Thin Films. Macromolecules 31(25) (1998): 8655-8659.
- [8] Miteva, T., Palmer, L., Kloppenburg, L., Neher, D., and Bunz, U.H.F. Interplay of Thermochromicity and Liquid Crystalline Behavior in Poly(*p*-phenyleneethynylene)s: π - π Interactions or Planarization of the Conjugated Backbone? Macromolecules 33(3) (2000): 652-654.

- [9] Wilson, J.N., Wang, Y., Lavigne, J.J., and Bunz, U.H.F. A biosensing model system: selective interaction of biotinylated PPEs with streptavidin-coated polystyrene microspheres. Chemical Communications (14) (2003): 1626-1627.
- [10] Yang, J.-S. and Swager, T.M. Fluorescent Porous Polymer Films as TNT Chemosensors: Electronic and Structural Effects. Journal of the American Chemical Society 120(46) (1998): 11864-11873.
- [11] Toal, S.J. and Trogler, W.C. Polymer sensors for nitroaromatic explosives detection. Journal of Materials Chemistry 16(28) (2006): 2871-2883.
- [12] Miranda, O.R., et al. Array-Based Sensing of Proteins Using Conjugated Polymers. Journal of the American Chemical Society 129(32) (2007): 9856-9857.
- [13] Sakai, R., et al. Fluorescence Turn-On Sensing of Anions Based on Disassembly Process of Urea-Functionalized Poly(phenylenebutadiynylene) Aggregates. Macromolecules 45(10) (2012): 4122-4127.
- [14] Wang, B. and Wasielewski, M.R. Design and Synthesis of Metal Ion-Recognition-Induced Conjugated Polymers: An Approach to Metal Ion Sensory Materials. Journal of the American Chemical Society 119(1) (1997): 12-21.
- [15] Breen, C.A., Deng, T., Breiner, T., Thomas, E.L., and Swager, T.M. Polarized Photoluminescence from Poly(*p*-phenyleneethynylene) via a Block Copolymer Nanotemplate. Journal of the American Chemical Society 125(33) (2003): 9942-9943.
- [16] VanVeller, B. and Swager, T.M. Biocompatible post-polymerization functionalization of a water soluble poly(*p*-phenyleneethynylene). Chemical Communications 46(31) (2010): 5761-3.
- [17] Xue, C., Donuru, V.R.R., and Liu, H. Facile, Versatile Prepolymerization and Postpolymerization Functionalization Approaches for Well-Defined Fluorescent Conjugated Fluorene-Based Glycopolymers. Macromolecules 39(17) (2006): 5747-5752.

- [18] Tolosa, J., Kub, C., and Bunz, U.H.F. Hyperbranched: A Universal Conjugated Polymer Platform. Angewandte Chemie International Edition 48(25) (2009): 4610-4612.
- [19] Lakowicz, J.R. Introduction to Fluorescence. in Principles of Fluorescence Spectroscopy, pp. 1-26: Springer US, 2006.
- [20] Sahoo, S.K., Sharma, D., Bera, R.K., Crisponi, G., and Callan, J.F. Iron(III) selective molecular and supramolecular fluorescent probes. Chemical Society Reviews 41(21) (2012): 7195-7227.
- [21] Ceroni, P. and Balzani, V. Photoinduced Energy and Electron Transfer Processes. Ceroni, P. (ed.). in The Exploration of Supramolecular Systems and Nanostructures by Photochemical Techniques, pp. 21-38: Springer, Dordrecht, 2012.
- [22] Fan, L.-J. and Jones, W.E. Studies of Photoinduced Electron Transfer and Energy Migration in a Conjugated Polymer System for Fluorescence "Turn-On" Chemosensor Applications. The Journal of Physical Chemistry B 110(15) (2006): 7777-7782.
- [23] Balzani, V., Bolletta, F., and Scandola, F. Vertical and "nonvertical" energy transfer processes. A general classical treatment. Journal of the American Chemical Society 102(7) (1980): 2152-2163.
- [24] Piedras, A., Gómez, B., Carmona-Espindola, J., Arroyo, R., and Gázquez, J.L. Intramolecular charge transfer model in fluorescence processes. Theoretical Chemistry Accounts 135(10) (2016): 243.
- [25] Haberhauer, G., Gleiter, R., and Burkhart, C. Planarized Intramolecular Charge Transfer: A Concept for Fluorophores with both Large Stokes Shifts and High Fluorescence Quantum Yields. Chemistry – A European Journal 22(3) (2016): 971-978.

- [26] Sapsford, K.E., Berti, L., and Medintz, I.L. Materials for Fluorescence Resonance Energy Transfer Analysis: Beyond Traditional Donor–Acceptor Combinations. Angewandte Chemie International Edition 45(28) (2006): 4562-4589.
- [27] Wu, J., Liu, W., Ge, J., Zhang, H., and Wang, P. New sensing mechanisms for design of fluorescent chemosensors emerging in recent years. Chemical Society Reviews 40(7) (2011): 3483-3495.
- [28] Wu, J.-S., et al. Fluorescence Turn On of Coumarin Derivatives by Metal Cations: A New Signaling Mechanism Based on C=N Isomerization. Organic Letters 9(1) (2007): 33-36.
- [29] Hong, Y., Lam, J.W.Y., and Tang, B.Z. Aggregation-induced emission: phenomenon, mechanism and applications. Chemical Communications (29) (2009): 4332-4353.
- [30] Thomas, S.W., Joly, G.D., and Swager, T.M. Chemical Sensors Based on Amplifying Fluorescent Conjugated Polymers. Chemical Reviews 107(4) (2007): 1339-1386.
- [31] Henary, M.M. and Fahrni, C.J. Excited State Intramolecular Proton Transfer and Metal Ion Complexation of 2-(2-Hydroxyphenyl)benzazoles in Aqueous Solution. The Journal of Physical Chemistry A 106(21) (2002): 5210-5220.
- [32] Kim, I.-B., Dunkhorst, A., Gilbert, J., and Bunz, U.H.F. Sensing of Lead Ions by a Carboxylate-Substituted PPE: Multivalency Effects. Macromolecules 38(11) (2005): 4560-4562.
- [33] Kim, I.-B. and Bunz, U.H.F. Modulating the Sensory Response of a Conjugated Polymer by Proteins: An Agglutination Assay for Mercury Ions in Water. Journal of the American Chemical Society 128(9) (2006): 2818-2819.
- [34] Liu, X., Zhou, X., Shu, X., and Zhu, J. A Polymer-Based Ultrasensitive Metal Ion Sensor. Macromolecules 42(20) (2009): 7634-7637.
- [35] Ma, X., Song, F., Wang, L., Cheng, Y., and Zhu, C. Polymer-based colorimetric and “turn-off” fluorescence sensor incorporating benzo[2,1,3]thiadiazole

- moiety for Hg²⁺ Detection. Journal of Polymer Science Part A: Polymer Chemistry 50(3) (2012): 517-522.
- [36] Nolan, E.M. and Lippard, S.J. Tools and Tactics for the Optical Detection of Mercuric Ion. Chemical Reviews 108(9) (2008): 3443-3480.
- [37] Zeng, W., et al. Conjugated polymers containing 2-thiohydantoin: Detection of cuprous ion, hydrogen peroxide and glucose. European Polymer Journal 61 (2014): 309-315.
- [38] Wu, Y., et al. Fluorescence Array-Based Sensing of Metal Ions Using Conjugated Polyelectrolytes. ACS Applied Materials & Interfaces 7(12) (2015): 6882-6888.
- [39] Gorman, A., Killoran, J., O'Shea, C., Kenna, T., Gallagher, W.M., and O'Shea, D.F. In Vitro Demonstration of the Heavy-Atom Effect for Photodynamic Therapy. Journal of the American Chemical Society 126(34) (2004): 10619-10631.
- [40] Fan, L.-J., Zhang, Y., and Jones, W.E. Design and Synthesis of Fluorescence "Turn-on" Chemosensors Based on Photoinduced Electron Transfer in Conjugated Polymers. Macromolecules 38(7) (2005): 2844-2849.
- [41] Fan, L.-J. and Jones, W.E. A Highly Selective and Sensitive Inorganic/Organic Hybrid Polymer Fluorescence "Turn-on" Chemosensory System for Iron Cations. Journal of the American Chemical Society 128(21) (2006): 6784-6785.
- [42] Pourghaz, Y., Dongare, P., Thompson, D.W., and Zhao, Y. Click functionalized poly(*p*-phenyleneethynylene)s as highly selective and sensitive fluorescence turn-on chemosensors for Zn²⁺ and Cd²⁺ ions. Chemical Communications 47(39) (2011): 11014-6.
- [43] Wang, H., He, F., Yan, R., Wang, X., Zhu, X., and Li, L. Citrate-induced aggregation of conjugated polyelectrolytes for Al³⁺-ion-sensing assays. ACS Applied Materials & Interfaces 5(16) (2013): 8254-9.
- [44] Xu, H., Wu, W., Chen, Y., Qiu, T., and Fan, L.J. Construction of response patterns for metal cations by using a fluorescent conjugated polymer sensor

- array from parallel combinatorial synthesis. ACS Applied Materials & Interfaces 6(7) (2014): 5041-9.
- [45] Osweiler G.D., C.T.L., Buck W.B., et al. Iron. in Clinical and diagnostic veterinary toxicology, pp. 104-106. Dubuque, Iowa: Kendall/Hunt Publishing Co., 1985.
- [46] Goyer, R.A. Toxic effects of metals. Klaassen, C.D. (ed.). in Casarett & Doull's toxicology: the basic science of poisons, pp. 715-716. New York City, NY: McGraw-Hill, 1996.
- [47] Hillman, R.S. Hematopoietic agents: growth factors, minerals, and vitamins. Hardman J.G., Limbird L.E., Molinoff P.B., et al, (ed.). in Goodman & Gilman's the pharmacological basis of therapeutics., pp. 1311-1340. New York City, NY: McGraw-Hill, 1995.
- [48] Halliwell, B. Reactive Oxygen Species and the Central Nervous System. Journal of Neurochemistry 59(5) (1992): 1609-1623.
- [49] Stevens , R.G., Jones , D.Y., Micozzi , M.S., and Taylor , P.R. Body Iron Stores and the Risk of Cancer. New England Journal of Medicine 319(16) (1988): 1047-1052.
- [50] Tenenbein, M. UNit-dose packaging of iron supplements and reduction of iron poisoning in young children. Archives of Pediatrics & Adolescent Medicine 159(6) (2005): 557-560.
- [51] McGuigan, M.A. Acute iron poisoning. Pediatr Ann 25(1) (1996): 33-8.
- [52] Fegley, M.E.A., Sandgren, T., Duffy-Matzner, J.L., Chen, A., and Jones, W.E. Detection and differentiation of ferrous and ferric ions using fluorescent metallopolymer and oligomer chemosensors. Journal of Polymer Science Part A: Polymer Chemistry 53(8) (2015): 951-954.
- [53] Lei, Y., et al. Water-soluble benzoselenadiazole-based conjugated polymer fluorescent sensor with high selectivity for ferric ions and mercury ions and possible applications as integrated molecular logic gates. Tetrahedron 71(21) (2015): 3453-3462.

- [54] Quang, D.T. and Kim, J.S. Fluoro- and Chromogenic Chemodosimeters for Heavy Metal Ion Detection in Solution and Biospecimens. Chemical Reviews 110(10) (2010): 6280-6301.
- [55] Lin, W., Yuan, L., Feng, J., and Cao, X. A Fluorescence-Enhanced Chemodosimeter for Fe³⁺ Based on Hydrolysis of Bis(coumarinyl) Schiff Base. European Journal of Organic Chemistry 2008(16) (2008): 2689-2692.
- [56] Lin, W., Yuan, L., and Cao, X. A rational approach to emission ratio enhancement of chemodosimeters via regulation of intramolecular charge transfer. Tetrahedron Letters 49(46) (2008): 6585-6588.
- [57] Lee, M.H., Giap, T.V., Kim, S.H., Lee, Y.H., Kang, C., and Kim, J.S. A novel strategy to selectively detect Fe(III) in aqueous media driven by hydrolysis of a rhodamine 6G Schiff base. Chemical Communications 46(9) (2010): 1407-1409.
- [58] Shen, B.-x. and Qian, Y. A novel triphenylamine-BODIPY dendron: click synthesis, near-infrared emission and a multi-channel chemodosimeter for Hg²⁺ and Fe³⁺. Journal of Materials Chemistry B 4(47) (2016): 7549-7559.
- [59] Jackson, R.K., Shi, Y., Yao, X., and Burdette, S.C. FerriNaphth: A fluorescent chemodosimeter for redox active metal ions. Dalton Transactions 39(17) (2010): 4155-4161.
- [60] Chen, Y.-Z., Bhorge, Y.R., Pape, A.J., Divate, R.D., Chung, Y.-C., and Yen, Y.-P. A New Schiff Base Chemodosimeter for Fluorescent Imaging of Ferric Ions in Living Cells. Journal of Fluorescence 25(5) (2015): 1331-1337.
- [61] Samanta, S., Goswami, S., Ramesh, A., and Das, G. A new chemodosimetric probe for the selective detection of trivalent cations in aqueous medium and live cells. Journal of Photochemistry and Photobiology A: Chemistry 310 (2015): 45-51.
- [62] Bunz, U.H.F. Poly(aryleneethynylene)s. Macromolecular Rapid Communications 30(9-10) (2009): 772-805.

- [63] Bunz, U.H.F. Poly(aryleneethynylene)s: Syntheses, Properties, Structures, and Applications. Chemical Reviews 100(4) (2000): 1605-1644.
- [64] Bunz, U.H.F. Synthesis and Structure of PAEs. Weder, C. (ed.) in Poly(arylene ethynylene)s: From Synthesis to Application, pp. 1-52. Berlin, Heidelberg: Springer Berlin Heidelberg, 2005.
- [65] Chinchilla, R. and Nájera, C. The Sonogashira Reaction: A Booming Methodology in Synthetic Organic Chemistry. Chemical Reviews 107(3) (2007): 874-922.
- [66] Kuroda, K. and Swager, T.M. Synthesis of a nonionic water soluble semiconductive polymer. Chemical Communications (1) (2003): 26-27.
- [67] Swager, T.M. The Molecular Wire Approach to Sensory Signal Amplification. Accounts of Chemical Research 31(5) (1998): 201-207.
- [68] Wilson, J.N., Bangcuyo, C.G., Erdogan, B., Myrick, M.L., and Bunz, U.H.F. Nanostructuring of Poly(aryleneethynylene)s: Formation of Nanotowers, Nanowires, and Nanotubules by Templated Self-Assembly. Macromolecules 36(5) (2003): 1426-1428.
- [69] Zhou, Q. and Swager, T.M. Fluorescent Chemosensors Based on Energy Migration in Conjugated Polymers: The Molecular Wire Approach to Increased Sensitivity. Journal of the American Chemical Society 117(50) (1995): 12593-12602.
- [70] Geng, J. and Zeng, T. Influence of Single-Walled Carbon Nanotubes Induced Crystallinity Enhancement and Morphology Change on Polymer Photovoltaic Devices. Journal of the American Chemical Society 128(51) (2006): 16827-16833.
- [71] Bunz, U.H.F. Poly(p-phenyleneethynylene)s by Alkyne Metathesis. Accounts of Chemical Research 34(12) (2001): 998-1010.
- [72] Brizius, G., Pschirer, N.G., Steffen, W., Stitzer, K., zur Loye, H.-C., and Bunz, U.H.F. Alkyne Metathesis with Simple Catalyst Systems: Efficient Synthesis of

- Conjugated Polymers Containing Vinyl Groups in Main or Side Chain. Journal of the American Chemical Society 122(50) (2000): 12435-12440.
- [73] Liu, J., Lam, J.W.Y., and Tang, B.Z. Acetylenic Polymers: Syntheses, Structures, and Functions. Chemical Reviews 109(11) (2009): 5799-5867.
- [74] Burke, D.J. and Lipomi, D.J. Green chemistry for organic solar cells. Energy & Environmental Science 6(7) (2013): 2053-2066.
- [75] Krebs, F.C., Nyberg, R.B., and Jørgensen, M. Influence of Residual Catalyst on the Properties of Conjugated Polyphenylenevinylene Materials: Palladium Nanoparticles and Poor Electrical Performance. Chemistry of Materials 16(7) (2004): 1313-1318.
- [76] Nielsen, K.T., Bechgaard, K., and Krebs, F.C. Removal of Palladium Nanoparticles from Polymer Materials. Macromolecules 38(3) (2005): 658-659.
- [77] Yin and Liebscher, J. Carbon–Carbon Coupling Reactions Catalyzed by Heterogeneous Palladium Catalysts. Chemical Reviews 107(1) (2007): 133-173.
- [78] Djakovitch, L. and Rollet, P. Sonogashira Cross-Coupling Reactions Catalysed by Copper-Free Palladium Zeolites. Advanced Synthesis & Catalysis 346(13-15) (2004): 1782-1792.
- [79] Djakovitch, L. and Rollet, P. Sonogashira cross-coupling reactions catalysed by heterogeneous copper-free Pd-zeolites. Tetrahedron Letters 45(7) (2004): 1367-1370.
- [80] Rollet, P., Kleist, W., Dufaud, V., and Djakovitch, L. Copper-free heterogeneous catalysts for the Sonogashira cross-coupling reaction: Preparation, characterisation, activity and applications for organic synthesis. Journal of Molecular Catalysis A: Chemical 241(1-2) (2005): 39-51.
- [81] Stevens, P.D., Li, G., Fan, J., Yen, M., and Gao, Y. Recycling of homogeneous Pd catalysts using superparamagnetic nanoparticles as novel soluble supports for Suzuki, Heck, and Sonogashira cross-coupling reactions. Chemical Communications (35) (2005): 4435-4437.

- [82] Kim, N., Kwon, M.S., Park, C.M., and Park, J. One-pot synthesis of recyclable palladium catalysts for hydrogenations and carbon–carbon coupling reactions. Tetrahedron Letters 45(38) (2004): 7057-7059.
- [83] Choudary, B.M., Madhi, S., Chowdari, N.S., Kantam, M.L., and Sreedhar, B. Layered Double Hydroxide Supported Nanopalladium Catalyst for Heck-, Suzuki-, Sonogashira-, and Stille-Type Coupling Reactions of Chloroarenes. Journal of the American Chemical Society 124(47) (2002): 14127-14136.
- [84] Novák, Z., Szabó, A., Répási, J., and Kotschy, A. Sonogashira Coupling of Aryl Halides Catalyzed by Palladium on Charcoal. The Journal of Organic Chemistry 68(8) (2003): 3327-3329.
- [85] Potts, K.T., Horwitz, C.P., Fessak, A., Keshavarz-K, M., Nash, K.E., and Toscano, P.J. Coordination of ethynylpyridine ligands with copper(I): x-ray structure of a novel triple-helical, tricuprous complex. Journal of the American Chemical Society 115(22) (1993): 10444-10445.
- [86] Samaritani, S. and Menicagli, R. Palladium on carbon catalyzed cross-coupling between alk-1-yne and 2-chloro-4,6-dialkoxy-1,3,5-triazines. Tetrahedron 58(7) (2002): 1381-1386.
- [87] Murakami, M., Hasegawa, N., Hayashi, M., and Ito, Y. Synthesis of (+-)-.alpha.-allokainic acid via the zinc acetate catalyzed cyclization of .gamma.-isocyano silyl enolates. The Journal of Organic Chemistry 56(26) (1991): 7356-7360.
- [88] Senra, J.D., Malta, L.F.B., de Souza, A.L.F., Medeiros, M.E., Aguiar, L.C.S., and Antunes, O.A.C. Phosphine-free Heck reactions in aqueous medium using hydroxypropylated cyclodextrins as supramolecular hosts. Tetrahedron Letters 48(46) (2007): 8153-8156.
- [89] Coelho, A.V., de Souza, A.L.F., de Lima, P.G., Wardell, J.L., and Antunes, O.A.C. Ligand-free Stille cross-coupling reaction using Pd/CaCO₃ as catalyst reservoir. Tetrahedron Letters 48(43) (2007): 7671-7674.

- [90] Sonogashira, K., Tohda, Y., and Hagihara, N. A convenient synthesis of acetylenes: catalytic substitutions of acetylenic hydrogen with bromoalkenes, iodoarenes and bromopyridines. Tetrahedron Letters 16(50) (1975): 4467-4470.
- [91] Chinchilla, R. and Najera, C. Recent advances in Sonogashira reactions. Chemical Society Reviews 40(10) (2011): 5084-5121.
- [92] Giesa, R. and Schulz, R.C. Soluble poly(1,4-phenyleneethynylene)s. Die Makromolekulare Chemie 191(4) (1990): 857-867.
- [93] Kong, K.C. and Cheng, C.H. Facile aryl-aryl exchange between the palladium center and phosphine ligands in palladium(II) complexes. Journal of the American Chemical Society 113(16) (1991): 6313-6315.
- [94] Goodson, F.E., Wallow, T.I., and Novak, B.M. Application of "Transfer-Free" Suzuki Coupling Protocols toward the Synthesis of "Unambiguously Linear" Poly(*p*-phenylenes). Macromolecules 31(7) (1998): 2047-2056.
- [95] Murage, J., Eddy, J.W., Zimbalist, J.R., McIntyre, T.B., Wagner, Z.R., and Goodson, F.E. Effect of Reaction Parameters on the Molecular Weights of Polymers Formed in a Suzuki Polycondensation. Macromolecules 41(20) (2008): 7330-7338.
- [96] Johansson Seechurn, C.C.C., Kitching, M.O., Colacot, T.J., and Snieckus, V. Palladium-Catalyzed Cross-Coupling: A Historical Contextual Perspective to the 2010 Nobel Prize. Angewandte Chemie International Edition 51(21) (2012): 5062-5085.
- [97] De La Rosa, M.A., Velarde, E., and Guzmán, A. Cross-Coupling Reactions of Monosubstituted Acetylenes and Aryl Halides Catalyzed by Palladium on Charcoal. Synthetic Communications 20(13) (1990): 2059-2064.
- [98] Tyrrell, E., Al-Saadi, A., and Millet, J. A Novel Silica-Supported Palladium Catalyst for a Copper-Free Sonogashira Coupling Reaction. Synlett (3) (2005): 487-488.

- [99] Zeng, M., et al. An efficient and recyclable heterogeneous palladium catalyst utilizing naturally abundant pearl shell waste. Green Chemistry 13(2) (2011): 350-356.
- [100] Saetan, T., Lertvachirapaiboon, C., Ekgasit, S., Sukwattanasinitt, M., and Wacharasindhu, S. Palladium Nanoparticles Immobilized on Individual Calcium Carbonate Plates Derived from Mussel Shell Waste: An Ecofriendly Catalyst for the Copper-Free Sonogashira Coupling Reaction. Chemistry – An Asian Journal 12(17) (2017): 2221-2230.
- [101] Jikei, M., Ishida, Y., Seo, Y., Kakimoto, M.-a., and Imai, Y. Preparation of Polycinnamamide Catalyzed by Palladium-Graphite through the Heck Reaction. Macromolecules 28(23) (1995): 7924-7928.
- [102] Guo, J., Ye, Y., Gao, S., and Feng, Y. Synthesis of polyketone catalyzed by Pd/C catalyst. Journal of Molecular Catalysis A: Chemical 307(1–2) (2009): 121-127.
- [103] Liu, S.-Y., et al. Pd/C as a Clean and Effective Heterogeneous Catalyst for C–C Couplings toward Highly Pure Semiconducting Polymers. Macromolecules 45(22) (2012): 9004-9009.
- [104] Bae, I.H., Lee, I.-H., Byun, S., Chung, J., Kim, B.M., and Choi, T.-L. Magnetically recyclable Pd-Fe₃O₄ heterodimer nanocrystals for the synthesis of conjugated polymers via suzuki polycondensation: Toward green chemistry. Journal of Polymer Science Part A: Polymer Chemistry 52(11) (2014): 1525-1528.
- [105] Hayashi, S., Kojima, Y., and Koizumi, T. Highly regioselective Pd/C-catalyzed direct arylation toward thiophene-based π -conjugated polymers. Polymer Chemistry 6(6) (2015): 881-885.
- [106] Kojima, Y., Hayashi, S., and Koizumi, T. Palladium on carbon-catalyzed direct C–H arylation polycondensation of 3,4-ethylenedioxythiophene with various dibromoarenes. Journal of Polymer Science Part A: Polymer Chemistry 55(7) (2017): 1183-1188.

- [107] Yong, X., et al. Thiourea-functionalized poly(phenyleneethynylene): fluorescent chemosensors for anions and cations. Polymer Chemistry 4(15) (2013): 4126.
- [108] Zhang, W. and Huang, P.C. Effect of the substituting groups and their positions on the optical properties of phenylacetylenic compounds. Materials Chemistry and Physics 96(2-3) (2006): 283-288.
- [109] Brouwer, A.M. Standards for Photoluminescence Quantum Yield Measurements in Solution (IUPAC Technical Report). 2011: Pure and Applied Chemistry. 2213.
- [110] Fery-Forgues, S. and Lavabre, D. Are Fluorescence Quantum Yields So Tricky to Measure? A Demonstration Using Familiar Stationery Products. Journal of Chemical Education 76(9) (1999): 1260.
- [111] Egbe, D.A.M., Roll, C.P., Birckner, E., Grummt, U.-W., Stockmann, R., and Klemm, E. Side Chain Effects in Hybrid PPV/PPE Polymers. Macromolecules 35(10) (2002): 3825-3837.
- [112] Sato, T., Jiang, D.-L., and Aida, T. A Blue-Luminescent Dendritic Rod: Poly(phenyleneethynylene) within a Light-Harvesting Dendritic Envelope. Journal of the American Chemical Society 121(45) (1999): 10658-10659.
- [113] Swager, T.M., Gil, C.J., and Wrighton, M.S. Fluorescence Studies of Poly(p-phenyleneethynylene)s: The Effect of Anthracene Substitution. The Journal of Physical Chemistry 99(14) (1995): 4886-4893.
- [114] Crisp, G.T. and Bubner, T.P. Preparation of sterically constrained arylalkyne oligomers. Tetrahedron 53(34) (1997): 11899-11912.
- [115] Chuentragool, P., Vongnam, K., Rashatasakhon, P., Sukwattanasinitt, M., and Wacharasindhu, S. Calcium carbide as a cost-effective starting material for symmetrical diarylethynes via Pd-catalyzed coupling reaction. Tetrahedron 67(42) (2011): 8177-8182.

- [116] Li, J., Kendig, C.E., and Nesterov, E.E. Chemosensory Performance of Molecularly Imprinted Fluorescent Conjugated Polymer Materials. Journal of the American Chemical Society 129(51) (2007): 15911-15918.
- [117] Corradi, E., Meille, S.V., Messina, M.T., Metrangolo, P., and Resnati, G. Halogen Bonding versus Hydrogen Bonding in Driving Self-Assembly Processes. Angewandte Chemie International Edition 39(10) (2000): 1782-1786.
- [118] Iraqi, A. and Wataru, I. 3,6-linked 9-alkyl-9H-carbazole main-chain polymers: Preparation and properties. Journal of Polymer Science Part A: Polymer Chemistry 42(23) (2004): 6041-6051.
- [119] Ramakrishna, J. and Venkatakrisnan, P. Bigger and Brighter Fluorenes: Facile π -Expansion, Brilliant Emission and Sensing of Nitroaromatics. Chemistry – An Asian Journal 12(2) (2017): 181-189.
- [120] Harriman, A., Mallon, L.J., Elliot, K.J., Haefele, A., Ulrich, G., and Ziesel, R. Length Dependence for Intramolecular Energy Transfer in Three- and Four-Color Donor–Spacer–Acceptor Arrays. Journal of the American Chemical Society 131(37) (2009): 13375-13386.
- [121] Wang, S., Wu, B., Liu, F., Gao, Y., and Zhang, W. A well-defined alternating copolymer based on a salicylaldehyde Schiff base for highly sensitive zinc(ii) detection and pH sensing in aqueous solution. Polymer Chemistry 6(7) (2015): 1127-1136.
- [122] Kim, W.Y., et al. Coumarin-decorated Schiff base hydrolysis as an efficient driving force for the fluorescence detection of water in organic solvents. Chemical Communications 52(56) (2016): 8675-8678.
- [123] Stringer, T., Chellan, P., Therrien, B., Shunmoogam-Gounden, N., Hendricks, D.T., and Smith, G.S. Synthesis and structural characterization of binuclear palladium(II) complexes of salicylaldehyde dithiosemicarbazones. Polyhedron 28(14) (2009): 2839-2846.

- [124] Keleş, M., Keleş, H., and Emir, D.M. Pd(II) complexes of Schiff bases and their application as catalysts in Mizoroki–Heck and Suzuki–Miyaura cross-coupling reactions. Applied Organometallic Chemistry 29(8) (2015): 543-548.
- [125] Baker, A.W. and Shulgin, A.T. Intramolecular Hydrogen Bonding. II. The Determination of Hammett Sigma Constants by Intramolecular Hydrogen Bonding in Schiff's Bases. Journal of the American Chemical Society 81(7) (1959): 1523-1529.
- [126] Freedman, H.H. Intramolecular H-Bonds. I. A Spectroscopic Study of the Hydrogen Bond between Hydroxyl and Nitrogen. Journal of the American Chemical Society 83(13) (1961): 2900-2905.
- [127] Mutai, T., Sawatani, H., Shida, T., Shono, H., and Araki, K. Tuning of Excited-State Intramolecular Proton Transfer (ESIPT) Fluorescence of Imidazo[1,2-a]pyridine in Rigid Matrices by Substitution Effect. The Journal of Organic Chemistry 78(6) (2013): 2482-2489.
- [128] Tiwari, K., Mishra, M., and Singh, V.P. A highly sensitive and selective fluorescent sensor for Al³⁺ ions based on thiophene-2-carboxylic acid hydrazide Schiff base. RSC Advances 3(30) (2013): 12124-12132.
- [129] Dekker, G.P.C.M., Elsevier, C.J., Vrieze, K., van Leeuwen, P.W.N.M., and Roobeek, C.F. Influence of ligands and anions on the insertion of alkenes into palladium-acyl and palladium-carbomethoxy bonds in the neutral complex (dppp)Pd(C(O)CH₃)Cl and the ionic complexes [(P–P)PdR(L)]+SO₃CF₃[–] (P–P = dppe, dppp, dppb; R = C(O)CH₃, L = CH₃CN, PPh₃; R = C(O)OCH₃, L = PPh₃). Journal of Organometallic Chemistry 430(3) (1992): 357-372.
- [130] Kamer, P.C.J., van Leeuwen, P.W.N.M., and Reek, J.N.H. Wide Bite Angle Diphosphines: Xantphos Ligands in Transition Metal Complexes and Catalysis. Accounts of Chemical Research 34(11) (2001): 895-904.
- [131] Markl, F., et al. Printing PPEs: Fundamental Structure–Property Relationships. ACS Macro Letters 3(8) (2014): 788-790.

- [132] Wang, Y., Park, J.S., Leech, J.P., Miao, S., and Bunz, U.H.F. Poly(aryleneethynylene)s with Orange, Yellow, Green, and Blue Solid-State Fluorescence. Macromolecules 40(6) (2007): 1843-1850.
- [133] Doucet, H. and Hierso, J.-C. Palladium-Based Catalytic Systems for the Synthesis of Conjugated Enynes by Sonogashira Reactions and Related Alkynylations. Angewandte Chemie International Edition 46(6) (2007): 834-871.
- [134] Fleckenstein, C.A. and Plenio, H. Sterically demanding trialkylphosphines for palladium-catalyzed cross coupling reactions-alternatives to PtBu_3 . Chemical Society Reviews 39(2) (2010): 694-711.
- [135] Bilbrey, J.A., Kazez, A.H., Locklin, J., and Allen, W.D. Exact ligand cone angles. Journal of Computational Chemistry 34(14) (2013): 1189-1197.
- [136] Bao, Z., Chan, W.K., and Yu, L. Exploration of the Stille Coupling Reaction for the Synthesis of Functional Polymers. Journal of the American Chemical Society 117(50) (1995): 12426-12435.
- [137] Carsten, B., He, F., Son, H.J., Xu, T., and Yu, L. Stille Polycondensation for Synthesis of Functional Materials. Chemical Reviews 111(3) (2011): 1493-1528.
- [138] Moroni, M., Le Moigne, J., and Luzzati, S. Rigid rod conjugated polymers for nonlinear optics: 1. Characterization and linear optical properties of poly(aryleneethynylene) derivatives. Macromolecules 27(2) (1994): 562-571.
- [139] Rubin, Y., Lin, S.S., Knobler, C.B., Anthony, J., Boldi, A.M., and Diederich, F. Solution-spray flash vacuum pyrolysis: a new method for the synthesis of linear polyynes with odd numbers of C-C bonds from substituted 3,4-dialkynyl-3-cyclobutene-1,2-diones. Journal of the American Chemical Society 113(18) (1991): 6943-6949.
- [140] Goodson, F.E., Wallow, T.I., and Novak, B.M. Mechanistic Studies on the Aryl-Aryl Interchange Reaction of ArPdL_2I (L = Triarylphosphine) Complexes. Journal of the American Chemical Society 119(51) (1997): 12441-12453.

- [141] Xiong, X., Cai, L., Jiang, Y., and Han, Q. Eco-Efficient, Green, and Scalable Synthesis of 1,2,3-Triazoles Catalyzed by Cu(I) Catalyst on Waste Oyster Shell Powders. ACS Sustainable Chemistry & Engineering 2(4) (2014): 765-771.
- [142] Al-Sogair, F.M., Operschall, B.P., Sigel, A., Sigel, H., Schnabl, J., and Sigel, R.K.O. Probing the Metal-Ion-Binding Strength of the Hydroxyl Group. Chemical Reviews 111(8) (2011): 4964-5003.
- [143] Bunz, U.H.F. Poly(aryleneethynylene)s. Macromolecular Rapid Communications 30(9-10) (2009): 772-805.



APPENDIX A

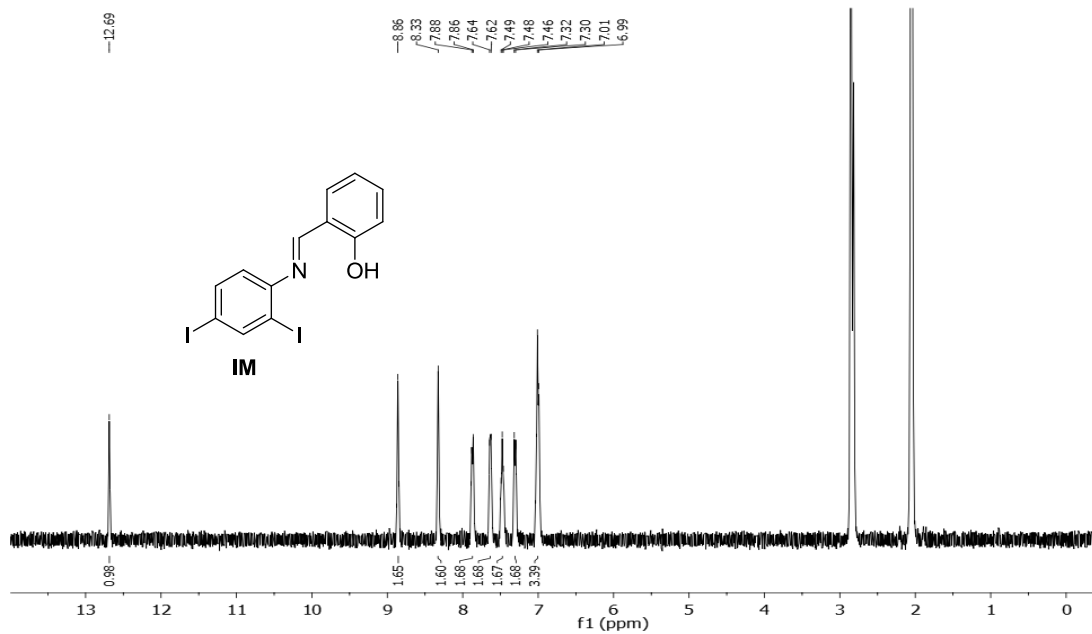


Figure A.1 ¹H NMR of IM in acetone-*d*₆

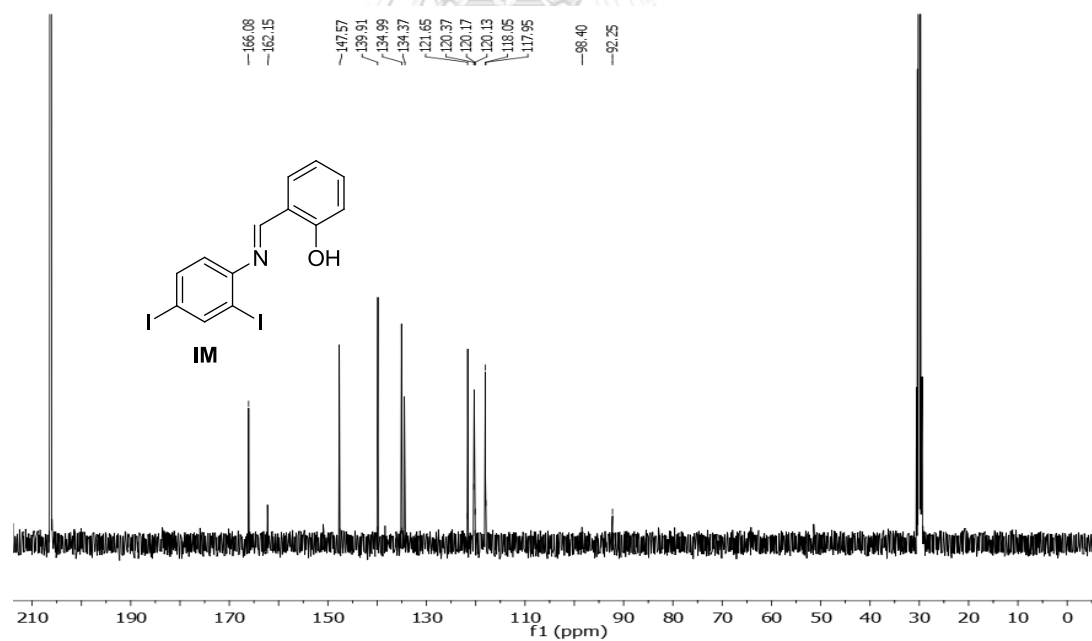


Figure A.2 ¹³C NMR of IM in acetone-*d*₆

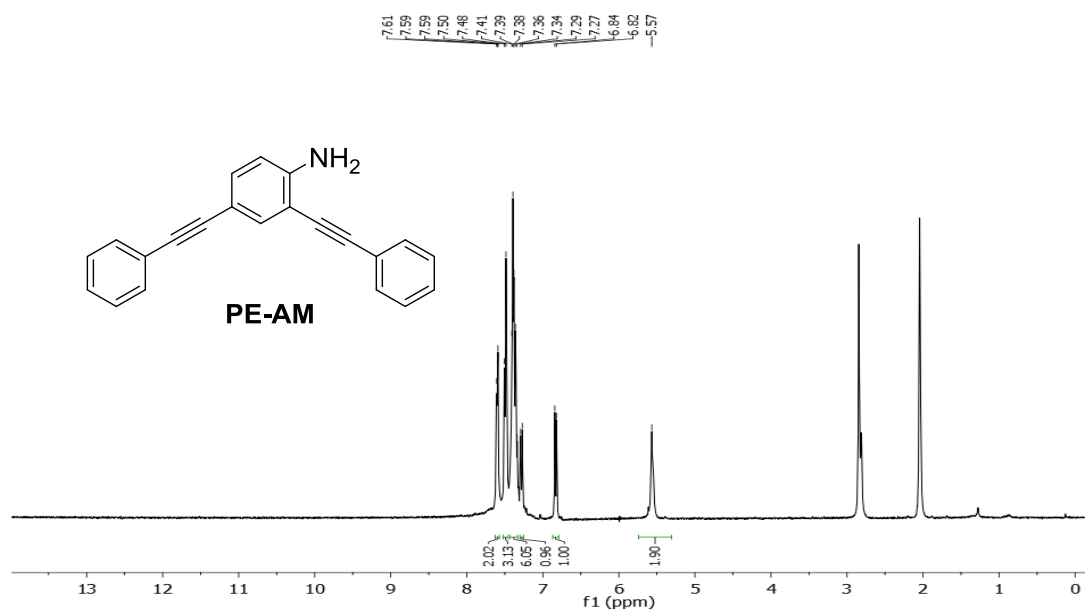


Figure A.3 $^1\text{H NMR}$ of PE-AM in acetone- d_6

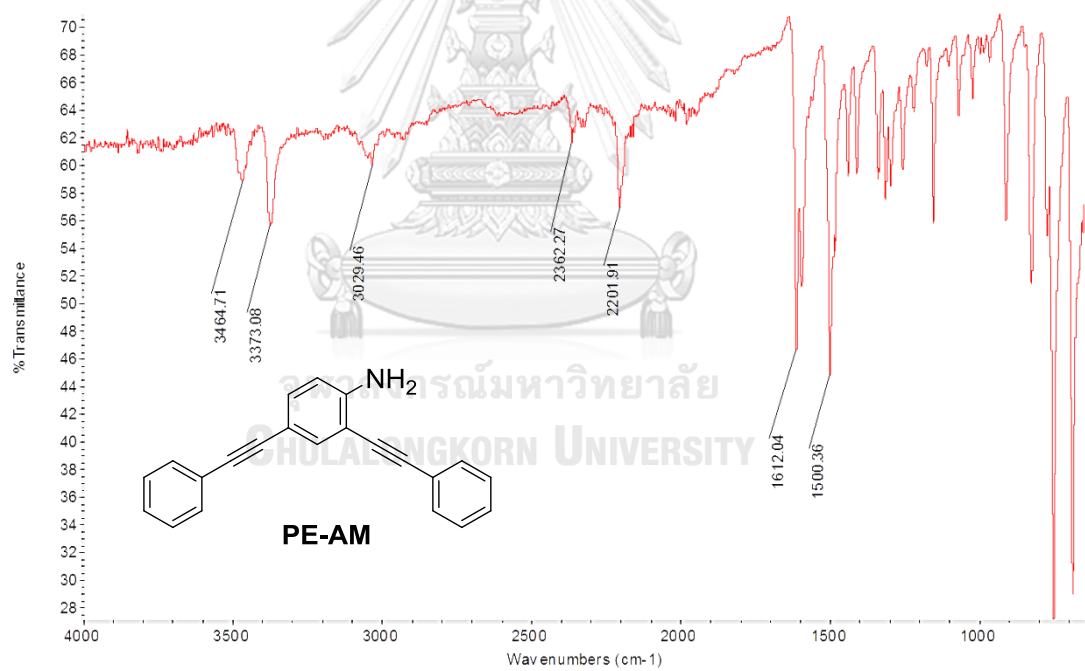


Figure A.4 FT-IR of PE-AM

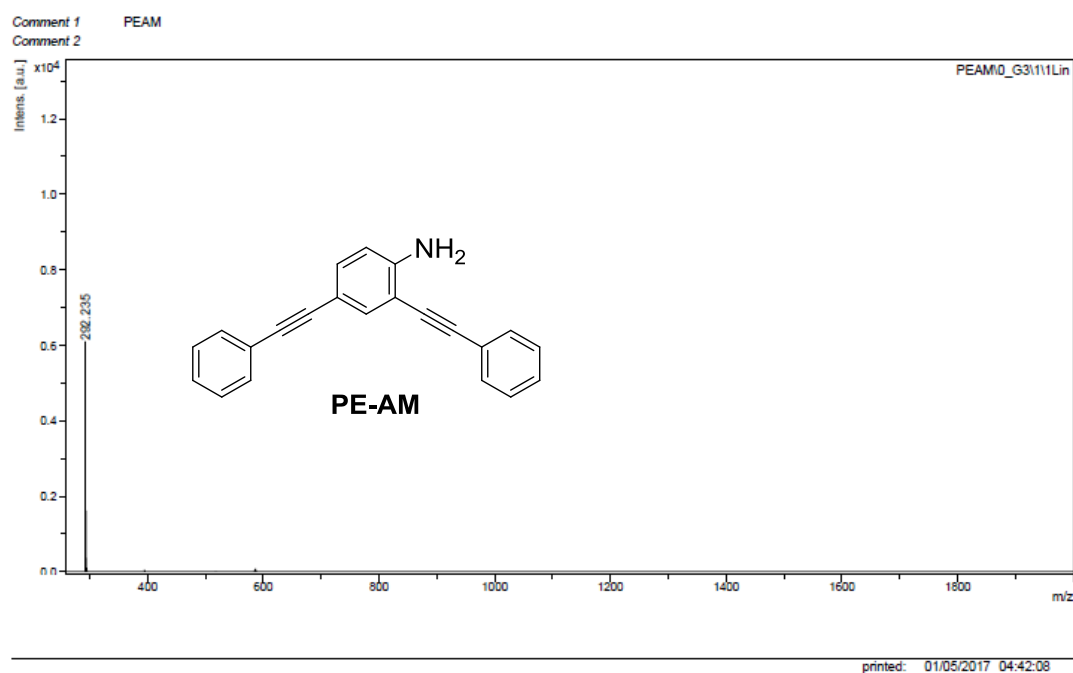
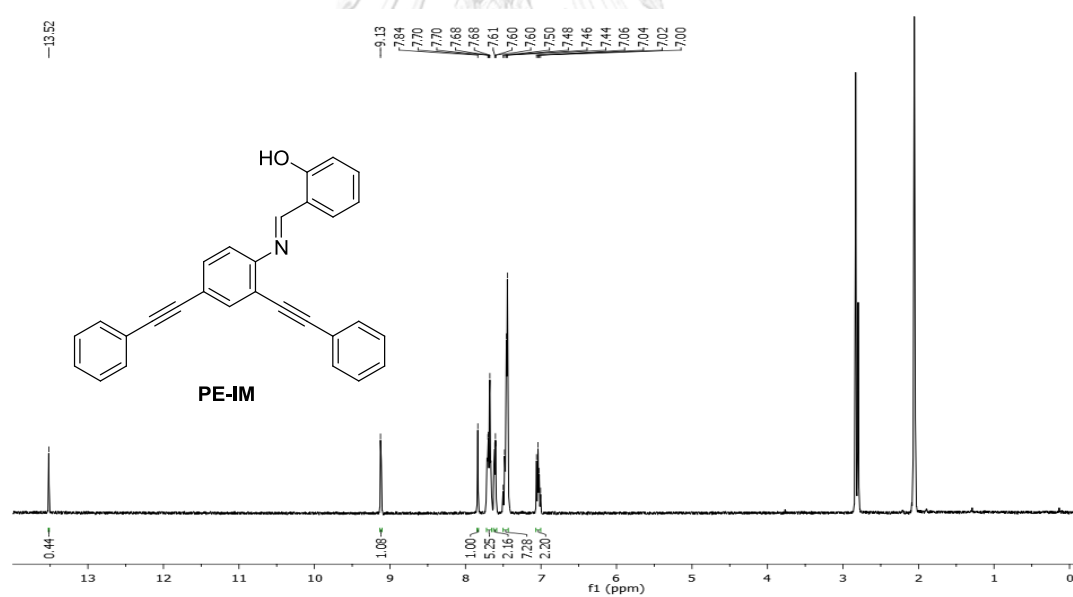


Figure A.5 MALDI-TOF MS of PE-AM

Figure A.6 ^1H NMR of PE-IM in acetone- d_6

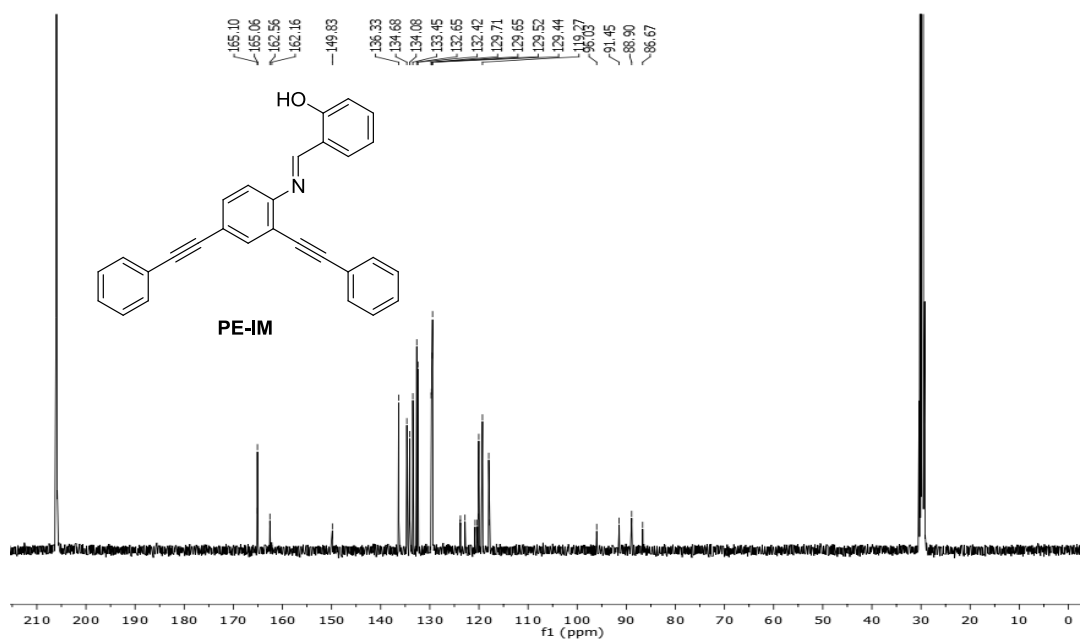


Figure A.7 ^{13}C NMR of PE-IM in acetone- d_6

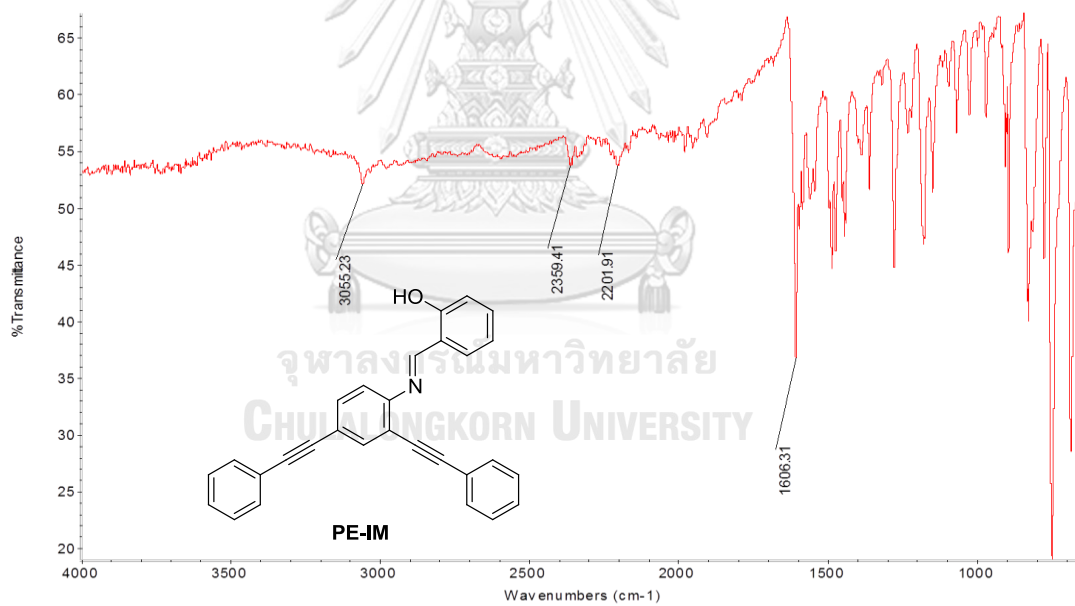


Figure A.8 FT-IR of PE-IM

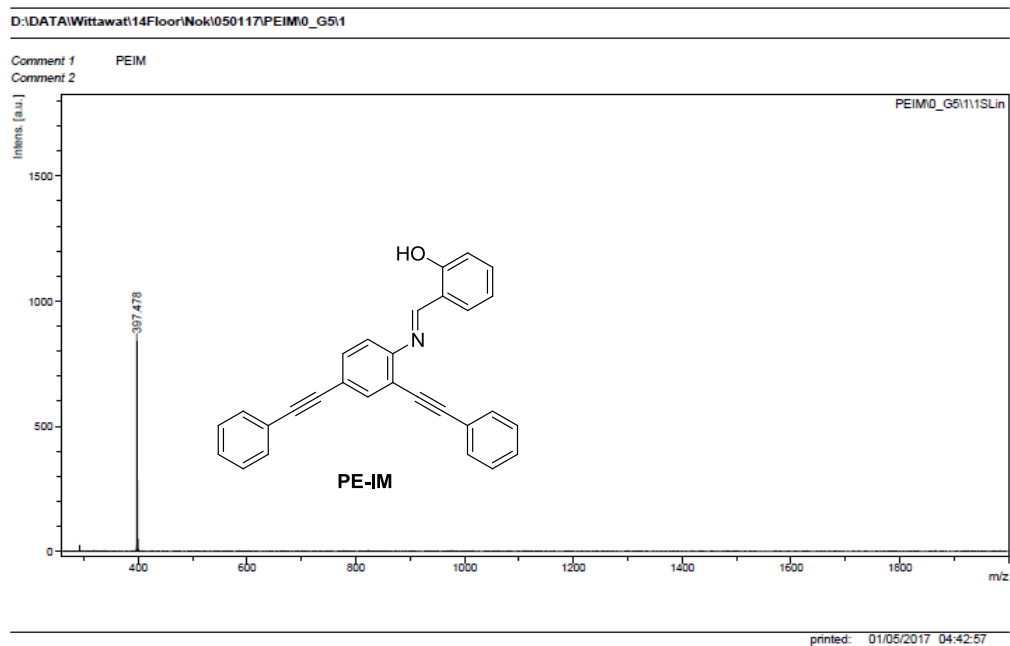
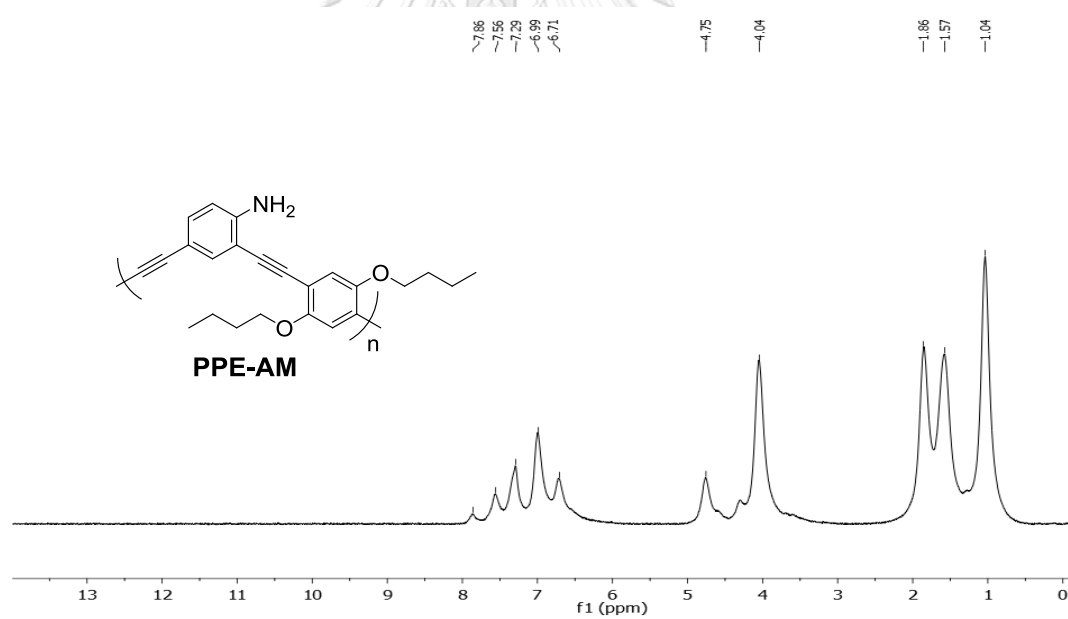


Figure A.9 MALDI-TOF MS of PE-IM

Figure A.10 ^1H NMR of PPE-AM in CDCl_3

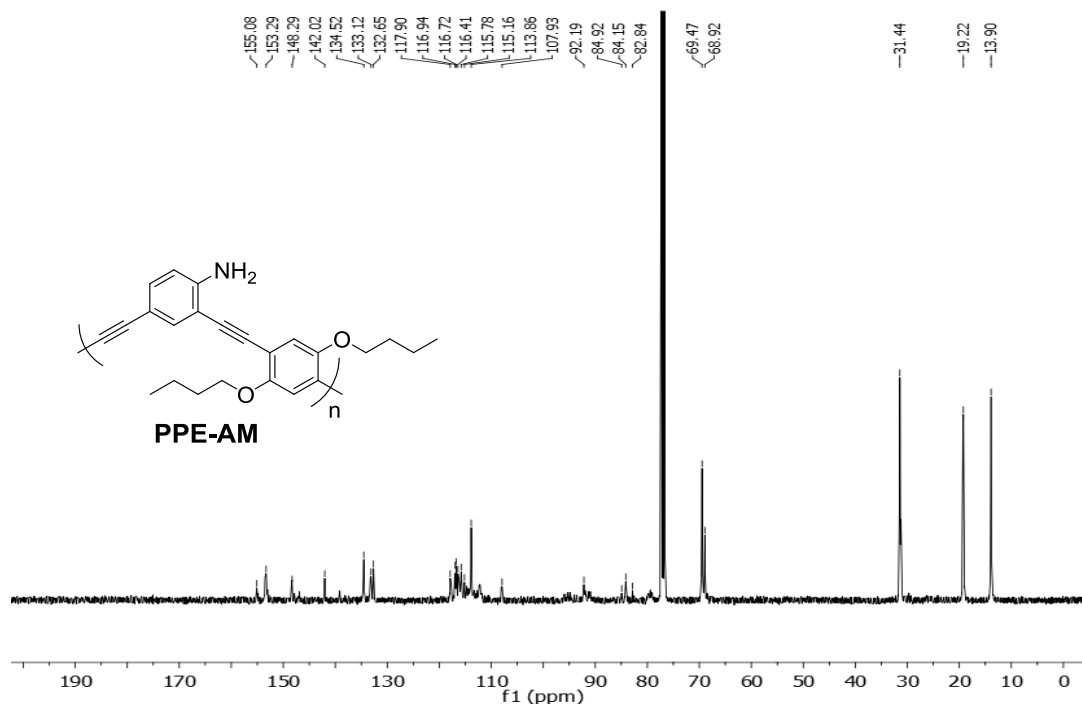


Figure A.11 ^{13}C NMR of PPE-AM in CDCl_3

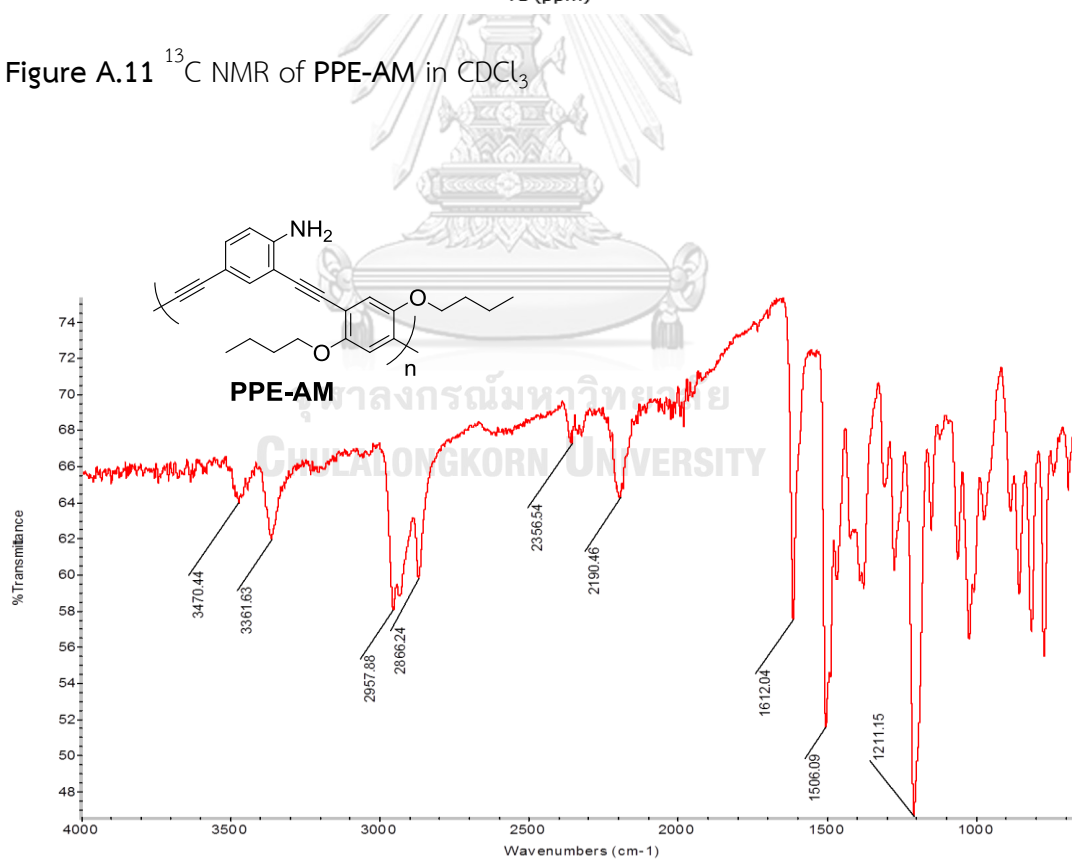


Figure A.12 FT-IR of PPE-AM

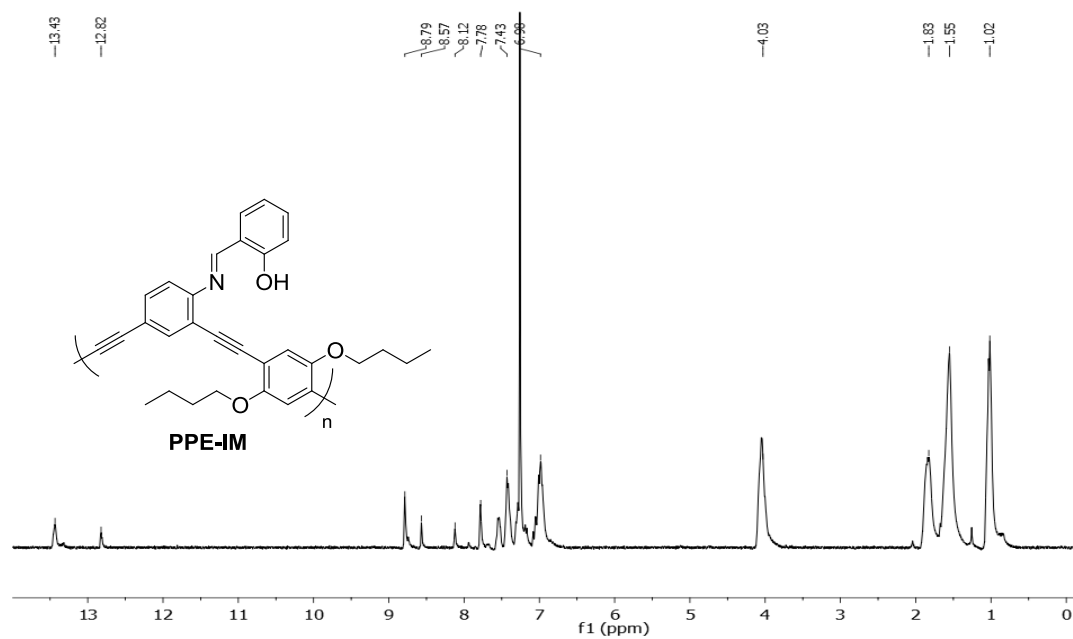


Figure A.13 ^1H NMR of PPE-IM in CDCl_3

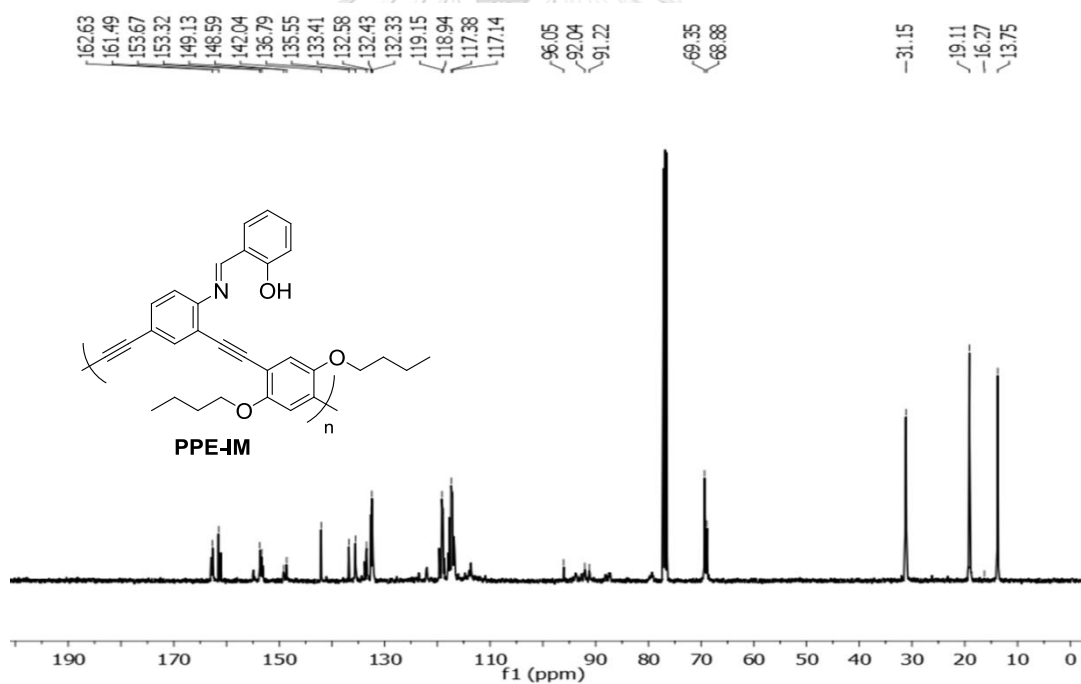


Figure A.14 ^{13}C NMR of PPE-IM in CDCl_3

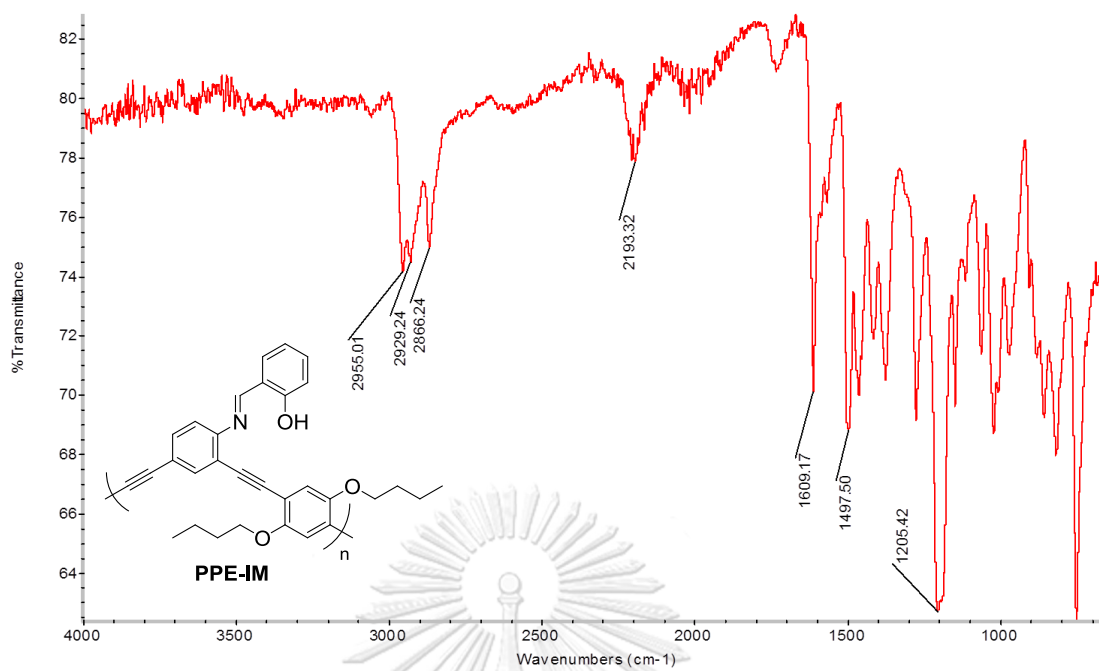
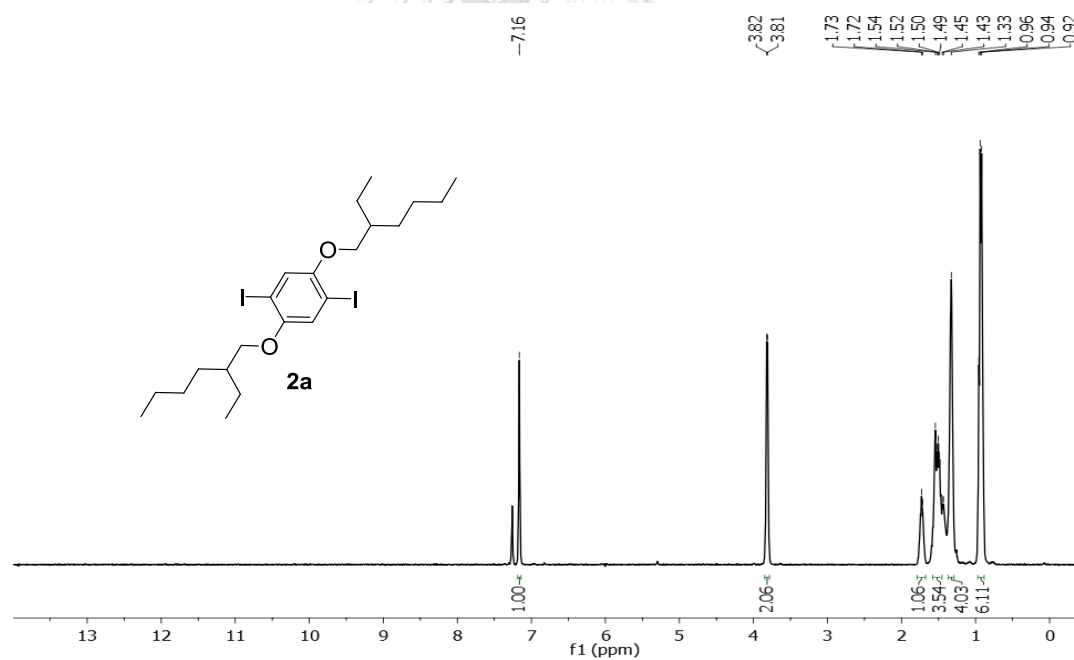
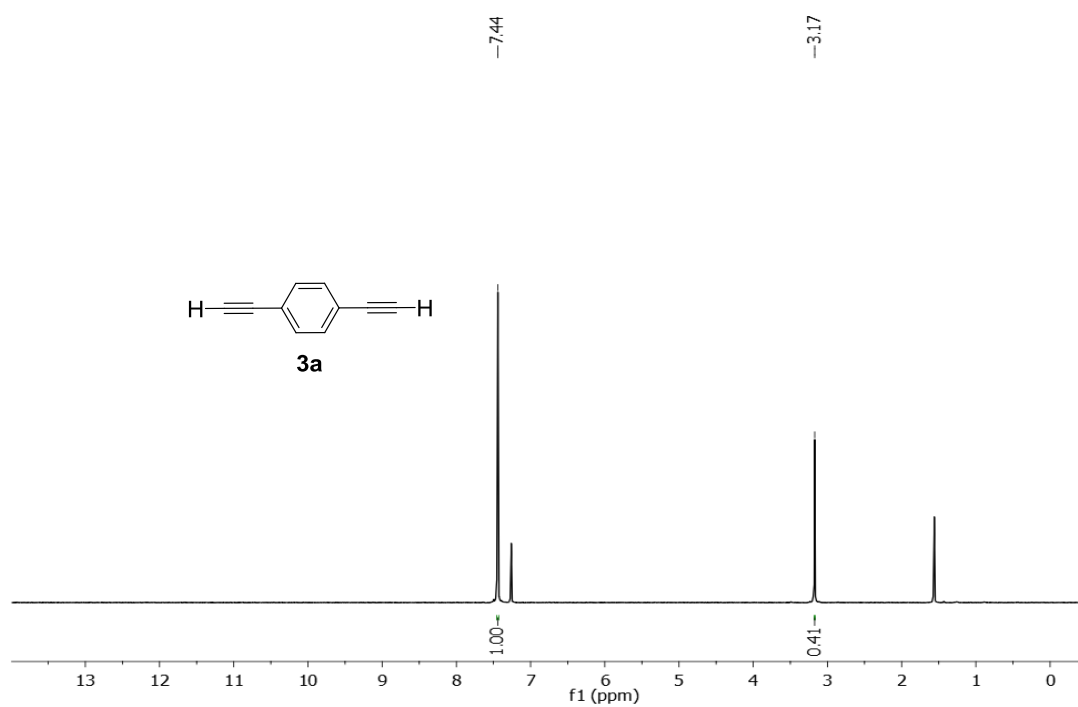
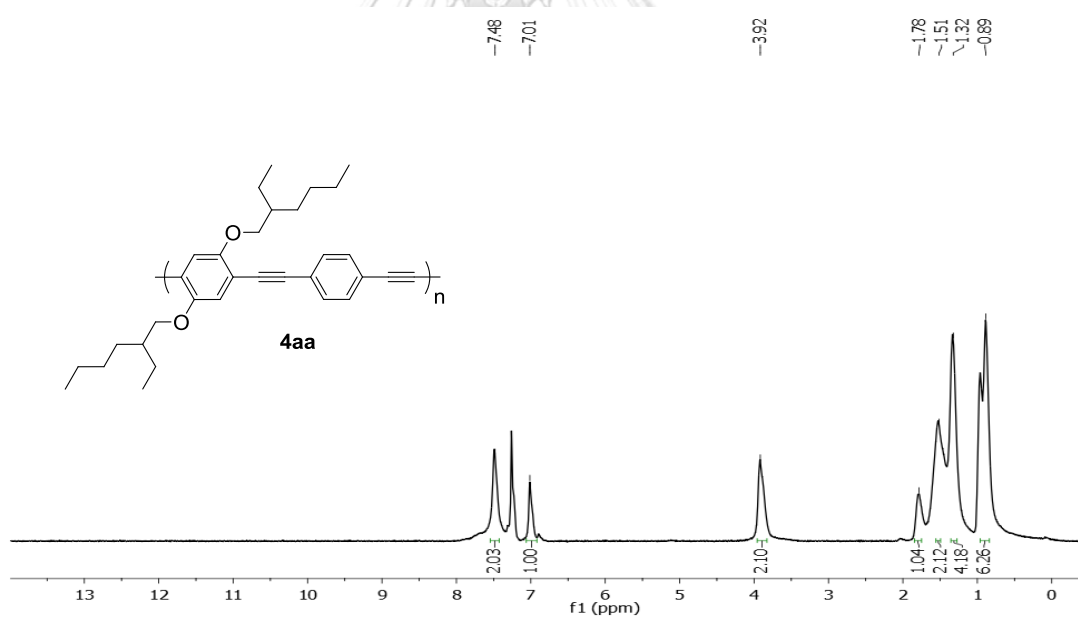


Figure A.15 FT-IR of PPE-IM

Figure A.16 ¹H NMR of 2a in CDCl₃

Figure A.17 ^1H NMR of **3a** in CDCl_3 Figure A.18 ^1H NMR of **4aa** obtained from Pd/CaCO_3 catalyst in CDCl_3

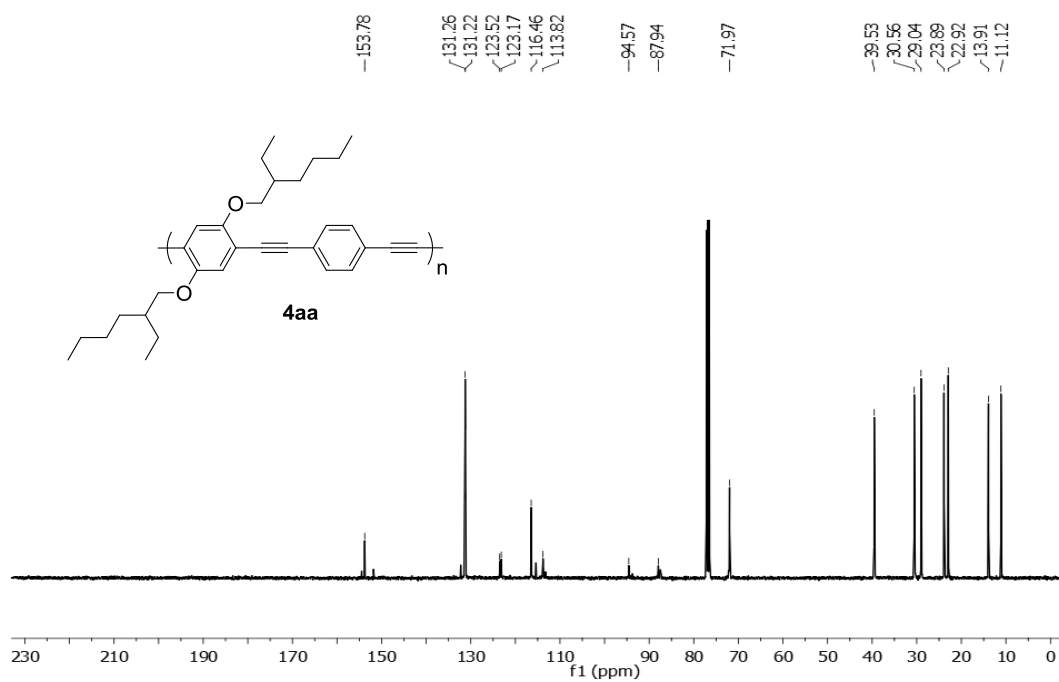


Figure A.19 ^{13}C NMR of **4aa** obtained from Pd/CaCO₃ catalyst in CDCl₃

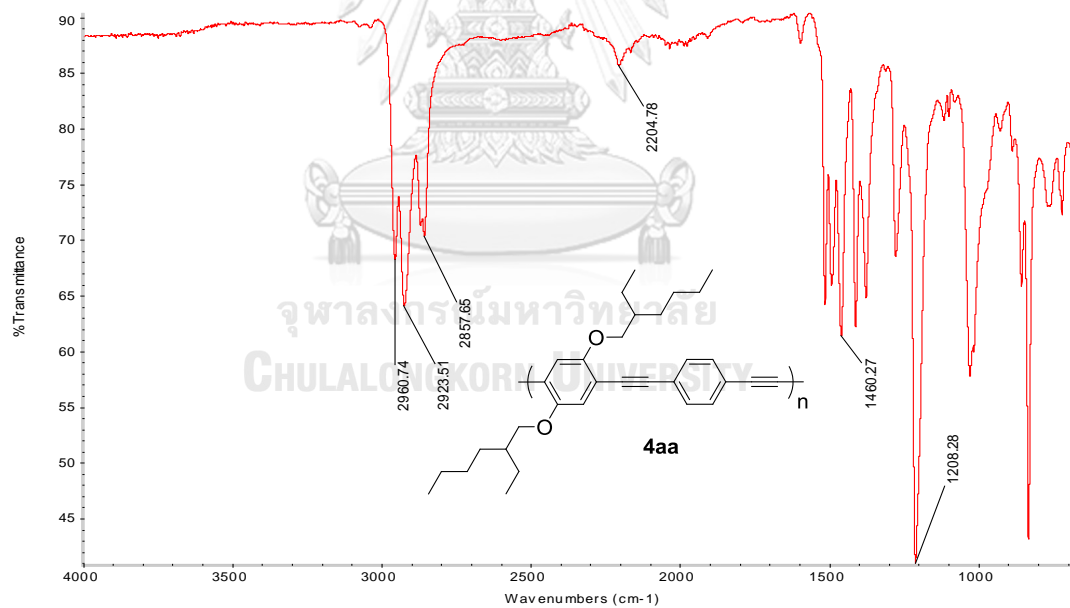


Figure A.20 FT-IR of **4aa** obtained from Pd/CaCO₃ catalyst

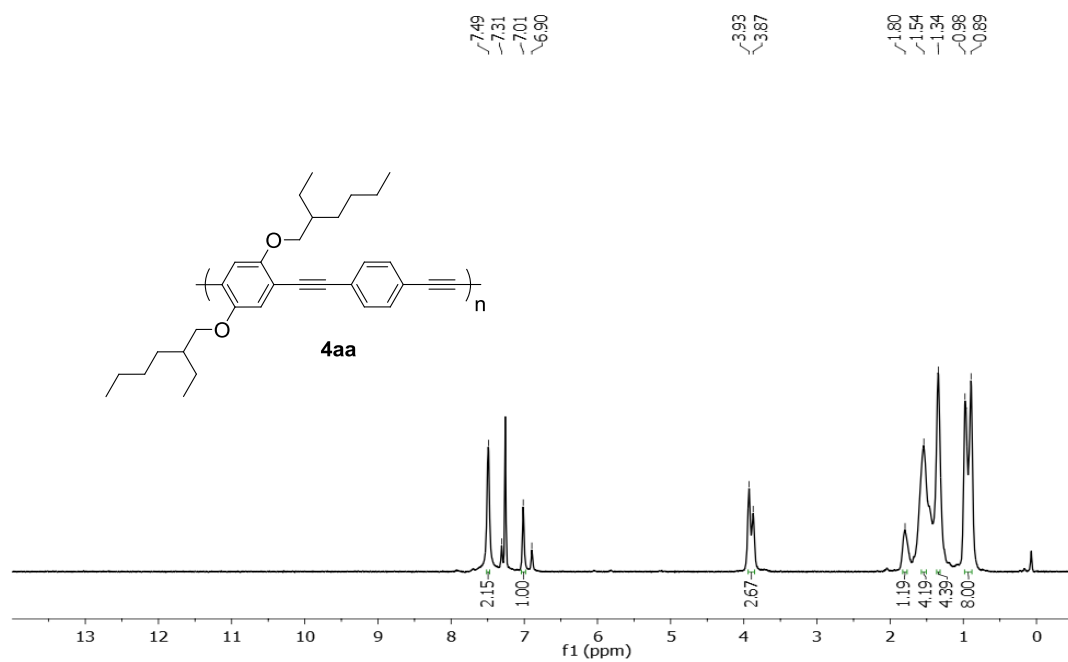


Figure A.21 ^1H NMR of **4aa** obtained from $\text{PdCl}_2(\text{PPh}_3)_2$ catalyst in CDCl_3

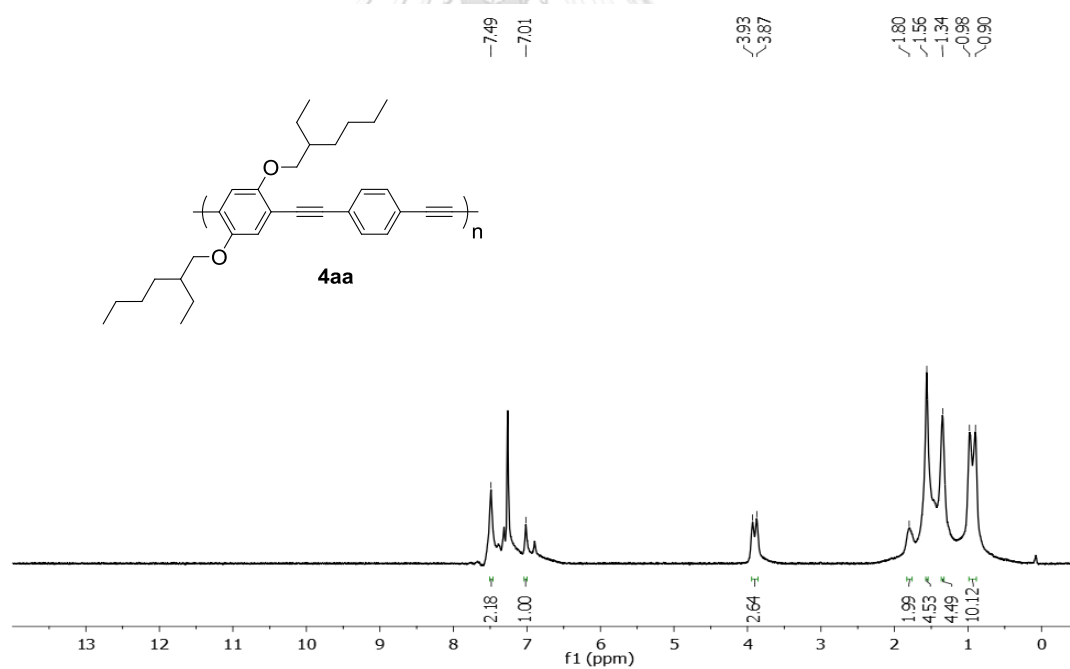


Figure A.22 ^1H NMR of **4aa** obtained from $\text{Pd}(\text{PPh}_3)_4$ catalyst in CDCl_3

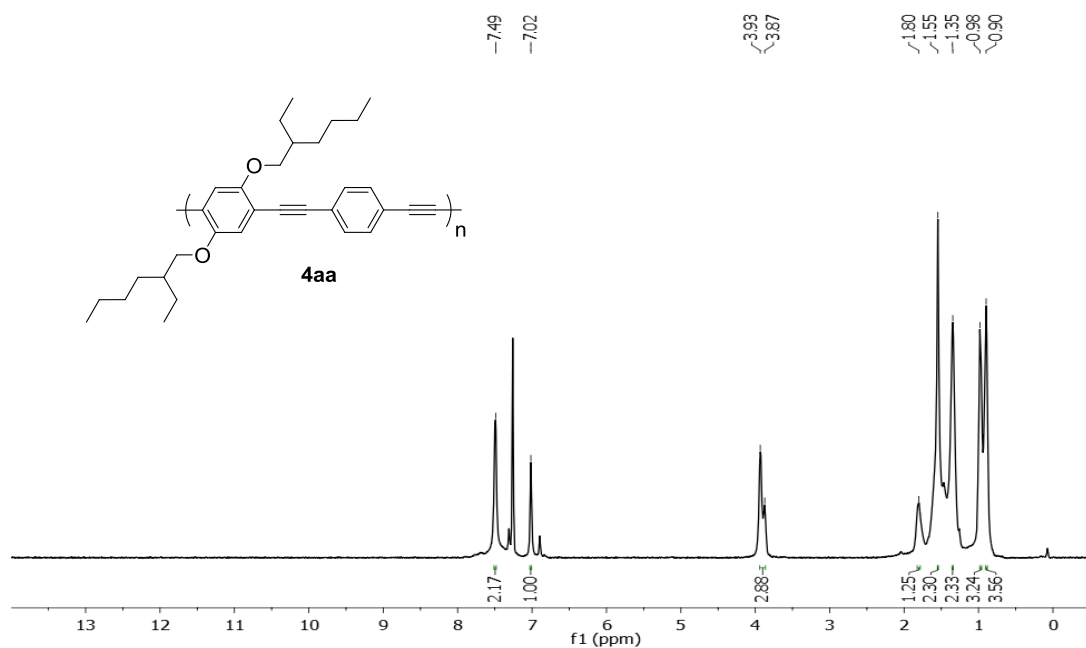


Figure A.23 ^1H NMR of **4aa** obtained from Pd/C catalyst in CDCl_3

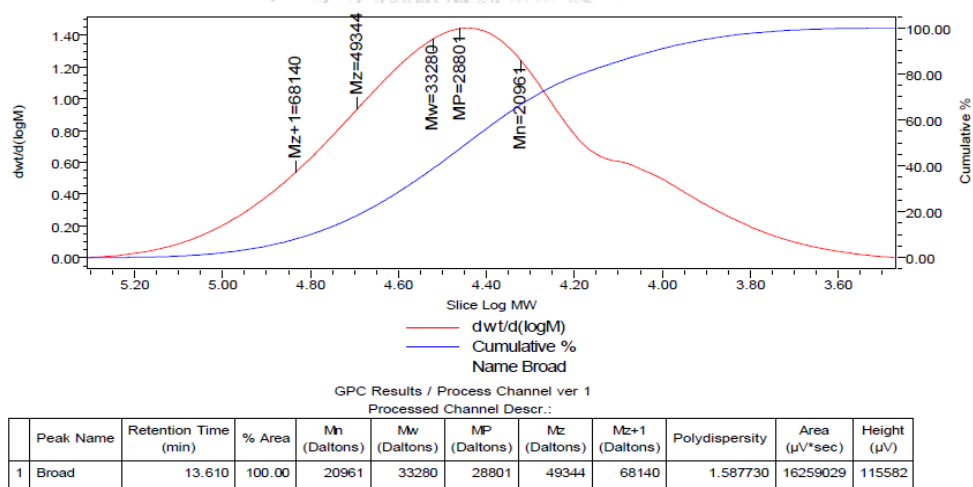
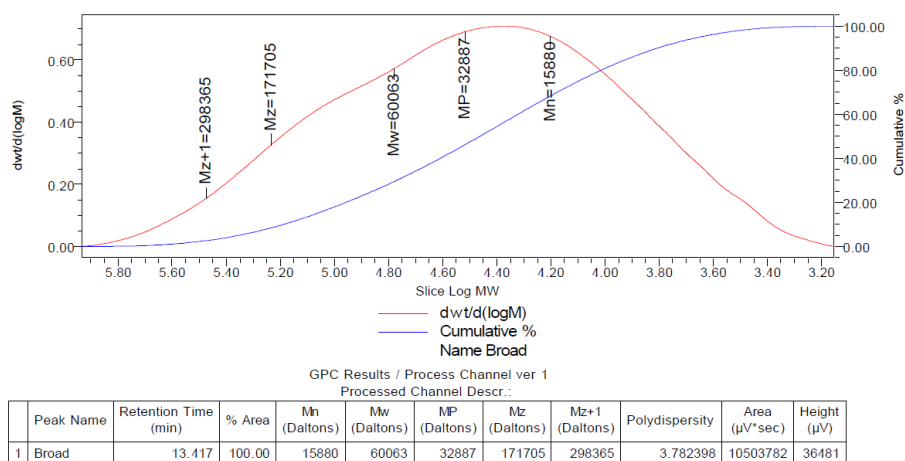
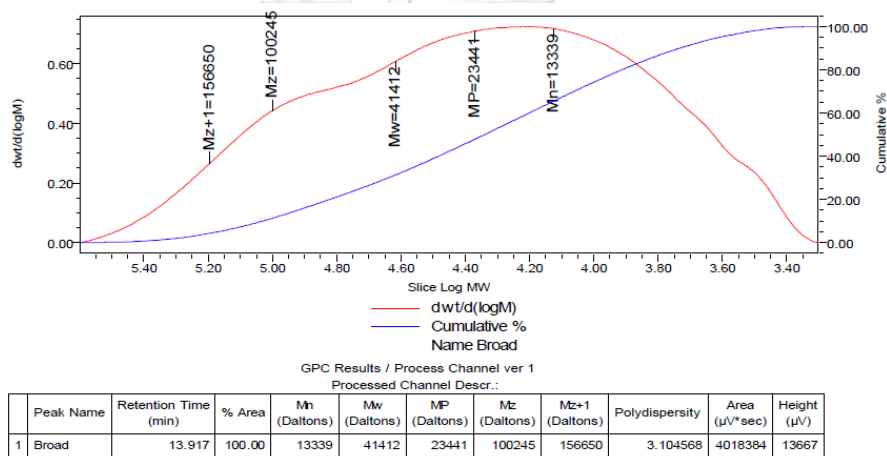
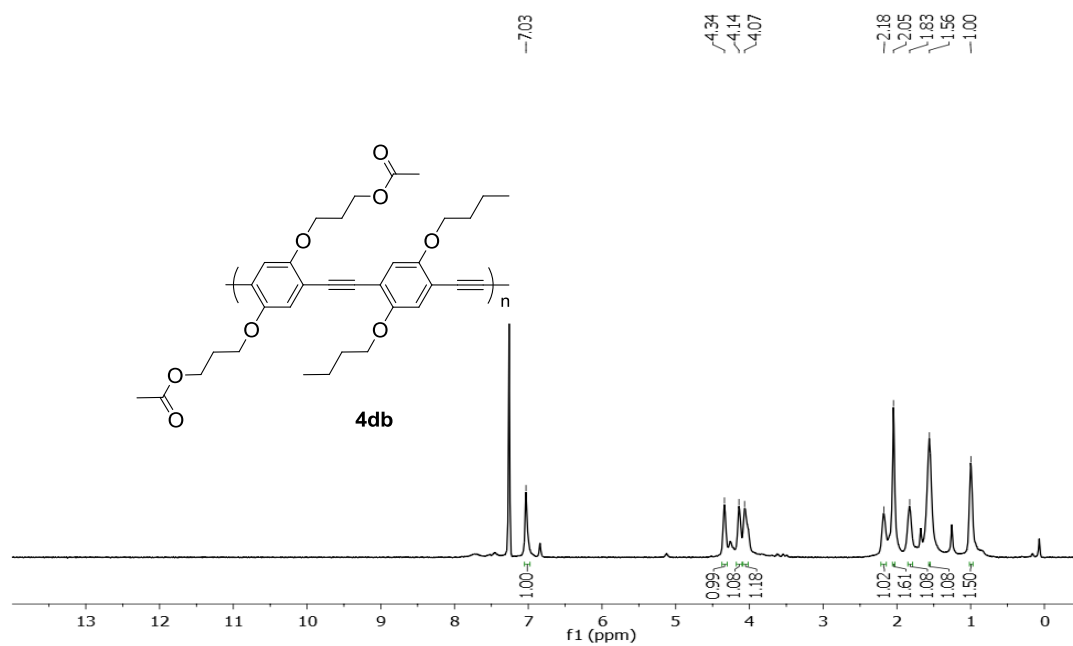
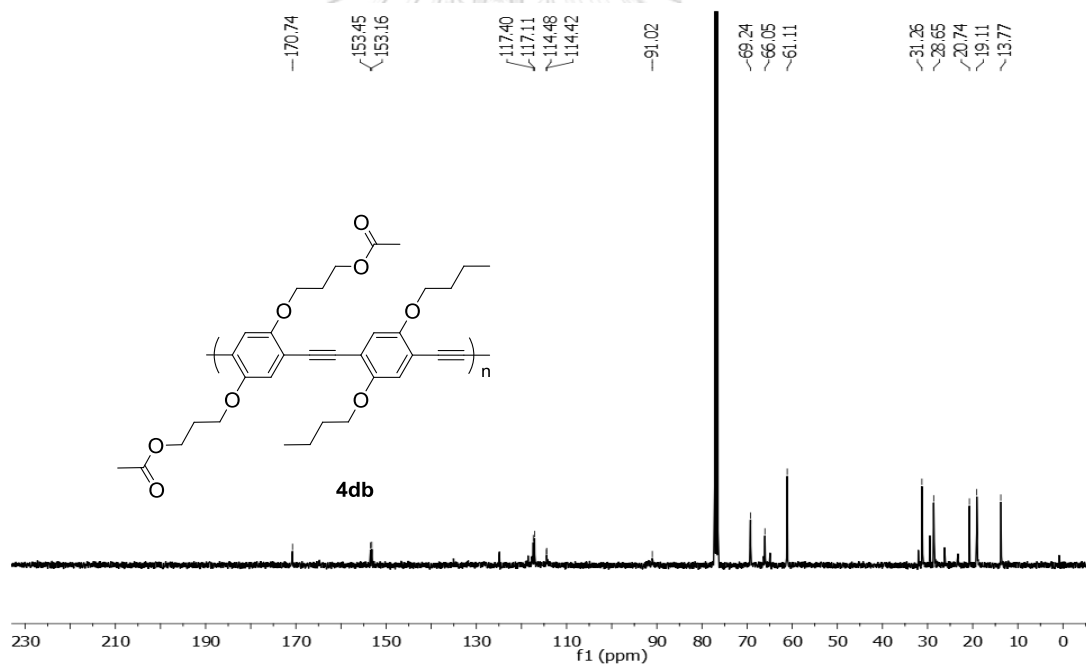
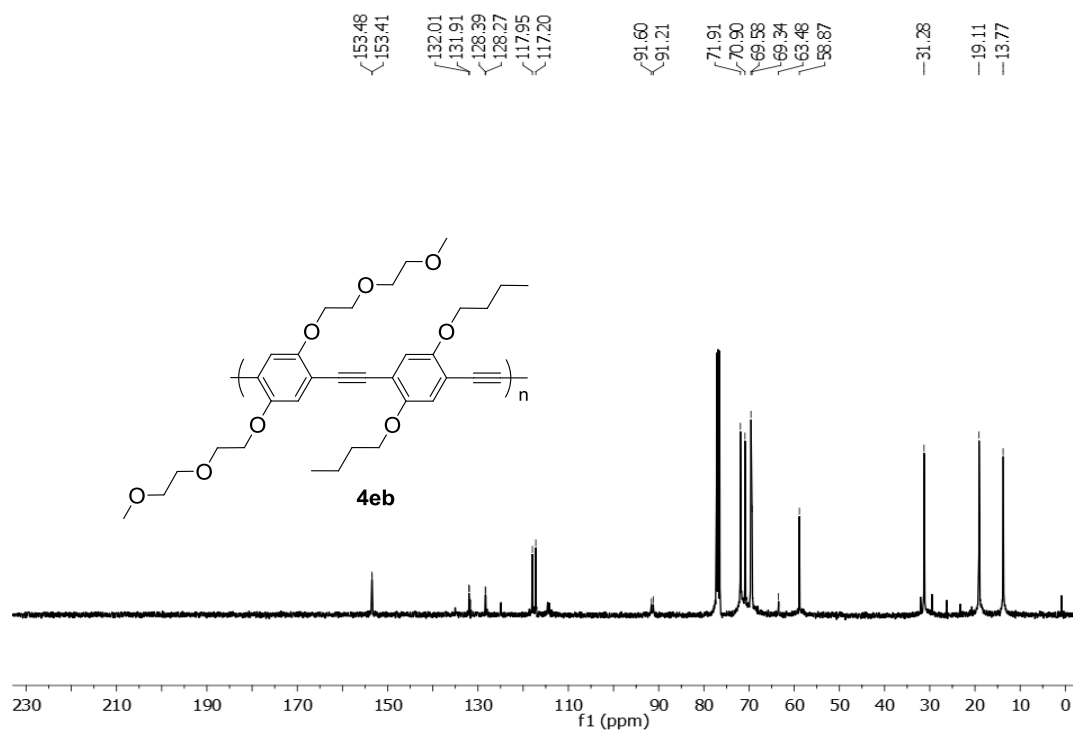
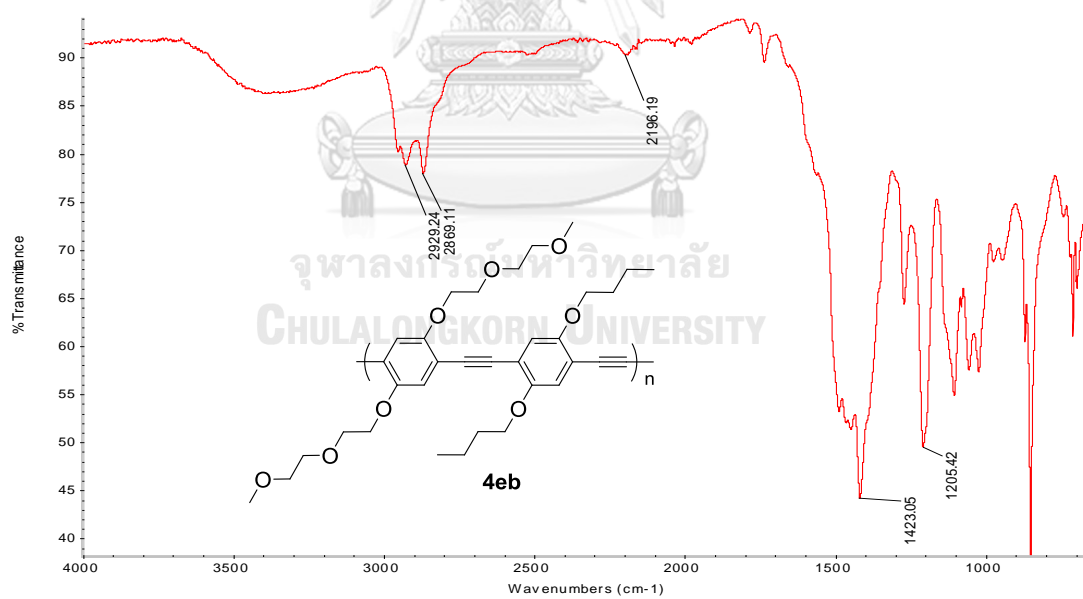
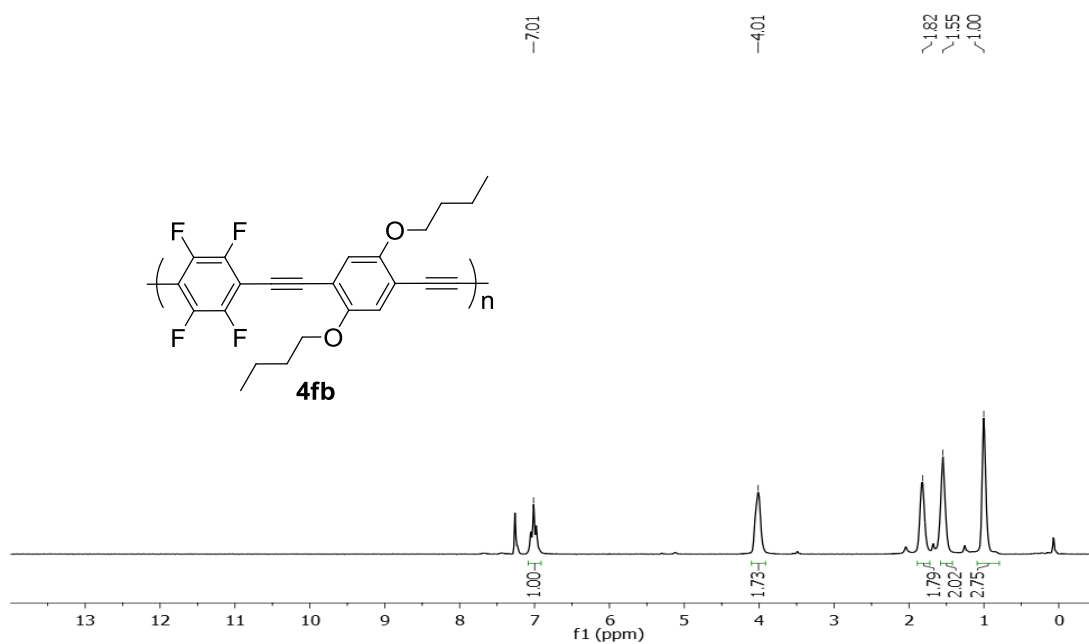
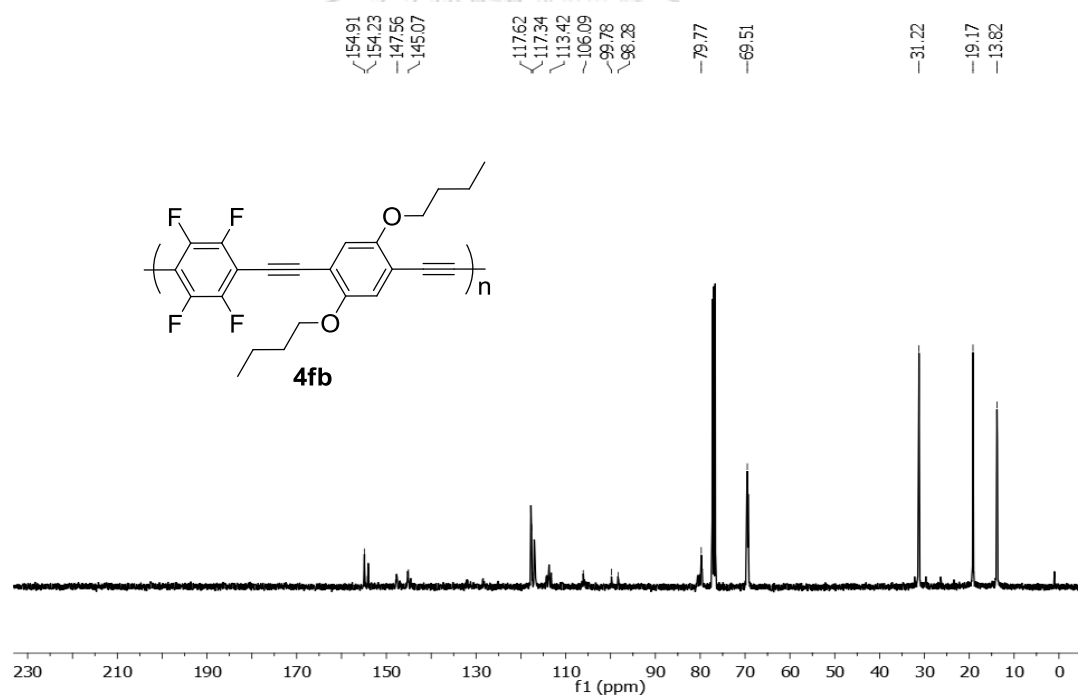


Figure A.24 GPC data of **4aa** obtained from $\text{PdCl}_2(\text{PPh}_3)_2$ catalyst

Figure A.25 GPC data of **4aa** obtained from $\text{Pd}(\text{PPh}_3)_4$ catalystFigure A.26 GPC data of **4aa** obtained from Pd/C catalyst

Figure A.27 ^1H NMR of **4db** in CDCl_3 Figure A.28 ^{13}C NMR of **4db** in CDCl_3

Figure A.31 ^{13}C NMR of **4eb** in CDCl_3 Figure A.32 FT-IR of **4eb**

Figure A.33 $^1\text{H NMR}$ of **4fb** in CDCl_3 Figure A.34 $^{13}\text{C NMR}$ of **4fb** in CDCl_3

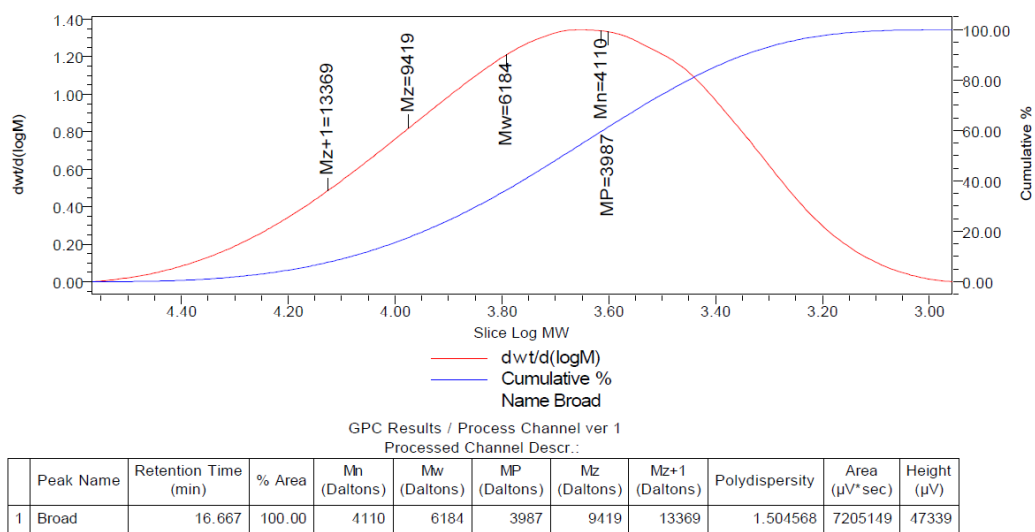
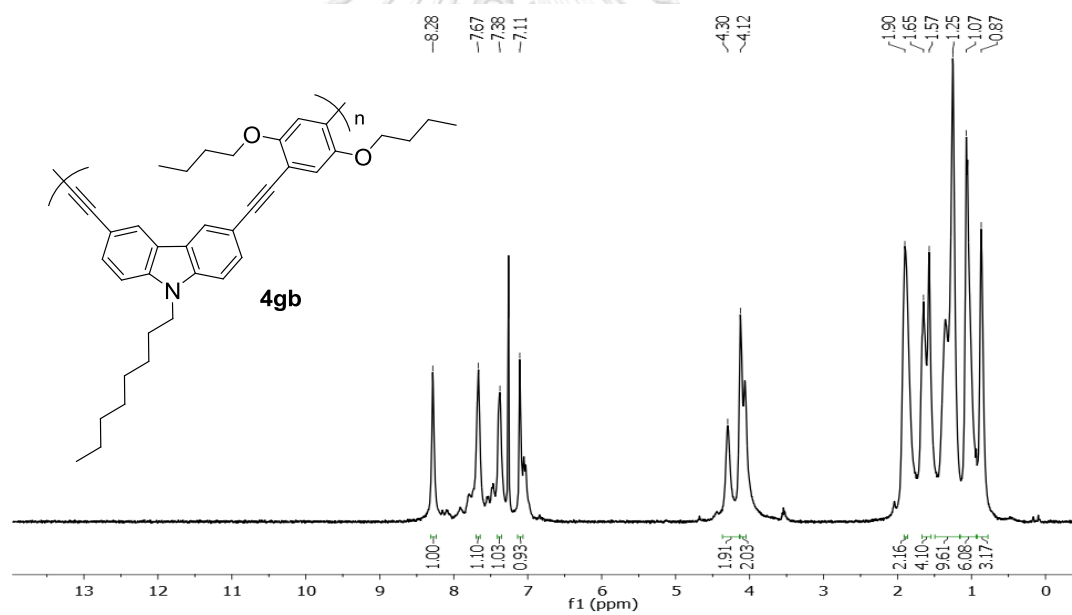
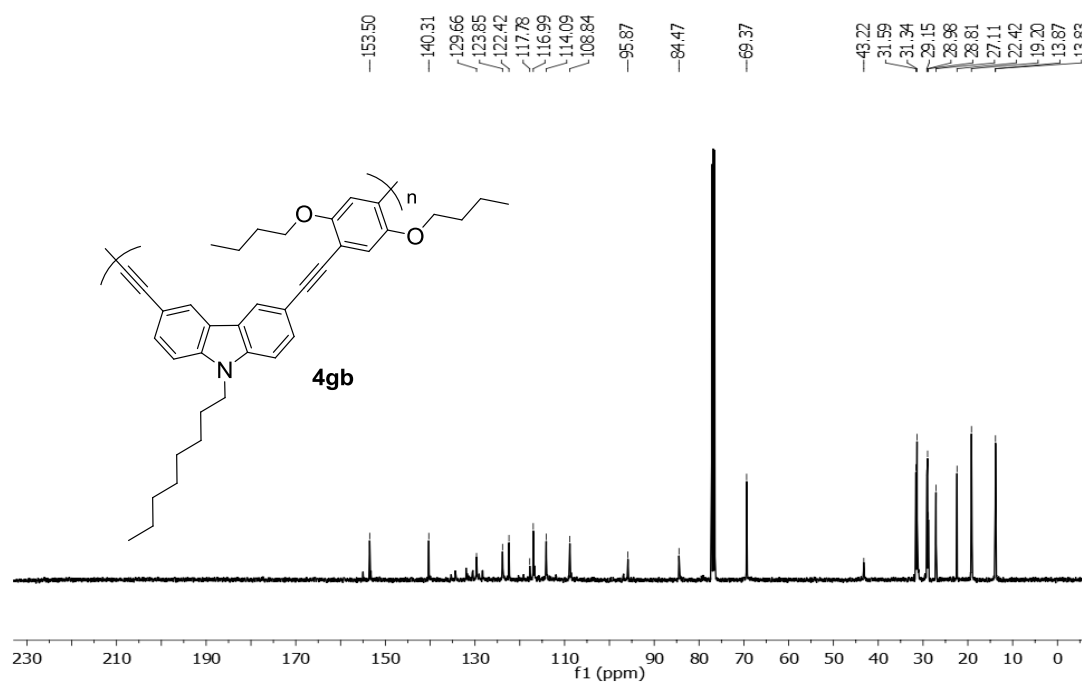
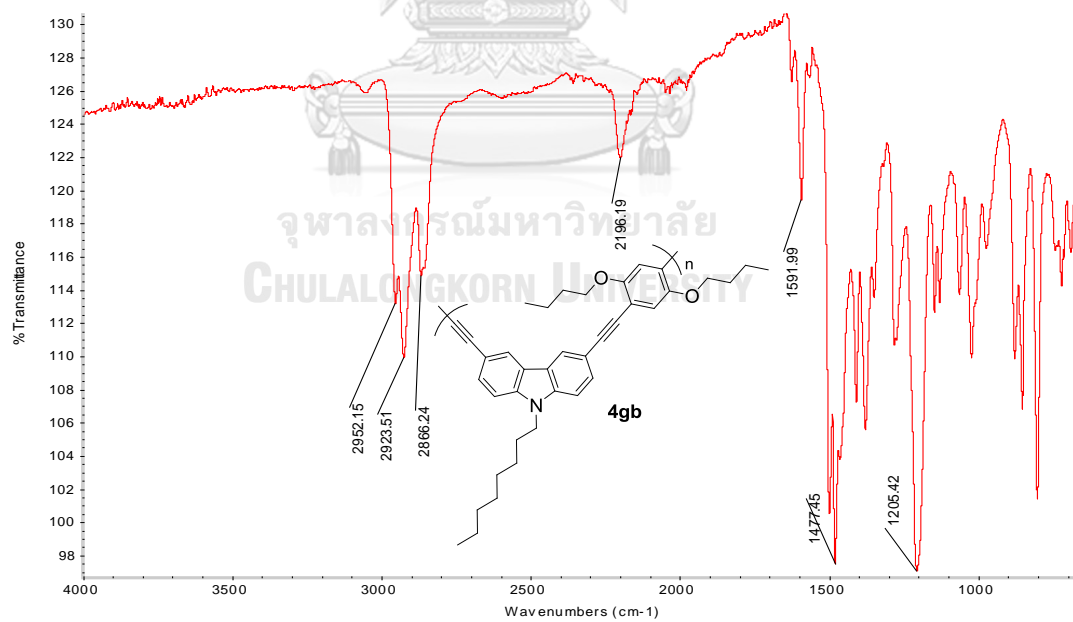
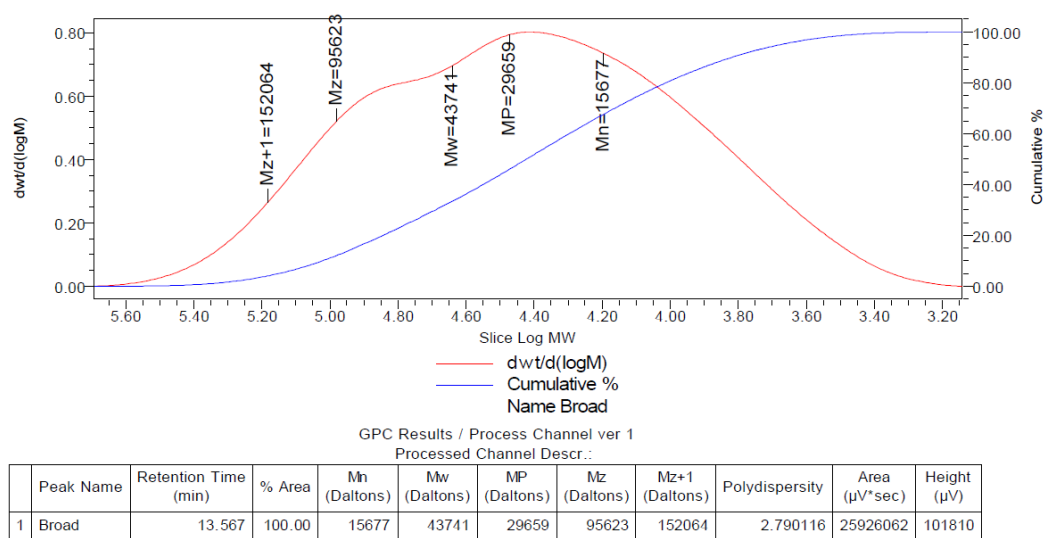
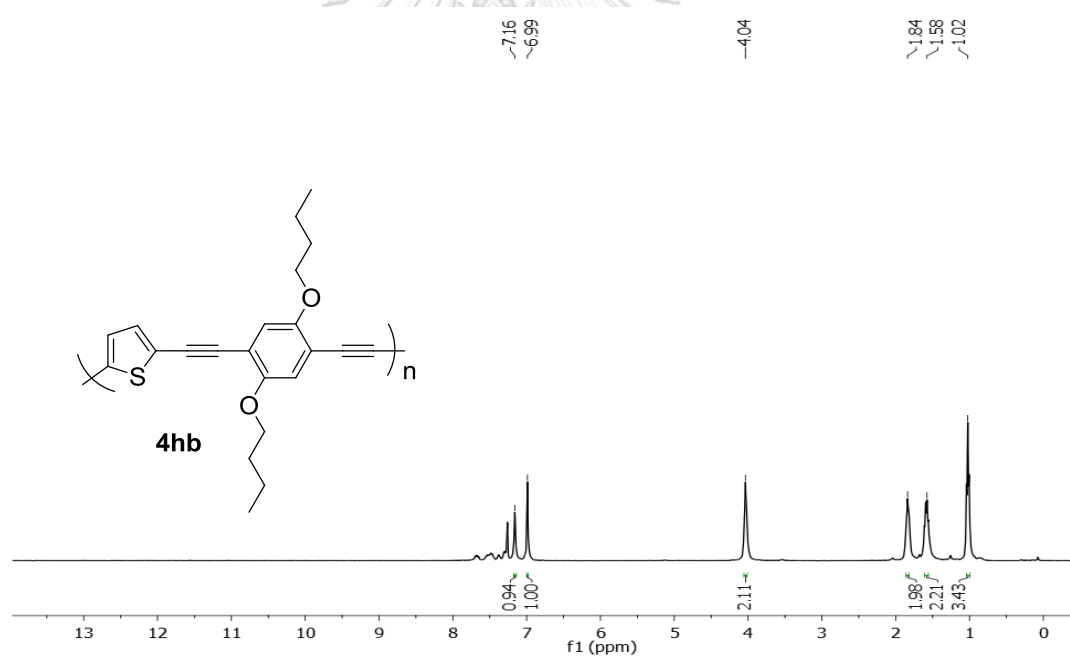


Figure A.35 GPC data of 4fb

Figure A.36 ^1H NMR of 4gb in CDCl_3

Figure A.37 ^{13}C NMR of **4gb** in CDCl_3 Figure A.38 FT-IR of **4gb**

Figure A.39 GPC data of **4gb**Figure A.40 ^1H NMR of **4hb** in CDCl_3

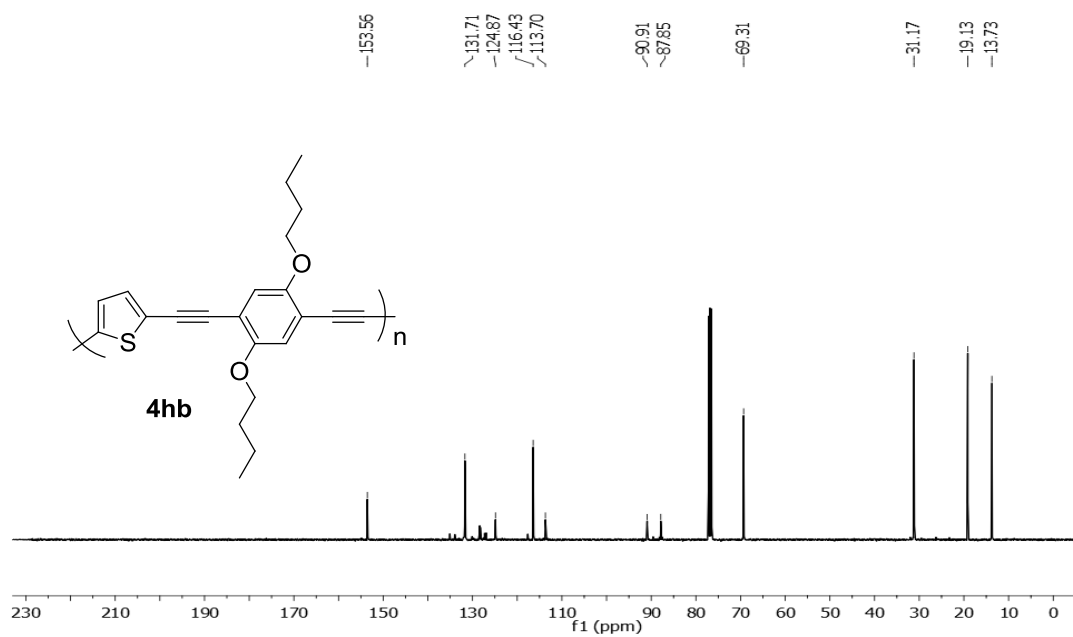


Figure A.41 ^{13}C NMR of **4hb** in CDCl_3

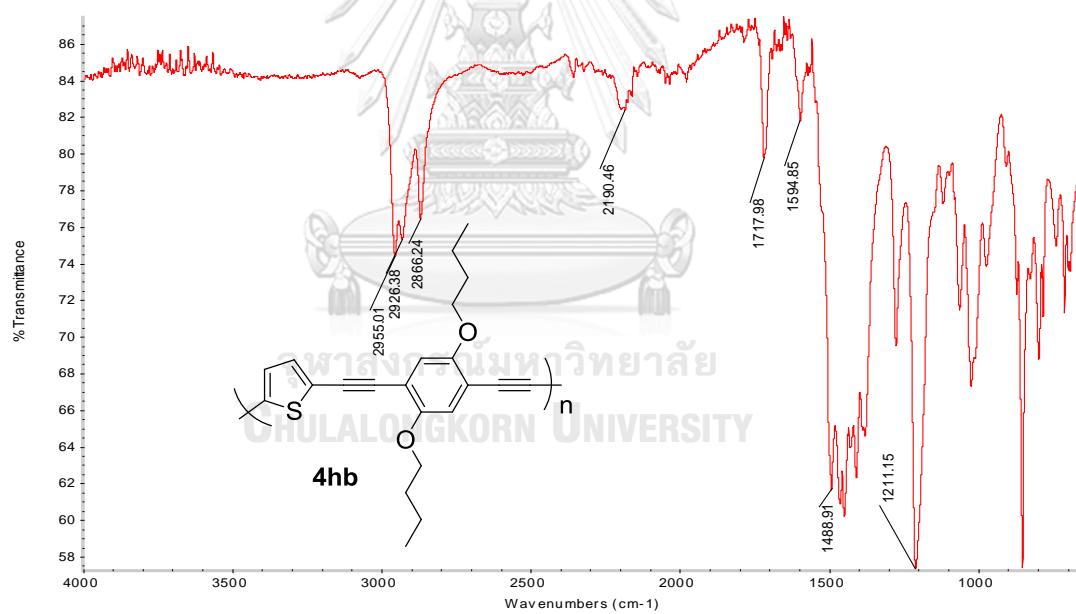


Figure A.42 FT-IR of **4hb**

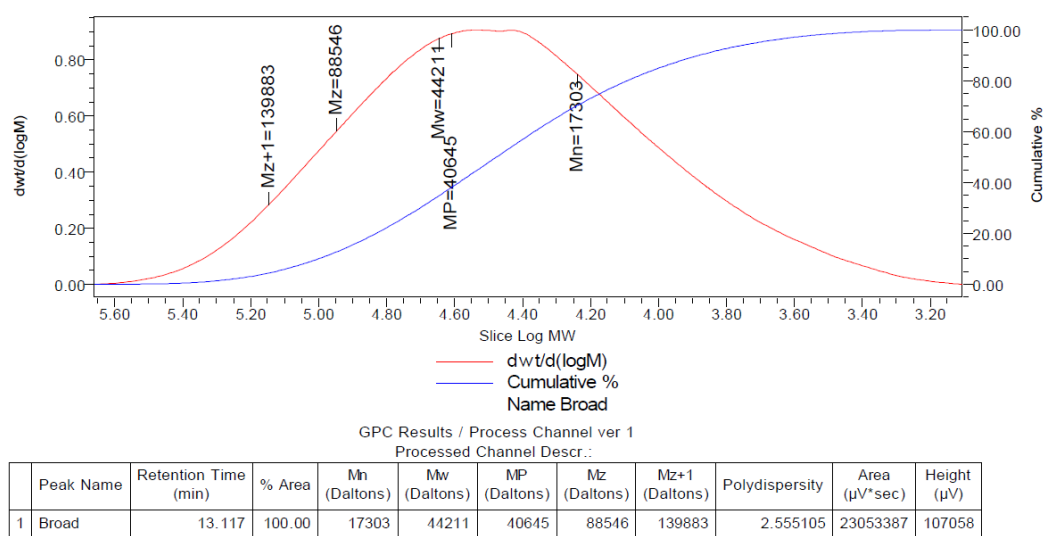
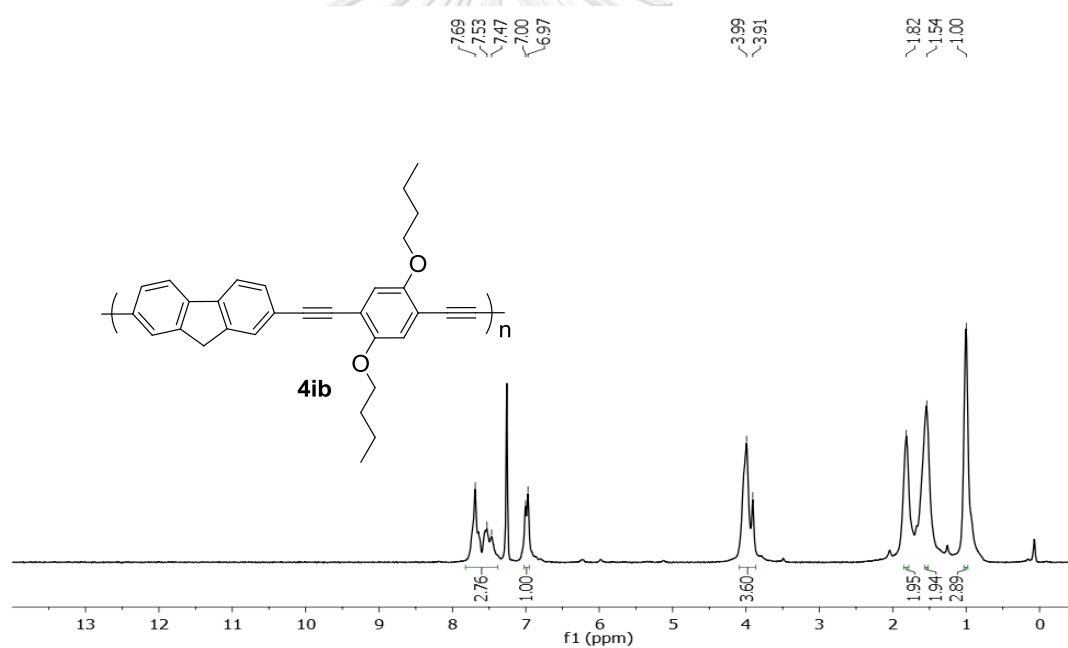
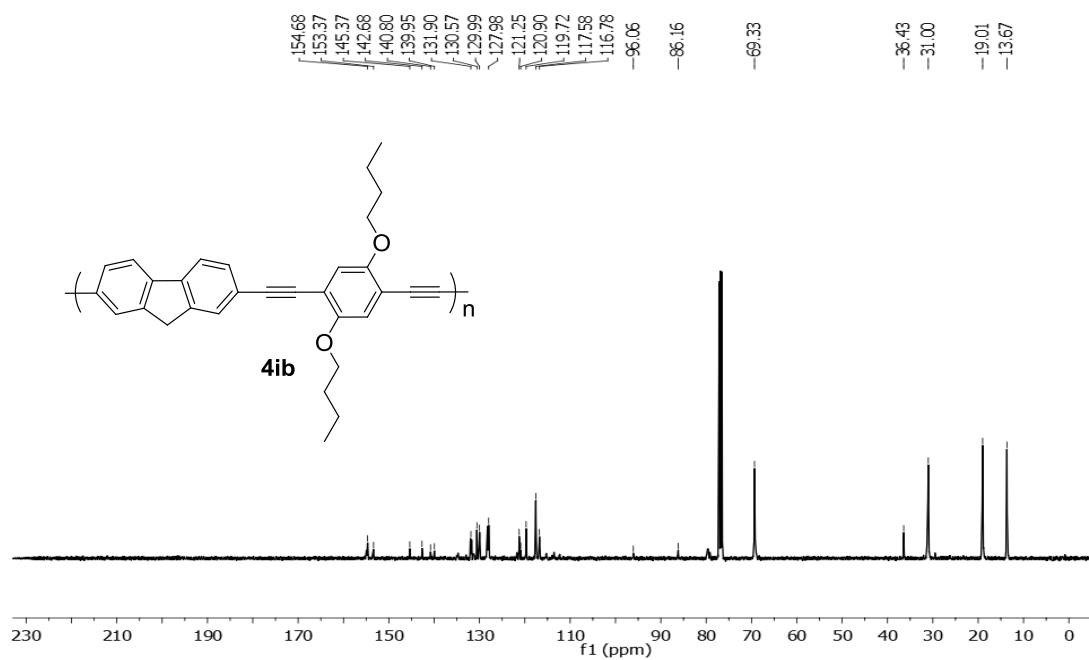
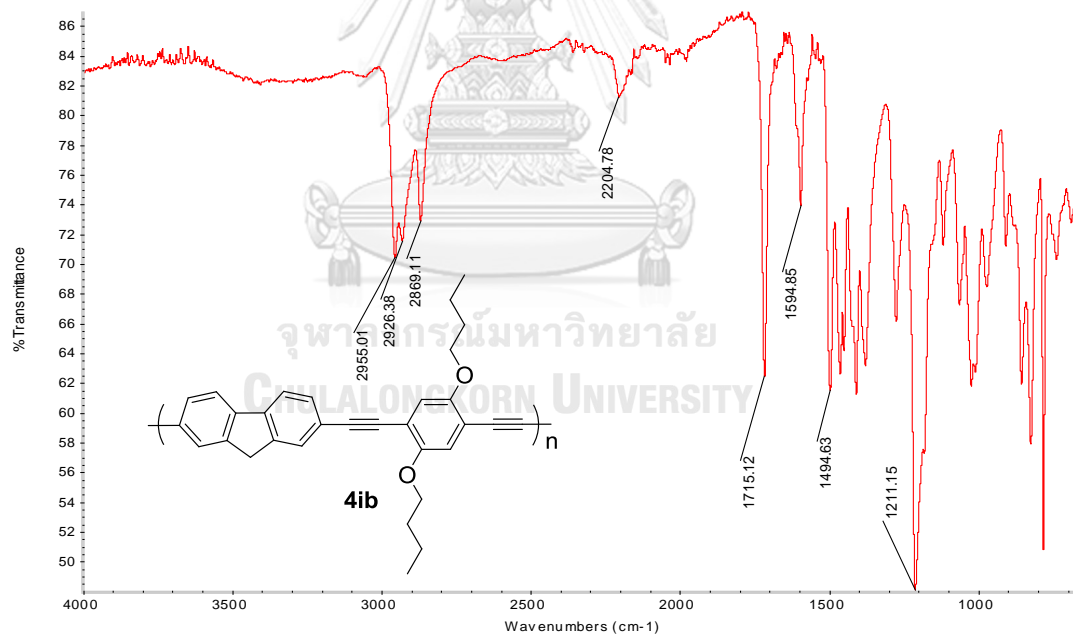


Figure A.43 GPC data of 4hb

Figure A.44 ^1H NMR of 4ib in CDCl_3

Figure A.45 ^{13}C NMR of **4ib** in CDCl_3 Figure A.46 FT-IR of **4ib**

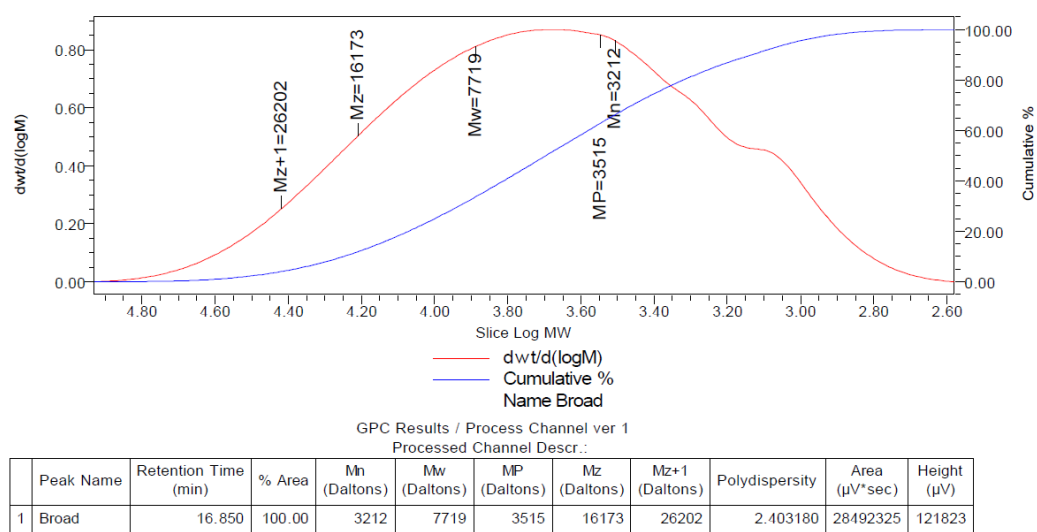
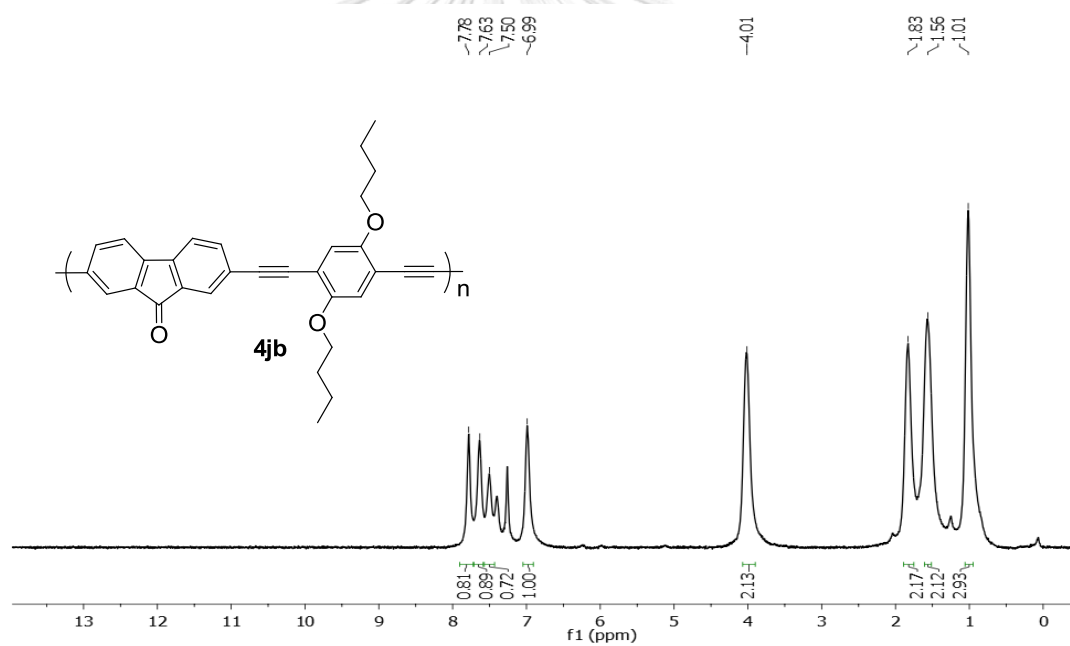
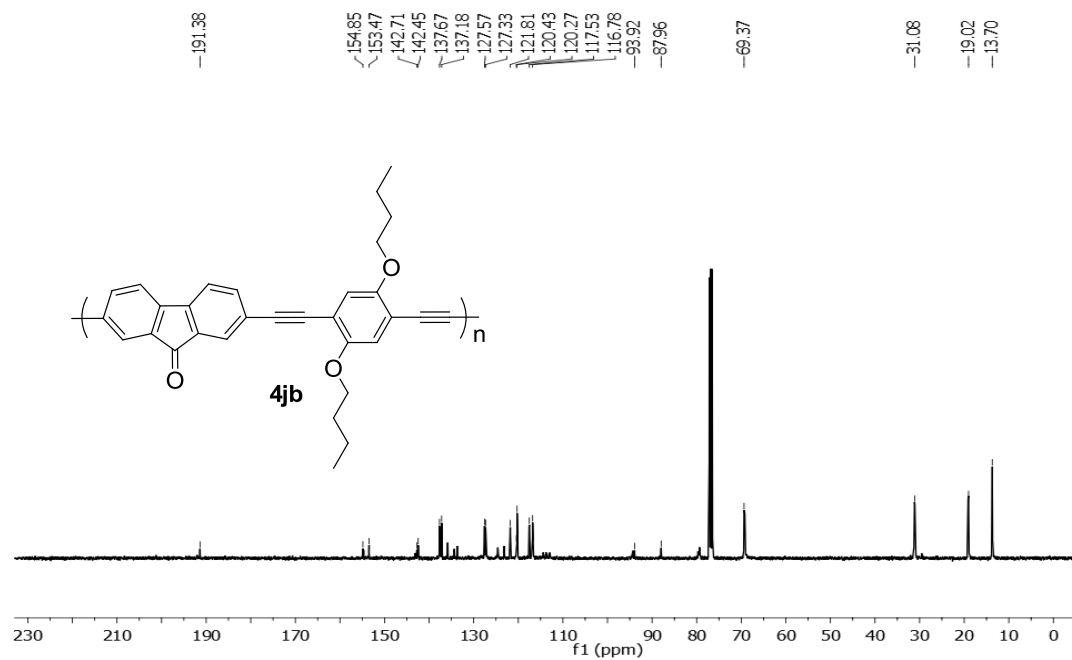
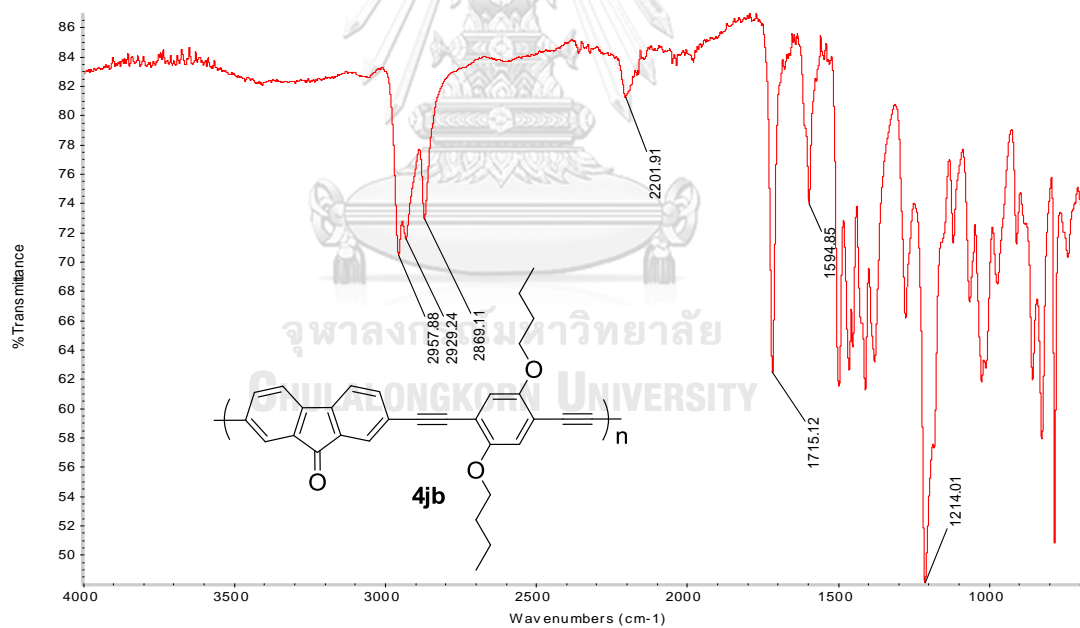
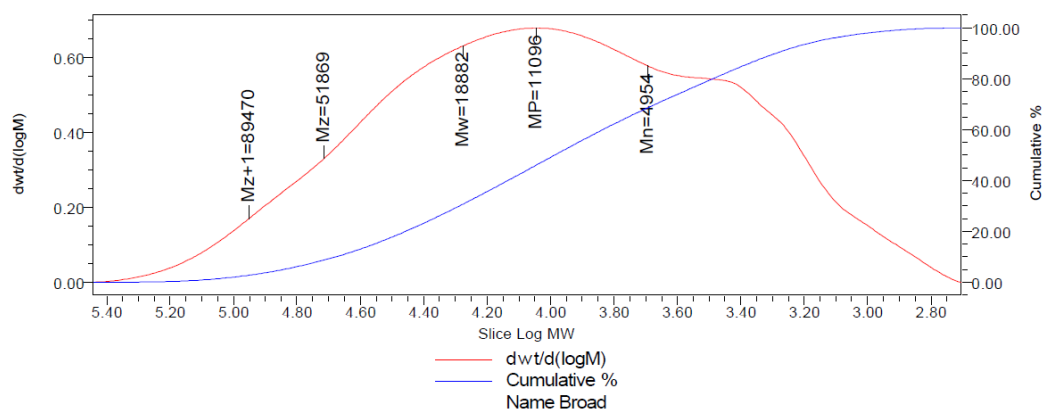


Figure A.47 GPC data of 4ib

Figure A.48 ^1H NMR of 4jb in CDCl_3

Figure A.49 ^{13}C NMR of **4jb** in CDCl_3 Figure A.50 FT-IR of **4jb**



GPC Results / Process Channel ver 1
 Processed Channel Descr.:

Peak Name	Retention Time (min)	% Area	Mn (Daltons)	Mw (Daltons)	MP (Daltons)	Mz (Daltons)	Mz+1 (Daltons)	Polydispersity	Area (μV*sec)	Height (μV)
1 Broad	15.083	100.00	4954	18882	11096	51869	89470	3.811577	18306154	56720

Figure A.51 GPC data of 4jb





จุฬาลงกรณ์มหาวิทยาลัย
CHULALONGKORN UNIVERSITY

VITA

Miss Nopparat Thavornsin was born on March 14, 1988 in Bangkok, Thailand. She got a Bachelor's Degree of Science in Industrial Chemistry from King Mongkut's Institute of Technology Ladkrabang in 2010. In 2013, she further received a Master Degree in Petrochemistry and Polymer Science program at Chulalongkorn University. Since 2013, she has been a graduate student in Petrochemistry and become a member of Material Advancement and Proficient Synthesis (MAPS) under supervision of Assoc. Prof. Dr. Sumrit Wacharasindhu and Prof. Dr. Mongkol Sukwattanasinitt. She graduated with a Ph. D. Degree in Petrochemistry in academic year 2017.

Her address is 43/530 Moo 8, Tiwanon Rd. Bangpood, Pakkred, Nonthaburi 11120, Thailand, Tel. 062-4796226.